Electrochemical Recovery of Copper from Distillery Spent Lees

Jonathan Boualavong
December 2018

A thesis presented for the degree of
Master of Philosophy

Department of Chemical and Process Engineering
University of Strathclyde

Declaration

This thesis is the result of the authors original research. It has been composed by the author and has not been previously submitted for examination which has led to the award of a degree.

The copyright of this thesis belongs to the author under the terms of the United Kingdom Copyright Acts as qualified by University of Strathclyde Regulation 3.50. Due acknowledgement must always be made of the use of any material contained in, or derived from, this thesis.

All data supporting this thesis has been deposited with the University of Strathclyde at: http://dx.doi.org/10.15129/53703157-f445-43c2-905a-d1332256eee0

Date:

Signed:

Contents

Declaration **i**

Contents **iii**

Acknowledgements **vii**

Abstract **ix**

List of Symbols **xi**

List of Figures **xiii**

List of Tables **xxvii**

1 Introduction **1**

1.1 Whisky Distillery Waste 1

1.2 Copper Economics 7

1.3 Research Overview 10

2 Fundamental Theory **13**

2.1 Metal Electroplating 13

2.2 Analytical Electrochemical Techniques 17

2.2.1 Cyclic Voltammetry 17

2.2.2 Polarization 18

2.3 Reaction Kinetics 18

3 Literature Review 21

3.1 Copper Treatment Technologies 21

3.2 Copper Recovery Processes 23

3.3 Reactors for Electrochemical Metal Recovery 27

3.3.1 Flow-based transport enhancement 27

3.3.2 Particulate electrodes 28

3.3.3 Porous mesh or matrix electrodes 32

3.3.4 Alternative electrode reactions 34

3.4 Past Work with the Porocell Test System 35

3.5 Comparison between Previous and Current Tests 41

4 Experimental Methods 47

4.1 Bench Scale Tests 47

4.1.1 Solution composition 47

4.1.2 Electrochemical cell 48

4.1.3 Cyclic voltammetry 48

4.1.4 Polarization experiments 50

4.1.5 Current efficiencies 51

4.2 Development of Process for Porocell Optimization 52

4.2.1 Copper measurement methods 52

4.2.2 Porocell design description 53

4.2.3 Flow rate validation 54

4.2.4 Comparison of carbon felt electrode pre-treatments 55

4.2.5 Determination of current limits 56

4.3 Porocell Copper Recovery Under Ideal Conditions 57

4.3.1 Optimization of current and flow rate 57

4.3.2 High power tests 58

4.3.3 Electrode imaging and analysis 58

4.4 Validation Against Spent Lees 60

5 Results and Discussion 61

5.1 Bench Scale Tests . . . 61

5.1.1 Cyclic Voltammetry . . . 61

5.1.2 Polarization experiments . . . 72

5.1.3 Bench Scale Plating . . . 79

5.1.4 Discussion . . . 87

5.2 Idealized Porocell Copper Recovery . . . 88

5.2.1 Flow rate and current density effects . . . 89

5.2.2 Reaction kinetics . . . 101

5.2.3 Energy consumption . . . 106

5.2.4 Extended time testing . . . 112

5.2.5 High voltage testing . . . 117

5.2.6 Discussion . . . 120

5.3 Validation against Spent Lees . . . 124

5.3.1 Results . . . 124

5.3.2 Discussion . . . 132

5.4 Copper Plating Distribution . . . 134

5.4.1 Physical appearance . . . 134

5.4.2 Image processing algorithm proof of concept . . . 137

5.4.3 Quantification of plating . . . 143

5.4.4 Discussion . . . 148

6 Conclusion 153

6.1 Summary . . . 153

6.2 Future Work . . . 157

Bibliography 159

Appendix A Statistical and Computational Methods 169

A.0.1 Power consumption . . . 169

A.1 Linear regression analyses 169

A.2 Statistical testing: ANOVA and Scheffe comparison 171

Appendix B Development of Procedures 175

B.1 Copper measurement method 175

B.2 Calibration of the cupric ion selective electrode 180

B.3 Flow rate validation 189

B.4 Comparison of carbon felt pre-treatments 190

B.5 Determination of current limits 192

Appendix C Additional Data and Statistical Tables 199

C.1 Bench scale tests 199

C.2 Porocell Copper Recovery Under Ideal Conditions 211

C.3 Validation Against spent lees 217

C.4 Electrode image analysis 217

Acknowledgements

This work would not have been possible alone, and to forget to mention everyone else who contributed would be a personal failing. I wish to acknowledge the following people for their support and assistance throughout this endeavor:

- My supervisors Sudipta Roy and Todd Green, for guiding me through the process, helping me understand the data, and suggesting avenues and paths to move forward with.
- Fellow students Priscila Valverde and Xiaomeng Su, for assistance both in the laboratory when trying to get experiments to work and helping make sense of the results that I obtained.
- Robbie Hughes of the Glengoyne Distillery, for providing spent lees for study and organizing their pickup.
- Cecilia Barrera and Chris Jones, for helping with laboratory procedures, primarily showing me how to operate and maintain my test reactor properly.

Finally, I must acknowledge the US-UK Fulbright Commission and the University of Strathclyde for their financial support, without which I would not have been able to perform this work.

Abstract

While the copper stills used in the whiskey purification process are vital to its flavor profile, low levels of copper corrosion lead to low but environmentally relevant copper concentrations in distillery waste. This is particularly the case for spent lees, the by-product of the second distillation, as, unlike the first distillation by-product, its only avenue is treatment and discharge.

With diminishing copper reserves, it is increasingly necessary to investigate ways that copper waste, including copper containing solutions, can be recovered for reuse. This work investigates electrochemical copper recovery from spent lees. Initial bench-scale studies investigated the impact of spent lees other waste constituents on copper recovery, finding insignificant or insufficiently large differences between the electrochemical behaviour of simulated waste and pure copper solution.

Consequently, copper recovery was tested with weakly acidic copper sulphate in a 4.5 L batch reactor using a porous carbon felt cathode. Application of currents of 105 mA (5 A/m^2) could reduce the copper concentration below the reliable detection limit of 2 ppm within 6 hours, albeit at a Coulombic efficiency less than 40 %. Applying less current resulted in lower efficiencies, suspected to be related to corrosion. The efficiency increased to 86.1 $\pm$ 1.4 % when the current was increased to 1.05 A, and the process duration decreased to under 2 hours.

When operating with real spent lees, the process was slower and less efficient. However, the difference was not statistically significant, predominantly due to uncertain copper concentration measurements. Real spent lees are notably more resistive, resulting in nearly double the energy cost compared to pure copper solution. Consequently, despite reasonable rates and efficiencies, the current process requires too much energy due to the high resistivity of the spent lees.

List of Symbols

Symbol	Definition
A	Electrode surface area (in cm^2)
D	Diffusion coefficient
E	Equilibrium electrode potential
E^0	Standard electrode potential
I	Absolute current
i_p	Peak current in a cyclic voltammogram
j	Current density
j_0	Exchange current density
k_0	Kinetic rate constant of a zeroth order reaction
k_1	Kinetic rate constant of a first order reaction
k_m	Mass transport coefficient of an electrochemical reactor
R	Gas constant
SD	Standard deviation
T	Temperature
t	Time
V	Solution volume
z	Number of electrons transferred in a redox half-reaction
$[X]$	Concentration of species X
α	Cathodic charge transfer coefficient
α_X	Chemical activity of species X
η	Electrode overpotential
ν	Scan rate (V/s)

List of Figures

3.1 A schematic diagram of a rotating drum electrode for electrochemical metal recovery. Diagram key: (1) Anolyte solution, (2) anode, (3) membrane, (4) metal deposit, (5) catholyte, (6) scraping mechanism, (7) rotating cathode, (8) insulating cover. From [37]. 28

3.2 (top) Example schematic diagram of a packed bed electrochemical reactor using graphite particles as the cathode from [33]. (bottom) Example schematic diagram of a fluidized bed electrochemical reactor from [58]. 29

3.3 Example diagram of a spouted vessel reactor as used in [54]. . . . 31

3.4 Pourbaix diagram of copper in water at concentration 10^{-4}, 25°C. Adapted from [38]. 43

3.5 Pourbaix diagram of copper in water at (left) concentration 10^{-6}, 25°C and (right) concentration 10^{-8}, 25°C. Adapted from [38]. . . 44

4.1 (top) Photograph of the bench-scale electrochemical cell. (bottom) Surface of the gold disk/platinum ring electrode. 49

4.2 Photograph (top) and simplified schematic (bottom) of the Porocell Test System. (A) Reservoir. (B) Pump (0.5-3.5L/min). (C) Flow meter. (D) Electrochemical reaction chamber. (E) Diaphragm valve. (F) Outlet. 53

4.3 (left) Cross section of the Porocell reaction chamber. Fluid flows from the bottom and gets forced through the carbon felt cathode due to a block in the flow path. Current is supplied to the felt from the inside steel rings. (right) Photograph of the cathode held in place against the current collector by its plastic mesh. 55

5.1.1 Cyclic voltammogram of the base electrolyte (dilute sulphuric acid at pH = 4, approximately 65 μM). WE = Au disk, CE = Pt wire 62

5.1.2 Scan rate effects on Cu^{2+}/Cu^0. All tests use 40 ppm Cu^{2+} at pH = 4. Arrow shows the direction of increasing scan rates. WE = Au disk, CE = Pt wire 63

5.1.3 Concentration effects on Cu^{2+}/Cu^0. All tests are at 35 mV/s and pH = 4. Arrow shows the direction of increasing concentration. WE = Au disk, CE = Pt wire 65

5.1.4 Magnitude of the oxidation (top) and reduction (bottom) peaks in the cyclic voltammograms along the range of scan rates from 10 mV/s to 100 mV/s. 66

5.1.5 Electrolyte composition effects on Cu^{2+}/Cu^0 (40 ppm Cu^{2+} at pH = 4). Cu (red) = only copper sulphate. Cu + M (green) = copper and trace metal salts as stated in Table 1.2. Sim. waste (purple) = detailed in Table 1.2 with 40 ppm Cu^{2+}. WE = Au disk, CE = Pt wire 67

5.1.6 Comparison of the reduction potentials of the Cu^{2+}/Cu^0 redox couple in the presence of other contaminants. *$p < 0.05$. 68

5.1.7 Comparison of the oxidation (top) and reduction peaks (bottom) in the cyclic voltammograms with additional compounds of spent lees. All tests use 40 ppm Cu^{2+}. 69

5.1.8 Diffusion coefficients of Cu^{2+}, determined by the cyclic voltammogram peaks using the Randles-Sevcik equation. Error bars indicate the standard error of the mean, aggregating across the three concentrations (n = 3). Individual data points are indicated by a $*$. (Bottom) Tabulation of means and standard deviations. . 70

5.1.9 Analysis of the possible concentration effects on the calculated diffusion coefficient of Cu^{2+}. 71

5.1.10 Polarization curves for each solution composition tested. Pure copper = 40 ppm Cu^{2+} at pH = 4 (approximately 65 μM sulphuric acid). Copper + Trace metals = 40 ppm Cu^{2+} + trace metal salts as stated in 1.2 at pH = 4. Simulated waste = Solution composition as detailed in 1.2 with 40 ppm Cu^{2+}. WE = Pt ring rotating at 100 rpm, CE = Pt wire 73

5.1.11 Normalized steady-state current after removal of the background. Vertical and horizontal dashed lines indicate the predicted reduction potential from the Nernst equation and the 0 A current line, respectively. WE = Pt ring rotating at 100 rpm, CE = Pt wire . 74

5.1.12 Polarization curve for 40 ppm Cu^{2+} for all solution compositions. Lines indicate the fit lines to the Tafel equation. WE = Pt ring rotating at 100 rpm, CE = Pt wire 75

5.1.13 Limiting current for copper reduction across the range of concentrations tested. WE = Pt ring rotating at 100 rpm, CE = Pt wire 76

5.1.14 Fraction of background current observed at steady state across the range of potentials in the polarization curve. WE = Pt ring rotating at 100 rpm, CE = Pt wire 77

5.1.15 High resolution polarization curves for 0 ppm (top) and 40 ppm (bottom) Cu^{2+} in each of the tested solution compositions. Vertical lines indicate the point at which the current switches from anodic to cathodic. 78

5.1.16 Current efficiencies of bench-scale copper plating for each current density, determined gravimetrically. Individual data points are represented by a ($*$). 80

5.1.17 Photographs of the electrode before (left) and after (middle and right) plating. (Middle) A normal, ideal copper electroplating result, showing a relatively uniform copper coat on the platinum ring. (Right) The result when electroplating copper when the electrode was not removed soon after completion, instead left rotating in the acidic electrolyte for at least 30 minutes. 81

5.1.18 Current efficiencies of bench-scale copper plating for each solution composition, determined gravimetrically. All tests applied a constant 25 μA. Individual data points are represented by a (*). 82

5.1.19 Change in the mass of the bare RRDE with time. A simple linear fit was used to determine how well it could estimate the mass loss due to polishing ($R^2 = 0.091$). 83

5.1.20 Electrode potentials of bench-scale copper recovery at each current density (symbols) and solution compositions (dashed and dotted lines). Data presented only samples the full dataset every 2 hours for simplicity of visualization. 85

5.1.21 Differences in energy consumption per Coulomb passed due to current density (top) and solution composition (bottom). 87

5.2.1 Measured concentration change of copper over the course of 3 hours of galvanostatic operation using the Porocell, starting with a 40 ppm Cu^{2+} (pH = 4) test solution. Error bars indicate the standard deviation (n = 4). 90

5.2.2 Concentration of copper before (top) and after (bottom) electrochemical recovery from a 40 ppm Cu^{2+} (pH = 4) test solution with the Porocell. Error bars indicate the standard deviation (n = 4). Dotted horizontal line indicates the known starting concentration of 40 ppm. 91

5.2.3 Net Coulombic efficiency for copper recovery from a 40 ppm Cu^{2+} (pH = 4) test solution using the Porocell, calculated using the measured concentration change over time. Error bars indicate the propagated standard deviation (n = 4). 93

5.2.4 Isolation of the net Coulombic efficiency for copper recovery from a 40 ppm Cu^{2+} (pH = 4) test solution for the first 10 minutes (top) and for the full test duration (bottom), calculated using the measured concentration change over time. Error bars indicate the propagated standard deviation (n = 4). Dotted horizontal lines note the realistic bounds of 0 % and 100 % efficiency for ease of interpretation. 94

5.2.5 Recalculation of net Coulombic efficiency for copper recovery from a 40 ppm Cu^{2+} (pH = 4) test solution for the full duration of 3 hours, assuming the initial concentration to be 40 ±2 ppm as prepared. Error bars indicate the propagated standard deviation (n = 4). Dotted horizontal lines note the realistic bounds of 0 % and 100 % efficiency for ease of interpretation. 95

5.2.6 Predicted change in copper concentration of the 40 ppm Cu^{2+} ($pH_{t\,=\,0} = 4$) test solution based on the change in pH. Error bars indicate the propagated standard deviation (n = 4). 97

5.2.7 Predicted Coulombic efficiency of copper reduction from a 40 ppm Cu^{2+} ($pH_{t\,=\,0} = 4$) solution based on the change in pH. Error bars indicate the propagated standard deviation (n = 4). 99

5.2.8 Coefficient of determination (R^2) when fitting the mean measured concentration profile (Fig. 5.2.1) to 0^{th} or 1^{st} order kinetics. . . . 102

5.2.9 Values for the rate constant, k, when fitting the mean measured concentration profile (Fig. 5.2.6) to 0^{th} order (top) or 1^{st} order (bottom) kinetics via linear regression. Error bars indicate the uncertainty of the fit. 103

5.2.10 Coefficient of determination (R^2) when fitting the predicted concentration change based on pH changes (Fig. 5.2.6) to 0^{th} or 1^{st} order kinetics. 104

5.2.11 Values for the rate constant, k, when fitting the predicted concentration change based on pH changes (Fig. 5.2.6) to 0^{th} order (top) or 1^{st} order (bottom) kinetics via linear regression. Error bars indicate the uncertainty of the fit. 105

5.2.12 Porocell voltage change over time when run galvanostatically with a 40 ppm Cu^{2+} (pH = 4) test solution. Plot shows samples every 10 minutes for ease of visualization. Error bars indicate the standard deviation (n = 4). 107

5.2.13 Total energy consumption of the Porocell when run galvanostatically for 3 hours of operation at each current with a test solution of 40 ppm Cu^{2+} (pH = 4). Error bars indicate the standard deviation (n = 4). 108

5.2.14 (top) Mass of copper recovered (top) and normalized electrical energy cost for 3 hours of operation of the Porocell (bottom), based on the measured starting and ending concentrations of a 40 ppm Cu^{2+} (pH = 4) test solution. Dotted horizontal line notes the total quantity of copper in the batch.
Error bars are the propagated standard deviation (n = 4). Data points are slightly offset on the x-axis for ease of visualization due to overlapping error bars. 109

5.2.15 Mass of copper recovered (top) and normalized electrical energy cost for 3 hours of operation of the Porocell (bottom), based on the known starting concentration of 40 ±2 ppm and the measured concentration at 3 hours.
Error bars are the propagated standard deviation (n = 4). Data points are slightly offset on the x-axis for ease of visualization due to overlapping error bars. 110

5.2.16 Mass of copper recovered (top) and normalized electrical energy cost for 3 hours of operation of the Porocell (bottom), based on the change in pH of a 40 ppm Cu^{2+} ($pH_{t=0} = 4$) test solution and Eq. 5.3.
Error bars are the propagated standard deviation (n = 4). Data points are slightly offset on the x-axis for ease of visualization due to overlapping error bars. 111

5.2.17 Porocell voltage change over the course of 26 hours of galvanostatic operation with a 40 ppm Cu^{2+} (pH = 4) solution. 113

5.2.18 Measured concentration of copper ions of a copper sulphate solution (pH = 4) over the course of 26 hours. Error bars indicate the uncertainty in the single measurement associated with the ISE. . . 114

5.2.19 Predicted change in copper concentration of a 40 ppm Cu^{2+} ($pH^{t\,=\,0}$) solution calculated from the change in pH and Eq. 5.3. 116

5.2.20 Porocell voltage change when operating galvanostatically at 1.05 A with a 40 ppm Cu^{2+} (pH = 4) solution. Potentials of 20 V indicate potentiostatic operation where greater than 20 V were needed to drive 1.05 A current. Error bars are the standard deviation (n = 3). 118

5.2.21 Measured copper concentration (top) and the change predicted by the change in pH and Eq. 5.3 (bottom) when recovering using 1.05 A in the Porocell. Error bars are the standard deviation (n = 4). 119

5.3.1 Copper concentration over the course of Porocell operation at 105 mA. Pure copper = 40 ppm Cu^{2+}, pH = 4, Sim. waste = see Table 1.2; Spent lees = waste provided by Glengoyne Distillery. 125

5.3.2 Porocell voltage profile over the course of operation at 105 mA. Error bars for all groups represent one standard deviation (n = 4). 128

5.3.3 Change in solution pH over the course of galvanostatic Porocell operation at 105 mA. Error bars for all groups represent one standard deviation (n = 4). 128

5.3.4 (top) Anticipated change in copper concentration during galvanostatic Porocell operation at 105 mA based on the change in pH. Error bars for all groups represent one standard deviation (n = 4). (bottom) Net current efficiency after 3 hours using the change in pH to estimate the change in copper concentration. 129

5.4.1 Photographs of the outside face of the carbon felt. Axes denote the direction of flow (Z) and the direction of radial symmetry (Θ). Scale bars in the bottom right of each image measure 1 cm across. (left) Representative electrode after 10 tests with the Porocell using copper only solution. (right) The electrode used only for tests involving simulated spent lees or Glengoyne spent lees.
Arrow (a) designates the height at which copper stops being plated. Arrow (b) indicates a region where the copper appears blue instead of red, suggesting a hydrated form of copper (II) ions. . . . 135

5.4.2 Sample photograph of an electrode cross section. Axes denote the direction of flow (Z) and the depth (r); the outside edge nearest the anode when assembled is to the left of the image. Scale bar measures 0.5 cm horizontally.
Arrow (a) points out a slight amount of copper on the face of the electrode, indicated by the reddish tint of the fibers. 136

5.4.3 Example of the basic breakdown of the front-facing image. (Top) The full color image, which is stored as (middle) relative contributions of green, red, and blue channels. (Bottom) The difference between the red channel and the other two channels gives a slightly clearer image of the copper. The images for the difference have had their intensities rescaled for ease of visualization. 138

5.4.4 Demonstration of the processing used to isolate the electrode from the background. A threshold value for the red channel was determined using Otsu's method to obtain a binary filter. 139

5.4.5 Demonstration of the processing used to isolate the copper from the rest of the image. A threshold value for the difference between the red and green channels was determined using Otsu's method to obtain a binary filter. 139

5.4.6 Visual comparison of the original front-facing photograph and the processed image. White designates copper, black indicates carbon felt, and gray indicates the background. 140

5.4.7 Example of the basic breakdown and calculation for the cross section image. (Top) The full color image, which is stored as (row 2) relative contributions of green, red, and blue channels. (Row 3) The difference between the red channel and the other two channels gives a slightly clearer image of the copper. (Bottom) Squaring the original color channels, which have intensities from 0 to 1, causes greater separation between the lightest and darkest regions, allowing for sharper distinction when calculating the difference between red and the other channels. 141

5.4.8 Demonstration of Otsu's method to isolate the regions likely to be copper. 142

5.4.9 Demonstration of the processing used to isolate an electrode cross section from the background. The yellow hue was isolated based on its expected relative intensities of red, green, and blue. 142

5.4.10 Visual comparison of the original cross section and the processed image. White designates copper, black indicates carbon felt, and gray indicates the background. 143

5.4.11 Relative fraction of copper at each height increment for 3 independent electrodes. Vertical dashed and dotted (−.−) lines represent the height at which copper begins to disappear, and vertical dashed lines (−−) represent the point highest point at which copper is present. 144

5.4.12 Change in copper fraction with change in distance. The circled minima are capable of noting when copper begins to disappear and when it ceases to appear. 145

5.4.13 Average profile for copper fraction with depth (n = 3) at sections close to the inlet (1 cm) and outlet (13 cm). Profiles have been smoothed using a 41 point linear interpolation window. 146

5.4.14 Perceived copper fraction of the centermost depths, 0.2 cm in from each edge. Error bars are one standard deviation (n = 3). 147

5.4.15 Estimated copper deposition depth penetration at each height increment. This depth represents the point at which the copper fraction is first becomes equal to the mean plus one standard deviation of the centermost region. Error bars are one standard deviation (n = 3). 148

B.1 Absorption spectra of dilute sulphuric acid, pH = 4 (approximately 65 μM) (top) and 40 ppm copper in dilute sulphuric acid, pH = 4 (bottom). 176

B.2 Calibration of UV-vis measurements for cupric ion detection. Error bars indicate the standard deviation (n = 3); the dotted line indicates the standard deviation of the fit line. 178

B.3 Calibration of the ion selective electrode for cupric ion detection. Error bars indicate the standard deviation (n = 3); individual replicates are also presented. The dotted line indicates the standard deviation of the fit line from 2 to 100 ppm. 179

B.4 Calibrations of the ion selective electrode at different pH values. The arrow shows the direction of increasing pH. 180

B.5 Quantification of the pH effect on the ISE calibration's slope (-x-, left axis) and intercept (-o-, right axis). Error bars indicate the uncertainty in the calibration fit line. 181

B.6 Change in the ISE calibration's slope (top) and intercept (bottom) with respect to pH and time. Error bars indicate the uncertainty in the calibration fit line. 183

B.7 Shift in the ISE measurement over time. Error bars indicate the standard deviation across all tested concentrations (n = 5). . . . 184

B.8 Change in the ISE calibration's slope (top) and intercept (bottom) with respect to pH during the month of August. Error bars indicate the uncertainty in the calibration fit line. Circled data points indicate tests with simulated spent lees. 185

B.9 Calibrations of the ion selective electrode at different pH values, aggregating tests performed in August together. (top) Error bars indicate the standard deviation. The arrows show the direction of increasing pH. (middle and bottom) pH dependence on the calibration slope and intercept. Error bars show the uncertainty in the fit line. 186

B.10 Comparison between the nominal flow rate displayed on the Porocell (abscissa) and the experimentally measured flow rate (ordinate). Error bars indicate the standard deviation (n = 3). The dashed line shows the expected values should the nominal and measured flow rates be equivalent. 190

B.11 Comparison of the steady state current when using carbon felt pre-treated under various conditions, using dilute sulphuric acid (top) or 40 ppm Cu^{2+} in dilute sulphuric acid. Untreated tests were performed with the Porocell circulating at 3.5 L/min; all other tests were performed with a static solution. 191

B.12 Current-voltage plot of 40 ppm Cu^{2+} in dilute sulphuric acid under each flow rate tested. Each trace indicates an independent replicate. Titles refer to the uncorrected nominal flow rate. . . . 193

B.13 Current-voltage plot comparing 65 μM sulphuric acid to 65 μM sulphuric acid with 40 ppm Cu^{2+}. An additional curve of 65 μM sulphuric acid scaled by a factor of 4 is included due to a factor of 4 increase in conductivity for more direct comparison. 194

B.14 Current-voltage plot for each flow rate (rows) and concentration (columns) tested. Titles refer to the uncorrected nominal flow rate. 195

B.15 Coefficient of determination of the linear fit of the steady state current (Fig. B.11) from 0 V to the specified upper voltage. The horizontal dotted line indicates the 0.95 cut-off point for a strong linear fit. The vertical dotted line is the estimated potential where the linear fit is no longer applicable. 196

C.1 Cyclic voltammetry with weakly acidified copper solution. Each row uses the same scale for the y-axis; each column uses the same scale for the x-axis. The estimated peak is circled. 200

C.2 Cyclic voltammetry with weakly acidified copper solution with trace metals found in spent lees. Each row uses the same scale for the y-axis; each column uses the same scale for the x-axis. The estimated peak is circled. 203

C.3 Cyclic voltammetry with simulated spent lees. Each row uses the same scale for the y-axis; each column uses the same scale for the x-axis. The estimated peak is circled. 206

C.4 Photographs of the electrodes' outer face. 219

C.5 Processed photographs of the electrodes' outer face. White regions are copper; black regions are the rest of the electrode surface. 220

C.6 Photographs and processed images of electrode E3 cross sections. 222

C.7 Photographs and processed images of electrode E4 cross sections. 224

C.8 Photographs and processed images of electrode E5 cross sections. 226

C.9 E3 cross sections: profile of copper with depth. 228

C.10 E4 cross sections: profile of copper with depth. 229

C.11 E5 cross sections: profile of copper with depth. 230

C.12 Electrode cross sections: mean profile of copper with depth, smoothed by a 41 point slope (40 mm window). 231

List of Tables

1.1 Reported average, minimum, and maximum values for the chemical makeup of distillery pot ale; n indicates the number of independent batches tested. The absence of data from the data indicates that it was unreported or untested. COD = chemical oxygen demand, BOD = biological oxygen demand, TOC = total organic carbon. 3

1.2 Reported average, minimum, and maximum values for the chemical makeup of distillery spent lees; n refers to the number of distinct distilleries whose waste were tested. All data from Yu et al. [6]. Concentrations are reported in ppm if not indicated otherwise. 4

1.3 List of environmental quality standards set by the SEPA. All regulations reported are set by supporting guidance document WAT-SG-53 [11]. 6

3.1 Summary of literature related to the Porocell.
*Source is a summary of other work and does not include all experimental details.
**Only source using low current (< 100 A/m^2, often < 10 A/m^2). 37

5.1.1 Coefficient of determination when fitting the cyclic voltammetry peaks to the Randles-Sevcik equation. Red = reduction peak, Ox = oxidation peak. 64

5.1.2 Calculated Tafel slopes and exchange currents from the polarization curves in Fig. 5.1.12. Error represents the uncertainty in the quality of the fit line. 74

5.1.3 Differences in mean electrode potential due to current density and solution composition. 85

5.2.1 Mean Coulombic efficiency of copper recovery from a 40 ppm Cu^{2+} (pH = 4) solution for each flow rate and current tested after 3 hours of Porocell operation, calculated based on the changes in pH. Uncertainty indicates one standard deviation (n = 4). 100

5.2.2 Operation time (hours) necessary to treat 40 ppm Cu^{2+} (pH = 4) to 2 ppm Cu using the Porocell, as predicted by zeroth order kinetics. The error is the standard deviation, based on the uncertainty of the kinetic fit. 106

5.2.3 Key values from galvanostatic Porocell operation with a starting solution of 40 ppm Cu^{2+} for 26 hours. 116

5.2.4 Key values from galvanostatic Porocell operation at 1.05 A from a feed solution of 40 ppm Cu^{2+} (pH = 4).
*Using the measured starting concentration
**Using the assumed starting concentration of 40 ±2 ppm as prepared 119

5.3.1 Measurements and calculations for comparison of pure copper sulphate (40 ppm Cu^{2+}, pH = 4) (n = 4) to simulated spent lees per Table 1.2 (n = 3) and Glengoyne spent lees (n = 4). Uncertainties represent one standard deviation. 126

5.3.2 Conductivities of pure copper, simulated waste, and Glengoyne spent lees before and after testing in the Porocell (105 mA for 3 hours). 130

5.4.1 Calculated values for the point at which copper starts to disappear and the point at which it ceases to appear. E3, E4, and E5 represent electrodes used in 8 tests of copper recovery each, all from solutions of pure copper. 146

A.1 List of variables used in 2-way ANOVA 172

B.1 Comparison between absorbance wavelengths of 760 nm and 805 nm for detection of copper at concentrations below 40 ppm. Values are mean ±measurement error (1 standard deviation of absorbance for the same solution, n = 3). 177

B.2 Quality of the fit line to the ISE calibration for different regions of interest. Data was fit to the following equation: $V_{ISE} = slope * \log_{10}[Cu^{2+}] + intercept$ 179

B.3 Coefficients of determination of the ISE calibration variables with respect to pH for each test date in July. 183

B.4 Coefficients of determination of the ISE calibration variables with respect to pH for each test date in August. 185

C.1 Current for each voltammogram peak: copper only. Current in μA. Uncertainty is one standard deviation. 201

C.2 Potential for each voltammogram peak, and the estimated reduction potential: copper only. Potential in mV vs Ag/AgCl. 202

C.3 Current for each voltammogram peak: copper and trace metals. Current in μA. Uncertainty is one standard deviation. 204

C.4 Potential for each voltammogram peak, and the estimated reduction potential: copper and trace metals. Potential in mV vs Ag/AgCl. 205

C.5 Current for each voltammogram peak: simulated waste. Current in μA. Uncertainty is one standard deviation. 207

C.6 Potential for each voltammogram peak, and the estimated reduction potential: simulated waste. Potential in mV vs Ag/AgCl. . . 208

C.7 Slope and subsequent diffusion coefficient when fitting the mean oxidation peak current and scan rate to the Randles-Sevcik equation. Uncertainty is one standard deviation. 209

C.8 p-values for the comparison of each pair of solution compositions for results from bench scale studies. 210

C.9 Solution pH of each individual sample from the Porocell when comparing different flow rate and current conditions. 212

C.10 Solution cupric ion concentration of each individual sample from the Porocell when comparing different flow rate and current conditions. Concentration determined from the ISE measurements. . 214

C.11 Tabular version of Figure 5.2.8: Coefficient of determination (R^2) when fitting the mean measured concentration profile to the zeroth and first order kinetics. 216

C.12 p-values from the 2-way ANOVA of the concentration at three hours, as measured by ISE. 216

C.13 p-values from the 2-way ANOVA of the mass of copper recovered after three hours. Comparison factors are the calculation method (top) and the current (bottom). The flow rate is known to have an insignificant effect compared to the effects of these factors and was ignored. Calculation method definition:
Measured = uses the measured concentrations from ISE for both t = 0 and t = 3 hours
Assumed = uses the measured concentrations from ISE for t = 3 hours and the known starting concentration of 40 ±2 ppm
pH = uses the change in copper ion concentration based on the change in [H^+] and the stoichiometric relation 217
C.14 Solution pH (top) and cupric ion concentration (bottom) of individual samples when validating Porocell behaviour with spent lees. 218
C.15 Photographs and processed images of electrode E3 cross sections. 221
C.16 Photographs and processed images of electrode E4 cross sections. 223
C.17 Photographs and processed images of electrode E5 cross sections. 225

Chapter 1

Introduction

1.1 Whisky Distillery Waste

Scotch whiskey production is one of the largest economic industries in Scotland [1], worth more than 5 bn in 2015 [2]. However, this industry amounts to a significant amount of liquid waste: for every liter of whiskey produced, an estimated 8 [1] to 32 [3] liters of wastewater are produced. The majority of this liquid waste comes from the distillation and wash steps following fermentation. These steps take place in large copper stills, helping remove not only large, undesirable organic compounds directly by distillation, but also the small flavor-fouling sulphur-containing compounds via adsorption to the copper surface [4]. Overall, an average sized whiskey distillery will generate nearly 500 thousand liters of wastewater per day of operation [5], of which approximately 0.4 tonnes/year will be copper leached from the stills [6]. In total, all of the Scottish distilleries combined generate just under 2 billion liters of liquid waste annually [7].

In a typical Scotch whiskey process, the liquid waste is derived from two distillations, yielding the pot ale and spent lees from the first and second distillations, respectively. Piggott [8] estimated that every liter of liquor produced yields 8.5 to 11.5 liters of pot ale and 16 to 21 liters of spent lees; on the other hand, Russell

[9] approximates about 10.8 kg pot ale and 12.1 kg spent lees per kg whiskey. The consistency in the quantity of pot ale, despite these two estimates being published in 1989 and 2003, respectively, suggests that there is roughly an order of magnitude more pot ale than liquor. On the other hand, the decline in spent lee estimates with time may be the result of more efficient wash and distillation processes being implemented, but it still is nearly equal to pot ale, if not slightly higher, in volume.

While the compositions of the two waste streams are similar, pot ale tends to be more concentrated than the spent lees, containing more of the impurities from the fermentation process. The major components found in pot ale and spent lees are listed in Table 1.1 and Table 1.2, respectively. The data is broken up by source, noting the differences both within and among studies to highlight the sources of variability. Only one source could be found reporting the contents of spent lees, likely due to the very low concentrations leading to less research in their utility. Additionally, no study was a fully systematic analysis of all components, only taking measurements of suspected compounds.

While many of these compounds are of concern, not all have related regulations surrounding discharge due to low environmental impact. Key regulations relevant to Scottish distillery wastewater are presented in Table 1.3. Interestingly, there are no strict regulations placed on the concentration of any of the pollutants in wastewater. Instead, regulations set the environmental quality standards (EQS), which dictate the concentration of pollutants of concern in the body of water as a whole. This metric accounts for wastewater dilution after it has been mixed into the environment, only using samples from outside of the mixing zones where wastewater and natural waters combine.

Table 1.1: Reported average, minimum, and maximum values for the chemical makeup of distillery pot ale; n indicates the number of independent batches tested. The absence of data from the data indicates that it was unreported or untested. COD = chemical oxygen demand, BOD = biological oxygen demand, TOC = total organic carbon.

	Graham et al. [1]				Tokuda et al. [3]				Kida et al. [10]			
	Mean	n	Min	Max	Mean	n	Min	Max	Mean	n	Min	Max
Physical												
pH	3.81		3.34	4.13			3.5	3.6	3.47	4	3.4	3.6
Organics (ppm)												
COD	46854	7	38476	62948	33000							
BOD	24908	6	12951	35327								
TOC							15380	17430	16415	4	15380	17460
Acetate	1000	8			600							
Lactate	120	8			6100							
Propionate	85	8			300							
Anions (ppm)												
NO_3^-									2.2	3	1.9	2.5
SO_4^{2-}									259.5	3	223	284.8
PO_4^{3-}							1560	1576	1645	3	1560	1800
Cations (ppm)												
Cu species		8	2	6								
Ca									53.4	3	46.0	57.3
Mg									221.5	3	148.2	276.6
Ammonium							58.8	79.5	61.3	4	44.7	79.5
K									741	3	290.6	971

Table 1.2: Reported average, minimum, and maximum values for the chemical makeup of distillery spent lees; n refers to the number of distinct distilleries whose waste were tested. All data from Yu et al. [6]. Concentrations are reported in ppm if not indicated otherwise.

	Mean	n	Min	Max
Physical				
Conductivity ($\mu S/cm$)	180	2	164	196
pH	4.35	2	4.28	4.41
Organics				
COD	1862	8	1302	2362
BOD	1392	8	900	1808
TOC	605	8	337	1062
Ethanol (v/v)	0.08	8	0.017	0.12
Aceteate	14.4			
Latate	55			
Propionate	1.8			
Formate	0.6			
i-Butyrate	2.9			
n-Butyrate	1.4			
i-Valerate	1.3			
Anions				
Cl^-	6.3			
NO_2^-	0.2			
NO_3^-	0.3			
SO_4^{2-}	15.7			
PO_4^{3-}	21.9			
Cations (all valence states)				
Cu	21.4	8	11.7	41.3
Zn	0.3			
Pb	0.1			
Ni	0			
Fe	0.6			
Ca	0.1			
Mg	0.2			
Na	0			

Thus, the Scottish Environmental Protection Agency [11] does not set an industry-wide limit on the any pollutant concentration; instead, it sets limits on a case-by-case basis when the discharger applies for a license [12]. For instance, the Glengoyne Distillery in Dumgoyne is able to discharge their spent lees by simply releasing it into a bed of reeds, which, after uptake and adsorption by the plants, allows the nearby water to fall below the EQS [13]. In contrast, the Glenallachie Distillery in Aberlour must treat their lees for biological oxygen demand (BOD), suspended solids, and copper prior to discharge [14].

These decisions take into account the geographic location of a distillery as well as its size. Distilleries in locations where they are able to discharge into large, well-mixed, low residence time waterways are able to discharge slightly higher concentrations of pollutants than distilleries of comparable size in locations near small, poorly mixed, high residence time waterways, as these hydrological features would allow pollutant build-up. The variety of distillery capacities - ranging from small, 50 thousand liters of pure alcohol (LPA) distilleries to large, over 100 million LPA distilleries [15] - also drives the variation in individual discharge limits, as much larger distilleries will, by definition, generate much more wastewater, which may not be diluted as much upon discharge. On average, malt whisky distilleries have capacities of around 3 million LPA.

The EQS values set by SEPA were based on the regulations by the EU, and are motivated by the desire to limit the environmental impact of discharge. Based on Tables 1.1-1.3, for distilleries this often means treatment for pH, heavy metals, and organics. The acidic pH has the potential to kill or impair local wildlife, particularly the microscopic organisms. Many heavy metal species also become more soluble at acidic pH, potentially leading to heavy metal toxicity, particularly via bioaccumulation in higher trophic levels [16]. High organic content, particularly in the presence of high nitrate and phosphate as is the case for some distilleries,

Table 1.3: List of environmental quality standards set by the SEPA. All regulations reported are set by supporting guidance document WAT-SG-53 [11].

Species	Environmental Quality Standard Range	Notes
Physical		
pH	4.03-5.1	Assuming humic waters (> 10 ppm DOC)
Organics (ppm)		
BOD		Dependent on body of water to which it is discharged

Species	Environmental Quality Standard Annual Average (ppm)	Maximum (ppm)	Notes
Anions			
Cl^-	250000		
SO_4^{2-}	400000		
Cations			
Cu	1		Bioavailable concentration
Zn	11.9		Bioavailable concentration
Pb	1.2	14	
Fe	1000	1000	
Na	unlimited		
NH^3	1.5-6.0		Dependent on location

can result in eutrophication, killing many aquatic organisms by oxygen depletion. Larger organic particles may also increase the turbidity, limiting photosynthesis at the base of the food chain [5].

In the case of pot ale, treatment with intent for discharge is not the most common route: the high concentrations of organic matter actually allow for condensation into a syrup that can be mixed into feedstock for cattle and pigs [17]. Spent lees, on the other hand, may need to be treated for organic content, acidity, and copper based on batch and location. Of these pollutants, copper is the most readily recovered into a useful product, turning the cost burden of waste treatment into a potential point of profit similar to the reuse of pot ale as feedstock.

For this study, distillery spent lees were selected as a model waste system for electrochemical copper recovery via electroplating based on the high ratio of copper to other constituents. This concentration, however, is still roughly 6 orders of magnitude lower than that of a typical electroplating bath. As a result, the system is expected to behave similar to a pure copper plating bath and should not require any pretreatment to eliminate potential interferents. However, the very dilute nature means that hydrogen evolution and oxygen reduction reactions are likely to limit copper recovery by limiting the electrochemical window or competing with copper at the cathode. This allows for a more in depth study of the reactor design and operation of a flow-through reactor for optimal copper recovery at extremely low copper concentrations while simultaneously maintaining relevance to a specific industrial problem.

Estimates based on the contents found by Yu et al. and the calculation of the EQS assume a discharge limit of around 1.8 ppm, much higher than the 0.33 ppm allowed for the Glenallchie Distillery [14], but lower than the untreated discharge for the Glengoyne Distillery. For the purposes of these experiments, the target is to reduce the copper concentrations below 2 ppm, based on the Scottish drinking water standard [18]. While this regulation is not relevant to Scottish distillery industry directly, it gives a discrete estimated target value that can be applied to other copper treatment purposes, and falls close to the lowest values of allowed discharge found.

1.2 Copper Economics

One of the largest concerns when deciding between simply treating copper and recovering the copper is economic. For instance, in a highly complex waste stream with many metals, nonspecific treatment processes that can remove the majority of those metals in a single step are likely to be cheaper and more efficient, particularly if there would be a large energy cost to a recovery and separation process. However, the value of the metallic copper produced should be taken into consideration to offset operation costs. Thus, designs should attempt to minimize energy consumption while maximizing the recovery efficiency. Market forces, though, will influence the desirability and value of copper, and thus influence whether a recovery process is economically viable. In all scenarios modeled by Elshkaki et al. [19], whether based solely on market forces, policies, personal interest, or social equity, copper mining is expected to deplete the current reserves around the middle of the present century as a result of increased use and manufacture of emerging electronic devices. In fact, if present consumption rates are maintained and the only copper input is from mining, easily accessible copper reserves will be fully consumed around 2040 [20], after which mining becomes significantly more expensive.

Offsetting this can be done through increased copper recycling processes, be that from stripping copper off of unused copper-containing solids or from recovering copper from waste streams as studied in this project. An additional benefit to recovery would be its low energy cost relative to primary mining. Estimates of the energy use of copper mining at mid-century place it around 2.4 % of the global energy production [19], but recycling only consumes 12 to 16 % of the energy used in primary mining [21, 22]. That reduction is expected to become larger as time goes on, as depleted mines will produce lower grade ores, leading to increased costs of separation [19, 23].

This high cost is the result of the low energy efficiency of pyrometallurgical purification, with average estimates of 10.9 GJ/tonne being almost 7 times higher than the theoretical expectation of 1.6 GJ/tonne [20]. This is in contrast to the energy costs of electrochemical recovery processes, which reported an energy cost of 21 kWh/kg (1.2 GJ/tonne) using a 3D electrode-based reactor called the

Porocell to recover copper from a dilute bath ($<$ 100 ppm Cu) despite working at around an unoptimized 13 % current efficiency [24]. This suggests that should copper become scarcer as a resource in the future, recovery processes may be more economically viable and favorable due to their lower cost.

In addition to the economics of energy and copper scarcity, the current social perspectives on environmental sustainability, while often not directly ascribed a monetary value, may also drive decision-making. Improved public image, tax incentives, and liability reduction are some of the practical reasons for recovering copper from waste [25]. The 12 principles of green chemistry proposed by Anastas and Warner [26], attempt to guide the design of processes while reducing their environmental impact. Broadly, these principles suggest the minimization of inputs, both materials and energy, particularly those from nonrenewable feedstocks or those that are toxic to the environmental or human health. Taking these principles into consideration, one can attempt to limit the negative environmental impacts of a process while enhancing or maintaining performance.

Simple changes, such as reducing the use of toxic organic solvents, are commonly suggested to make a process more sustainable, but these changes can detrimentally impact downstream processes. Therefore, one should evaluate and redevelop the overall design to determine the best approach for making the entire process more sustainable. Generally, reduction, reuse, recycling, and recovery of energy and hazardous inputs will lead to the greatest reduction in environmental impact compared to the simple treatment and secure disposal of waste [25]. In the case of copper recovery from spent lees, recovering copper may reduce the environmental impact of copper discharge, indirectly reducing energy costs of the entire supply chain by reducing the quantity of primary copper mining. Importantly, an electrochemical process as proposed would not require any pretreatment or inputs. Only electrons are added in this process, and this input is consumed by copper reduction. As a result, no secondary pollutant, such as solid sludge or increased salinity, would be generated while simultaneously producing a useful product.

1.3 Research Overview

The objective of this work is to understand the parameters affecting copper recovery from distillery spent lees using the Porocell Test System (C-Tech Innovation, henceforth simply Porocell) as an electrochemical reactor. By applying a constant cathodic current, copper from the spent lee waste will be plated onto the porous carbon cathode of the Porocell. Doing so will achieve two aims: (1) assess the feasibility of recovering metallic copper from very dilute mixed aqueous waste and (2) determine the ideal operational conditions for the Porocell for this process.

While the additional waste constituents in spent lees are present at very low concentrations relative to copper, due to their total quantity, one must be aware of the impact that they may have on the ability to remove copper selectively from the waste. In particular, the other metal ions may compete with the copper plating reaction, resulting in lower current efficiency, while the nucleophiles can complex with either aqueous or metallic copper, making plating less favorable [27]. While these effects are not dictating the overall process design, an understanding of the interaction between copper and the other constituents will provide an upper bound for later optimizations, as well as indicate whether it is even feasible to recover copper from this type of waste. The key variables to test are copper transport characteristics (e.g. diffusion coefficient), kinetic characteristics (e.g. exchange current), and selectivity (e.g. current efficiency), all of which would be affected by complex formation.

Finally, the Porocell will be optimized by varying the flow rate and current density. These two operational parameters are easily varied, and a literature review [28, 29] suggests a potentially large impact, as the electric field and mass transport control the evenness of copper plating. The current efficiency and electrical energy cost at a variety of operation conditions should be tested and correlated against microscopy images to assess plating distribution as a potential cause. Ultimately, this should lead to a better understanding of how best to optimize a flow-through porous electrode for metal recovery from dilute waste streams in general, with direct application to the whiskey industry.

Chapter 2

Fundamental Theory

2.1 Metal Electroplating

Metal electroplating is the process of taking an aqueous metallic ion and depositing it onto one of the electrodes as one of the oxidation/reduction half-reactions. In the case of copper electroplating as used in these experiments, the process follows the cathodic half reaction set in Eq. 2.1; the anodic reaction is most often oxygen evolution.

$$Cu^{2+}(aq) + 2e^{-} \rightarrow Cu(s) \tag{2.1}$$

For each half reaction, there is a reduction potential where the system will be at equilibrium, defined by the Nernst equation (Eq 2.2).

$$E = E^{0} - \frac{RT}{zF} \ln\left(\frac{\alpha_{red}}{\alpha_{ox}}\right) \tag{2.2}$$

where E is the equilibrium reduction potential, E^0 is the standard reduction potential, defined as the equilibrium potential at standard conditions, R is the gas constant, T is the absolute temperature, z is the number of electrons transferred per reaction, F is the Faraday constant, α_{red} is the activity of the reduced species,

α_{ox} is the activity of the oxidized species [30, 31]. While the activity of the species often deviates from the concentration as ionic strength increases, the very dilute nature of spent lees allows for approximating the activity of cupric ions to be equal to its concentration. Since the reaction of concern is metal plating, z is the same as the valence of the metal cation and will be used to represent both parameters for simplicity of the report.

Thermodynamically, when the electrode potential is more negative than the reduction potential, the reduction reaction will proceed; when the potential is more positive, the reaction proceeds in the oxidation direction. However, in practice, the potential needs to be driven further than expected to overcome the activation, Ohmic, and concentration overpotentials. These additional barriers are related to the activation energy, electrolyte resistivity, and mass transport, respectively, resulting in a larger than expected amount of electrical energy necessary to drive the reaction [30].

These potentials are limited by the solvent, as at sufficiently high and low potentials, the solvent will be oxidized and reduced, respectively. These bounds, called the electrochemical window, limit the range of potentials that can be used in an electrochemical process without solvent breakdown [30]. Not only will solvent breakdown cause problems involved in the stability of the solution, but these redox reactions will compete for electrons, lowering process efficiency. For instance, in the aqueous copper system used in these experiments, the electrochemical window is dictated by oxygen and hydrogen evolution at the anode and cathode, respectively. Cathodic hydrogen evolution will compete with copper reduction, particularly as the Nernst potential decreases at low concentrations. Anodic oxygen evolution will act as the counter reaction to generate the electrons used in copper reduction, limiting the minimum cell potential between the anode and the cathode. Any oxygen generated by this reaction will also preferentially reduce at the cathode if accessible [31].

Driving any electrochemical reaction forward can be done by setting either the electrode potential (potentiostatic) or the current (galvanostatic). While potentiostatic design allows for finer control of the supplied energy to prevent side reactions, it is more difficult and expensive to achieve due to the requirement of a stable reference electrode and the design of a constant electric field across the electrode surface [30]. Instead, industrial applications of electroplating use galvanostatic control, which controls the rate of the reaction according to Faraday's law:

$$it = zFV\Delta\left[M^{z+}\right] \tag{2.3}$$

where i is the current, t is the time, V is the solution volume, and $[M^{z+}]$ is the bulk metal ion concentration, assuming metal reduction is the only reaction at the electrode [31]. The primary issue with this assumption is that it does not account for parasitic side reactions that are possible when the potential is not controlled, and thus Faraday's law only provides the upper limit of metal removal. This is used to calculate the Coulombic efficiency of an electroplating reaction, ϵ, as the ratio between the observed and expected changes, assuming only the desired reaction occurs at the electrode [32].

$$\epsilon = \frac{\Delta\left[M^{z+}\right]_{observed}}{\Delta\left[M^{z+}\right]_{expected}} = \frac{\Delta\left[M^{z+}\right]_{observed}}{\left(\frac{it}{zFV}\right)} \tag{2.4}$$

In copper electroplating, this number varies depending on the conditions of the plating bath and applied current, with typical industrial plating baths designed to operate at 95 to 99 % efficiency [31] but values as low as 3 % have been reported when attempting to recover copper from very dilute solutions [24]. The high efficiencies for plating baths is partially due to the contribution of the bath composition, where additives may help the copper reaction proceed or prevent side reactions, and the highly acidic solution acts as a supporting electrolyte [33, 34, 31, 35].

In contrast, poor efficiencies when plating from dilute solutions can often be attributed to the low limiting current i_{lim}, when the reaction is limited by mass transport supplied to the electrode surface and therefore cannot proceed any faster. The limiting current for consumption of a metallic species M is shown in Eq. 2.5, where A is the electrode area and k_m is the mass transport coefficient. For the case of the 1-dimensional flat plate, k_m is equal to the diffusion coefficient (D) divided by the diffusion layer thickness (δ).

$$i_{lim} = zFk_mA\left[M^{z+}\right] \tag{2.5}$$

Application of currents beyond the limiting current will result in the excess current being consumed by side reactions such as hydrogen evolution, thereby reducing the Coulombic efficiency [32]. Since this parameter is proportional to concentration, for a metal recovery system where the goal is to decrease the concentration, the current efficiency is expected to drop over time. If adjustments are not made to accommodate for the drop in concentration over time, low current efficiencies are likely. This problem has been partially addressed by setting the current to decrease at known intervals related to the decrease in limiting current [36, 37].

Measurable net efficiency can also be influenced by copper oxidation reactions. This is particularly important to consider given the solubility of copper in acidic solutions [38], including distillery waste, as well as the use of hydrolysis as the anodic half-reaction. Anodic hydrolysis produces oxygen gas, which is known to be parasitic in consuming electrons at the cathode and may corrode the copper, ultimately resulting in lower recovery efficiencies.

2.2 Analytical Electrochemical Techniques

Two primary analytical techniques will be used to obtain values relevant to the conditions for copper electroplating: cyclic voltammetry and polarization. Generally, cyclic voltammetry is a dynamic technique whereby the electrode potential is changed with time, whereas polarization seeks to obtain data regarding the steady state. As a result, they give different information about the system by decoupling the mass-transport controlled and kinetically controlled components of an electrochemical reaction.

2.2.1 Cyclic Voltammetry

Cyclic voltammetry is a dynamic electrochemical technique where a triangle wave voltage input is applied to obtain the resultant current. With this technique, one can obtain diffusion-related information, as the mass transport will be the slowest to respond, limiting the observed current. In the absence of a Faradaic reaction, the current will behave as a pure capacitor between the electrodes due to the formation of an electric double layer. When a Faradaic reaction is possible with the compounds in solution, the current will increase, but only after passing the reduction potential. Continuing the voltage change beyond the reduction potential will increase the reaction rate, and thus the current, until the point where transport becomes limiting, at which point the current will drop back to its steady-state condition. This results in a peak current that can be related to the diffusion coefficient of the reacting species according to the Randles-Sevcik equation:

$$i_p = 2.69 * 10^5 z^{3/2} A_{cm} D^{1/2} \left[M^{z+}\right] \nu^{1/2} \tag{2.6}$$

where i_p is the current at the peak (Amps), A_{cm} is the electrode area in square centimeters, D is the diffusion coefficient (cm^2/s), and ν is the scan rate (V/s). When the voltage sweep reverses with the other side of the triangle wave, the reverse reaction will occur, giving another peak. The mean of the potentials of these two peaks will equal the standard reduction potential of the redox reaction for this particular system [30].

2.2.2 Polarization

Polarization experiments hold the potential of the system constant until the current reaches steady state, continuing this process over a wide range of potentials. The steady-state current density will be related to the amount of excess energy is available to drive the reaction, as defined by the Butler-Volmer equation:

$$j = j_0 \left(e^{-\alpha \frac{zF}{RT}\eta} - e^{-(1-\alpha)\frac{zF}{RT}\eta} \right) \tag{2.7}$$

where j_0 is the exchange current density, α is the cathodic charge transfer coefficient, and η is the applied overpotential [31]. Polarization experiments, as steady state experiments, are also able to obtain information related to the limiting current [30]. This is simply the largest current magnitude that is possible despite increases in the voltage, and thus can be estimated as the current measured when a sufficiently large overpotential is applied.

2.3 Reaction Kinetics

As the goal of these experiments is to optimize the process for electrochemical copper recovery at a relatively large scale, knowledge of the reaction rate will be necessary to set process times and conditions. A generic form for the rate of change of copper ions per Eq. 2.1 is presented in Eq. 2.8, which is then simplified to be a function of only copper with rate order x.

Since the concentration of electrons bears little physical meaning, the system can be simplified to be either first or zeroth order kinetics with respect to copper, depending on which reactant supply (*i.e.* electrons or copper) is limiting. These simplify to give the following copper concentration profiles for zeroth (Eq. 2.9) and first (Eq. 2.10) order:

$$\frac{d\,[Cu^{2+}]}{dt} = -k[Cu^{2+}][e^{-}]^2 = -k_x[Cu^{2+}]^x \tag{2.8}$$

$$[Cu^{2+}] = [Cu^{2+}]_{t=0} - k_0 t \tag{2.9}$$

$$[Cu^{2+}] = [Cu^{2+}]_{t=0} e^{-k_1 t} \tag{2.10}$$

In the zeroth order case, also called the current-limited case, the amount of copper is high relative to the supply of electrons, resulting in the rate, k_0 , being determined by the supply of electrons, not copper, to the electrode surface. Combining this equation with Faraday's Law (Eq. 2.3) and the definition of Coulombic efficiency (Eq. 2.4), one can define the rate constant, k_0, using the applied current, i, and the current efficiency, ϵ, according to Eq. 2.11 [31].

$$k_0 = \frac{\epsilon i}{zFV} \tag{2.11}$$

In the first order case, also ocalled the mass-transport limited case, the supply of electrons is sufficient that the copper concentration is important to the rate, leading to an exponential decay with rate constant k_1. Therefore, the absolute amount of current applied is not as consequential as the limiting current (Eq. 2.5). Combining these equations yields Eq. 2.12 [31].

$$k_1 = \frac{-k_m A}{V} \tag{2.12}$$

While a first order kinetic system would be ideal as it implies operation at the fastest possible rate, the fact that the copper supply is limiting suggests that this would only occur near or above the limiting current. Thus, while determination of the order of the reaction is important for determination of process duration, it can also be useful in optimizing the Coulombic efficiency to minimize energy consumption.

Chapter 3

Literature Review

3.1 Copper Treatment Technologies

As a consequence of environmental and public health motivated policies, metals such as copper must be below a certain concentration prior to discharge. For the purposes of this report, copper removal from aqueous waste will be broken down into two categories: treatment or recovery. Treatment processes remove copper, but do so in a way that the by-product would require additional steps to produce useful copper, either due to its speciation or the presence of impurities. The goal to a treatment process is simply the rapid and efficient removal of copper, without consideration for its utility afterwards. Recovery processes remove copper in a highly selective manner, resulting in high purity metallic copper at the end. The tradeoff for this highly selective process comes at the cost of time, energy, or removal efficiency, sometimes requiring further treatment before being allowed to be discharged.

Treatment processes are relatively fast and easy, often being nonspecific to treat many heavy metals in a single step to make the overall treatment process cheaper and faster. However, they often do not adhere to the principles of green chemistry, requiring additional inputs, often resulting in a possible secondary pollutant such as sludge as a result of the treatment process. Common processes include precipitation, adsorption, bioremediation, and electrocoagulation.

Precipitation is the simplest method, requiring the addition of anions such as sulphide, oxide, and oxalate that will precipitate out copper minerals. The resulting solid can then be settled and filtered out of the wash to remove the heavy metals. In order to remove enough copper, though, an excess of these anions must be added to accommodate the solubility products, potentially polluting the wastewater further with common monovalent cations like potassium and sodium, though these discharge limits are much higher. The non-specificity of this process makes it a simple method for metal removal [30, 39], though this is a detriment if only copper is desired. The minerals produced are often acid soluble, thus requiring pH adjustment prior to processing if not using hydroxide as the precipitating anion [38, 30].

Adsorption removes the copper onto a solid substrate via physical attraction to another surface. The selection of appropriate sorbents is an active area of research, with some options including sand [5] and humics [40]. One study specific to distillery waste also investigated the use of spent grain, the solid by-product of fermentation [41]. Like precipitation, this process is highly pH dependent and nonspecific for metal species [5, 41], but it has been shown to be effective at removal down to the ppm level [30].

Bioremediation methods are a broad class of mechanisms that require the addition of specific organisms to remove the copper. This process is most often used for the removal of organics via respiration, but some species such as the bacteria *S. putrefaciens* [42], the Lemnaceae plant subfamily [5], and the plant *C. alternifolius* [43] are known to remove heavy metals. The Glengoyne Distillery reported disposal of their spent lees by simply pouring over a nearby reedbed, which served to sufficiently remove its pollutants [13]. The organisms typically remove metals by precipitation, adsorption, or bioaccumulation, but utilize a biological component to make the process faster or more favorable without external inputs. As a result of biological metabolism and reproduction, many systems are self-sustaining, particularly if the species is native to the local ecosystem and can be repopulated around the point of discharge [43].

Conversely, electrocoagulation requires significant external inputs. This process utilizes sacrificial iron or aluminium anodes to generate iron or aluminium hydroxides. The resulting hydroxides will coprecipitate with other metals in the wastewater [30, 32]. At times, the gas formation at the cathode will assist by providing nucleation sites or buoying particles to the surface for easy separation without filtration [32]. The cathodic reaction has also been shown to be useful in the breakdown of organic chelates such as EDTA that inhibit copper precipitation [44], which makes it more attractive than simply adding iron or aluminium salts. There have been studies of electrocoagulation with spent lees specifically [45], which found the process to be highly pH dependent with best results around neutral pH and energetically costly due to the low conductivity.

3.2 Copper Recovery Processes

Recovery processes are much less common in industry as they tend to require higher energy inputs or tighter controls to produce metal of high enough purity that an additional separation process is not needed. While metal separation through a recovery process is useful and potentially profitable, in a highly complex system with many different metals, it is often much faster and cheaper to treat the waste with a single nonspecific step such as precipitation.

However, being able to produce the metal in its metallic form may offset the cost of operation, as the metallic form is generally the most valuable [30]. Due to the difference in valence state between dissolved metal ions and the metallic state, many copper recovery processes are electrochemical, involving copper ions plating to metallic copper at the cathode. In this setup, two electrodes are inserted into the waste solution and electricity is applied. By tuning the potential of the cathode, either directly by referencing it to a stable electrode or indirectly by carefully choosing the current density, the process can be made selective for the most thermodynamically preferable reduction reaction, i.e. the highest reduction potential [30].

This process serves the benefit of only requiring electrodes and electricity, so no secondary pollutant such as sludge is necessarily created. At most, the salinity of the solution may need to be increased to reduce Ohmic overpotentials, although this can also be counteracted by placing the anode and cathode closer together. The anode reaction may also be able to treat other oxidizable molecules such as cyano- compounds, potentially countering any efficiency losses observed due to the presence of organic chelates by breaking down those inhibitors [45]. If there is no feasible anodic reaction that is necessary in treatment, capture of the oxygen evolving from hydrolysis is a potential cost-saving alternative [30].

In general, copper electroplating is a mature technology, used often in the electronics industry [46, 47]. These applications use excess copper to assume whatever is consumed in plating is negligible to the concentration of the bath, with the simplest being simply 2 M H_2SO_4 and 0.1 to 1 M $CuSO_4$ [31]. Past fundamental studies have been conducted to find important data for copper electroplating, such as its diffusion coefficient ($5.83 \pm 0.08 * 10^{-6}$ cm^2/s) [48] and its exchange current (11 ± 4 A/m^2) [49], generally finding that the range of potentials for kinetic control is very small, rapidly reaching a point of transport control. Various process variations, such as changing the temperature or using pulsed instead of constant current, can result in grain size refinement or altered surface morphologies [50].

However, these studies have all been conducted with the same assumption of insignificant changes to the copper concentration, an assumption counter to the goal of a waste recovery system. The differences between typical industrial applications and waste recovery lead to numerous problems that are the focus of much work for this application, most notably: low limiting currents, poor throwing power, and variability in electrolyte contents.

The low limiting currents are a direct result of the low concentration, as limiting current is proportional to concentration (Eq. 2.5). This has led to a number of design decisions, detailed in Section 3.3, to counter this effect. Each approach can be summarized as an attempt to enhance the mass transport coefficient (k_m) and the electrode surface area, both of which will proportionally increase the limiting current [33, 30]. Only one design was found still to use a large flat cathode, taking advantage only of high flow rates to cause local turbulences [37]. The remainder of results use some form of 3-dimensional electrode, where small pores create both local turbulences and higher surface areas [51, 52, 53, 54].

The increased surface area comes at the cost of more complex electrode geometries, leading to unevenness in the electric field. This results in localized regions of high overpotential, where plating occurs quicker, and regions of anodic potential, where corrosion may occur [53]; the extent to which the plating is uneven is quantified as the throwing power. Only one study has attempted to quantify the extent of plating with a complex porous 3D electrode [29]; in this study, plating on a carbon felt electrode was found to only occur on 12 to 23 % of the electrode s surface area. These localizations became more pronounced the larger the difference between the electrode conductivity and the solution conductivity became [29, 55]. With highly dilute waste, solution conductivity can be quite low at times, resulting in very poor throwing power when using standard highly conductive metallic or graphitic electrodes. Generally, one would find the greatest amount of copper to plate on the side of the cathode closest to the anode, as this outer surface does not have any stagnant areas [56] and shows the most concentrated electric field [28]; ultimately, this localized plating will cause the pores of the 3-dimensional electrode to plug at this surface and require intermittent replacement.

Finally, the greatest uncertainty involved in waste recovery is the batch-to-batch variability of waste. Concentrations tend to fall within a specified range, but when the limiting current is related to the concentration of copper, if the range is wide enough, it affects process duration and efficiencies. Additionally, the other compounds in waste are likely to influence results. Metal ions may compete with copper for electrons at the electrode surface, reducing Faradaic efficiency and the purity of the final plated copper [30]. In the case of some metals like iron, they may oxidize plated copper and resolubilize it [36]. Nucleophiles, particularly polydentate organics, will form complexes with copper [57], usually reducing the reduction potential and making plating less thermodynamically favorable [27]. They may adsorb to the surface of the electrode instead, blocking reaction sites and slowing the process down [30]. All of these unfavorable conditions will act in concert with each other. In many cases, the effects of compounds found in industrial waste on electroplating are poorly studied, if at all, leading to a number of inefficiencies that cannot be reduced without potentially difficult or costly pretreatments. This dearth of information is one of the reasons why the technique has not been widely adopted.

3.3 Reactors for Electrochemical Metal Recovery

A broad survey of reactors for electrochemical metal recovery are detailed below. These designs have been developed for a wide range of solution inputs, ranging from concentrated (> 1000 ppm) to fairly dilute (< 100 ppm). All utilize some means of enhancing the turbulence and electrode area, serving to increase the maximum rate that metal can be recovered, thereby reducing process time. While most metals would behave similar to copper, due to the breadth of literature on the topic, this literature survey is limited to reports specific to copper recovery.

3.3.1 Flow-based transport enhancement

Only one paper was found where the electrode geometry was left simple and unchanged and only the flow rate affected. Walsh et al. [37] used a rotating cylinder cathode and annular anode, taking advantage of the high rotation speeds of the cathode to enhance transport to the cathode. Build-up on the cathode was removed by scraping, releasing particles that could be later collected with a filter. A diagram of this type of reactor design is presented in Figure 3.1.

Multiple reactors of this configuration were connected in series, with successive reactors applying lower current densities to accommodate the decreasing concentration. As a result, current efficiencies were relatively high at 68 to 81 %, reducing an inlet concentration of 100 ppm Cu (1 N H_2SO_4 supporting electrolyte) to about 1.5 ppm. Highest efficiencies were obtained when operated at 60°C rather than at 30°C. This report also tested a larger system that applied a total current of 900 A across all of the reactors in series, which maintained an efficiency at 65 % at similar inlet and outlet concentrations. This report shows that even at

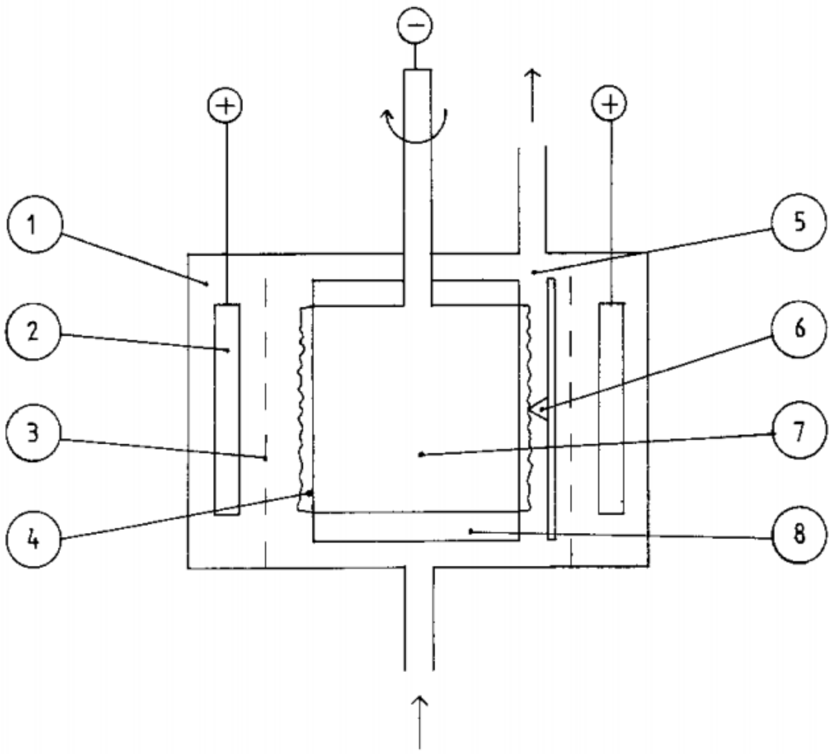

Figure 3.1: A schematic diagram of a rotating drum electrode for electrochemical metal recovery. Diagram key: (1) Anolyte solution, (2) anode, (3) membrane, (4) metal deposit, (5) catholyte, (6) scraping mechanism, (7) rotating cathode, (8) insulating cover. From [37].

dilute concentrations and use of a relatively simple electrode geometry, one can achieve fairly efficient copper recovery.

3.3.2 Particulate electrodes

The most commonly reported method for enhancing the recovery rate is to use some form of conductive particulates as the electrode. These particles increase the electrode surface area, as well as force solution to flow through small pores, causing local turbulence. Examples schematics of these types of designs are presented in Figures 3.2 and 3.3.

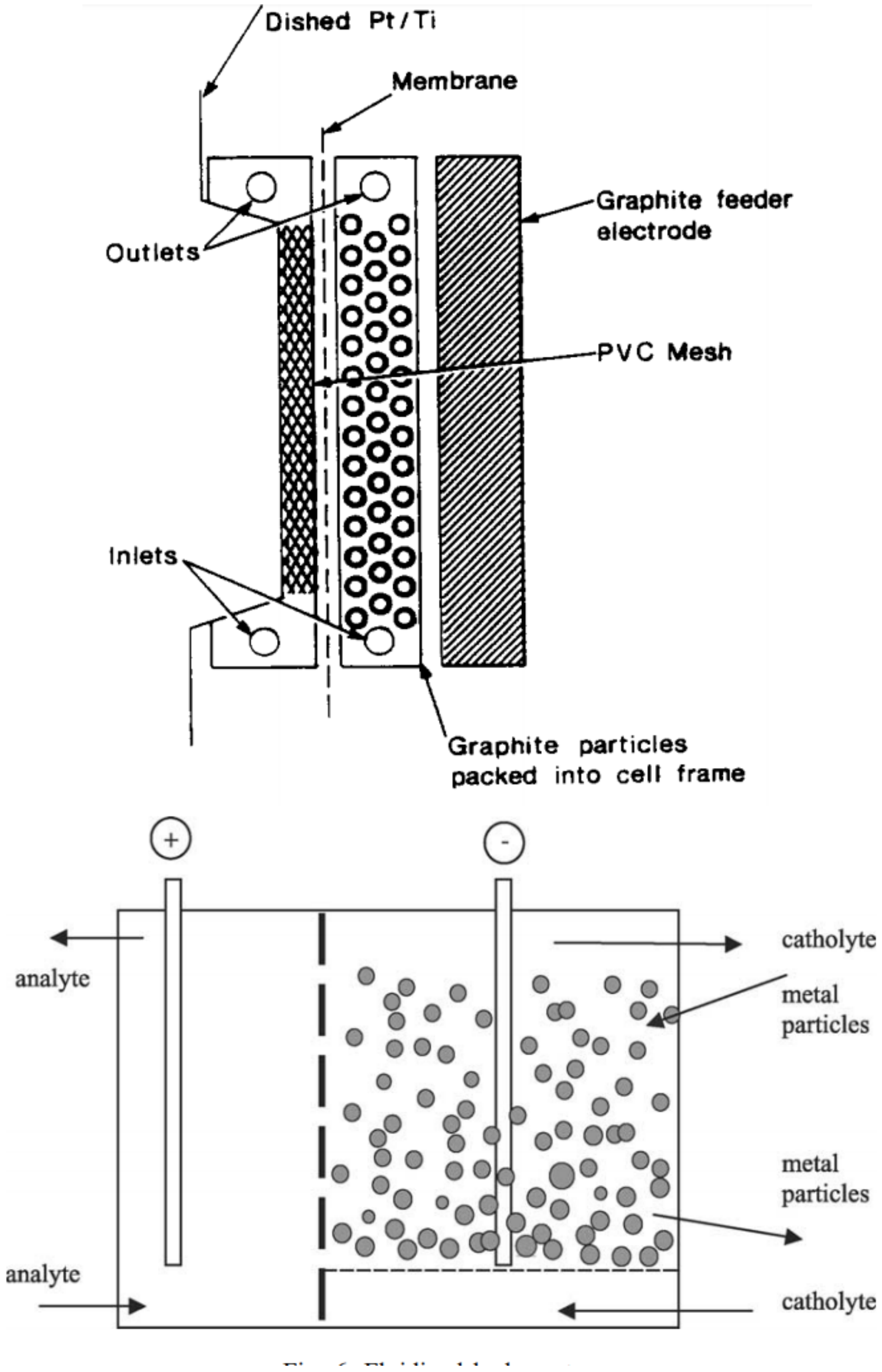
Dished Pt/Ti
Membrane
Outlets
Graphite feeder electrode
PVC Mesh
Inlets
Graphite particles packed into cell frame
+
-
analyte
catholyte
metal particles
metal particles
analyte
catholyte

Figure 3.2: (top) Example schematic diagram of a packed bed electrochemical reactor using graphite particles as the cathode from [33].
(bottom) Example schematic diagram of a fluidized bed electrochemical reactor from [58].

The simplest form of this type of reactor is to use a packed bed. In this setup, the cathode is composed of either graphite or metal particulates and the solution flowed through it [30]. Studies on particle size [33] have showed that different sizes contribute to different current efficiencies at the same current density, implying that the particle size, and likely its shape, determines what fraction of that area is usable in plating. Generally, for a given particle size, there will be a current density at which efficiency reaches its maximum; lower currents result in pockets of anodic potential, and higher currents exceed the limiting current. Efficiency when removing copper from 60 ppm to 1 ppm was found to be at about 30 %. While these packed beds provide adequate surface areas and turbulences, they face the problem of having static particles which may fuse together and clog. These beds also require the addition of a membrane to keep the particles from washing away, and these membranes can be potentially expensive [51].

An alternative to the packed bed would then be to use a fluidized bed, in which the particles are in constant motion. This results in a trade-off between potential clogging and intermittent particle-particle contact [58] which leads to temporarily anodic particles. A well-designed system can optimize the particle sizes and flows to minimize this problem, producing more uniform potential and current distributions compared to static packed beds [30].

A systematic review of fluidized beds [52] showed that current efficiencies seem to increase with current density until a critical threshold value, after which it remains stable. This is likely the result of localized anodic regions near the middle of the bed. This anodic region becomes large and more pronounced at lower concentrations, resulting in copper corrosion [53], but sufficiently high current densities can counteract those anodic regions.

Regimes of corrosion are also found when extending the fluidized state to a fully circulating bed, such as the spouted vessel reactor [54, 59] as seen in Figure 3.3. These reactors observe reduced recovery rates at lower pH values, suggesting some influence of corrosion. When using the spouted vessel specifically for copper plating [54], increasing the temperature to attempt to increase the limiting current does not help the current efficiency as corrosion exhibited greater temperature dependence, resulting in lower current efficiencies at higher temperatures and its best current efficiency (60 %) at ambient temperature.

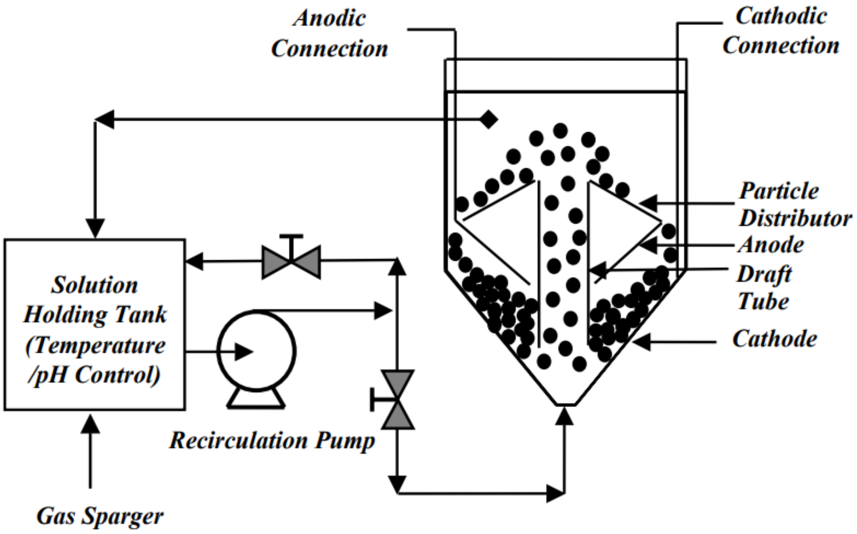
Anodic Connection
Cathodic Connection
Particle Distributor
Anode
Draft Tube
Cathode
Solution Holding Tank (Temperature /pH Control)
Recirculation Pump
Gas Sparger

Figure 3.3: Example diagram of a spouted vessel reactor as used in [54].

A combination of these two designs, the pulsed bed reactor, was developed, where the bed alternates between a static packed state and a dynamic fluidized state [51]. This reactor was only used in electrowinning applications, and thus quite high Cu concentrations (35 to 40 g/L), but showed a wide range of efficiencies, from negative efficiencies from only causing corrosion to plating at about 60 % efficiency, depending on the relative duration of the packed and fluidized states. It is believed that the fluidized state duration led to the majority of the inefficiencies, as this time contributed to the most corrosion.

3.3.3 Porous mesh or matrix electrodes

An alternative to the use of particles would be the use of various conductive meshes or matrices as the electrodes. The most common of these in the literature is carbon felts, as with a 10 micron fiber diameter, the total surface area is about 1000 m^2/g. Use of graphitic carbon generally requires some form of treatment to enhance the wettability. Typical efficiencies appear to be around 20 to 60 %, but reproducibility is low [30].

As mentioned previously, studies have indicated that only a small fraction of the total surface area, estimated at 12 to 23 % [29] is used in plating even when pre-treated for wettability. In this study using graphite felt as the cathode in a hybrid flow battery, the low surface area utilization was found to be due to unevenness in the current distribution across the electrode. Increasing the solution conductivity closer to that of the electrode material led to the increase in active surface area. This suggests that the distribution of the electric field dictates some of the plating distribution, as matching the conductivity of the carbon felt with the solution would lead to a more uniform field distribution.

Further tests have also shown that there is an effect of flow rate and direction on the distribution as well. Experiments by Medvedev et al. [28], later explained by models [60, 61], indicate that while the fastest plating occurs on the side of the cathode closest to the anode (i.e. where the electric field is strongest), supply direction and flow rate can be balanced against the current density to obtain more even distribution profiles.

The experimental results found here are consistent with those predicted by models by Trainham and Newman [62] and Alkire and Ng [63]. Trainham and Newman's model for flow-through configurations, where the fluid flow is parallel to the current flow, highlighted how the plating distribution is predominantly driven by the electric field distribution within the electrode-solution matrix, and the focusing effect on the side of the electrode nearest the anode will result in higher reaction rates at that side. On the opposite side, the reaction will often be that of a side reaction like hydrogen evolution, decreasing the overall current efficiency.

Trainham and Newman's model focused on modeling flow-by configurations, where fluid flow is orthogonal to current. They found that less plating would occur on the side of the electrode opposite the supply of fresh solution due to the reduced concentration because of consumption of the metal ions nearer the inlet. While Medvedev et al.'s results [28] used a flow-through configuration, Trainham's explanation for their observed phenomenon also explains how directing the flow from the cathode to the anode with sufficiently slow flow rates and high current densities can drive the opposite plating distribution of what one would expect from the field alone. Together, these two models and the experimental results show that both flow direction and electric field distribution influence the resulting plating distribution, and the relative effects are determined by both system configuration and also the magnitude of the flow rate and electric field.

Other models have been developed for carbon felt due to their widescale use in electrosynthesis and energy applications [56], including models of flow rate effects on reaction rates [64] and models for the hydrodynamics within the electrode [56]. However, these models provide little information relevant to the scope of this project for metal recovery from dilute solutions.

While carbon felt is the mostly widely used in the literature due to its low cost and ease of manipulation into arbitrary electrode geometries [65], other 3 dimensional electrodes exist, notably metal meshes (e.g. platinum mesh) and foam electrodes (e.g. reticulated vitreous carbon). Metal meshes are simply networks of metal to form a porous net-like structure, increasing surface area and porosity [66]. Therefore, these metal meshes do not sacrifice any benefits of using inert metals for the improved geometry, but are often more expensive than using carbon electrodes due to the more expensive material.

In contrast, as a foam of glassy carbon, reticulated vitreous carbon (RVC) is relatively cheap. These electrodes have been used to remove metal contaminants, including copper, at very low (< 100 ppm) concentrations [67]. However, RVC is relatively fragile because vitreous carbon is more ceramic-like than graphite. This improved stiffness makes it more suitable to certain environmental conditions compared to graphitic carbon felts, but limits its use in environments where it must be more malleable.

3.3.4 Alternative electrode reactions

The most recent development in copper recovery is the possibility of using other kinds of electrodes to alter the rates, energy consumption, or product. For instance, biocathodes have been employed, making use of natural biochemical pathways of electrogenic bacteria to catalyze the reaction, making it more selective to avoid the reduction of dissolved oxygen and potentially generating nanoparticle catalysts instead of pure copper as an alternative product [6].

Alternatively, the anodic reaction, which is typically oxygen evolution, could be changed to consume organics in the waste. Doing so would provide the additional benefit of limiting current inefficiencies associated with oxygen gas, which reduces more preferentially at the cathode. Approaches have included use of bioanodes [6, 68], which may also generate small amounts of electricity instead of consuming it, or using boron doped diamond, which poisons the hydrolysis reactions sufficiently to allow for the higher potentials needed to oxidize many organic compounds [69]. All of these approaches are still relatively young compared to the simpler schemes described previously, and thus would require significant amounts of optimization before they can be industrially viable.

In addition, one of the largest barriers to adoption of these alternative electrodes is difficulty of manufacture, increasing their cost. Bioelectrodes are often made as-needed, as the biological component of the electrode does not have a long shelf life. Boron doped diamond is made through like low throughput methods chemical vapor deposition [70], requiring tight process controls to produce usable electrodes. This is in contrast to the more standard electrodes mentioned previously, which have been around for decades [65] and are relatively cheap and simple to mass produce.

3.4 Past Work with the Porocell Test System

Like many of these approaches, the Porocell Test System used in this project utilizes a porous carbon felt in a flow-through configuration for a batch recirculation reactor. This design is specifically intended for metal recovery from dilute solutions and commercially available through C-Tech Innovation, and thus readily applied to industrial use. In accordance to its patent [71], it can operate at flow rates from 2 to 80 L/min, optimally at 15 to 30 L/min, with currents of 300 to 800 A/m^2 (referenced to the geometric electrode area) to recover metals of approximately 50 ppm down to below 1 ppm. The reactor us available with a divided cell, which employs an ion exchange membrane between the cathode and anode, or an undivided cells [72]. Official operation procedures for the 0.5 m cell, the size used in these experiments, anticipate approximately 20 to 60 A for most solutions, assuming no upper limit to the voltage [73], although it is unclear whether this is the total current for multiple cells in series or the current for a single cell.

Initial official work from E.A. Technology with the Porocell has demonstrated some success in metal recovery applications (helping grant it the patent in 1997 [71]) as have more recent work from independent researchers. Interestingly, despite the recommended flow rate and current density ranges from the patent [71] and operation procedures [73], all tests reported in the literature fall within the lower half of the recommended current density range (up to 400 A/m^2), and no test used flow rates exceeding 4 L/min, roughly one third of the recommended flow rate. A summary of all literature discussed related to the Porocell can be found in Table 3.1.

Bancroft and Dalrymple [72] summarized many of the developments and applications in their overview. Typical values for copper recovery from moderately acidic copper sulphate solutions, for instance, come to approximately 14 to 28 kWh/kg Cu, assuming cell voltages of 5 to 10 V and a change from 100 ppm to 1 ppm. Case studies have been conducted with waste from printed circuit board manufacturing, whiskey spent lees, cadmium plating waste, and photographic fixers.

The circuit board etch solution used in this case study contained an upper limit of 290 ppm Cu in a solution of pH 1.4 to 1.9 [72]. Application of 300A/m^2, starting at 40 V due to the high resistivity of the solution but dropping to 10 V over the course of an hour due to the generation of ions from the hydrolysis reaction, managed to remove copper down to concentrations as low as 0.15 ppm. Continuous operation of 6 cells was able to process the etch solution generated by the manufacturer at a sufficient rate relative to its production, yielding approximately 22 kg Cu per week.

Operation conditions for these other three applications - whiskey spent lees, cadmium plating waste, and photographic fixers - were not reported in the case

Table 3.1: Summary of literature related to the Porocell.
*Source is a summary of other work and does not include all experimental details.
**Only source using low current (< 100 A/m^2, often < 10 A/m^2).

Source	Solution	Contaminant	Starting concentration	Final concentration	Duration	Net Coulombic efficiency
[72] *	Whiskey spent lees	Copper	13 ppm	< 1 ppm	1 hour	
	Printed circuit board waste	Copper	290 ppm	0.15 ppm		
	Cadmium plating waste	Cadmium		< 20 ppm		
	Photographic fixer solution	Silver	3600 ppm	1 ppm		
[74]	Acidic cadmium waste	Cadmium	1.1 g/L	24 ppm	8 hours	
			650 ppm	< 1 ppm	6.5 hours	1 to 5 %
[74]	Alkaline cadmium waste	Cadmium	300 to 500 ppm	11 ppm	5.5 hours	1 to 3 %
		Cyanide	470 ppm	< 15 ppm		
		(simultaneous)				
[24]	HCl process waste	Copper	50 ppm	< 10 ppm	0.5 to 3 hours	3 to 13 %
	Acidic nitrate solution	Copper	0.3 to 1.5 g/L	< 1 ppm	1 to 3 hours	11 to 33 %
[75]**	Simulated ^{99}Tc waste	Permanganate	300 ppm Mn	< 1 ppm Mn	< 5 hours	> 100 %
[76]	Galvanix sludge leachate	Copper	7 g/L	< 70 ppm	7 hours (3 A)	29 %
					2.5 hours (18 A)	90 %

study, but generally reported successful results [72]. Whisky spent lees from Whyte & Mackay were treated using the Porocell, treating copper from about 13 ppm to under 1 ppm in about 1 hour of operation. Estimates of the total removal were 1 kg Cu/day, although how that estimate was made was not reported in the study. Cadmium waste, generated from plating of corrosion resistant cadmium coatings, was treated to maintain Cd concentrations below 20 ppm, with the added benefit of also removing some of the cyanide additives via the anodic reaction. This resulted in possible reuse of this solution for rinsing, reducing water consumption while generating 1 kg Cd for every 32 kWh electricity. Photographic fixer solutions were treated for their silver content, starting at 3600 ppm and decreasing it to 1 ppm in a single batch reactor at the cost of 2.7 kWh/kg.

More detailed and controlled studies were conducted for cadmium [74] and copper [24, 77] recovery from a variety of solution compositions. Cadmium removal studies [74] used rinse wastes from both alkaline and acidic cadmium plating processes, investigating how differences in the composition could cause differences in the results. Results with acidic rinse wastes showed that there is an equilibrium concentration at which the rate of cadmium corrosion equals the rate of cadmium plating, thus requiring pretreatment to make the pH more neutral to obtain concentrations below 30 ppm. This pH pretreatment provided the additional benefit of increasing the salt concentration of the solution, and thus making it more conductive, reducing the necessary potential. Interestingly, operation at 400 A/m^2 stabilized at a concentration double that when operating at 200 A/m^2. This is potentially due to differences in the starting pH and concentration leading to differences in the concentration at which the rate of corrosion equalled the rate of plating, but this hypothesis cannot be confirmed as the starting conditions were not reported for the 400 A/m^2 test. Current efficiencies are generally quite low, particularly as the concentration drops, giving a maximum efficiency of around 45 % in pH treated liquors during the first 15 minutes, but dropping to net efficiencies around 5 %.

Alkaline cadmium plating liquors were contaminated with other metals - iron, zinc, copper, and nickel - at trace concentrations as well as cyanide. Treatment with the Porocell was found to simultaneously treat cadmium via reduction to concentrations below 20 ppm and cyanide via oxidation down to concentrations as low as 15 ppm, although the cyanide removal rate is generally slower than that of cadmium. Operation at higher current densities led to removal of other metals, although the majority of the removal appeared to be that of cadmium, primarily because its concentration was 10 to 40 times higher than the other metals. Removal from alkaline liquors was generally much less efficient compared to from acidic liquors, with no current efficiencies exceeding 10 %, even at the start when cadmium concentrations are highest [74].

Two different copper removal studies were conducted, one with hydrochloric acid process liquors [24] and one with a proprietary acidic nitrate solution [77]. Both contained additional iron, with the proprietary solution also containing chromium and nickel. Recovery from hydrochloric acid liquors showed relatively low current efficiencies, particularly at low current densities: operation at 200A/m^2 ran at 3 % current efficiency, while 300 A/m^2 and 400 A/m^2 ran at about 13 % current efficiency. This is likely due to corrosion from the strongly acidic conditions reversing the electroplating reaction, supported by the finding that copper concentrations would increase if processed solutions were stored in the Porocell without current. Strangely, use of sulphuric acid as the supporting electrolyte instead of sodium sulphate reduced process costs from 24 kWh/kg Cu to 21 kWh/kg Cu, likely due to a higher conductivity leading to a reduction in the necessary cell potential.

Recovery from nitrate solution [77] found much better efficiencies of around 45 %, but this is due to starting concentrations of 310 ppm or higher, compared to 50 ppm in the hydrochloric acid solutions. When at similar concentrations, the current efficiency was similar if not lower, possibly due to pH values of 1.2 to 1.4 contributing to corrosion. In both of these solution compositions, the additional metals did not appear to have any effect nor did they change significantly from start to end of each trial.

Beyond internal studies conducted by EA Technologies, two independent groups have explicitly reported use of the Porocell. Griffiths, et al. [75] conducted a technical report of the use of the Porocell as a means of removing permanganate as manganese oxide, studied as a cheaper and safer analogue to treating pertechnate, a pollutant of concern due to ^{99}Tc found in radioactive waste.

Their conditions simulated an alternative treatment as part of the typical pump and treat method for environmental hazards, supported by their previous work finding that cathodic potentials can prevent radioactive leachate. Permanganate concentrations dropped from 300 ppm Mn to < 1 ppm without redissolution of the solid oxide in the alkaline electrolyte. This study worked at much lower current densities than the EA Technology tests, applying 0.5 to 2 A (20 to 75 A/m^2) when Mn concentrations were high and decreasing it to 0.05 to 0.2 A (2 to 7.5 A/m^2) when concentrations were below 10 ppm. Results showed that application of current rapidly decreased soluble Mn concentrations to undetectable levels, although a notable fraction of the MnO_2 was found suspended in the solution rather than on the electrode surface. At both high and low concentrations, Coulombic efficiencies exceeded 100 %, potentially attributed to adsorption onto the carbon felt, which was found to be significant.

Huyen et al. [76] also used the Porocell to recover copper from galvanic sludge leachate. Copper was leached from galvanic sludge using concentrated (0.1 to 2 M) sulphuric acid to relatively high concentrations (5 to 21 g/L). Despite these high concentrations, the Porocell was able to remove significant fractions of it, particularly at high current densities of 1200 A/m^2. In this case, the high concentrations of both copper and acid provided highly conductive solutions and high limiting currents. Flow rate was found to negatively impact current efficiencies at all current densities, potentially suggesting the parasitic side reactions are transport limited. Higher currents yielded better current efficiencies, potentially due to the highly corrosive electrolyte, given that it was initially used to leach copper from sludge. At the highest current density, current efficiency was as high as 90 %, while it became as low as 29 % at the lowest current density. Given that current efficiency tends to drop when concentrations are low, these values are not representative of what is expected for recovery from dilute streams like spent lees.

3.5 Comparison between Previous and Current Tests

Despite the Porocell's use in these reports and papers, fundamental studies seeking to optimize or characterize its operation are sparse in the literature. Most of the aforementioned studies did not conduct rigorous statistical analysis, with many studies lacking replicates necessary to perform any statistics, creating uncertainty in the validity of conclusions drawn. In many cases, there is little stated justification for the selected process parameters, particularly when the process covers a wide range of concentrations and limiting currents. This dearth in the literature, combined with the wide range of results obtained by previous tests and the known impacts of flow rate and current density as established by carbon felt studies [28], is the motivation for the optimization studies with the Porocell.

Additionally, while the majority of tests with the Porocell study copper recovery, they were designed as case studies, using actual waste from real processes or simulating complicated waste compositions. While doing so is useful for specific application, it provides no general information, and thus no reference value in ideal conditions. Therefore, this study will attempt to perform the optimization using only dilute acidic copper sulphate solution. Due to the ultimate desire to process distillery spent lees, the pH will be kept closer to neutral (pH 4) [6] compared to most other studies (pH 1 to 2); while this is likely to result in increased energy costs from poor conductivity causing large Ohmic losses, it both prevents the need to add additional secondary pollutants to increase the conductivity and limits the acid-based corrosion [38] observed in many of the aforementioned studies [24, 77, 76].

A less acidic pH will also result in a more forgiving electrochemical window. As mentioned previously, the electrochemical window defines the potentials at which the solvent breaks down. In water, both the anodic and cathodic hydrolysis reactions are pH dependent: solving the Nernst equation (Eq. 2.2) shows that it decreases at a rate of 59.1 mV per pH unit. In contrast, copper reduction is relatively pH independent so long as the pH is below values around 4 (Fig. 3.4). As a result, a less acidic pH has a larger window of potentials in which the system can reduce copper without losing Coulombic efficiency to the hydrogen evolution reaction. This also has the added benefit of reducing the potential necessary for oxygen evolution, thereby slightly reducing the energy requirement of the net reaction.

A systematic approach will be used to understand the effects of additional waste components (Table 1.2) on Porocell performance. While the low concentrations

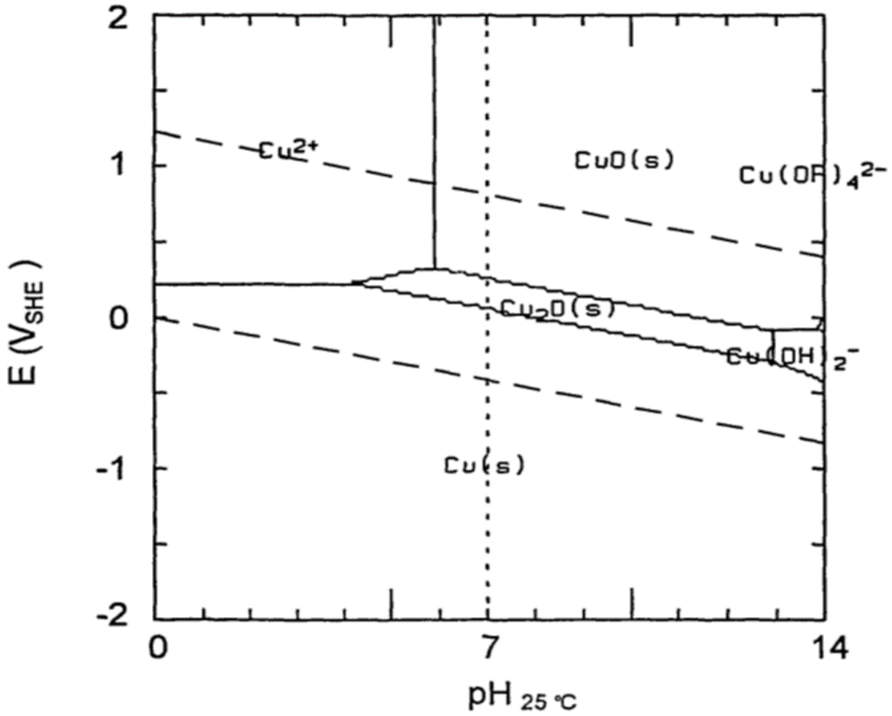

Figure 3.4: Pourbaix diagram of copper in water at concentration 10^{-4}, 25°C. Adapted from [38].

relative to copper are expected to have little impact, particularly given the small impact observed in other similar Porocell studies [24, 77, 76], there may still be some difference. Specifically, other metals, as well as protons from the acidic pH, are likely to compete with copper for electrons at the electrode surface, or oxidize copper that was already plated. The high organic content, particularly organic acids, are likely to complex with either the soluble copper, chelating it and decreasing its reduction potential, or the plated copper, forming a barrier to electron transfer.

The low concentration of copper is particularly a concern with spent lees, which seem to have concentrations of less than 40 ppm (0.63 mM) to start, not only because of its low limiting current. Pourbaix diagrams generated for total copper content at 10^{-4}, 10^{-6}, and 10^{-8} M (Fig. 3.4-3.5) indicate that the Cu^+ species seems to have a larger regime of potentials where it is stable as the concentration drops,

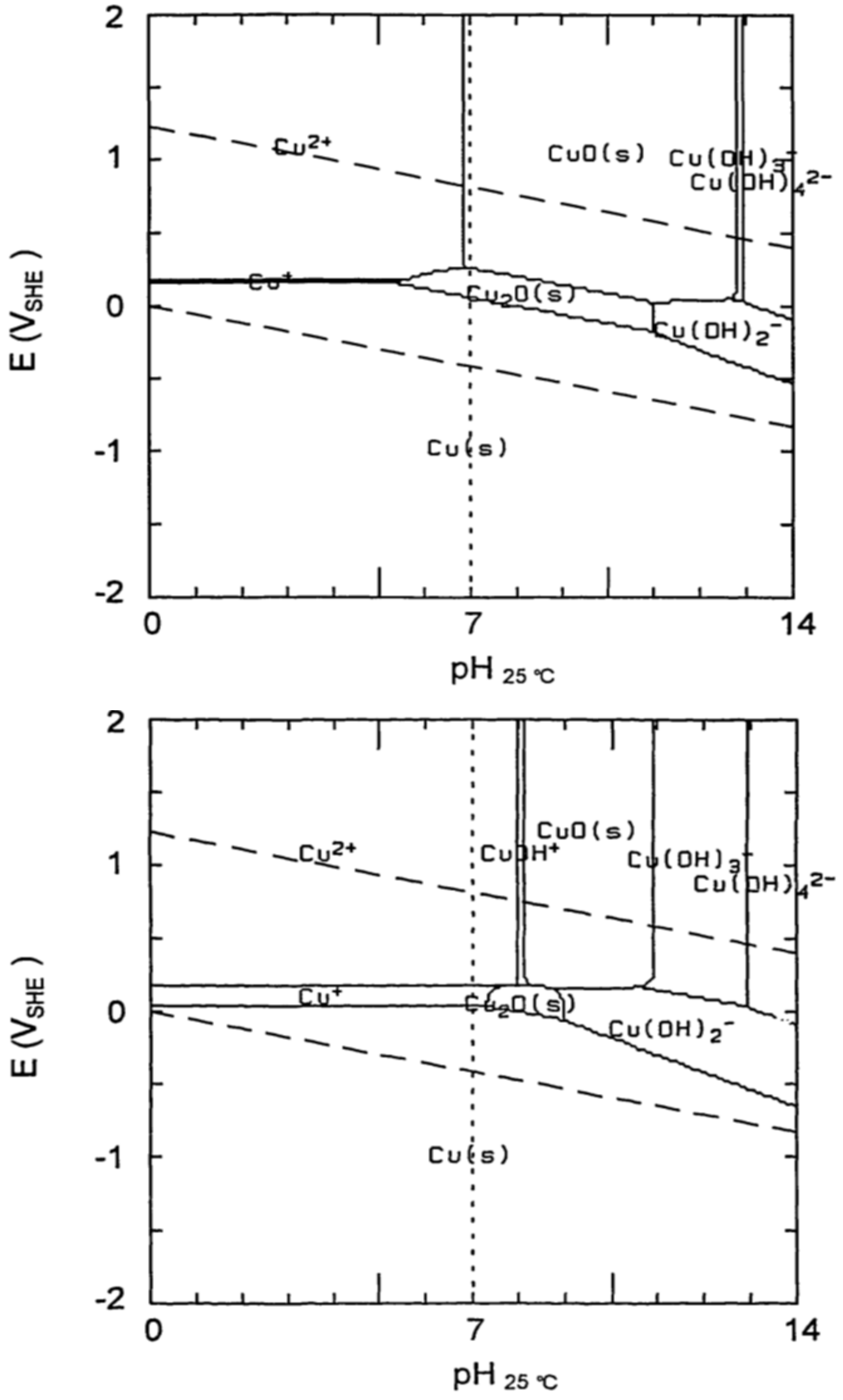

Figure 3.5: Pourbaix diagram of copper in water at (left) concentration 10^{-6}, 25°C and (right) concentration 10^{-8}, 25°C. Adapted from [38].

changing from non-existent in the 10^{-4} M diagram but increasing to a roughly 200 mV range of being the most thermodynamically stable species in acidic media at

10^{-8} M [38].

This is important because of the possible disproportionation reaction, whereby Cu^{2+} oxidizes solid Cu, producing two Cu^{+} molecules. A regime where the Cu^{+} species is not only stable, but the dominant form, is likely to produce noticeable corrosion. Sufficiently reducing potentials can drive the reaction to form solid Cu, but the more acidic the environment, the smaller the window before hydrolysis occurs, decreasing the net current efficiency through another mechanism. This information also implies that for processing spent lees, each batch should be drained after completion, as letting it rest in the Porocell afterwards is likely to result in corrosion.

Therefore, tests at the bench scale will be performed to determine the magnitude of the impact of these additional waste constituents compared to plating from a pure copper sulphate bath. This will then follow with optimization of the Porocell's operational parameters using only copper, which will then be validated against simulated and true spent lees. This experiment design allows for more robust and generalizable conclusions beyond spent lees, granting a better fundamental basis for Porocell use in other metal recovery applications.

Chapter 4

Experimental Methods

4.1 Bench Scale Tests

Due to the complex composition of distillery spent lees, an intensive study of the impact of each individual waste constituent, as well as their combinatorial effects, was deemed infeasible. However, most of the waste constituents are at least 1 order of magnitude lower in molar concentration than the starting concentration of copper. Additionally, all of the known constituents fell within three categories: molecules known to be inert relative to copper reduction, other trace metals, and nucleophiles. As a result, only three sets of tests were performed: copper only, copper with other metals, and copper with metals and nucleophiles, using the inert molecules to maintain charge balances when additional constituents were added.

4.1.1 Solution composition

Copper solutions were made in dilute sulphuric acid (65 μM) only, trace metal solution, or fully simulated spent lees. The list of compounds and their concentrations are listed in Table 1.2. All solutions were made using deionized water (DirectQ, 18.2 MΩ) and pH corrected using H_2SO_4 to a value of 4 ± 0.2. All electrochemical tests were done in ambient room temperature (20 to 25°C).

4.1.2 Electrochemical cell

All experiments utilized a BioLogic SP-300 potentiostat and accompanying EC-Lab software (v. 11.17) to control or measure the current and voltage. A 3-electrode setup was used, with a Ag/AgCl (3 M NaCl) reference electrode and platinum wire counter electrode; unless otherwise stated, all voltages are reported relative to this reference. The RRDE-3A (ALS co. Ltd.) gold disk (4 mm diameter) or platinum ring (5 mm inner diameter, 7 mm outer diameter) was used as the working electrode, depending on the experiment being performed. The working electrode was mechanically polished using 0.5 μm alumina (PK-3 electrode polishing kit, ALS co. Ltd), followed by an electrochemical polish via cyclic voltammetry from 0.1 to 1.7 V at 100 mV/s in dilute sulphuric acid (pH = 4, approximately 65 μM) until repeated voltammograms overlapped each other [78, 79].

4.1.3 Cyclic voltammetry

Cyclic voltammetry (CV) was performed with the Au disk electrode and test electrolytes of 4, 20, or 40 ppm Cu. As evident from Table 1.2, there are more reported cations than anions in full simulated spent lees. In order to adequately represent both the anions and pH without adding new cations into solution, a minimum of 6 ppm copper was necessary when testing with this electrolyte. Each test electrolyte was cycled from 0.6 to 0.1 V twice, at each of the following scan rates: 10, 25, 35, 50, and 100 mV/s. Due to the digital quantization of the linear sweep, data was acquired by sampling during the final 25 % of each digital voltage step and averaging over every 50 steps to obtain smooth data outputs. The second cycle at each scan rate was used for analysis for consistency to minimize charging effects observed in the beginning of the first scan.

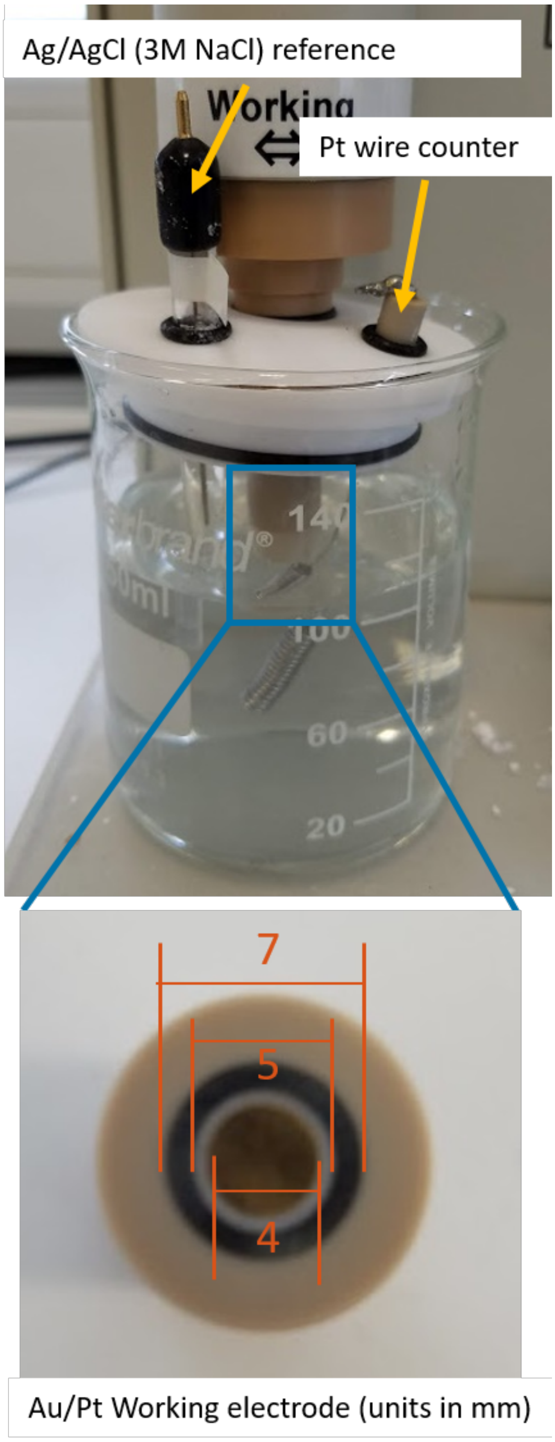
Ag/AgCl (3M NaCl) reference
Working
⇔
Pt wire counter
7
5
4
Au/Pt Working electrode (units in mm)

Figure 4.1: (top) Photograph of the bench-scale electrochemical cell. (bottom) Surface of the gold disk/platinum ring electrode.

The values of i_p for copper reduction and copper oxidation for each scan rate were determined by first subtracting out the capacitive contribution of the curve by linearly fitting the region right before the peak, then performing a fit to a quadratic equation on the region around the local extrema. Each test was performed in triplicate to obtain a mean value for the i_p at each scan rate and concentration. The relationship between i_p and $\nu^{1/2}$ was then fit to the Randles-Sevcik equation (Eq. 2.6), from which the diffusion coefficient could be calculated from this fit's slope. A mean value for the diffusion coefficient for each solution was determined by taking the mean across the three copper concentrations.

4.1.4 Polarization experiments

Polarization curves were obtained using the Pt ring electrode rotated at a rate of 100 rpm, selected as the lower limit of the RRDE-3A's rotation speed. Tests in stagnant solution or with the Au disk rapidly reached the transport limited current, preventing analysis of the reaction kinetics, so the rotating ring was used.

The electrode was first charged by holding it at 0.4 V for 10 minutes. Afterwards, the electrode potential was decreased by 0.1 V and held for 5 minutes. This decrease of 0.1 V was then repeated until a final potential of -0.5 V. The current was sampled every 0.5 s. The steady state current was determined as the mean current of the final 30 seconds at each potential. This experiment was performed using copper concentrations of 0, 4, and 40 ppm with additional waste constituents as desired. In the case of simulated spent lees, the tested copper concentrations were 6, 10, and 46 ppm due to aforementioned charge imbalance between cations and anions in the reported composition of spent lees.

The current at 4 and 40 ppm Cu was normalized by subtracting out the contribution from the corresponding 0 ppm polarization curve, thereby eliminating the background contribution. The resulting data was plotted on a semilog plot to fit to the Tafel approximation of the Butler-Volmer equation for high overpotentials (Eq. 4.1) [31].

$$\ln(i) = \ln(i_0) + (1-\alpha)\frac{zF}{RT}\eta \tag{4.1}$$

The equilibrium potential used to obtain η was estimated based on the mean standard reduction potential of copper, as determined experimentally by CV, and adjusted for concentration using the Nernst equation (Eq. 2.2). The mass transport limiting current was estimated as the current at steady state when held at -0.5 V, as beyond this voltage a very large background contribution is observed. An additional replicate was conducted for the range 1 to -1 V with 50 mV steps to obtain higher resolution results, particularly for identification of the potential where the system switches from anodic to cathodic current.

4.1.5 Current efficiencies

Copper from a 40 ppm copper sulphate bath was plated on the Pt ring electrode rotating at 100 rpm at 50 %, 25 %, or 12.5 % of the initial mass transport limiting current for 24, 48, or 96 hours, respectively. This corresponded to the length of time required to plate a measurable mass of 1.4 mg at 100 % Coulombic efficiency. A maximum of 50 % of the transport limiting current was selected to avoid dendritic copper growth, which is known to occur at higher current densities [31]. Initial tests plating with high current resulted in dendrites causing a short circuit between the Pt ring and Au disk, leading to a sudden increase in electrode surface area.

The mass of the electrode was measured after mechanical and electrochemical polishing, rinsing, and drying for at least 5 minutes at 60°C, then again after copper plating to determine the amount of copper plated. This data was combined with Faraday's law (Eq. 2.3) to obtain the current efficiency. The 25 % i_{lim} condition was then used to test current efficiency with the two other waste compositions as this condition provided reliably consistent results when testing with weakly acidified copper sulphate solution.

4.2 Development of Process for Porocell Optimization

4.2.1 Copper measurement methods

Spectrophotometric measurements (Shimadzu UV mini 1240) were obtained at 805nm [36] at copper concentrations ranging from 0 to 40 ppm, and then assessed with a linear fit according to Beer-Lambert law.

The open circuit potential of a cupric ion selective electrode (SLS PHE0372) was measured using a potentiostat at copper concentrations ranging from 0.5 to 100 ppm. Instrument noise was eliminated by taking the average potential every second. All solutions were adjusted to a pH of 4, and all measurements performed in triplicate. The open circuit potential was defined as the average potential over a 30 second period after equilibration, which took approximately 4 to 4.5 minutes after placing in a new solution. The potential was related to concentration according to the Nernst equation (Eq. 2.2).

The ion selective electrode's pH dependence was determined by performing calibrations over the range of expected pH values in copper recovery tests. Stock solutions were made at 2 to 75 ppm copper, and pH adjusted with sulphuric acid to 5.25, 4.25, 4.05, 3.75, 3.40, 3.25, and 3.05 ($\pm$ 0.05). This calibration was performed periodically to account for any drift in the reading with time.

4.2.2 Porocell design description

The Porocell reactor used in these experiments is a circulation batch reactor, composed of a reservoir, pump, and reaction chamber with leads connected to the electrodes (Fig. 4.2). The total volume of the system is approximately 4.5 L. The volume of the reservoir alone is slightly larger than 3 L, while the reaction chamber is approximately 0.8 L. Due to process controls inherent to the reactor, the pump will only operate continuously if at least 4.2 L of solution are present.

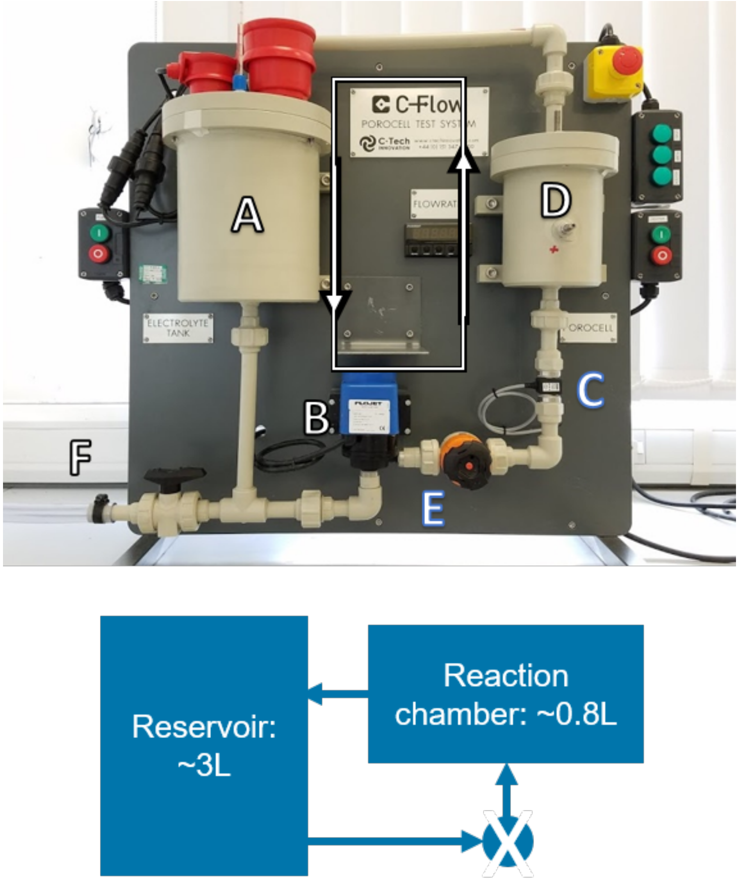
C-Flow
POROCELL TEST SYSTEM
C-Tech INNOVATION
A
D
FLOWRATE
ELECTROLYTE TANK
POROCELL
C
B
F
E
Reaction chamber: ~0.8L
Reservoir: ~3L

Figure 4.2: Photograph (top) and simplified schematic (bottom) of the Porocell Test System. (A) Reservoir. (B) Pump (0.5-3.5L/min). (C) Flow meter. (D) Electrochemical reaction chamber. (E) Diaphragm valve. (F) Outlet.

A flow meter (Omega, FTB602) is attached between the pump and the reaction chamber, and its reading in liters per minute displayed on an LED screen. The pump (FloJet, model NDP14/2) is capable of generating up to about 3.8 L/min of flow. The flow rate is able to be attenuated through a diaphragm valve down to 0.5 L/min, below which the flow meter reading becomes inaccurate, displaying an effective 0 L/min.

The reaction chamber (Fig. 4.3) contains two electrodes, a steel plate (20 x 9 cm) that is screwed and curved to sit along the chamber's outer wall and a removable and replaceable carbon felt (cut to 1 x 14 x 15 cm for this experiment). The carbon felt is wrapped around a 15 cm tall, 5.2 cm diameter hollow cylindrical plastic frame that links the inlet and outlet pipes. The frame contains a hard plastic blockage 10 cm from the base, preventing flow from only passing through the frame without passing through the porous cathode. A steel rod is attached to the outside of the frame to act as the current collector. Steel bands (0.5 cm tall) are wrapped around the plastic frame at 2 cm intervals starting at the base and ending at the plastic blockage; these rings serve to supply a more uniform electric field to the carbon felt. The carbon felt is held in place against the current collector with a plastic mesh (0.2 cm thickness and 1 cm square windows).

4.2.3 Flow rate validation

A test of the Porocell's flow meter was conducted to confirm the validity of the reading and determine the system's dynamic range. The Porocell's diaphragm valve was adjusted such that the desired flow rate ($\pm$ 0.1 L/min) was displayed for 1 continuous minute. Afterwards, the pump was turned off and the piping reoriented such that the pipe linking the reservoir and the reaction chamber (i.e. the pipe from D to A in Fig. 4.2) was removed, instead acting as an outlet. Beneath the new outlet was a 5 L beaker atop a lab scale. The flow was started

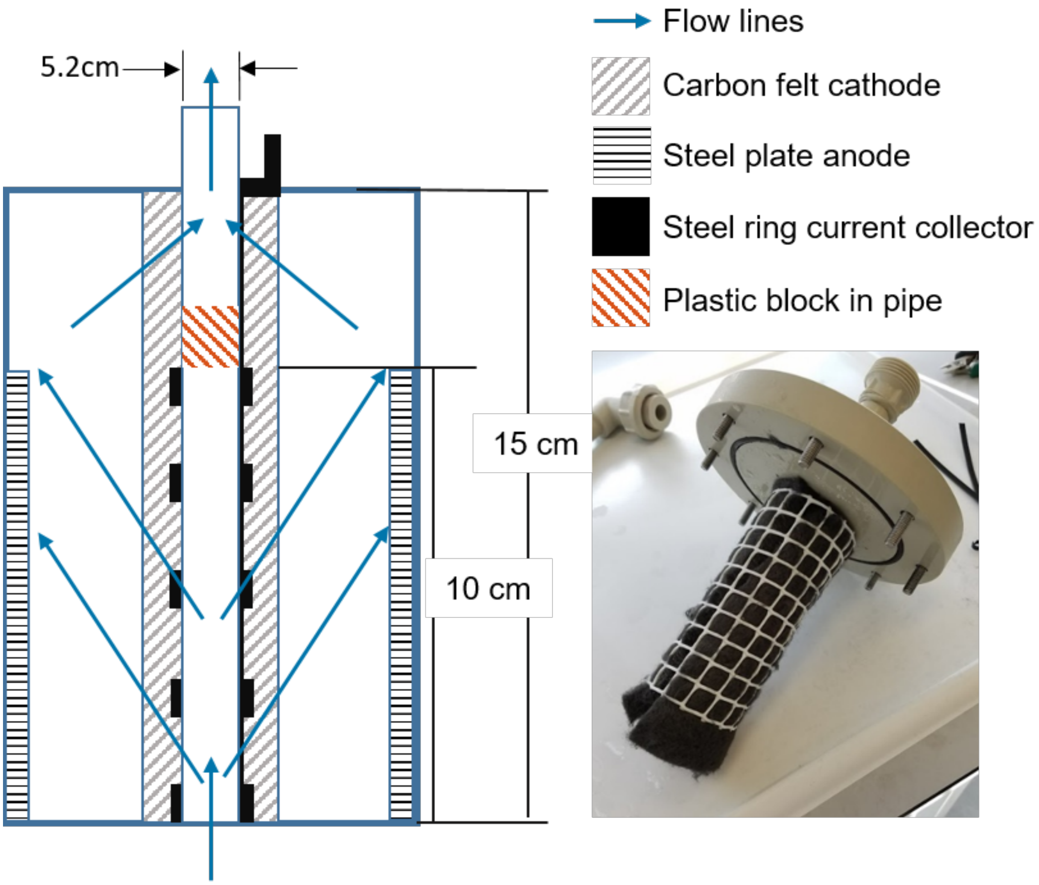
Flow lines
Carbon felt cathode
Steel plate anode
Steel ring current collector
Plastic block in pipe
5.2cm
15 cm
10 cm

Figure 4.3: (left) Cross section of the Porocell reaction chamber. Fluid flows from the bottom and gets forced through the carbon felt cathode due to a block in the flow path. Current is supplied to the felt from the inside steel rings. (right) Photograph of the cathode held in place against the current collector by its plastic mesh.

and allowed to continue for up to 20 seconds. On occasions where the pump was stopped prematurely due to volume depletion in the reservoir, the amount of time that the pump was running, estimated to the nearest second, was recorded. The mass change of the beaker was recorded, and a measured flow rate determined using an estimated density of water of 1 g/mL and the known duration of flow.

4.2.4 Comparison of carbon felt electrode pre-treatments

Preliminary tests with the carbon felt showed very low current, potentially related to its hydrophobicity leading to air pockets that limited contact between the electrode and solution. Therefore, a test was conducted to compare the electrochemical behaviour of unaltered carbon felt to its behaviour after three different pre-treatment conditions to assess the optimal pre-treatment for later tests.

All three pre-treatments involved submerging the electrode in a specified solution for 1 hour, followed by continuous rinsing with distilled water until the pH of the rinsate was the same as as the distilled water ($\pm$ 0.5, measured by Mettler Toledo InLab Expert Pro pH probe). The three pre-treatment solutions were: 1 M H_2SO_4, 1 M NaOH, and distilled water. Both 1M H_2SO_4 and 1 M NaOH have been previously shown to improve the hydrophilicity by altering the surface chemistry [58]. Distilled water was tested as a control condition because submerging the electrode resulted in an observable degassing, which will also improve electrode-solution contact.

The treated electrodes were compared using a modified polarization experiment using the Porocell as the electrochemical cell. The Porocell's 2-electrode setup was held at 0 V until a steady state current was measured, after which the voltage was increased by 0.5 V. This was repeated until a final voltage of 9 V. For tests with the untreated electrode, the Porocell pump was active and recirculating solution; for all other tests, the solution was stagnant. This test was performed in both dilute H_2SO_4 (pH = 4, approximately 65 μM H_2SO_4) and in weakly acidic 40 ppm copper solution.

4.2.5 Determination of current limits

Carbon felt pretreated in 1 M H_2SO_4 was tested by sweeping the voltage from -9 to 9 V at a scan rate of 10 mV/s at nominal flow rates of 0.5, 1.5, 2.5, and 3.5 L/min. This was performed using both 0 and 40 ppm copper at a pH of 4. The voltammograms were analyzed to determine the minimum necessary current for noticeable copper reduction and the maximum current that can be achieved at each flow rate.

4.3 Porocell Copper Recovery Under Ideal Conditions

4.3.1 Optimization of current and flow rate

A matrix of flow rate and current conditions were selected based on the observed limits. Due to the small differences observed in the current as a result of flow rate, only the fastest and slowest flow rates, 3.5 to 3.8 L/min and 0.4 to 0.6 L/min, respectively, were used in plating experiments. Currents of 0, 35, 70, and 105 mA were selected from on the voltage-current behaviour for comparison. While the Porocell is usually run at much higher currents, the SP-300 potentiostat that was used is limited to $\pm$10 V cell voltage, and exceeding 105 mA resulted in cell voltages greater than 10 V.

The reactor was filled with 4.5 L weakly acidic copper sulphate solution (40 ppm Cu in 66.7 μM H_2SO_4). The solution was allowed to circulate and mix in the reactor at the highest flow rate for 5 minutes before the test flow and current conditions were set. Samples were obtained periodically over the course of 3 hours, and were tested for pH and copper concentration. Carbon felt electrodes were replaced every 8 to 10 tests to prevent potential issues with pore clogging.

Additional tests were performed at all applied currents overnight to obtain information regarding the expected necessary process duration. Samples for pH and copper testing were taken every half hour from the start until 4 hours, and then again from 23.5 to 26 hours.

4.3.2 High power tests

Due to the limited range of the potentiostat, higher currents could only be achieved with a power supply (Aim TTi CPX400S). The power supply was run in compliance mode, with a desired current of 1.05 A and upper voltage limit of 20.20 V. In this mode, the power supply would automatically lower the current according to its compliance if the necessary voltage exceeded this upper limit. Samples were taken as in Section 4.3.1, and the current and potential were manually recorded at the same time as sample collection.

4.3.3 Electrode imaging and analysis

Electrodes were rinsed and air dried, then laid flat for photographing. Photos were taken of the outside face (*i.e.* the side nearest the anode when assembled) of the electrodes. The inside face of the electrodes showed no visible copper plating and therefore was not photographed for analysis. The 1 cm square windows from the plastic mesh were used as the image scale.

Images taken of the carbon felt were analyzed for spatial distribution of copper. The distribution with respect to height was determined from the photographs of the outside face. Images were cropped and rotated as needed to minimize the amount of background present and so that all electrodes were in the same orientation. Images were processed using custom scripts in MatLab as follows.

Each image file contained its individual red, green, and blue color channels, with values scaled to a 0 to 1 range, where 0 is the absence of that color. Copper, due to its reddish hue, could be differentiated from the black of the carbon felt by subtracting the green channel from the red channel. The difference was then run through a threshold filter whose threshold value was calculated by Otsu's method [80] in order to separate which regions were plated copper and which were carbon felt. The percentage of pixels determined to be copper at each height increment was calculated for analysis. A representative example of this algorithm is discussed in Section 5.5.2, and can be seen in Figures 5.5.3-5.5.6.

To acquire a profile of plating throughout the electrode thickness, a section from the center of the electrode was removed and segmented into approximately 1 cm slices along the height direction (*i.e.* the direction of flow), starting at the base and continuing until a height of 14 cm. Due to the small scale, photographs were taken with a microscope camera to obtain data on the copper plating profile with respect to electrode thickness. Due to handling issues leading to warping, a standardized scale was not obtained; instead, since the carbon felt has a known starting thickness of 1 cm, the images were analyzed using that as the scale.

Each image was aggregated such that results from a single image represented a single discrete height value and not a continuous height (*i.e.* an image of the lowest cross section represented height $h = 1$ cm, rather than all heights h from 0.1 to 1.0 cm). This aggregation allowed for sufficient data of the depth profile at each height for analysis and comparison.

Microscopy images were processed similar to the previous method, with slight algorithmic differences due to the differences in the cameras used. Pixels designating copper were determined by the difference between the red and blue channels instead of red and green, and the individual channels were raised to the 2$^{\text{nd}}$ power to increase the signal-to-noise ratio and amplify the difference between copper and carbon felt. The image background, which showed a slight yellow hue, was removed by finding pixels whose red and green values were similar (± 0.1 on a 0 to 1 intensity scale) and whose blue value was much lower than the red and green values (at least 0.2 lower on a 0 to 1 intensity scale). The percentage of pixels determined to be copper at each depth increment for each height section was calculated for analysis. A representative example of this algorithm is discussed in Section 5.5.2, and can be seen in Figures 5.5.7-5.5.10.

4.4 Validation Against Spent Lees

Simulated spent lees contained the same composition as established in Section 4.1.1. Spent lees were collected from the Glengoyne Distillery (Dumgoyne, Scotland) on 15 August 2018.

Simulated and Glengoyne spent lees were tested using 105 mA and the highest flow rate for 3 hours based upon results with pure copper. An additional overnight test was conducted for both solutions. Solution conductivities (InLab 730 Conductivity Probe) at the start and after 3 hours of operation were measured for comparison to those of pure copper.

Chapter 5

Results and Discussion

5.1 Bench Scale Tests

A fundamental understanding of the copper electrochemical parameters is necessary to discern whether the inefficiencies found when recovering copper are a result of engineering design or of solution chemistry. Conducting these tests at the bench scale helps mitigate, although not completely eliminate, the effects of the high resistivity of spent lees [6] by bringing the electrodes closer together. For this section, unless otherwise stated, errors presented in the figures and tables represent the standard deviation (n = 3), accounting for propagation of errors when relevant.

5.1.1 Cyclic Voltammetry

Cyclic voltammograms (CV) were conducted across five scan rates with the intent of measuring the cupric ion diffusion coefficient. The potential window of the scan was selected to minimize the influence of the background electrolyte (Fig. 5.1.1). It is evident from the voltammograms of the electrolyte that there is a large peak that starts around 0.1 V, likely associated with either hydrolysis or oxygen reduction, as these are the only reactants in solution that would reduce at such this potential. There is also a possible peak observed around 0.5 V, but this is present only at the highest scan rates and only when the potential sweep starts at 0.7 V. Starting the scan at 0.6 V eliminated the presence of this peak.

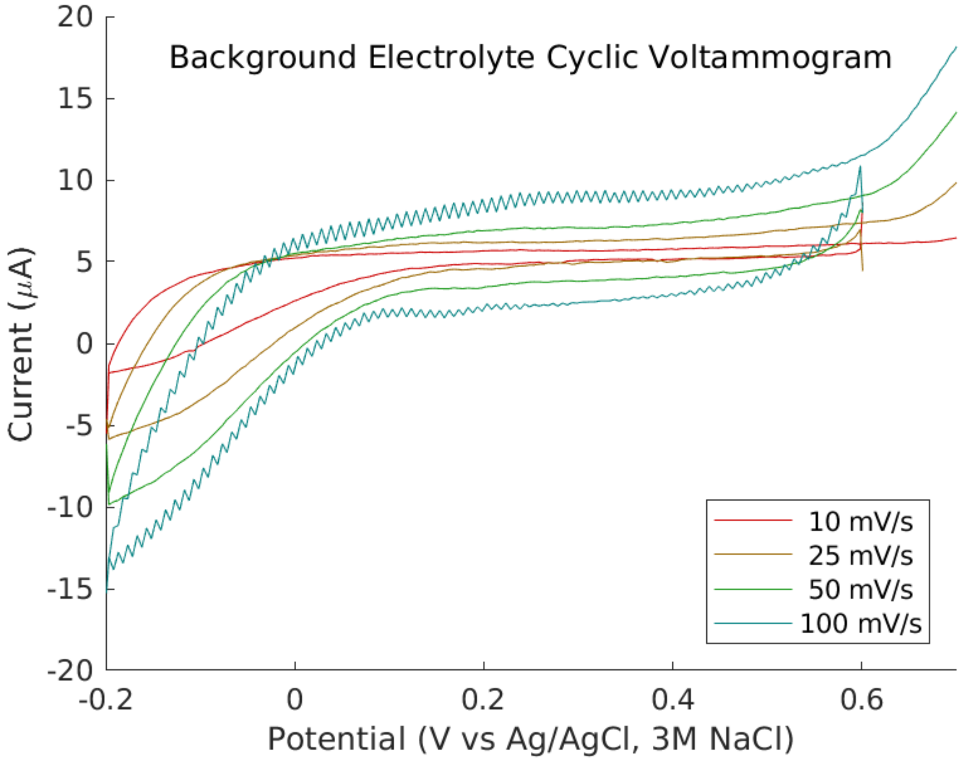

Figure 5.1.1: Cyclic voltammogram of the base electrolyte (dilute sulphuric acid at pH = 4, approximately 65 μM). WE = Au disk, CE = Pt wire

As evident in the representative CVs with 40 ppm Cu^{2+} in Fig. 5.1.2, a distinct anodic and cathodic pair of peaks that were not present in the absence of copper are visible. As the scan rate increases, the peak current increases, as predicted by Eq. 2.6, but the peaks also separate, a behaviour related to the large Ohmic drop. This resulted in many of the cathodic peaks being cut off in the scan. An attempt was made to extend the window of potentials in the CV to include more negative potentials, but it is clear from the CV of the background electrolyte that another peak would mask the copper signal at potentials more negative than 0 V vs Ag/AgCl.

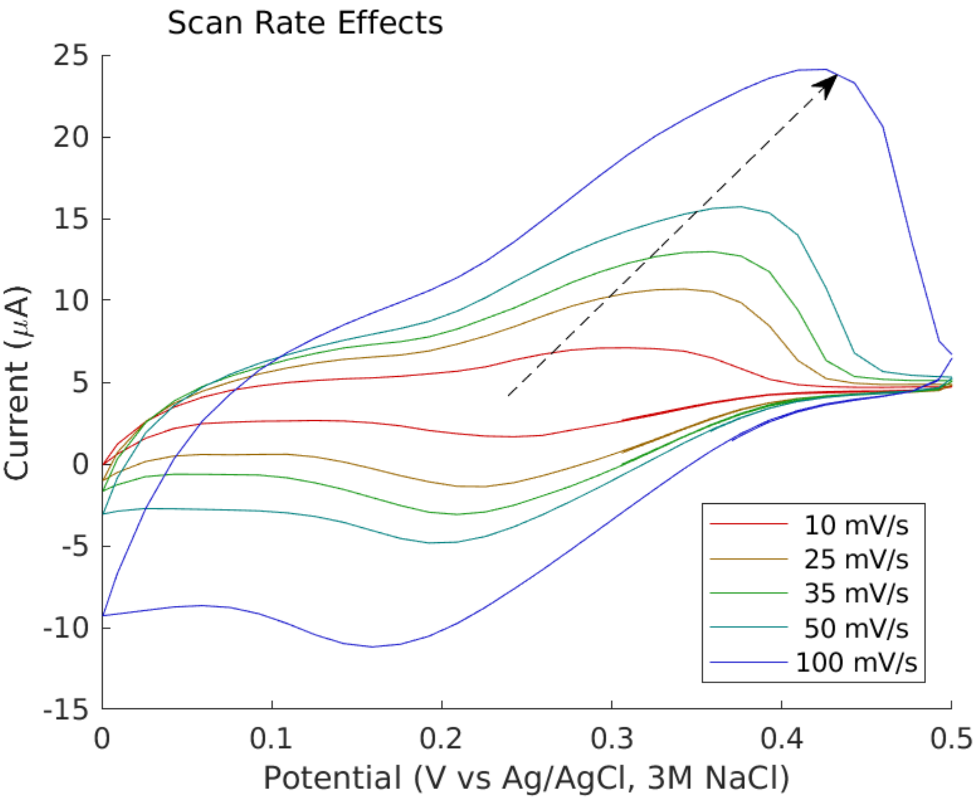

Figure 5.1.2: Scan rate effects on Cu^{2+}/Cu^0. All tests use 40 ppm Cu^{2+} at pH = 4. Arrow shows the direction of increasing scan rates. WE = Au disk, CE = Pt wire

While it is possible that the second peak could indicate a two-step process of $Cu^{2+} \rightarrow Cu^{+} \rightarrow Cu^{0}$, it is believed that the signal can be attributed to hydrogen evolution or oxygen reduction due to the presence of that peak when copper was absent from solution. One could determine which of these two reactions it is if the solution were sparged with inert gas prior to each scan, as this would eliminate any oxygen gas for possible reduction.

Importantly, the extension of the potential window created a second anodic peak that also overlapped the copper-related anodic peak, so the narrow potential window was selected to avoid this secondary reversible reaction altogether. While i_p could still be determined by extrapolating the peak out using a parabolic fit, using this narrow potential window causes significant error in determining both the reduction i_p and the voltage at which this peak occurs. Additionally, by cutting off a part of the reduction peak, the magnitude of the oxidation peak should also become smaller than expected, as there would be less plated copper for the reverse scan to oxidize. Despite these issues, the peak currents still appear to fit to the Randles-Sevcik equation (Table 5.1.1).

Table 5.1.1: Coefficient of determination when fitting the cyclic voltammetry peaks to the Randles-Sevcik equation. Red = reduction peak, Ox = oxidation peak.

	4 ppm Cu		20 ppm Cu		40 ppm Cu	
	Red	Ox	Red	Ox	Red	Ox
Copper only	0.997	0.995	0.998	0.998	0.992	0.999
Copper and and trace metals	0.993	0.951	0.999	0.989	0.998	0.999
Simulated spent lees	0.959	0.980	0.995	0.950	0.980	0.984

One feature of note is that the baseline current prior to the peak is not at 0 A, but is slightly positive throughout the scan. This difference is small, making up less than 5 μA for all scans, and likely only has impact on the CV due to the low copper concentration leading to low current. This small shift means that calculating a current efficiency by comparing the charge passed in the oxidation and reduction scans would not give reasonable results. For instance, the 10 mV/s CV only shows anodic current despite there being a distinct reduction peak due to the peak being smaller in amplitude than the baseline current.

Similarly, the concentration of copper affects the clarity with which the peaks can be observed (Fig. 5.1.3). At 4 ppm, the cathodic peak is effectively invisible, instead levelling off at a stable current at potentials more negative than 200 mV. This may be observed due to the rapid approach of the mass transport limit due to the low concentration. The peaks at 20 ppm show significantly wider spread than both the 4 ppm and 40 ppm tests, potentially due to slight differences in conductivity from subtle differences in pH: a more neutral solution will be more

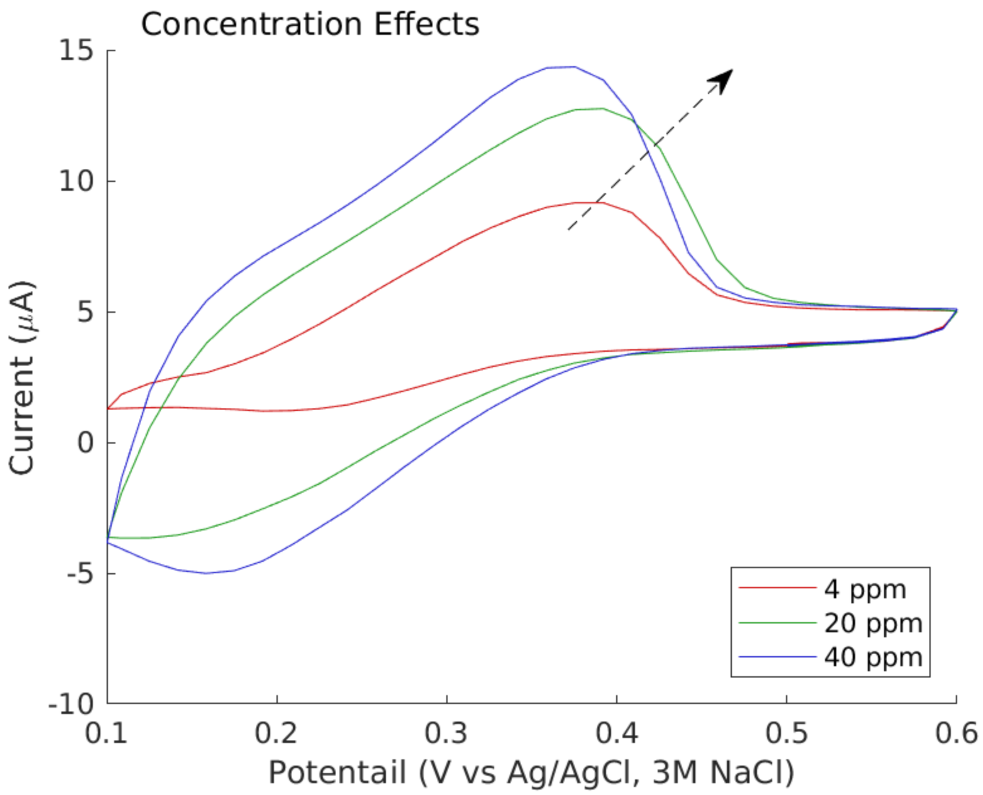

Figure 5.1.3: Concentration effects on Cu^{2+}/Cu^0. All tests are at 35 mV/s and pH = 4. Arrow shows the direction of increasing concentration. WE = Au disk, CE = Pt wire

resistive, causing the peaks to spread further apart.

Despite these imperfections in the CVs, estimates of the peak current and potential could be obtained by fitting the relevant part of the CV to a quadratic equation, whose minimum or maximum can be determined algebraically. While there is large uncertainty associated with this method, the estimated i_p still show strong fits to the Randles-Sevcik equation for both oxidation and reduction peaks (Fig. 5.1.4), with coefficients of determination all greater than 0.95 and many greater than 0.99 (Table 5.1.1).

The addition of other compounds present in spent lees did not show any notable effects on the shape of the CV (Fig. 5.1.5). While the addition of trace metals seemed to cause both peaks to occur at slightly more positive potentials, the

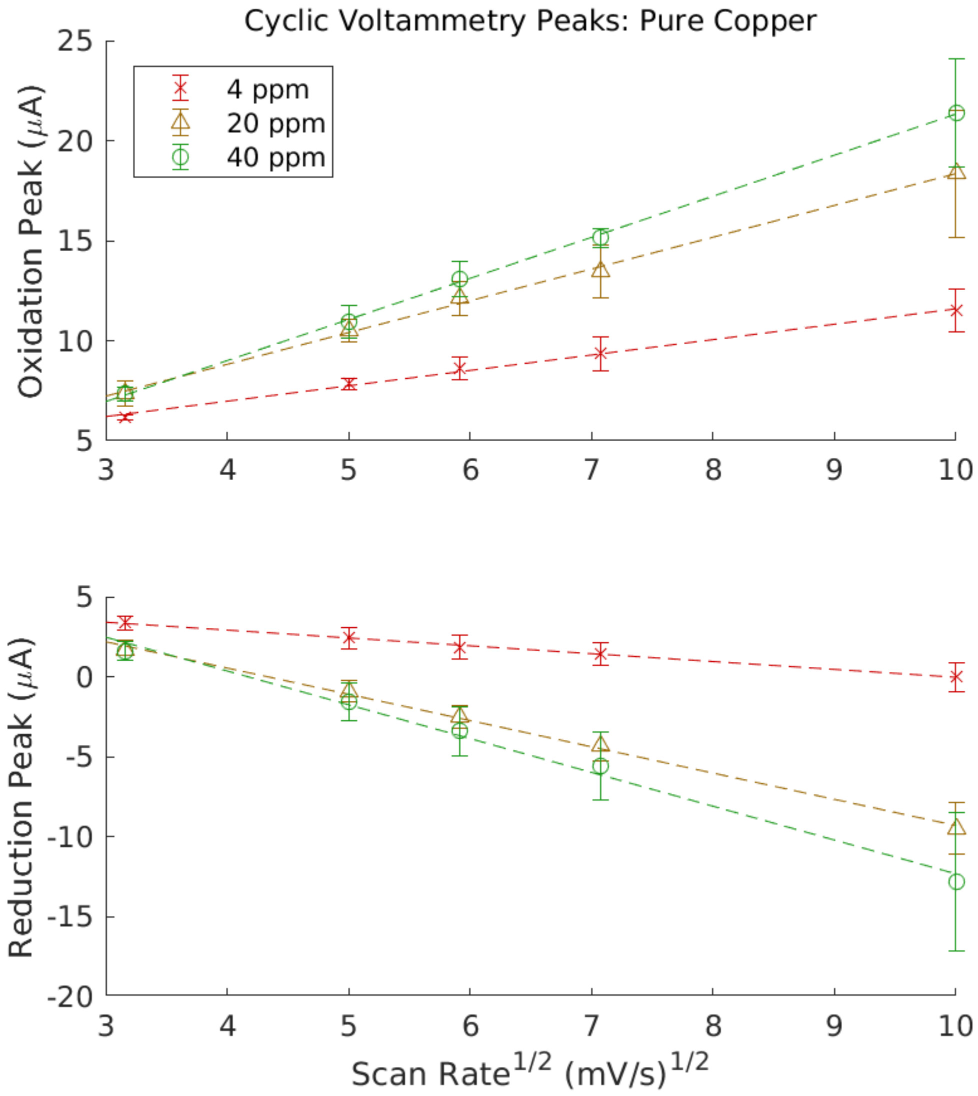

Figure 5.1.4: Magnitude of the oxidation (top) and reduction (bottom) peaks in the cyclic voltammograms along the range of scan rates from 10 mV/s to 100 mV/s.

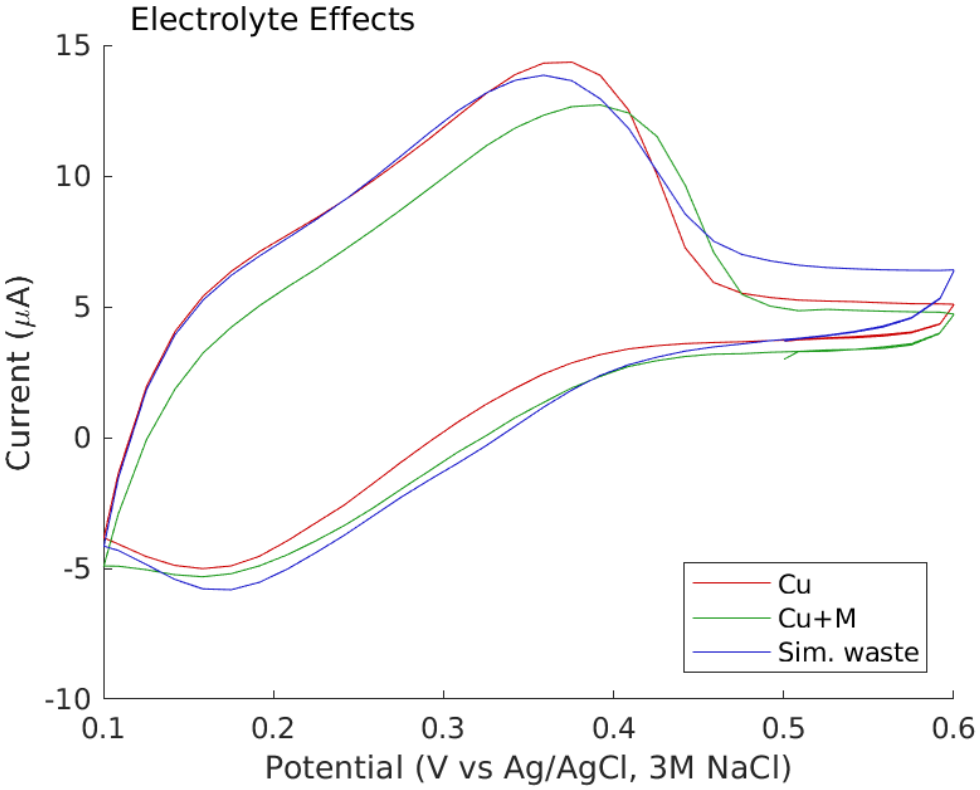

Figure 5.1.5: Electrolyte composition effects on Cu^{2+}/Cu^0 (40 ppm Cu^{2+} at pH = 4). Cu (red) = only copper sulphate. Cu + M (green) = copper and trace metal salts as stated in Table 1.2. Sim. waste (purple) = detailed in Table 1.2 with 40 ppm Cu^{2+}. WE = Au disk, CE = Pt wire

difference appeared to be corrected with the addition of the organic acids and inorganic anions.

However, in aggregate across multiple replicates (Fig. 5.1.6), the addition of organic acids and inorganic anions in simulated waste causes the peaks to shift to more negative potentials compared to both other conditions ($p < 0.05$), changing from 271 ± 38 mV without additives and 267 ± 30 mV with trace metals to 245 ± 46 mV when simulating spent lees. This negative shift in potential indicates that reduction becomes less favorable, likely a result of copper complexes forming with these nucleophilic additives, resulting in more stable copper ions.

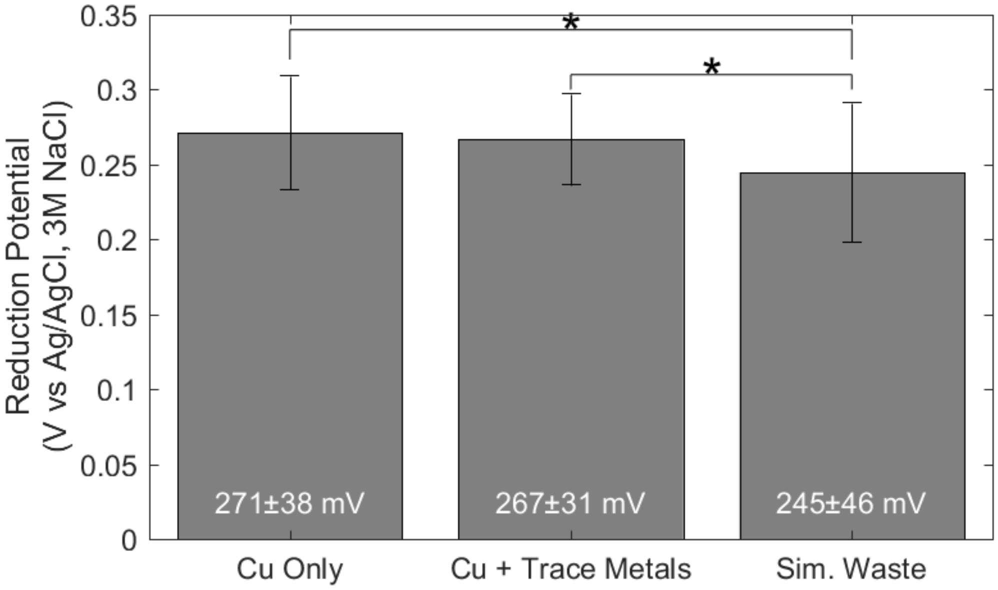

Figure 5.1.6: Comparison of the reduction potentials of the Cu^{2+}/Cu^0 redox couple in the presence of other contaminants. $^*p < 0.05$.

The subtle differences in the peak amplitudes of copper alone and copper with trace metals observed in the CV could be attributed to experimental error. In contrast, simulated spent lees consistently show slightly more negative currents for both oxidation and reduction peaks (Fig. 5.1.7). The fact that both the oxidation and the reduction peaks become more negative suggests that the difference is not related to the copper reaction, but the background behaviour of the solution, such as the solution's resistance and capacitance, which are expected to change as more ions and organic compounds are added.

This belief that it is not related to the copper reaction is supported by the result that the diffusion coefficients across all solution compositions, regardless of whether using the oxidation or reduction peak, show similar diffusion coefficients (Fig. 5.1.8), ranging from $0.249 \pm 0.151 * 10^{-5}$ cm^2/s (reduction peak, copper and trace metals) to $0.680 \pm 0.838 * 10^{-5}$ cm^2/s (oxidation peak, copper only). In fact, not only are all diffusion coefficients similar to each other ($p = 0.797$), but

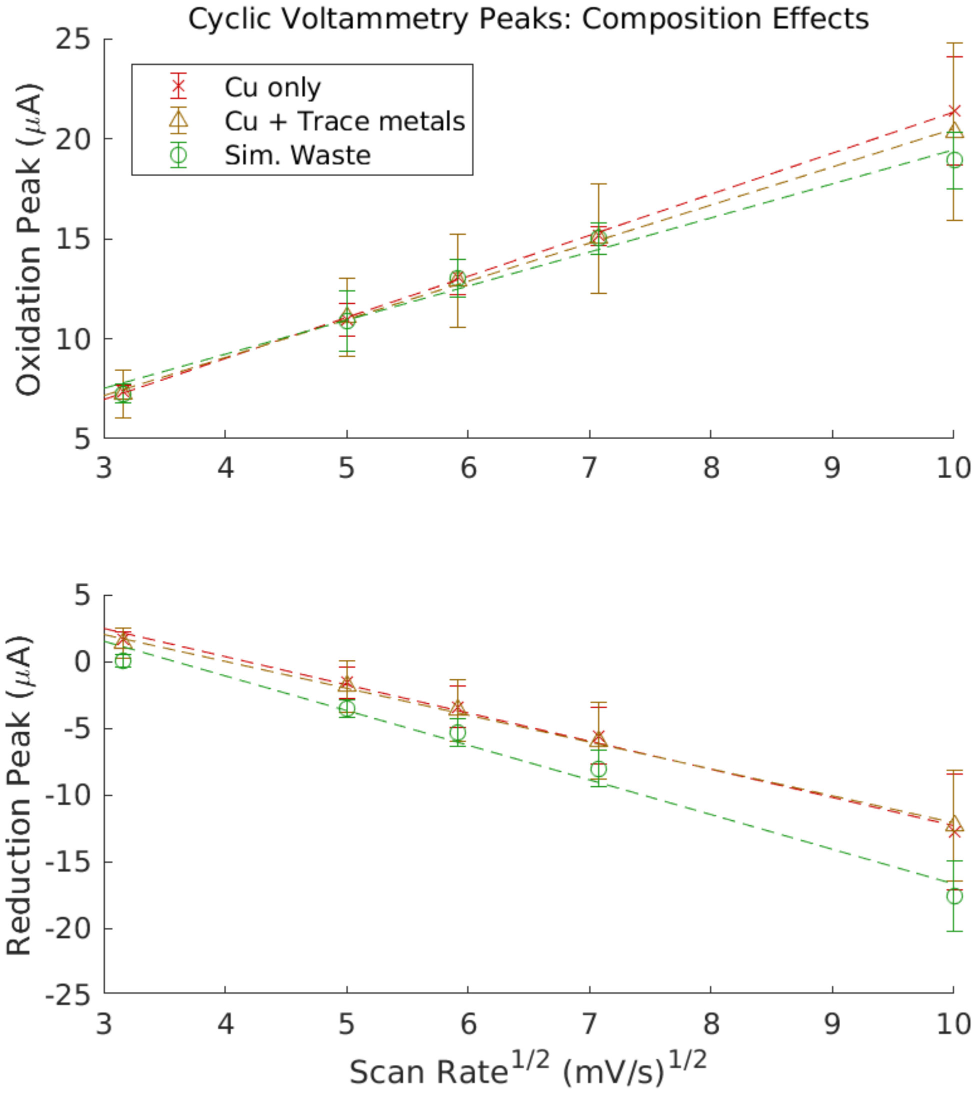

Figure 5.1.7: Comparison of the oxidation (top) and reduction peaks (bottom) in the cyclic voltammograms with additional compounds of spent lees. All tests use 40 ppm Cu^{2+}.

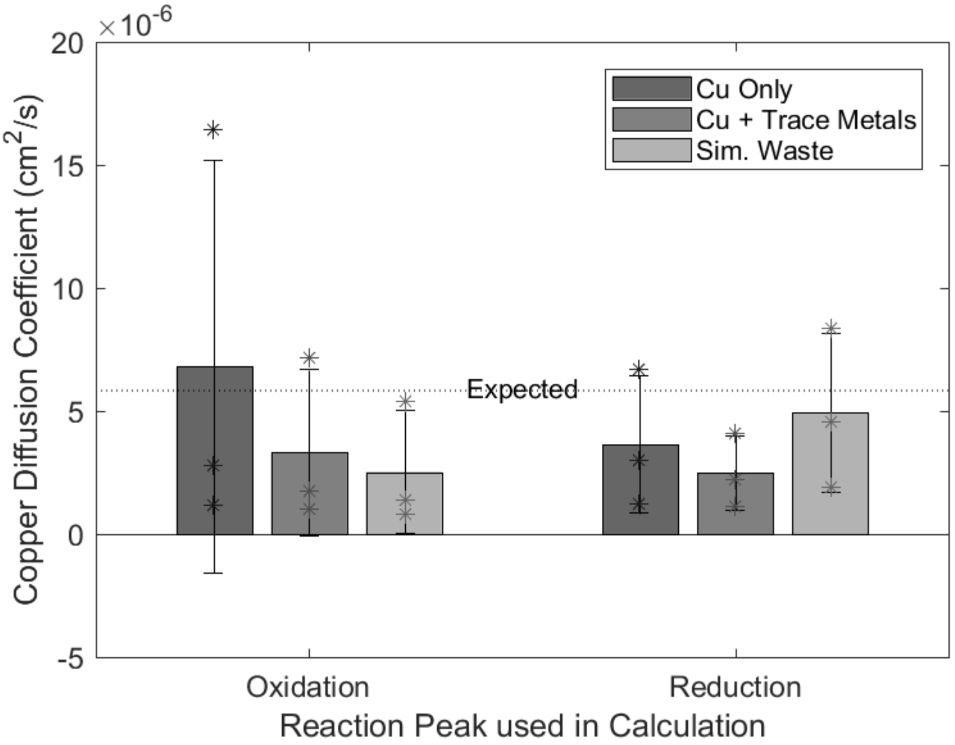

	Reduction peaks	Oxidation peaks
Copper only	$0.36 \pm 0.28 * 10^{-5}$	$0.68 \pm 0.84 * 10^{-5}$
Copper and trace metals	$0.25 \pm 0.15 * 10^{-5}$	$0.31 \pm 0.34 * 10^{-5}$
Simulated spent lees	$0.49 \pm 0.33 * 10^{-5}$	$0.25 \pm 0.25 * 10^{-5}$

Figure 5.1.8: Diffusion coefficients of Cu^{2+}, determined by the cyclic voltammogram peaks using the Randles-Sevcik equation. Error bars indicate the standard error of the mean, aggregating across the three concentrations (n = 3). Individual data points are indicated by a $*$. (Bottom) Tabulation of means and standard deviations.

they are also similar to the expected value based on the literature ($p = 0.788$) [48].

Notably, there is significant error in these results caused by the differences in apparent diffusion coefficient at different concentrations (Fig. 5.1.9). It appears that when conducting a CV at lower concentrations, the apparent diffusion coefficient seems to increase; as the concentration increases, the diffusion coefficient seems to decrease. The decrease seems to behave asymptotically, although additional data would be necessary to make concrete conclusions about this relationship. This trend is observed in all conditions, whether using the oxidation or reduction peaks to calculate the diffusion coefficient, or using copper with or without any of the additives.

While this finding is in contrast to the reported relationship between copper diffusion coefficient and concentration [48], that experiment only tested to concentrations of 10^{-4} M, while these concentrations are on the order of 10^{-7} M. This result is consistent with models of diffusion coefficient with other materials at such low concentration [81], which indicate that at this concentration, there is a notable effect of sorption, resulting in measurably higher diffusion coefficients at low concentration.

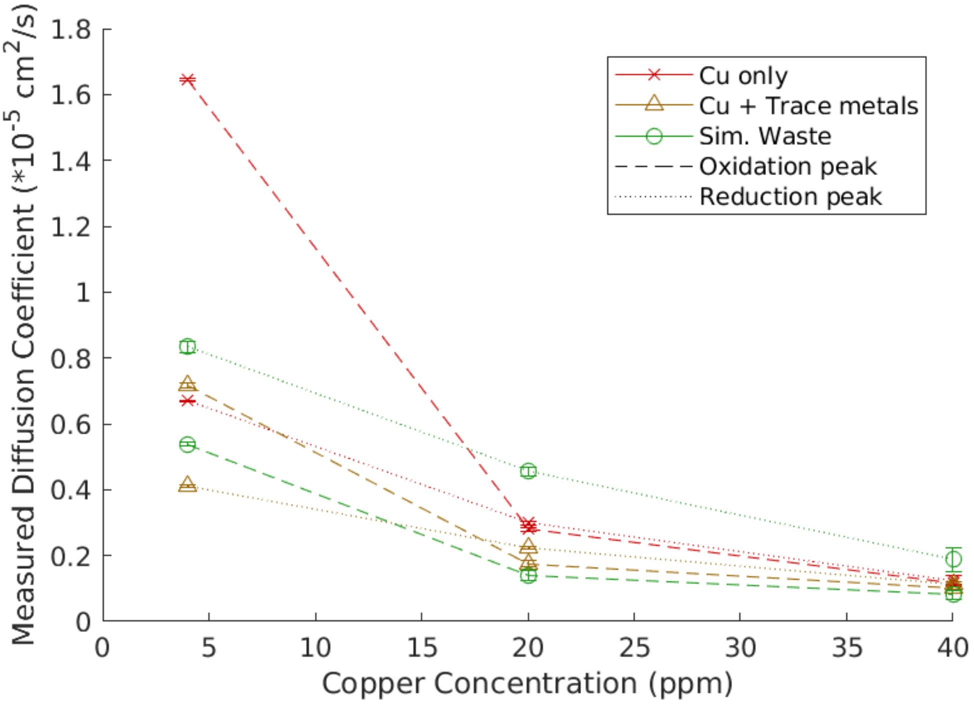

Figure 5.1.9: Analysis of the possible concentration effects on the calculated diffusion coefficient of Cu^{2+}.

5.1.2 Polarization experiments

The steady state current for potentials more cathodic than the equilibrium potential generally seem to follow the shape expected by the Butler-Volmer equation (Fig. 5.1.10), particularly at 40 ppm Cu^{2+}. At one order of magnitude lower, the trend is much weaker, likely because that concentration is so low that the copper signal contribution is too small to detect beyond the variation in the background. For potentials more anodic than the expected equilibrium potential, the currents are more erratic, likely because the only possible reactant at these potentials is water, which would form a gaseous product, whose bubbles would result in significant noise.

Normalizing the current by subtracting the current observed in the absence of copper highlights the unreliability of the 4 ppm data (Fig. 5.1.11). When adding copper, one would expect copper reduction at potentials below the expected equilibrium potential, leading to more negative currents. However, adding 4 ppm copper to dilute (65 μM) sulphuric acid seemed to result in more oxidative current, implying that another signal is dominating at this concentration.

This is in contrast to the results with 40 ppm copper, where, despite a small initial oxidative current from 0 to 0.1 V, it becomes strongly reducing as the overpotential is increased. This initial oxidative current suggests that the actual equilibrium potential is more negative than calculated by the Nernst equation, potentially the result of the increasing relative stabilization of the Cu^+ species as predicted by the Pourbaix diagrams [38] leading to other redox reactions besides the expected $Cu^{2+} \rightarrow Cu^0$ reaction, including Cu^0 oxidation to Cu^+.

Comparing the different solution compositions, the simulated spent lees, as with the CVs, appear to have more negative currents overall. While this leads to the simulated waste reaching higher current magnitudes at lower overpotentials,

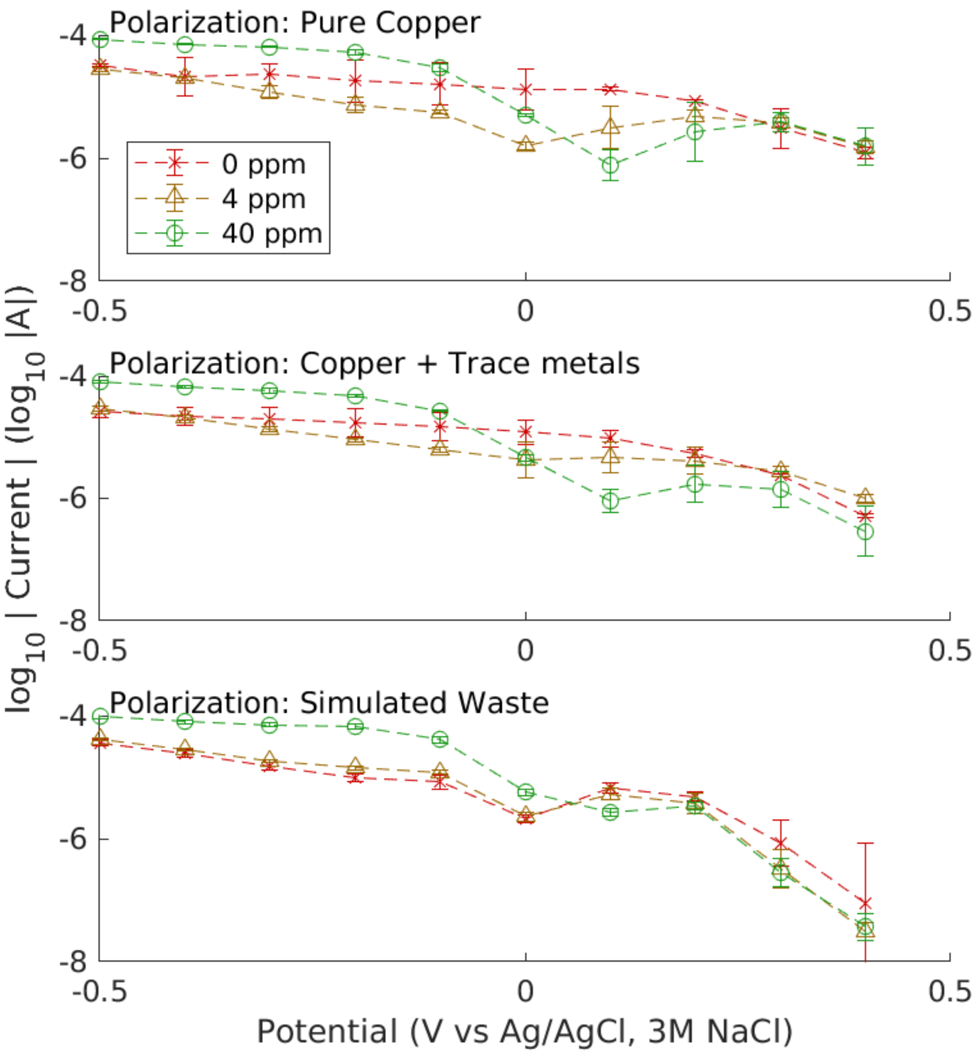

Figure 5.1.10: Polarization curves for each solution composition tested. Pure copper = 40 ppm Cu^{2+} at pH = 4 (approximately 65 μM sulphuric acid). Copper + Trace metals = 40 ppm Cu^{2+} + trace metal salts as stated in 1.2 at pH = 4. Simulated waste = Solution composition as detailed in 1.2 with 40 ppm Cu^{2+}. WE = Pt ring rotating at 100 rpm, CE = Pt wire

all conditions appear to reach the same transport limiting current, agreeing with the finding that all diffusion coefficients are similar to each other.

Since the 4 ppm polarization results do not appear to show clear copper reduction, further polarization analyses will only report and discuss the 40 ppm results. The polarization curve seems to fit well to the Tafel equation at potentials more

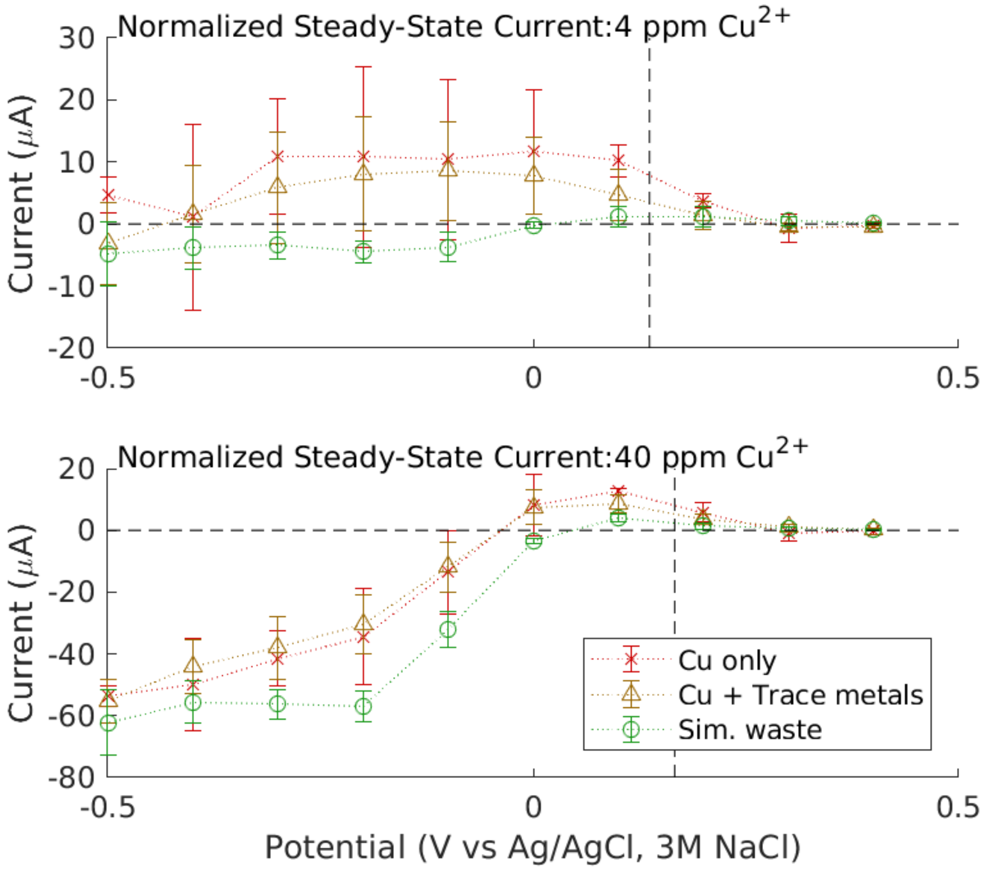

Figure 5.1.11: Normalized steady-state current after removal of the background. Vertical and horizontal dashed lines indicate the predicted reduction potential from the Nernst equation and the 0 A current line, respectively. WE = Pt ring rotating at 100 rpm, CE = Pt wire

negative than -0.1 V (Fig. 5.1.12). At lower overpotentials, the effect of the small positive currents result in a weaker and less reliable fit.

Table 5.1.2: Calculated Tafel slopes and exchange currents from the polarization curves in Fig. 5.1.12. Error represents the uncertainty in the quality of the fit line.

	Tafel slope (decades/V)	Exchange Current (μA)
Copper only	-2.43 ± 0.93	1.59 ± 0.48
Copper and and trace metals	-2.51 ± 0.89	1.55 ± 0.48
Simulated spent lees	-1.23 ± 0.74	1.45 ± 0.35

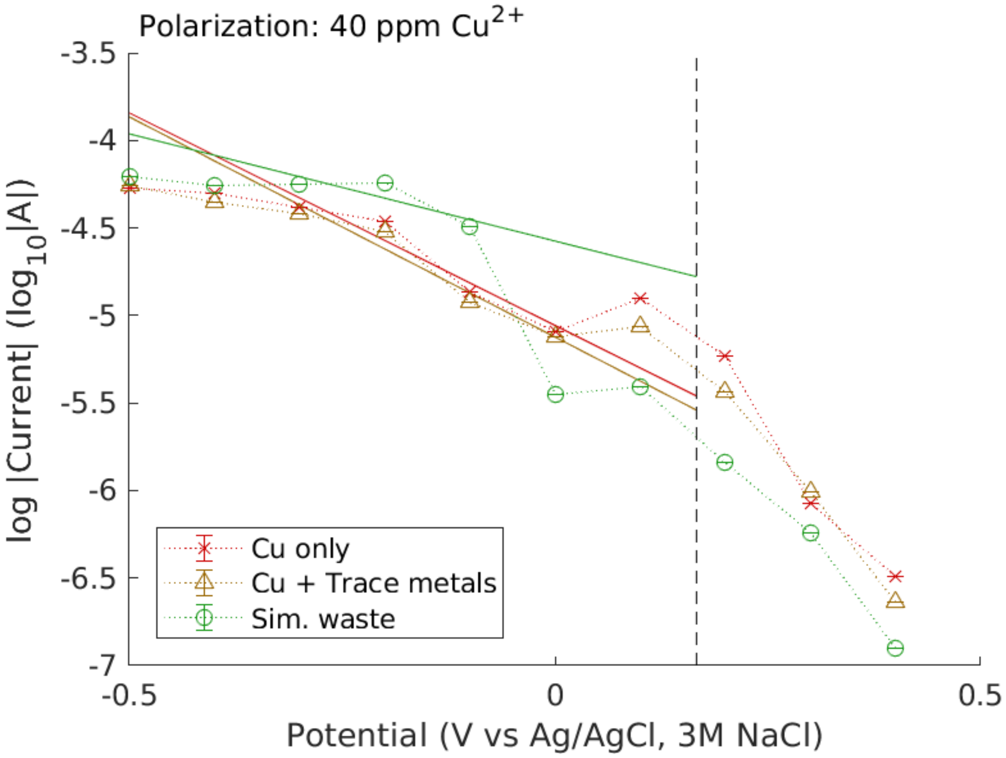

Figure 5.1.12: Polarization curve for 40 ppm Cu^{2+} for all solution compositions. Lines indicate the fit lines to the Tafel equation. WE = Pt ring rotating at 100 rpm, CE = Pt wire

This fit produces the Tafel slopes and exchange currents (Table 5.1.2). While the Tafel slope of simulated spent lees appears to be less steep, the difference is not significant ($p > 0.25$). The difference may, in fact, simply be an artefact of the range of potentials used in determining the Tafel fit. The Tafel approximation is only valid at sufficiently high overpotentials, but the current must not have reached the mass transport limit. Copper reaches the mass transport limit quickly, so only a narrow range of potentials could be used in calculating this fit line. Simulated spent lees appear to reach the mass transport limiting current at lower overpotentials, so it is uncertain if the entire potential range used in the fit can be approximated by the Tafel equation. Inclusion of high overpotentials that may have already reached the transport limit would artificially decrease the magnitude of the slope, leading to the observation.

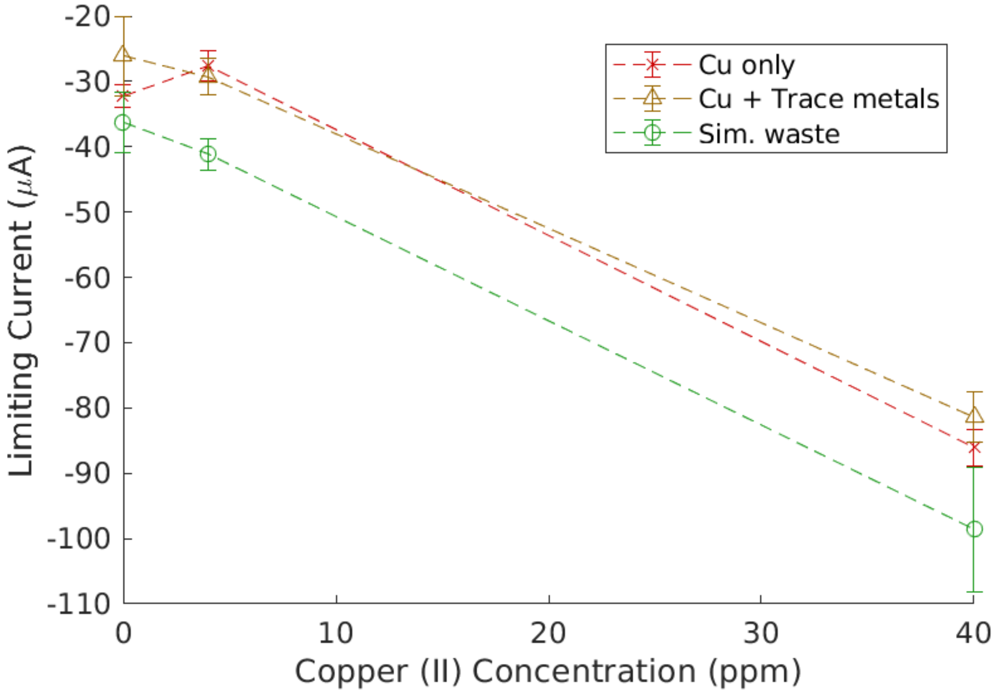

Figure 5.1.13: Limiting current for copper reduction across the range of concentrations tested. WE = Pt ring rotating at 100 rpm, CE = Pt wire

The exchange currents are nearly identical ($p > 0.92$). However, this conclusion should be taken in the context of the uncertainty of the equilibrium potential as well as the rapid approach of the mass transport limiting current, both of which cause a degree of unquantified uncertainty not included in the statistics. An uncertain equilibrium potential means that the exchange current would be higher or lower should the actual equilibrium potential be more negative or positive, respectively. The inclusion of data after reaching the mass transport limit would, in flattening the slope, result in a higher apparent exchange current.

In contrast, the results for the limiting current for all conditions follow a more expected trend (Fig. 5.1.13). All three conditions show a similar slope between limiting current and concentration, although additional data at other concentrations would be necessary to make more than a qualitative assessment. Again, the fully simulated waste shows more negative currents than either other condition

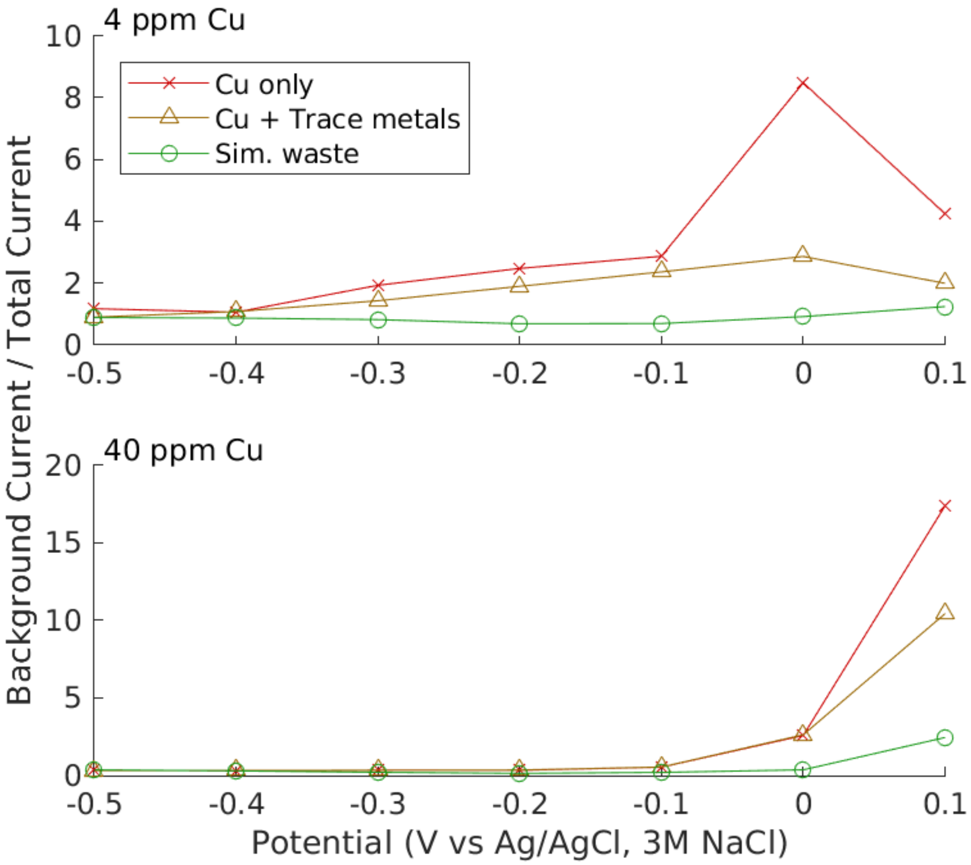

Figure 5.1.14: Fraction of background current observed at steady state across the range of potentials in the polarization curve. WE = Pt ring rotating at 100 rpm, CE = Pt wire

across all copper concentrations, which appears to be a result of the more negative background current. Knowing that this occurs in both dynamic (CV) and steady state (polarization) conditions, this difference is not likely to be related to changes to the solution capacitance, instead the result of the reduction of another compound or the difference in resistivity.

The range of approximately 80 to 100 μA at 40 ppm to 30 to 40 μA at 4 ppm does pose a problem for recovery, as the large range means selection of an appropriately fast current for galvanostatic electroplating would likely be higher than the limiting current at lower concentrations. The high baseline current at 0 ppm Cu^{2+} relative to the total current when copper is added is important to note (Fig. 5.1.14), particularly at lower copper concentrations. This ratio across the range of possible potentials shows that a sufficiently high overpotential, and thus sufficiently high current density, is needed to ensure that the entirety of the current can be assumed to result in copper reduction and not a background signal. If this were not the case, the current efficiency would have a non-ideal maximum. To obtain a range of results, bench scale plating was conducted at 50, 25, and 12.5 μA.

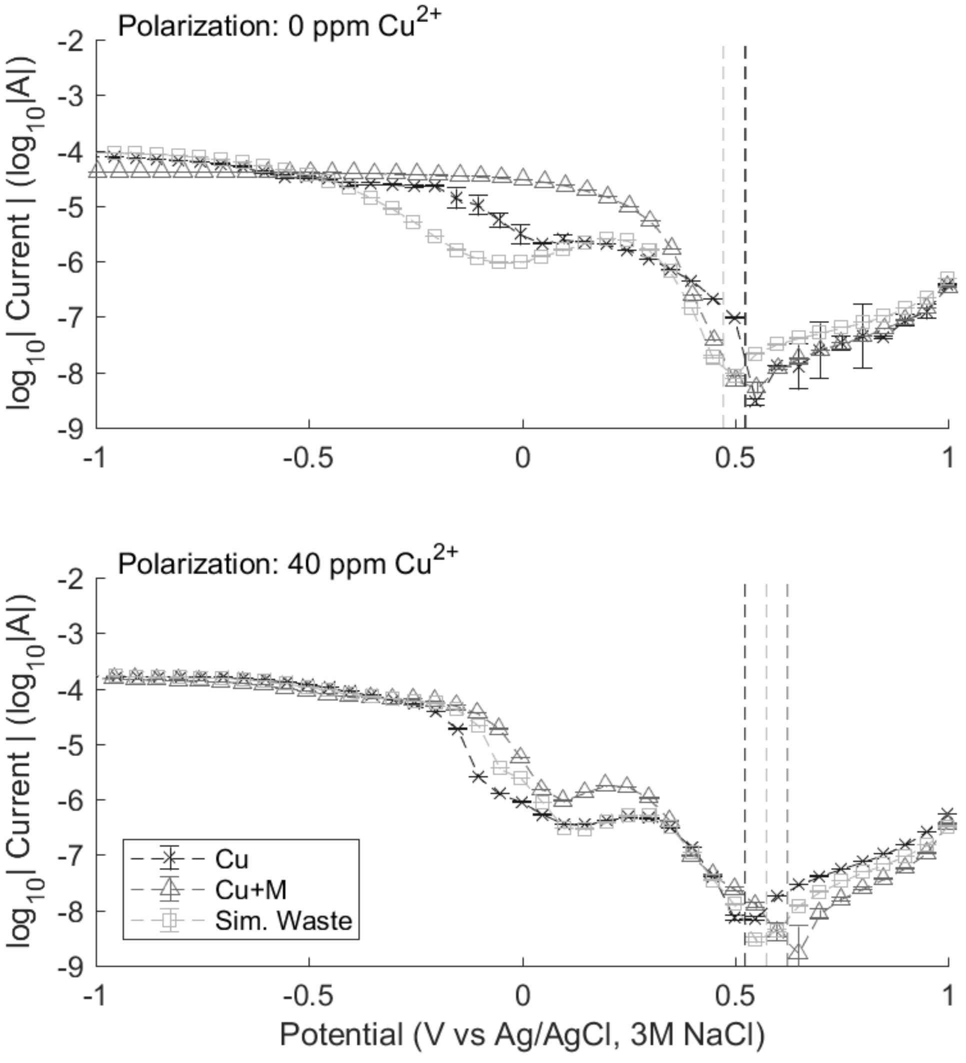

Figure 5.1.15: High resolution polarization curves for 0 ppm (top) and 40 ppm (bottom) Cu^{2+} in each of the tested solution compositions. Vertical lines indicate the point at which the current switches from anodic to cathodic.

One concern about the polarization curves was in the selection of the 0.5 to -0.5 V range and 0.1 V resolution, as this may have been too narrow and coarse to see any features clearly. Tests were conducted over the larger range of 1 to -1 V, using smaller potential steps (Fig. 5.1.15). These curves show that the initial shift from anodic to cathodic current occurs at significantly more positive potentials than expected at about 0.5 V, although there does appear to be a second decrease in current around the expected equilibrium potential of around 0.1 V.

While the current drop at 0.1 V does not appear when trace metal solution without copper is tested, both features are found in every other condition whether copper is present or not. This result seems to suggest that at this concentration, the contribution copper has to the polarization curve shape is very small and undetectable, and all conclusions made based on the previous polarization curves, most notably the Tafel slope and exchange current, may not actually describe behaviour specific to copper reduction. The only clear difference as a result of adding copper is in the current at sufficiently negative potentials, where the current is slightly more cathodic, agreeing with the findings presented in Fig. 5.1.13.

5.1.3 Bench Scale Plating

While electroplating copper using the RRDE setup is notably different than in the Porocell, it provides a more reproducible setup for analyzing the differences associated with the additional waste constituents. Thus, the motivation was not to optimize the current efficiency and minimize energy consumption at this scale, but rather to choose conditions that were highly consistent to compare results with and without compounds found in spent lees.

Measured net current efficiencies, calculated based on gravimetric changes to the cathode, are presented with respect to applied current in Fig. 5.1.16. For this experiment, all tests were scaled to pass the same number of Coulombs, leading to an expected change in mass of 1.4 mg at 100 % current efficiency. Looking simply at the distribution of the individual replicates, it is apparent that application of 25 μA led to the most consistent results. This is likely due to this current being high enough to avoid corrosion and low enough to avoid significant amounts of gas bubbles from hydrolysis.

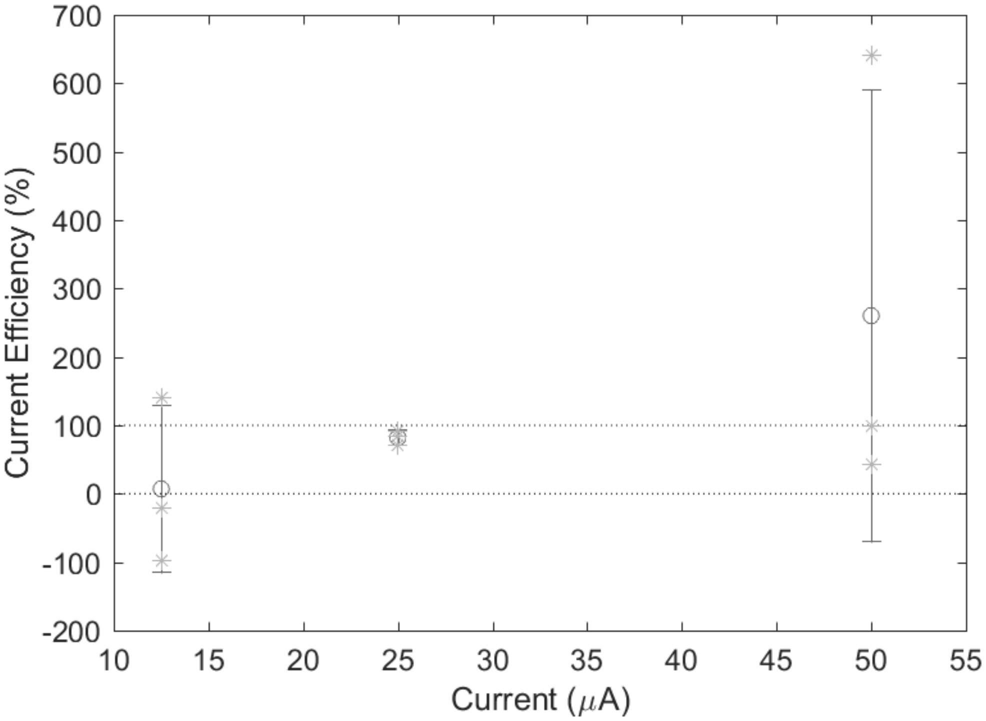

Figure 5.1.16: Current efficiencies of bench-scale copper plating for each current density, determined gravimetrically. Individual data points are represented by a (∗).

It was observed when conducting these tests that the timely removal of the electrode from the acidic copper solution was necessary to obtain accurate results. Otherwise, the copper on the electrode showed a spiral pattern reminiscent of the flow lines in a RRDE (Fig. 5.1.17). In fact, the direction of the spiral, where copper is only present on the outside of the ring and absent from the inside edge, is consistent with what one would expect if corrosion were the source. In an RRDE, solution passes from the center of the disk outward. As it passes over the copper, it would corrode that which was plated and increase in concentration, decreasing the driving force of corrosion as it moves toward the outside of the ring, resulting in more copper corrosion nearer the center.

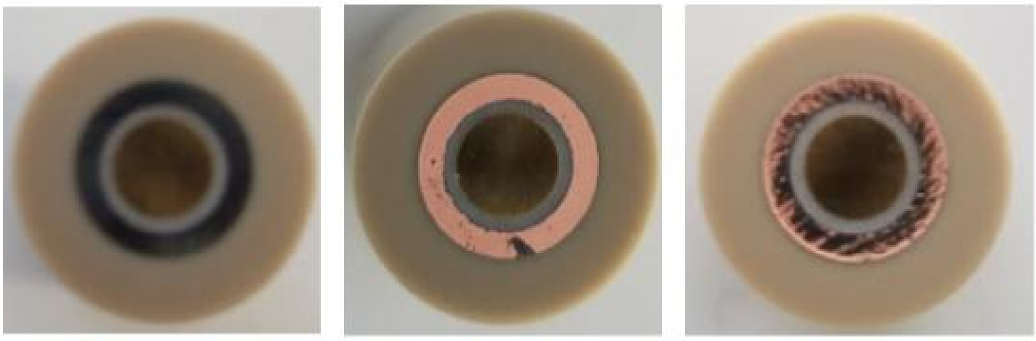

Figure 5.1.17: Photographs of the electrode before (left) and after (middle and right) plating. (Middle) A normal, ideal copper electroplating result, showing a relatively uniform copper coat on the platinum ring. (Right) The result when electroplating copper when the electrode was not removed soon after completion, instead left rotating in the acidic electrolyte for at least 30 minutes.

Knowing that a baseline quantity of corrosion occurs, slowly plating with a lower current would be impacted more by corrosion, leading to generally low current efficiencies. On the other hand, high current densities would also drive the rapid anodic production of oxygen gas, which may react with copper to form copper oxide. Since the efficiency was calculated gravimetrically, additional oxygen atoms in the oxide would increase the mass, leading to a higher calculated efficiency than reality. This may explain the abnormally high > 600 % current efficiency at 50 μA observed in Fig. 5.1.16. Given the consistency of the 25 μA test, this condition was used for comparison with the other solutions.

However, it became apparent that the observed reproducibility was not solely a result of the selection of the current density, as the addition of trace waste constituents did not produce similarly small standard deviations (Fig. 5.1.18), leading to statistically similar results ($p = 0.89$). While it is possible that this inconsistency is the result of the additives, the fact that the standard deviations are roughly similar in magnitude to the previous tests seems to imply that it is a procedural issue. Consequently, these results cannot lead to a confident conclusion about the effect of trace metals or of organic acids and anions on copper plating current efficiency, as any impact would be masked by the error associated with the process.

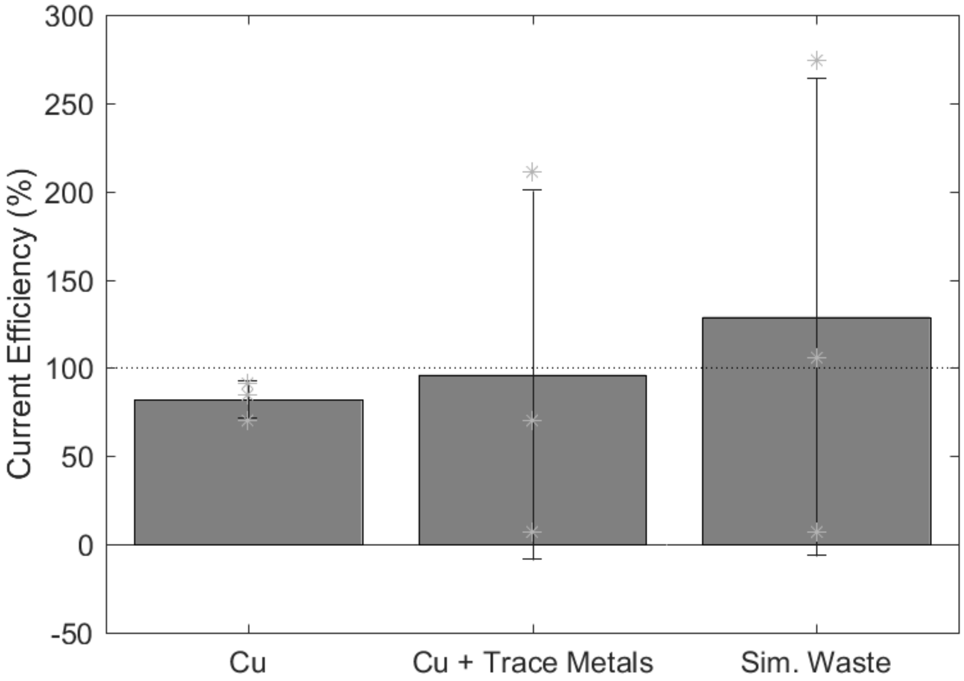

Figure 5.1.18: Current efficiencies of bench-scale copper plating for each solution composition, determined gravimetrically. All tests applied a constant 25 μA. Individual data points are represented by a (*).

One note to make is that some of the current efficiencies are very low, less than 10 %, with even some trials with 12.5 μA yielding negative efficiencies. With a gravimetric measurement, a negative Coulombic efficiency is only possible if the electrode lost mass over time. This cannot be due to corrosion, as the electrode starts with only a polished Au disk and Pt ring electrode, both of which would not corrode in conditions as mild as an aqueous metal solution of pH 4. This suggests that one of the major sources of error is the gravimetric measurement itself. A plot of the masses of the bare electrode before each test is presented in Fig. 5.1.19, showing the wide variability over time. Generally, one would expect the electrode to decrease in mass over time due to the mechanical polish slowly eroding the surface, and this trend is roughly true, albeit very weak and essentially negligible ($R^2 = 0.091$).

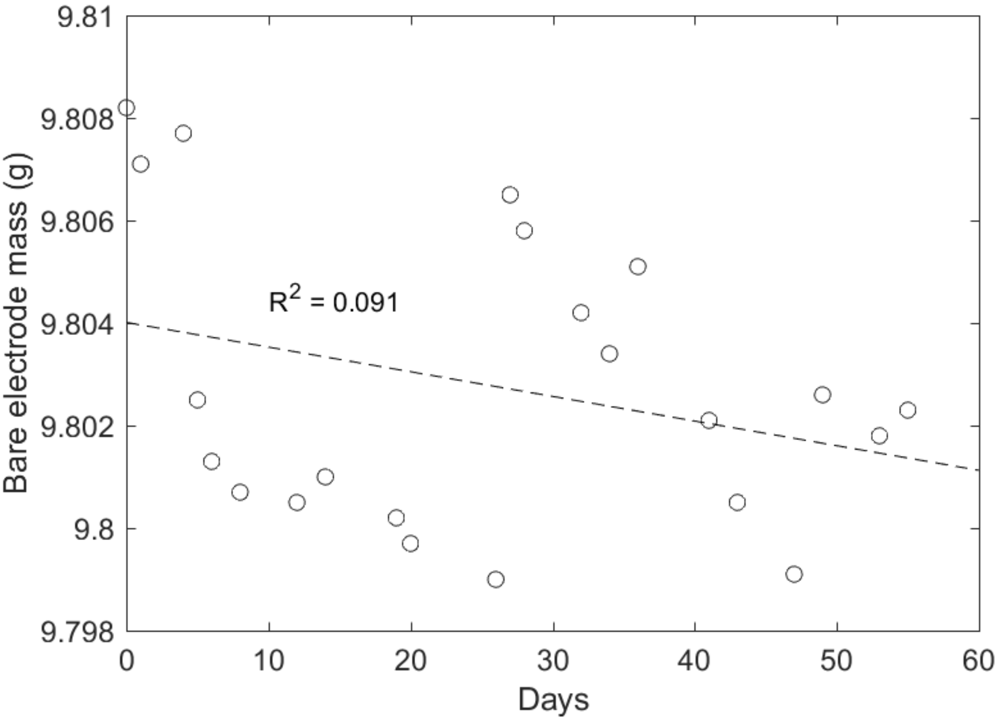

Figure 5.1.19: Change in the mass of the bare RRDE with time. A simple linear fit was used to determine how well it could estimate the mass loss due to polishing ($R^2 = 0.091$).

However, the day-to-day variability, due either to uncertainty in the analytical balance or due to insufficient washing and drying steps, spans approximately 10 mg. Since the tests were designed at the bench scale, a difference of only 1.4 mg was expected, so any current efficiencies are doubtfully accurate. While the test time could be extended to plate more copper to be much larger than 10 mg, a 100 mL solution of 40 ppm copper as used in these experiments only contains 4 mg of copper total, and test durations at 25 μA were already 48 hours long. Continuing tests for longer makes it more susceptible to ambient changes since the benchtop environment is not tightly controlled for factors such as temperature. On the other hand, shortening the time by increasing the current density becomes infeasible due to the low limiting current, and results at 50 μA have already demonstrated that a 2-fold increase is notably more inconsistent. The only other option would be to use a much larger electrode area, but doing so would require optimization with a new and potentially costly setup.

Therefore, current efficiency results at this scale are deemed inconclusive. Instead, the primary analysis performed with this data used results of high confidence: the measured potential. Profiles for the potential over time for all tests are presented in Fig. 5.1.20. It is apparent that application of higher currents led to higher magnitude electrode potentials, thereby increasing the cell voltage. Meanwhile, the difference due to addition of waste components appears to be small.

The difference is more apparent when using the mean potential after the first 5 hours when it had stabilized (Table 5.1.3). While the anode potentials do not change much with current magnitude, with the two lowest currents producing similar anodic potentials ($p = 0.49$), the cathode potentials are all statistically different ($p < 0.01$). This difference between changes in anodic and cathodic potentials simply means that the Tafel slopes for the anodic and cathodic reactions are different, with the cathodic plating reaction requiring greater increases in overpotential to achieve the same change in reaction rate.

Comparing the solution compositions, all anode potentials differ ($p < 0.01$), but the cathode potentials are all the same ($p = 0.52$). Here, the difference is promising, as it suggests that copper plating at this rate occurs at similar poten-

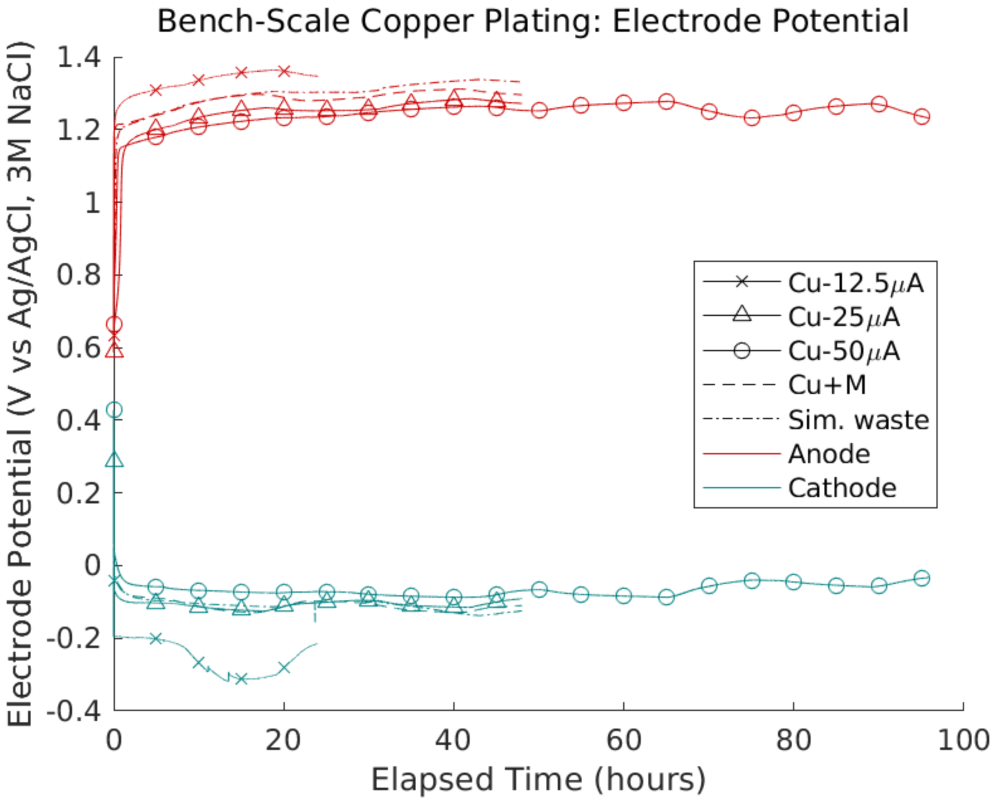

Figure 5.1.20: Electrode potentials of bench-scale copper recovery at each current density (symbols) and solution compositions (dashed and dotted lines). Data presented only samples the full dataset every 2 hours for simplicity of visualization.

Table 5.1.3: Differences in mean electrode potential due to current density and solution composition.

	Current (μA)	Cathode (mV)	Anode (V)
Copper only	12.5	-57 ± 10	1.22 ± 0.04
	25	-103 ± 9	1.25 ± 0.01
	50	-274 ± 7	1.33 ± 0.02
Copper and trace metals	25	-105 ± 23	1.28 ± 0.01
Simulated waste	25	-118 ± 16	1.31 ± 0.01

tials independent of the additional waste components. The difference observed in the CV regarding the standard reduction potential may be true, but it is small enough relative to the necessary overpotential that the difference is negligible. However, the anodic potentials are 1.25 ± 0.01, 1.28 ± 0.01, and 1.31 ± 0.01 V for copper alone, copper with trace metals, and simulated spent lees, respectively. The higher anodic potential for the oxidation reaction may suggest (a) that hydrolysis is impeded by the other reactants, (b) that another oxidation reaction is also occurring, such as Fe^{2+} to Fe^{3+} or the oxidation of the organic contaminants, or (c) that the solution is more resistive and requires a more extreme electrode potential to compensate, and the flatter anodic Tafel slope means that it is more readily observed with the anode potential than with the cathode potential.

However, when scaled up to the size of the Porocell, it is expected that these differences of less than 100 mV will not be observable due to the very high potentials needed at this scale. Also, if the hydrolysis reaction is simply being impeded, that is in part due to the platinum material of the counter electrode, which has a different chemical behaviour to the steel anode of the Porocell. Therefore, while this is useful to know that possible alternative anodic reactions may be occurring, or that the anodic reactions may be impeded due to the additives, this finding has less direct implication to the Porocell's operation.

One final calculation was performed using these potentials and currents to determine the amount of energy passed (Fig. 5.1.21). Due to the impracticality of normalizing to the mass of copper plated for easy comparison to reports in the literature [20, 24], the energy consumption was normalized instead to the number of Coulombs passed; doing so allows for a simple calculation in the future should a more definitive current efficiency be established for these conditions. As expected, higher currents required more energy due to the larger electrode potentials. On the other hand, the only statistically significant difference among solution compositions was observed between copper alone (5.79 ± 0.03 J/C) and the simulated waste (6.12 ± 0.07 J/C), $p = 0.005$, potentially due to the higher resistivity associated with the addition of all of the large organic compounds. This means that assuming similar current efficiencies, calculations of energy cost based on pure copper solution will underestimate the cost of recovery from spent lees, but likely by less than 10 %. This difference, however, would magnify the farther apart the anode and cathode are should this difference be the result of resistivity differences.

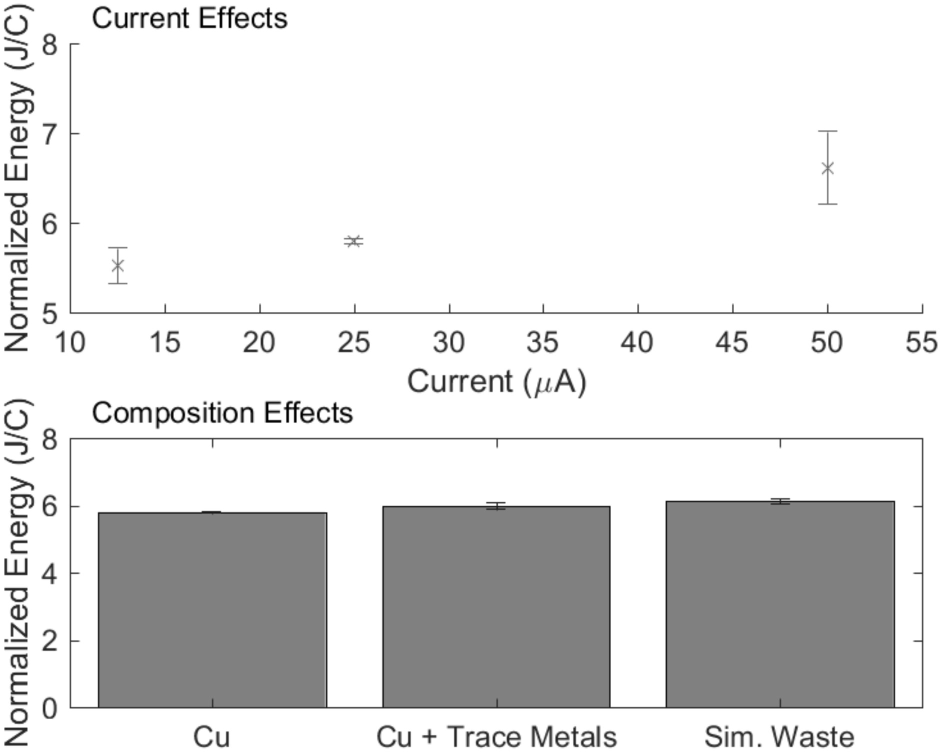

Figure 5.1.21: Differences in energy consumption per Coulomb passed due to current density (top) and solution composition (bottom).

5.1.4 Discussion

Generally, it was found that the addition of trace metals to pure copper solution led to negligible differences, if at all detectable. The further addition of organic acids and inorganic anions led to a slight negative shift in the reduction potential, but this difference did not seem to affect plating behaviour.

However, all of these measurements show notable errors attributable to the experimental methods, which may mask the differences between these conditions. Uncertainties in the diffusion coefficient were based on range of potentials of the

CV, which were narrower than desirable due to the observation of large background currents that would mask the copper plating reaction peaks. Polarization curves, due to the low concentration, rapidly reached the limiting current, resulting in almost no region from which reasonable kinetic data could be extrapolated. Finer resolution polarization curves place doubt in the validity of attributing many features to copper reduction. Attempts to quantify the amount of copper plated at this scale resulted in mass differences too small for reliable measurements, limiting the analyses to comparisons based on the electrode potentials.

Despite these uncertainties, in being too small to detect, the differences that may exist as a result of the other components in spent lees all appear to be too small to have any appreciable effect on the Porocell operation. For instance, prior literature with the Porocell [24, 77, 76] tends to operate at voltages greater than 3 V, so the differences of less than 300 mV are likely to have negligible impacts compared to the independent variables tested. Therefore, one can say with confidence that despite the inconclusiveness of many of these results, the fact that possible differences to copper electrochemistry due to other waste constituents are inconclusive indicates that the differences are too small to have an appreciable impact at the scale used in copper recovery.

5.2 Idealized Porocell Copper Recovery

Preliminary tests (Appendix B) were performed to establish the constraints and analytical methods for assessing copper recovery the Porocell. Briefly, due to the good sensitivity and selectivity of the ion selective electrode, it was selected as the analytical method to determine how much copper was plated. It does show some dependence with time and pH, but correction factors have been established to accommodate those variables. The Porocell's flow rate limits were measured and validated, showing that the actual range of flow rates is about 1.0 to 3.7 L/min; since this difference is less than a factor of 4 apart, only the two extremes were tested. The electrodes were treated with strong acid to degas the electrode and improve surface wetting, which was believed to impede the current. Due to the high solution resistance and the 10 V limit of the potentiostat used, a current range of 35 to 105 mA was selected. While this is slower than other tests in the literature, it may prove to be more economic at this concentration due to the copper's low transport limited current as previously established.

The bench scale tests demonstrated that there are small, if significant, differences between weakly acidic copper sulphate solution and simulated spent lees. This allowed for simplification of the test solution from simulated spent lees, which contain a number of trace metal ions and organic compounds, to 40 ($\pm$ 2) ppm Cu^{2+} at pH 4. The copper can then be recovered using the Porocell by applying current, which would result in copper reduction at the cathode. These experiments are intended to test how flow rate and current will affect how fast, efficient, and energy intensive copper recovery from spent lees would be if using the Porocell.

5.2.1 Flow rate and current density effects

Changes to the cupric ion concentration over time for operation with the Porocell for all combinations of flow rate and current density are presented in Fig. 5.2.1. When no current is applied, the concentration of copper in solution appears to increase, likely the result of any copper plated onto the electrode from previous tests corroding. This may be the reason why the higher flow rate resulted in higher concentrations for all time points, as faster flow rates would likely accelerate corrosion by increasing transport from the electrode surface back into the bulk.

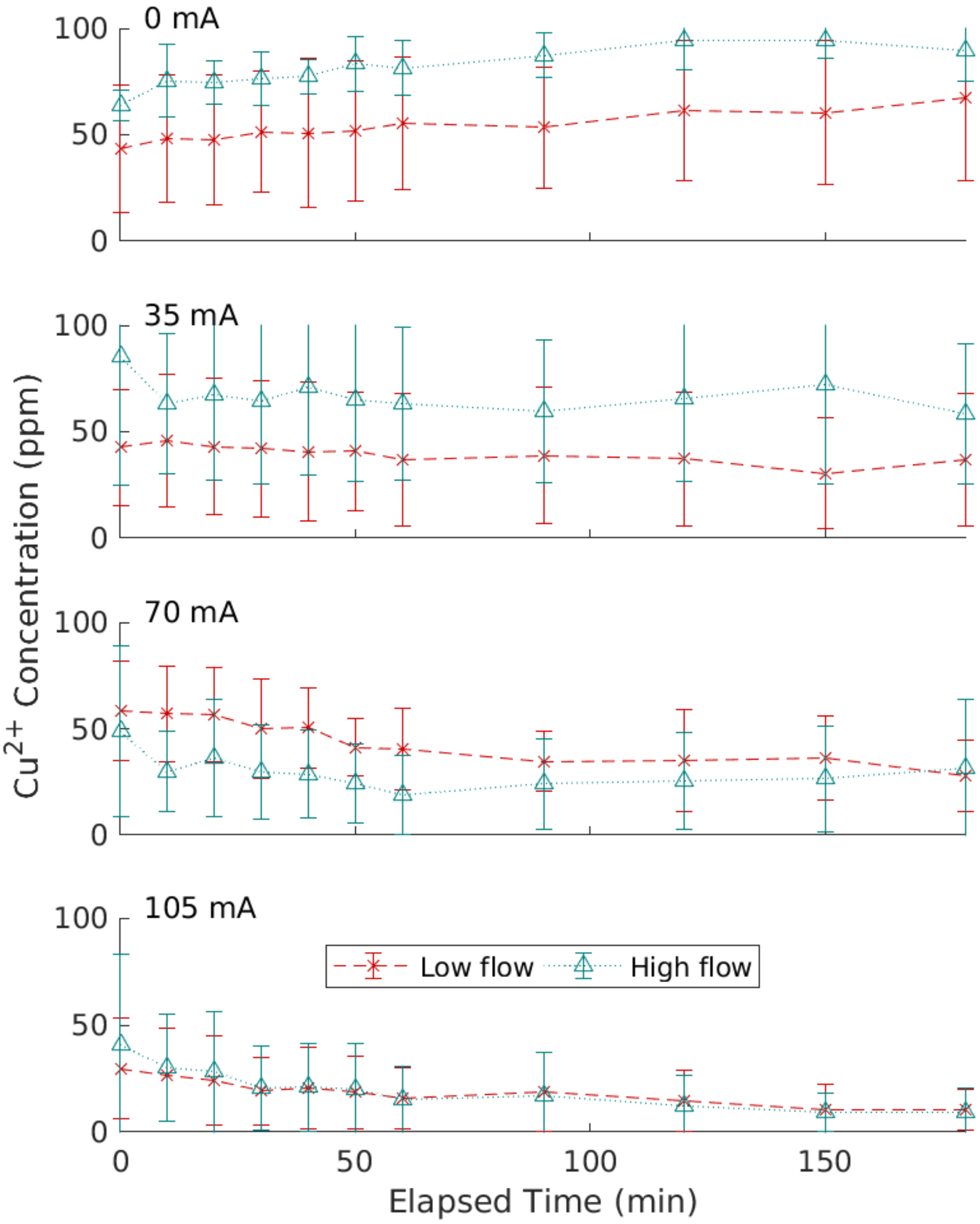

Figure 5.2.1: Measured concentration change of copper over the course of 3 hours of galvanostatic operation using the Porocell, starting with a 40 ppm Cu^{2+} (pH = 4) test solution. Error bars indicate the standard deviation (n = 4).

While this difference between the high and low flow rate is small relative to the error, the small difference in measurements may be due to the small difference in flow rate that can be achieved. Alternatively, it appears that the measurement of the starting concentration for the high flow rate is slightly larger than the starting concentration of the low flow rate despite both solutions starting exactly the same, so the difference in flow rate may be negligible.

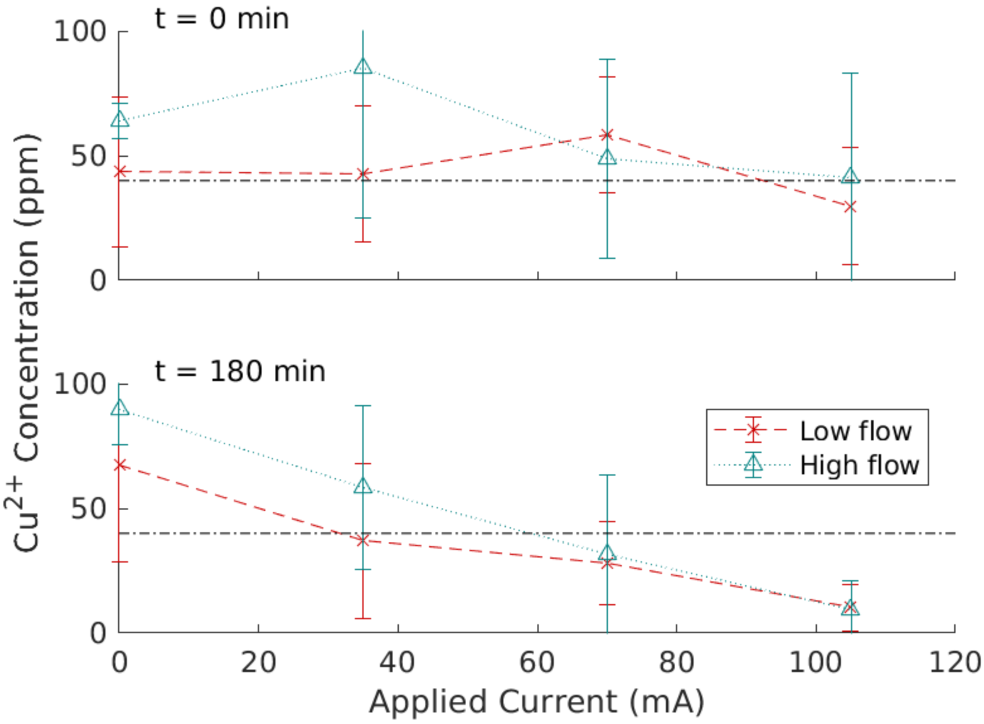

Figure 5.2.2: Concentration of copper before (top) and after (bottom) electrochemical recovery from a 40 ppm Cu^{2+} ($pH = 4$) test solution with the Porocell. Error bars indicate the standard deviation ($n = 4$). Dotted horizontal line indicates the known starting concentration of 40 ppm.

As expected, when current is applied, the copper concentration decreases, with higher currents accelerating the rate of copper plating. At 35 mA, this difference is small enough that the concentration is nearly constant over the 3 hour tests, suggesting that this is near the minimum current necessary to counteract the corrosion rate. When the current is increased, the rate at which the concentration drops accelerates, leading to lower copper concentrations at the end of 3 hours. This difference is more easily seen in Fig. 5.2.2, which isolates the starting and ending concentrations for comparison.

The concentration differences at the start are notable given that all tests were performed with a solution of 40 $\pm$ 2 ppm Cu^{2+} in 66.7 μM H_2SO_4, designated in the figure with the horizontal dotted line. Most starting measurements are within one standard deviation of the known concentration, but the accuracy is relatively low, varying from 85.1 $\pm$ 60.0 ppm (35 mA, high flow rate) to 29.7 $\pm$ 23.5 ppm (105 mA, low flow rate). The low accuracy with this measurement places uncertainty in the remainder of the results for later time points.

Despite this uncertainty, there is a clear trend at 3 hours, where higher currents lead to lower concentrations. This is what one would expect for a current-limited system, as increasing the current leads to faster reduction. While it may appear that the measurements are more consistent at 3 hours, this may be because the measurement error is proportional to concentration, making it more reliable at lower concentrations, as shown in Eq. 5.1.

$$d\left[Cu^{2+}\right] = \left[Cu^{2+}\right]\left(dV_{ISE} - d(int) + \frac{int - V_{ISE}}{slp^2}d(slp)\right) \tag{5.1}$$

The uncertainties associated with the high concentrations do present a problem with determining the net Coulombic efficiency, which was calculated based on the change in concentration (Eq 2.4). This leads to propagated errors where the Coulombic efficiency seems to be either much higher than 100 % or lower than 0 % (Fig 5.2.3). The values becomes more reasonable as time progresses, likely because the lower concentrations at later times provide more confidence in at least one measurement; this trend is easily apparent in Fig. 5.2.4, which compares the net efficiency of the first 10 minutes to the net efficiency for the full 3 hour duration.

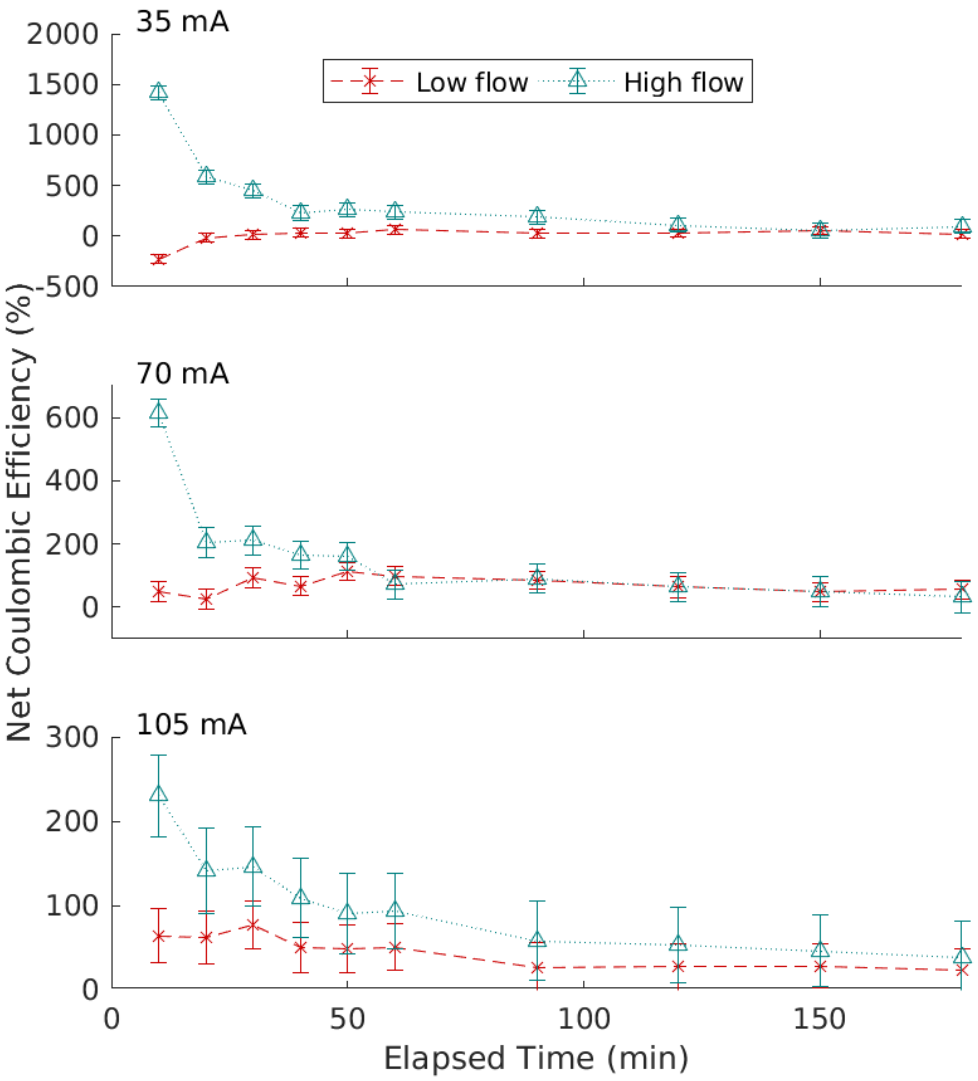

Figure 5.2.3: Net Coulombic efficiency for copper recovery from a 40 ppm Cu^{2+} (pH = 4) test solution using the Porocell, calculated using the measured concentration change over time. Error bars indicate the propagated standard deviation (n = 4).

Interestingly, the initial 10 minutes consistently show the low flow rate condition to be less efficient than the high flow rate condition independent of current magnitude. This is counter to what one would expect based on the observed faster corrosion at the high flow rate, which should cause the efficiency to decrease. The difference between flow rates does decrease over time, becoming negligible at 3

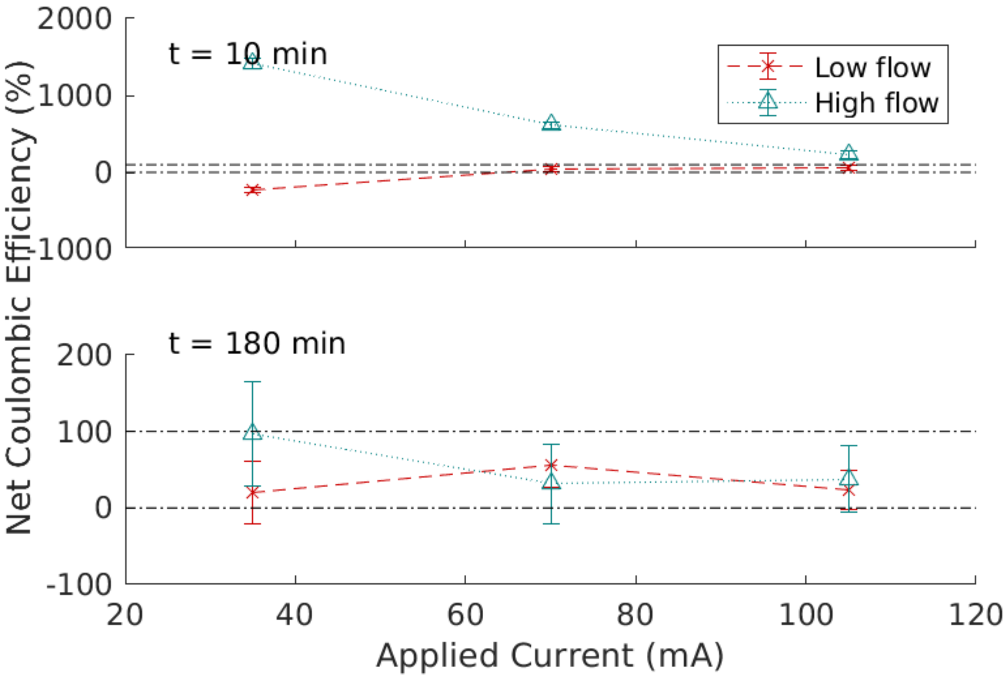

Figure 5.2.4: Isolation of the net Coulombic efficiency for copper recovery from a 40 ppm Cu^{2+} (pH = 4) test solution for the first 10 minutes (top) and for the full test duration (bottom), calculated using the measured concentration change over time. Error bars indicate the propagated standard deviation (n = 4). Dotted horizontal lines note the realistic bounds of 0 % and 100 % efficiency for ease of interpretation.

hours (p = 0.23). It is likely that the initial difference is related to the start up time of the process, as the Coulombic efficiencies do not appear to be stable until 90 minutes have elapsed. Initial flow rate differences also appear to decrease as the current increases, likely because the higher current leads to lower concentrations, which produce more reliable measurements. Overall, though, there is no difference in net current efficiency with current (n = 0.46), implying that the net efficiency is around 30 %.

This similarity, however, seems to be related to the large uncertainty associated with measuring the starting concentration. If performing the calculation based on the starting concentration as prepared (40 ± 2 ppm Cu^{2+}), the Coulombic efficiencies show a consistent trend between the low and high currents (Fig. 5.2.5).

Lower current generally leads to lower efficiency, likely related to the larger relative contribution of corrosion. This is supported by the fact that high flow rates, which may accelerate corrosion by increasing transport, tend to lower Coulombic efficiency, and flow rate becomes less of a contributor as the current increases.

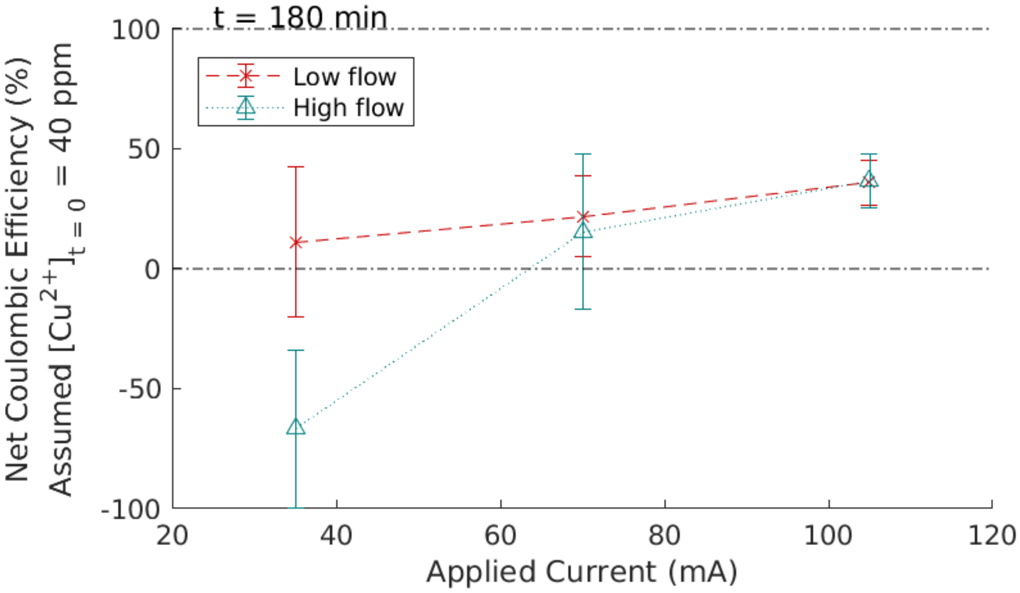

Figure 5.2.5: Recalculation of net Coulombic efficiency for copper recovery from a 40 ppm Cu^{2+} (pH = 4) test solution for the full duration of 3 hours, assuming the initial concentration to be 40 ± 2 ppm as prepared. Error bars indicate the propagated standard deviation (n = 4). Dotted horizontal lines note the realistic bounds of 0 % and 100 % efficiency for ease of interpretation.

However, using the known starting concentration still does not yield reasonable results for all conditions. The negative efficiency for the 35 mA, high flow rate condition does not reflect the measured result that the concentration appears to decrease with time from 85.1 ± 60.0 ppm to 58.4 ± 32.9 ppm (Fig. 5.2.1). The high concentration and subsequently large uncertainty of this measurement does suggest that the change in concentration would be small, so the trend of high current leading to higher efficiency is still supported in spite of the uncertainty.

As a consequence of the uncertainties associated with the ISE measurements, an alternative calculation was devised to determine the change in concentration. The measurements with the ISE rely on changes to the solution composition as a result of the cathodic half reaction. However, one could instead use the changes caused by the anodic half reaction to infer the cupric ion concentration change based on the reaction stoichiometry. In the present conditions for the Porocell, the most favorable anodic reaction is oxygen evolution:

$$H_2O \rightarrow 2H^+ + \frac{1}{2}O_2 + 2e^- \tag{5.2}$$

Therefore, in order for copper to be reduced at the cathode, protons must be generated at a stoichiometric ratio of one mole of copper to two moles of protons. Conveniently, the pH must already be measured due to the ISE's pH sensitivity. Therefore, the starting pH (pH_0) and the pH at time t (pH_t) can be used to estimate the change in copper concentration ($\Delta \left[Cu^{2+}\right]_t$) according to Eq. 5.3:

$$\Delta \left[Cu^{2+}\right]_t = -\Delta \left[H^+\right]_t /2 = (10^{-pH_0} - 10^{-pH_t})/2 \tag{5.3}$$

While one might expect this method to overestimate the copper ion change with a low Coulombic efficiency 30 %, where the anodic half-reaction is the same whether the cathodic half reaction is copper reduction or a parasitic reaction, the solution chemistry allows for this relationship to hold true independent of Coulombic efficiency. With this solution composition, the parasitic cathodic reactions are likely to be oxygen reduction, which is simply the reverse of Eq. 5.2, or hydrogen evolution, which would consume the protons that were generated by the anodic half-reaction. As a result, no pH change would be expected if no copper were removed. The only other compound in solution that could react with

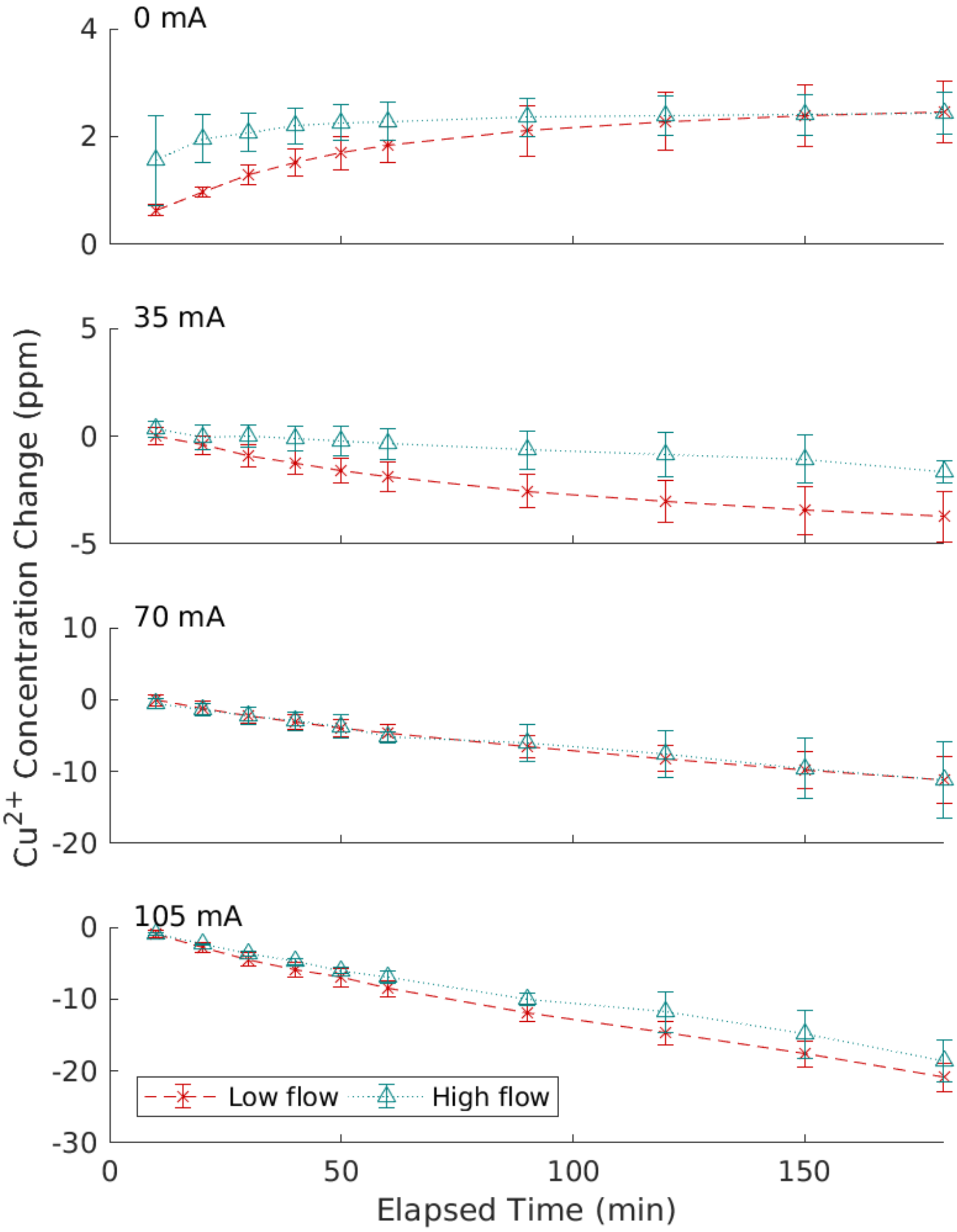

Figure 5.2.6: Predicted change in copper concentration of the 40 ppm Cu^{2+} ($pH_{t=0} = 4$) test solution based on the change in pH. Error bars indicate the propagated standard deviation (n = 4).

protons are the sulphate ions, which have a pK_a of -3 and thus will not bind to protons at pH 3 to 4.

Using the pH changes, the expected change in copper concentration is presented in Fig. 5.2.6. These changes are generally smaller than those observed with the ISE, but with much smaller standard deviation. The trends are also very similar, with high flow rates appearing to cause more positive changes (higher concentration), and this effect is lost as current increases.

When no current is applied, the rate at which the copper concentration increases appears to asymptotic (Fig. 5.2.6), suggesting that while copper will corrode, it does not progress beyond a certain point. At that point, the copper concentration is potentially high enough that the equilibrium potential for copper reduction is the same as the equilibrium potential for oxygen reduction, leading to no net reaction. As with measurements with the ISE, as current increases, the change in concentration becomes more rapid, leading to lower concentrations at the end of 3 hours.

The calculated current efficiency with this method provides much more reliable results (Fig. 5.2.7), with all but two individual measurements across all conditions and times (0 mA, high flow rate, $t = 10$ min and $t = 30$ min) falling within the realistic bounds of 0 and 100 %. The flow rate and current density effect observed before is repeated, with high flow rates generally causing lower Coulombic efficiency, and the effect decreasing at higher current densities. The consistency in this finding between these two calculation methods suggests that this effect is not simply a result of random chance, as it could have been with the highly uncertain ISE measurements.

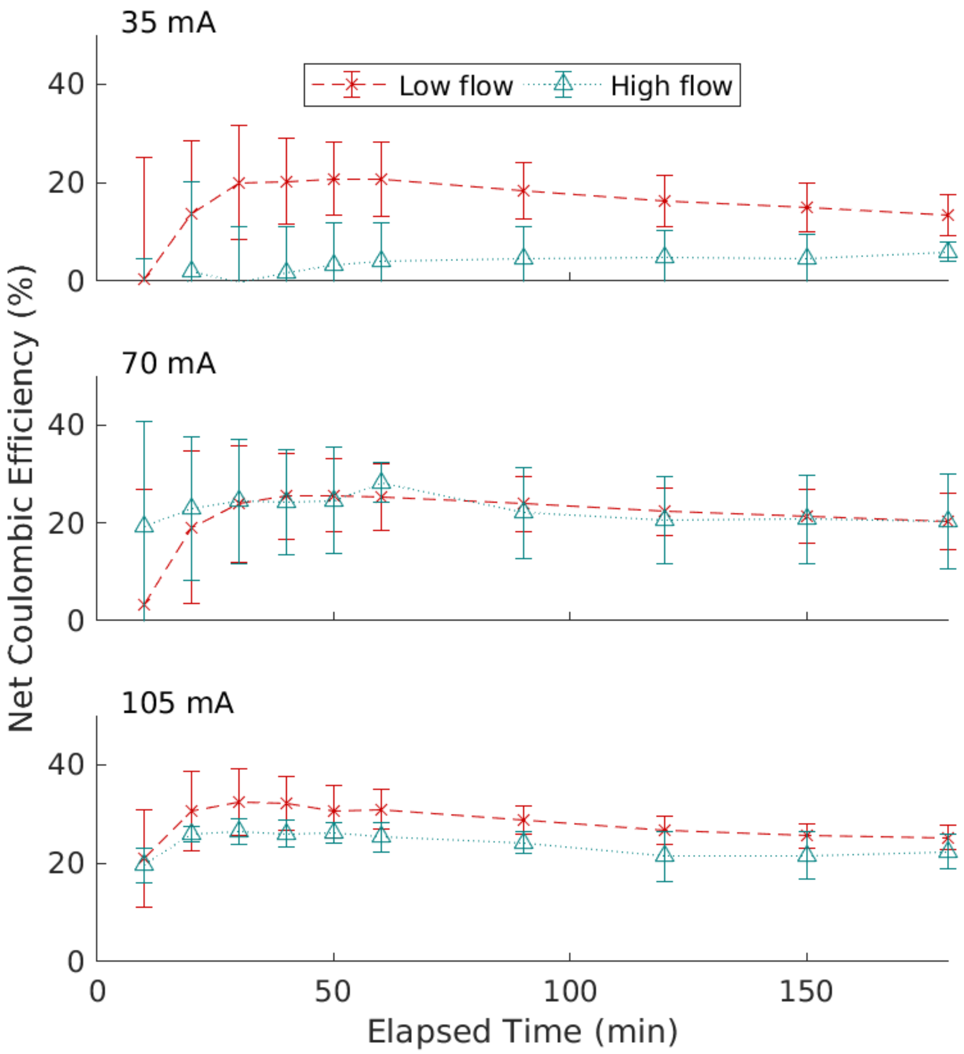

Figure 5.2.7: Predicted Coulombic efficiency of copper reduction from a 40 ppm Cu^{2+} ($pH_{t\,=\,0} = 4$) solution based on the change in pH. Error bars indicate the propagated standard deviation (n = 4).

Interestingly, the current efficiency starts low, but then increases and stabilizes over time, despite the lower concentration leading to a lower limiting current. The low starting efficiency may be the result of capacitive charging, where little reaction is occurring. The stabilization over time may mean that the currents remain below the mass transport limit despite the decreasing concentrations. Stabilization at such low efficiencies suggests there may be significant parasitic side reactions or the corrosion reactions counteracting copper plating. The net current efficiency for the 3 hour duration are presented in Table 5.2.1.

Table 5.2.1: Mean Coulombic efficiency of copper recovery from a 40 ppm Cu^{2+} (pH = 4) solution for each flow rate and current tested after 3 hours of Porocell operation, calculated based on the changes in pH. Uncertainty indicates one standard deviation (n = 4).

	Low flow rate (1 L/min)	High flow rate (3.7 L/min)
35 mA	13.5 $\pm$ 4.2 %	6.0 $\pm$ 1.9 %
70 mA	20.3 $\pm$ 5.8 %	20.3 $\pm$ 9.6 %
105 mA	25.2 $\pm$ 2.5 %	22.3 $\pm$ 3.5 %

While it does appear that the Coulombic efficiency of the high flow rate condition is generally lower, the difference is not large enough across all current conditions to yield statistically significant differences ($p = 0.12$). There is, however, a notable difference between applying 35 mA and applying either 70 mA ($p = 0.003$) and 105 mA ($p < 0.001$). The difference between the net Coulombic efficiency when applying 70 mA or 105 mA is not large enough to be significant ($p = 0.42$).

This general trend with current does suggest it may be possible to achieve higher current efficiencies at higher currents, so long as it is below the mass transport limit. Based on the changes in copper concentration (Fig. 5.2.6), 105 mA already causes an order of magnitude larger difference to concentration (20.1 $\pm$ 2.0 ppm decrease over 3 hours) compared to corrosion (2.5 $\pm$ 0.6 ppm increase over 3 hours). Therefore, it is possible another order of magnitude difference may lead to a completely insignificant contribution from corrosion, at which point the maximum current efficiency would be achieved. Doing so requires use of a different potentiostat, as the one used in these experiments could not accommodate a sufficient voltage for this amount of current; results from tests using a power supply capable of generating this much voltage are reported in Section 5.3.5.

5.2.2 Reaction kinetics

A complete analysis of this process requires knowledge of the necessary duration to achieve the desired final concentration of 2 ppm. For each condition tested, the final concentration never fell below 9.5 ppm as measured by ISE, or 19.1 ppm as predicted by the change in pH and the known starting concentration. Therefore, the concentration profiles were fit to kinetic models to estimate the necessary process duration.

For the zeroth order case, the concentration will decrease linearly over time, with the slope of the line equal to the zeroth order rate constant (Eq. 2.9). Therefore, a linear regression was performed (Eq. A.3) between $[Cu^{2+}]$ and t. For the first order case, the concentration follows an exponential decay (Eq. 2.10). In this case, $\ln[Cu^{2+}]$ will be proportional to t, and the slope of this linear regression will be the first order rate constant.

Since it is unknown whether the reactor is operating under zeroth or first order kinetics, the concentration measurements were fit to both models, and the coefficient of determination (R^2) of the fits compared (Fig. 5.2.8). This metric, broadly speaking, estimates the percentage of variance that can be attributed to the model, so the rate order should be discernible by comparing the results. Generally, it appears that low current densities fit better to zeroth order kinetics, while higher currents tend to operate closer to first order kinetics. However, the strength of both fits are not particularly strong, with all R^2 values less than the desired 0.95. The difference between zeroth and first order is small, with the largest difference of 0.14 for 105 mA at high flow rates more than double the next largest difference of 0.064 for 105 mA at low flow rates.

As a result, the rate constants for both rate orders are presented in Fig. 5.2.9. The trends follow what is expected based on the concentration profiles, with faster

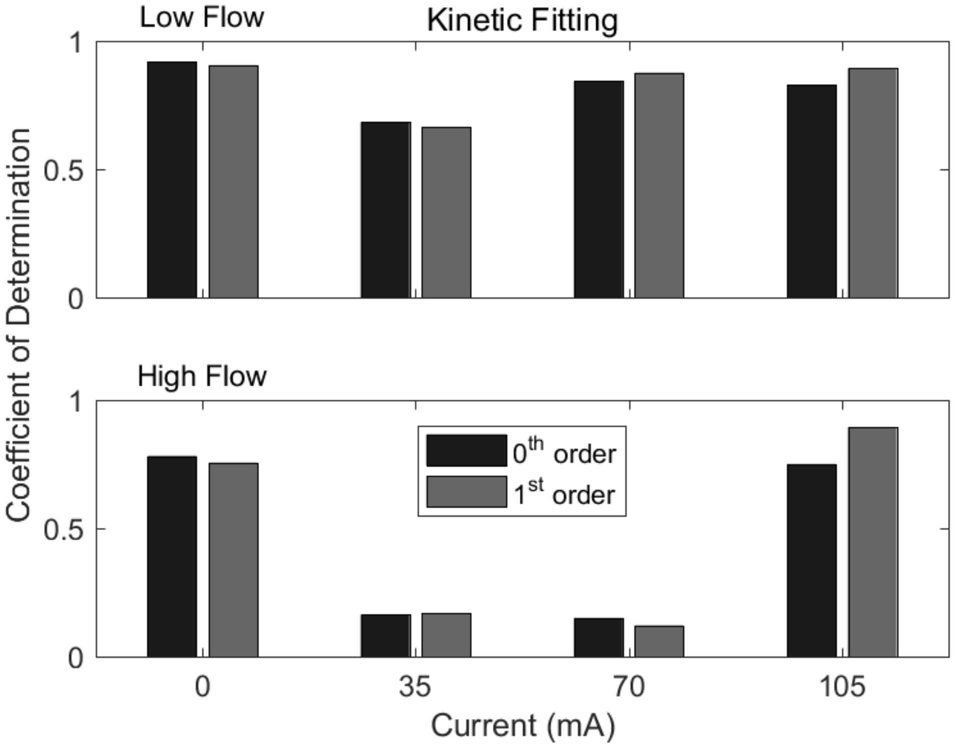

Figure 5.2.8: Coefficient of determination (R^2) when fitting the mean measured concentration profile (Fig. 5.2.1) to 0th or 1st order kinetics.

rates associated with higher current. The exact values help discern a possible reason for why the rate order cannot be determined: the magnitude of the first order rate constants are less than 10^{-2} min^{-1}. Such a low first order rate constant would mean the 180 minute test duration would be less than or nearly equal to all time constants, so the concentration profile will appear similar to a line even if it is first order.

The trend of higher current densities appearing more first order while the lower current densities appear more zeroth order agrees with the initial hypothesis that the higher the current, the more likely the kinetics will be limited by the copper concentration and transport. However, this result does not agree with previous results, which suggest that the mass transport limit requires potentials greater than those tested (Fig. B.14) and that the current efficiency, which drops when

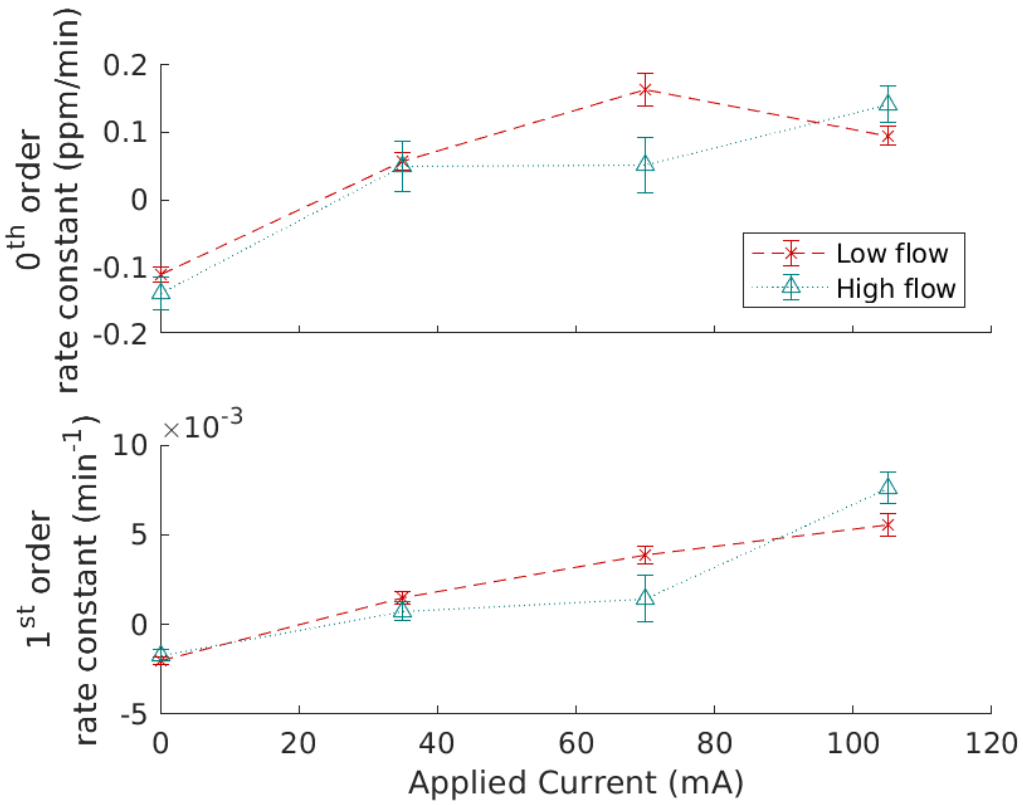

Figure 5.2.9: Values for the rate constant, k, when fitting the mean measured concentration profile (Fig. 5.2.6) to 0th order (top) or 1st order (bottom) kinetics via linear regression. Error bars indicate the uncertainty of the fit.

applying current above the limiting current, seems to increase with current in the range tested (Table 5.2.1).

A more reasonable result is found when fitting the copper concentration changes predicted by pH to the kinetic models (Fig. 5.2.10). All conditions strongly prefer zeroth order kinetics. At these low current densities, this result makes more sense, as the slow supply of electrons are likely to drive the kinetics. The poor quality of the first order kinetic fits lead to large uncertainties in those rate constants, particularly compared to the small uncertainties associated with the zeroth order rate constants (Fig. 5.2.11). These values also do not have the same physical meaning, as negative first order rate constants are defined as increases in copper concentration, which is not what was observed.

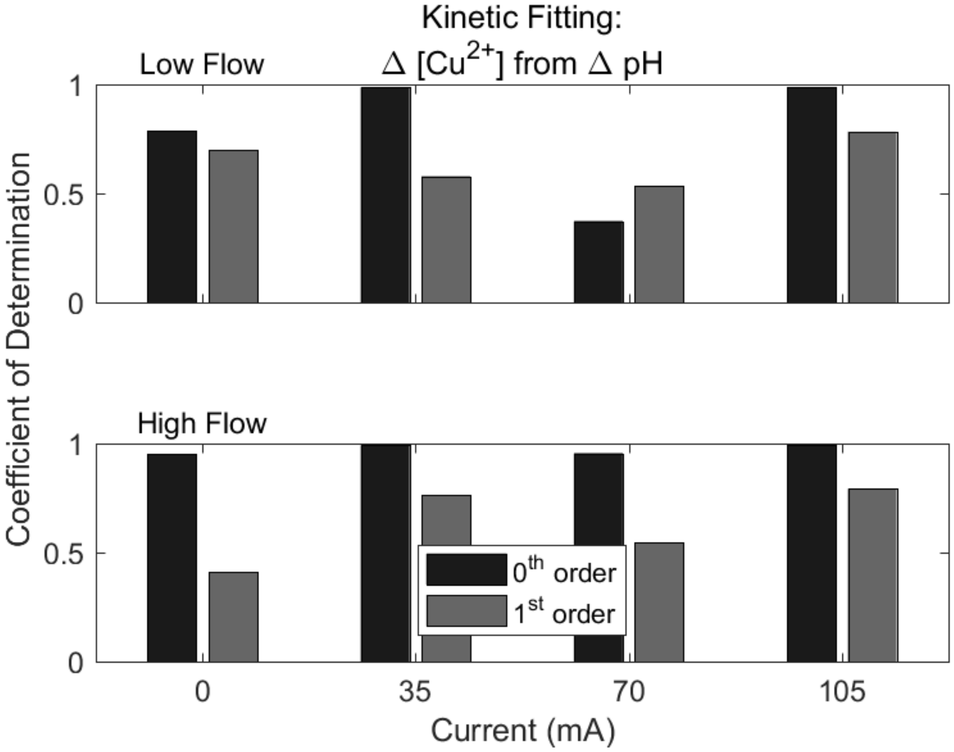

Figure 5.2.10: Coefficient of determination (R^2) when fitting the predicted concentration change based on pH changes (Fig. 5.2.6) to 0^{th} or 1^{st} order kinetics.

Additionally, the values for the zeroth order rate constants are of similar magnitude whether using pH or the ISE measurements, but first order kinetic rate constants are of different orders of magnitude. Given that the zeroth order kinetics both fit the more consistent pH-based measurements better and also have calculation method-independent rate constants, it is more likely that the reaction operates under zeroth order kinetics.

As a result, the zeroth order rate constants from fitting the ISE and pH-based measurements were used to calculate the operation time necessary to recover enough copper to change the starting concentration of 40 ppm to the target concentration of 2 ppm according to Eq. 2.9. Solving for time, t, gives Eq. 5.4.

$$t = \frac{[Cu^{2+}]_{t=0} - [Cu^{2+}]_{t=end}}{k_0} = \frac{38}{k_0} \tag{5.4}$$

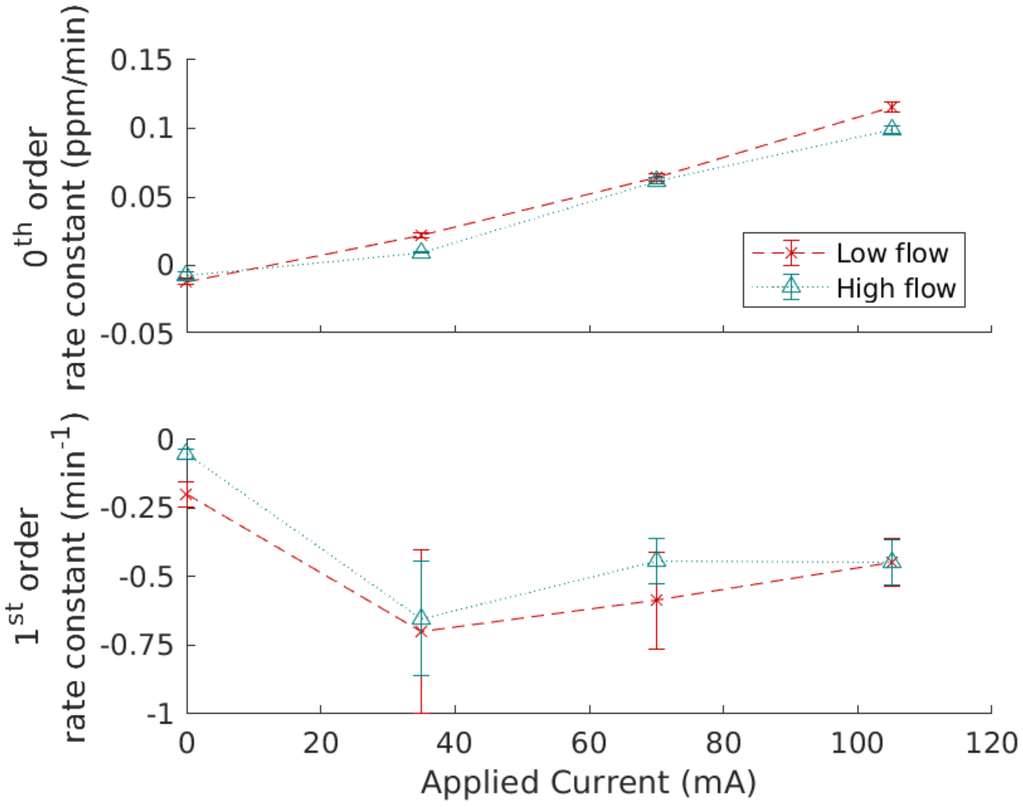

Figure 5.2.11: Values for the rate constant, k, when fitting the predicted concentration change based on pH changes (Fig. 5.2.6) to 0th order (top) or 1st order (bottom) kinetics via linear regression. Error bars indicate the uncertainty of the fit.

Applying the general form for propagation of error (Eq. A.8) gives the standard deviation of this result, s_t, which is a function of the uncertainty of the zeroth order rate constant, s_{k_0}, according to Eq. 5.5.

$$s_t = \frac{[Cu^{2+}]_{t=0} - [Cu^{2+}]_{t=end}}{k_0^2} * s_{k_0} = \frac{38}{k_0^2} * s_{k_0} \tag{5.5}$$

As a result of the uncertainties of the ISE leading to a worse quality fit, the uncertainties using this kinetic model are much higher and the expected trend of higher current leading to shorter operation times is not as evident. However, using the rate constant based on pH changes leads to a clear and obvious trend with much smaller standard deviations.

Table 5.2.2: Operation time (hours) necessary to treat 40 ppm Cu^{2+} (pH = 4) to 2 ppm Cu using the Porocell, as predicted by zeroth order kinetics. The error is the standard deviation, based on the uncertainty of the kinetic fit.

	Low flow rate	High flow rate
Based on fit to concentration from ISE		
35 mA	10.96 ± 2.49	12.72 ± 9.61
70 mA	3.87 ± 0.56	12.33 ± 9.75
105 mA	6.67 ± 1.01	4.48 ± 0.86
Based on fit to concentration change from pH		
35 mA	28.85 ± 2.18	66.53 ± 4.77
70 mA	9.82 ± 0.40	10.28 ± 0.40
105 mA	5.49 ± 0.17	6.37 ± 0.17

These operation times are likely underestimates for the desired process, as lower concentrations of copper should lead to lower limiting currents, which may lead to an eventual switch to slower first order kinetics as the copper concentration becomes limiting. However, in using 40 ppm Cu as the starting concentration, which is the highest recorded concentration in spent lees and roughly double its mean concentration, this operation time is a good starting point from which the process can be optimized. Additional analysis confirmed these results by extending the process duration (Section 5.3.4).

5.2.3 Energy consumption

While a shorter operation time is desirable, one must consider that the shorter operation times require higher current, and thus may require greater energy. This is because as current increases, more voltage is needed to drive that increase. The Porocell voltage change over time is presented in Fig. 5.2.12.

It is evident from the plot that the higher the current, the higher the voltage, but the relationship is not linear. The open circuit potential is approximately 0.8 V, and there is a large difference of 2 V between no current and 35 mA. However, doubling the current to 70 mA only requires 5 V to start and 3.8 V after 3 hours;

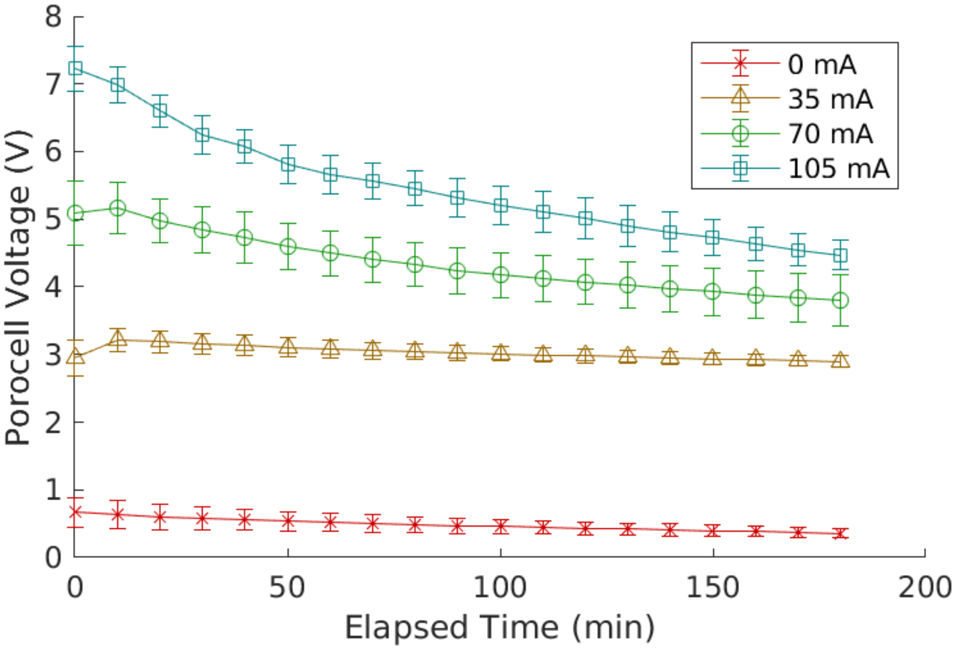

Figure 5.2.12: Porocell voltage change over time when run galvanostatically with a 40 ppm Cu^{2+} (pH = 4) test solution. Plot shows samples every 10 minutes for ease of visualization. Error bars indicate the standard deviation (n = 4).

105 mA requires 7.2 V at the start and only 4.5 V after 3 hours.

The initially high voltage to start is typical of a plating reaction, as the energy barrier for nucleation tends to be larger than the energy barrier for grain growth [50]. While one would expect the necessary voltage to increase with time due to the lower copper concentration and the Nernst equation, the difference in equilibrium potential of the cathode changes from 150 mV at the start to 111 mV vs Ag/AgCl when at the limit of detection. As a result, the cell voltage difference due to the concentration change is very small compared to the activation and Ohmic overpotentials, which collectively are on the order of multiple volts.

The nonlinear relationship between current and voltage is expected based on the Butler-Volmer equation for Faradaic current, as large differences in current can be achieved with small changes in voltage with sufficient activation overpotentials.

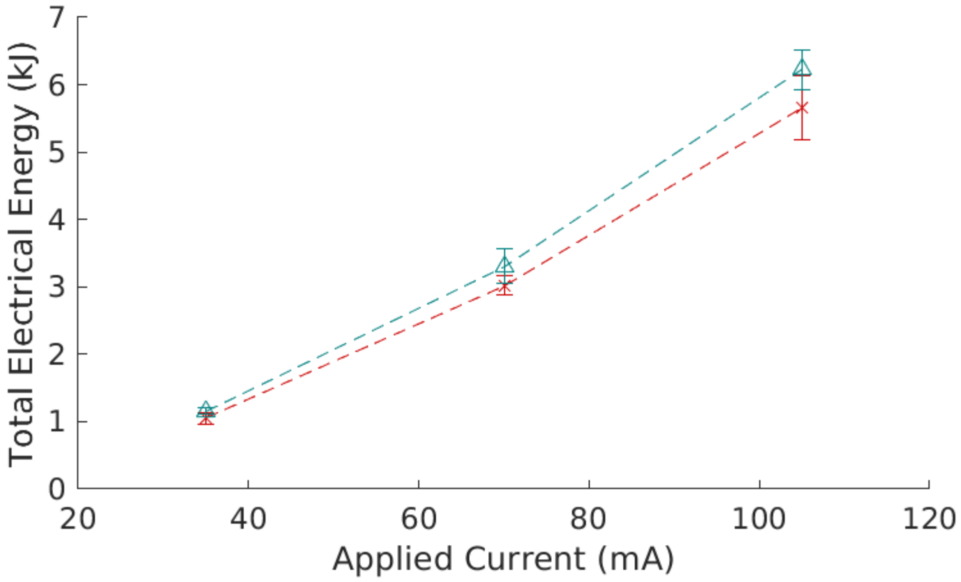

Figure 5.2.13: Total energy consumption of the Porocell when run galvanostatically for 3 hours of operation at each current with a test solution of 40 ppm Cu^{2+} (pH = 4). Error bars indicate the standard deviation (n = 4).

As a result, the relationship between current and electrical energy used in the reaction is close to a line, not a quadratic as it would be if this were a simple resistor (Fig. 5.2.13). This value alone is not useful, though, as while the 105 mA condition requires the most electrical energy, it also recovers the most copper in 3 hours. Therefore, the energy required per unit of copper recovered is presented in Fig. 5.2.14.

As with current efficiency calculations, the ISE's inherent imprecision, particularly at higher concentrations, is the result of the large uncertainty in the amount of copper recovered. This then propagates to an uncertainty in the normalized energy cost that is greater than the value itself. As a result, one cannot make any conclusion about the trends, as they all appear to be similar to each other. Some of that uncertainty can be eliminated by using the known starting concentration

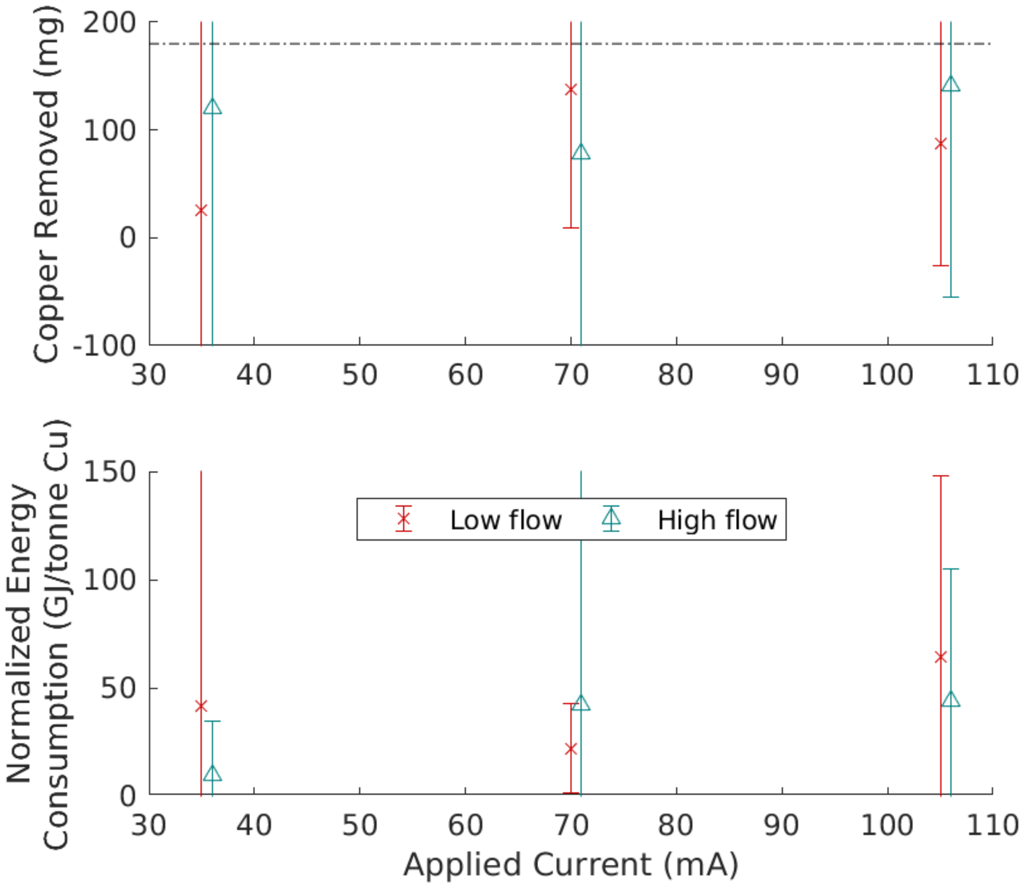

Figure 5.2.14: (top) Mass of copper recovered (top) and normalized electrical energy cost for 3 hours of operation of the Porocell (bottom), based on the measured starting and ending concentrations of a 40 ppm Cu^{2+} (pH = 4) test solution. Dotted horizontal line notes the total quantity of copper in the batch.
Error bars are the propagated standard deviation (n = 4). Data points are slightly offset on the x-axis for ease of visualization due to overlapping error bars.

of 40 ± 2 ppm (Fig. 5.2.15), thereby showing that 105 mA, by virtue of recovering more copper in 3 hours, results in lower energy costs per gram of copper.

If instead using the change in pH (Fig. 5.2.16), the difference among different currents decreases, with almost all results approximately the same at about 60 GJ/tonne. The only exception is when applying 35 mA with a high flow rate, where the high corrosion rate likely causes the necessary energy cost to more than double to 156 ± 50 GJ/tonne. As a result of this one outlier, the statistics imply

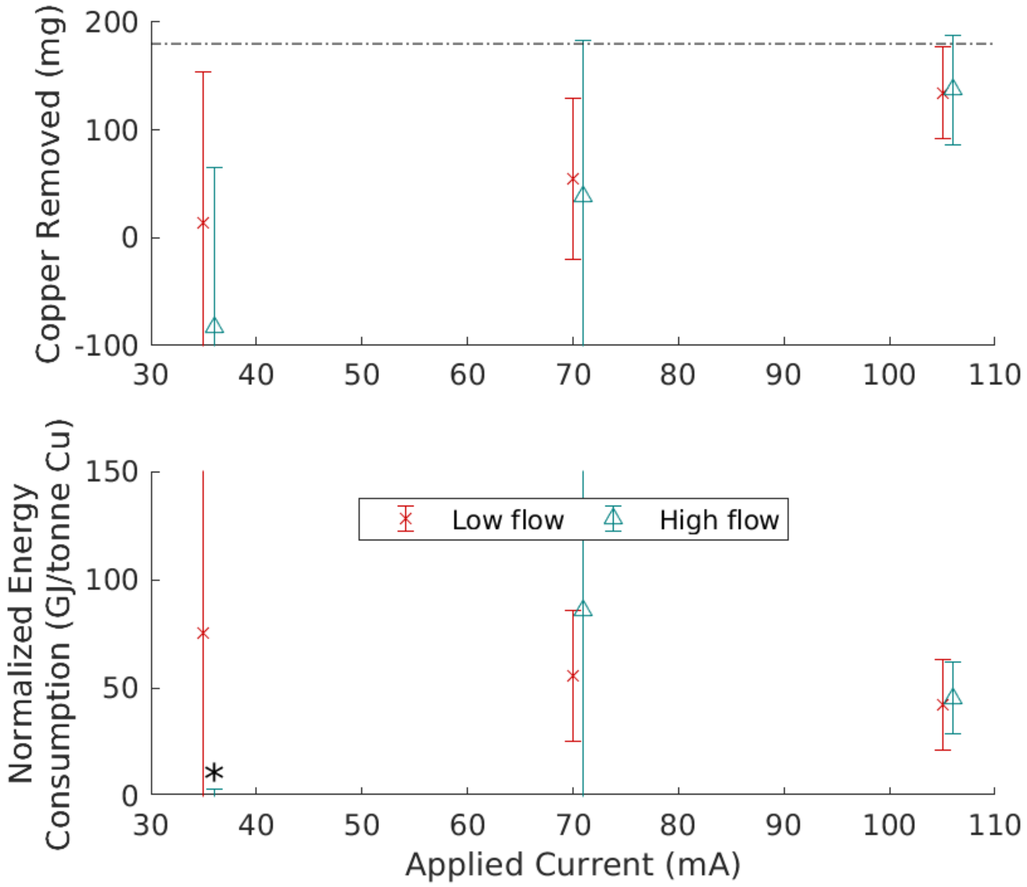

Figure 5.2.15: Mass of copper recovered (top) and normalized electrical energy cost for 3 hours of operation of the Porocell (bottom), based on the known starting concentration of 40 ± 2 ppm and the measured concentration at 3 hours. Error bars are the propagated standard deviation (n = 4). Data points are slightly offset on the x-axis for ease of visualization due to overlapping error bars.

that both flow rate and current have significant effects ($p = 0.002$ and 0.005, respectively), but only when the 35 mA condition is included; 70 mA and 105 mA are nearly indistinguishable independent of flow rate ($p = 0.94$).

Comparing the calculations with pH to the other methods, while the trend is different, the similarity in the magnitude of the value, which is consistent independent of what assumption are made, indicates that 40 to 60 GJ/tonne is a suitable estimate for this process.

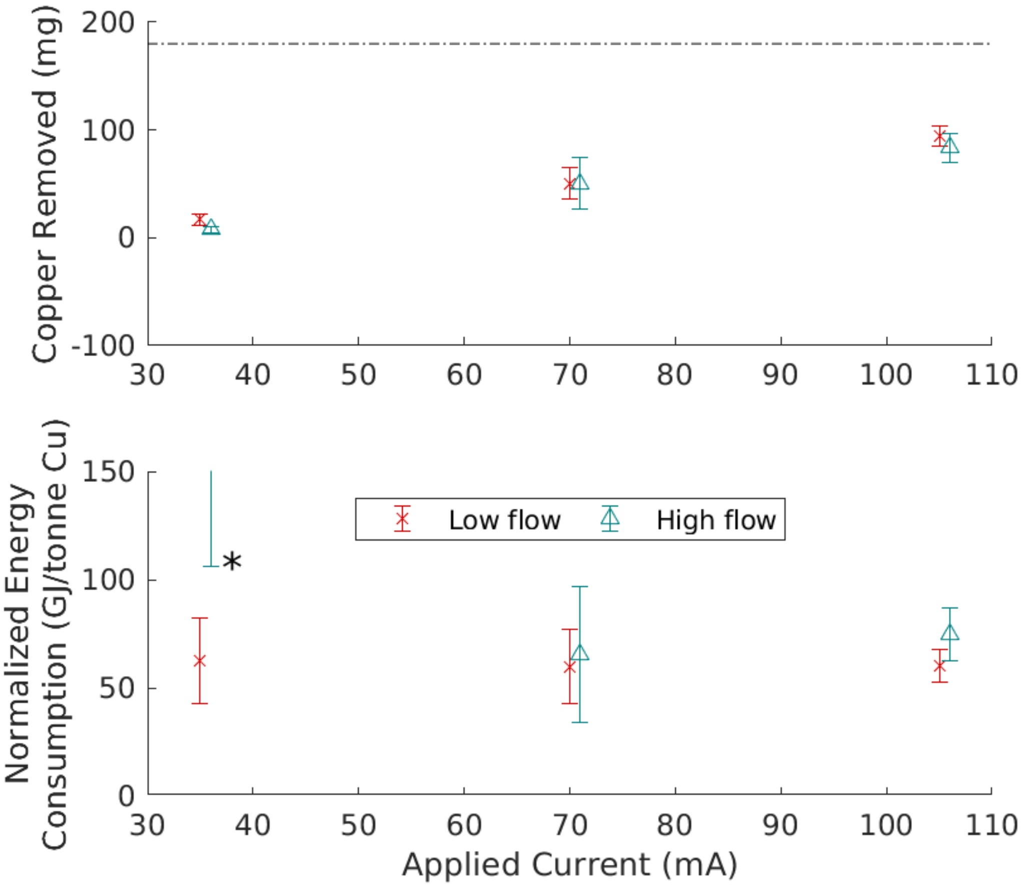

Figure 5.2.16: Mass of copper recovered (top) and normalized electrical energy cost for 3 hours of operation of the Porocell (bottom), based on the change in pH of a 40 ppm Cu^{2+} ($pH_{t\,=\,0} = 4$) test solution and Eq. 5.3.
Error bars are the propagated standard deviation (n = 4). Data points are slightly offset on the x-axis for ease of visualization due to overlapping error bars.

Compared to existing copper-producing processes, this estimate is high, as the benchmark of pyrometallurgical ore purification consumes about 10.9 GJ/tonne [20], and recovery processes should be cheaper in order to be industrially feasible. However, primary mining is expected to require more energy as time goes on due to mine depletion leading to lower grade ores [19, 23], so this may become more economic in the coming years.

Even when compared to other copper recovery attempts with the Porocell, the value is high. However, the reported 1.2 GJ/tonne [24] used significantly more conductive waste. Given that these results have a higher current efficiency of 25 to 35 % compared to their reported 13 %, the increased energy cost is entirely related to the high resistivity. Therefore, decreasing the energy cost is simply a matter of reducing the Ohmic drop.

5.2.4 Extended time testing

While initial kinetic estimates for the operation time have been made, the calculations rely on the assumption that the process will remain at zeroth order kinetics for the full duration. This assumption may be false, for there will be a point where the concentration of copper is sufficiently low that its transport will limit the kinetics. At that point, the kinetics will decrease according to first order kinetics, leading to a slightly longer process duration. At present, it is unknown what the limiting current for 2 ppm Cu is with the Porocell, so it is unknown how valid that assumption is.

Therefore, each current was tested once at high flow rate for 26 hours, for the initial kinetic calculations predict at least the 70 mA and 105 mA current conditions will reach 2 ppm in less than half that time. The voltage profile for these long tests is presented in Fig. 5.2.17. The open circuit potential does slightly decrease over time, potentially due to differences on the electrode surface while plated copper corrodes, the pH increases, and ions adsorb or desorb.

While the expected trend of higher current requiring higher voltage is true initially, it does not remain true for all time. The 70 mA condition requires the greatest voltage between hours 4 and 8, but requires less voltage than the 35 mA condition after about 19 hours of operation. This may be due to the difference in current leading to different rates at which protons are generated as a byproduct, thereby making the solution more conductive at different rates.

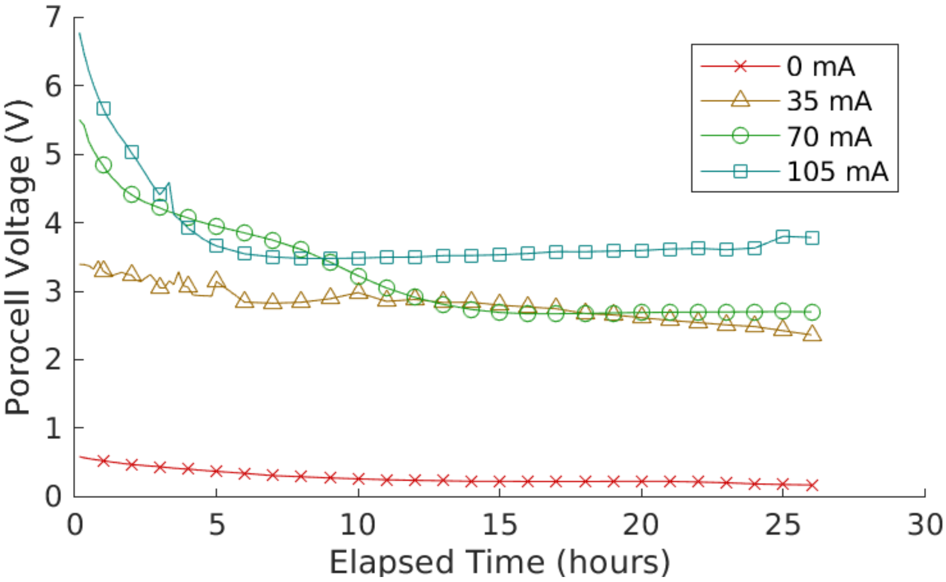

Figure 5.2.17: Porocell voltage change over the course of 26 hours of galvanostatic operation with a 40 ppm Cu^{2+} (pH = 4) solution.

As previously m-entioned, as copper ions are plated, they are replaced by two protons to maintain the charge balance. Since protons are much smaller than copper ions, they would be able to migrate in the electric field more easily, making the solution more conductive. At higher currents, this change will occur more rapidly, leading to a more rapid decrease in resistivity and therefore more rapid decrease in voltage. Since it is believed the majority of the voltage is related to the solution resistance, the voltage should be highly responsive to these changes, leading to the shifts in relative voltage over time.

This change in voltage will only continue until there is no net change in copper concentration. Based on the concentration measurements (Fig. 5.2.18), this occurs sometime between hour 4 and 23 for the 70 and 105 mA conditions, after which the measured concentration is 0.24 and 2.6 ppm, respectively. The lower concentration for 70 mA than 105 mA may simply be an artefact of the ISE's accuracy, as it was previously established that the calibration is most accurate between 2 and 100 ppm (Table B.2).

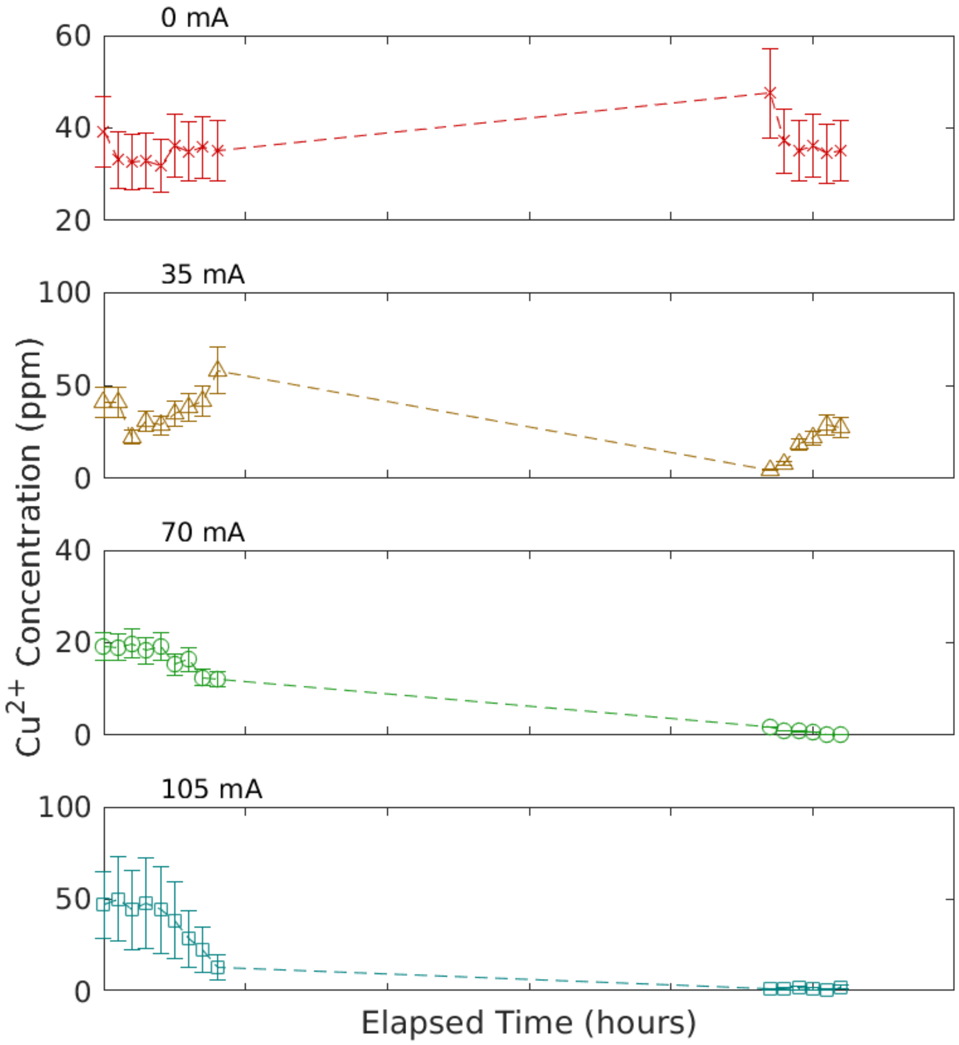

Figure 5.2.18: Measured concentration of copper ions of a copper sulphate solution (pH = 4) over the course of 26 hours. Error bars indicate the uncertainty in the single measurement associated with the ISE.

It is uncertain whether the 0 mA baseline corrosion test equilibrates, as it appears to have increased between hours 4 and 23, but decreases after that. Knowing that the uncertainty is greater at higher concentrations, this may simply be a stochastic measurement error, particularly since all measurements after 23 hours are within a standard deviation of each other.

The abnormal behaviour for the 35 mA condition, however, cannot be as easily explained, as it is unknown why the concentration would start to increase again after 23 hours. It is possible that the increased acidity due to copper plating increased the corrosion rate, but given how slow the process is from the kinetic analysis, it is not likely that the system would underdamped, which it would need to be in order for this overshoot to occur. Additional replicates of this test are necessary to have more confidence in whether this is a repeatable phenomenon or an inaccuracy in the measurements.

When using Eq. 5.3 to estimate copper concentration change using the change in pH, the copper concentration seems to continue to drop for all applied current conditions despite the increases the ISE measurement implies (Fig. 5.2.19). These pH measurements confirm both that there is no notable change after 23 hours when applying 0, 70, or 105 mA and that the total concentration change when 70 or 105 mA current is applies is roughly 40 ppm, the total amount of copper present at the start.

Since when copper is no longer being plated, the only reactions occurring are anodic and cathodic hydrolysis, the conductivity of the solution after that point should remain constant. Since the voltage is believed to be predominantly the effect of solution resistance, while the exact time at which copper concentration stopped changing was not measured directly, it can be estimated by finding the time at which the voltage reaches steady state. These estimates are reported in Table 5.2.3.

As expected, the higher current of 105 mA takes less time to reach a steady state voltage, at which point the copper concentration should be similar to the concentration measured after 23 hours. Applying 70 mA requires more than double the time, despite applying 66 % of the current, likely a result of the

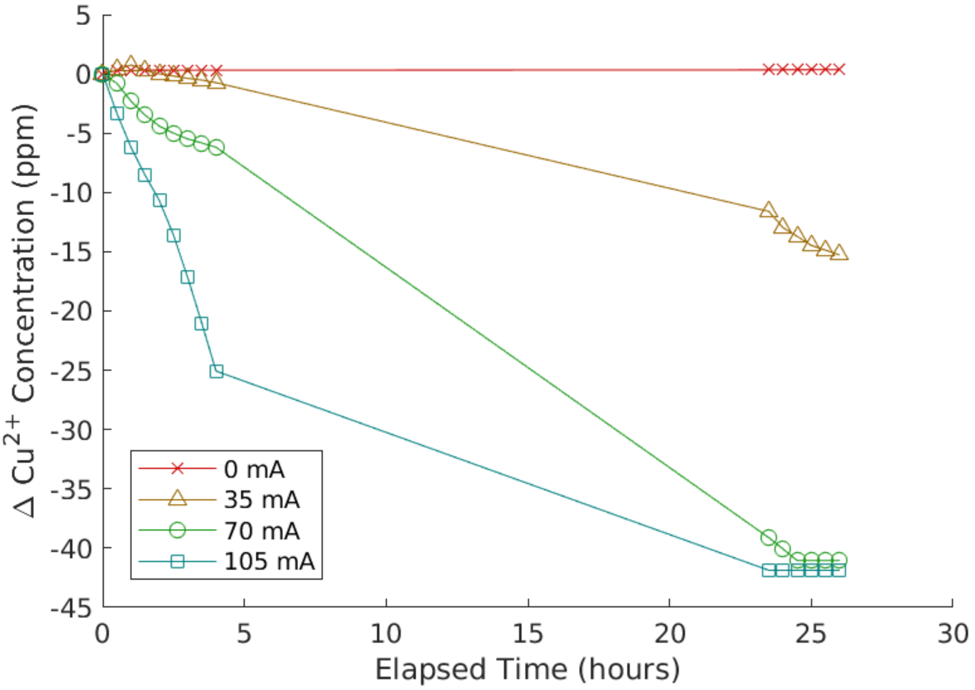

Figure 5.2.19: Predicted change in copper concentration of a 40 ppm Cu^{2+} ($pH^{t\,=\,0}$) solution calculated from the change in pH and Eq. 5.3.

Table 5.2.3: Key values from galvanostatic Porocell operation with a starting solution of 40 ppm Cu^{2+} for 26 hours.

	0 mA	35 mA	70 mA	105 mA
pH (t = 0)	4.89	4.09	4.25	4.21
pH (t = 26 hr)	5.72	3.25	2.87	2.86
[Cu^{2+}] (t = 26 hr) (ppm)	35	27	0.24	2.6
Time to steady state (H:MM)	NA	> 26:00	13:15	5:37

lower current efficiency. Interestingly, the time for 105 mA is roughly the same as the prediction based on zeroth order kinetics, while the time for 70 mA is about 3 hours longer than the prediction. While the exact cause of the deviation is unknown, it may be related to the lower pH accelerating corrosion, thereby making it more significant and reducing the current efficiency even further over time, and this effect being more pronounced with a slower plating rate.

5.2.5 High voltage testing

As previously mentioned, current efficiencies are generally quite low, with estimates less than 50 %, despite the current being much lower than the mass transport limited current. Thus, while parasitic side reactions may be occurring, it is not likely to explain the entirety of the low efficiency, as they are more significant at currents above the transport limit. The presence of a corrosion reaction in the absence of current and the near-zero recovery rate at 35 mA suggests that the inefficiency may be related to corrosion reactions reversing the plating reaction. As current increases, the rate at which plating occurs increases, causing a reduction to the effect of corrosion relative to plating.

To test this hypothesis, an additional test was conducted at 1.05 A using a power supply, as an additional order of magnitude higher current should make the corrosion reaction effectively negligible. This should lead to an even higher Coulombic efficiency assuming the transport limit has not been achieved. The voltage profile for this test is presented in Fig. 5.2.20. Before 20 minutes, the voltage is capped due to the power supply switching to potentiostatic mode if it requires more than 20.20 V to drive the 1.05 A. After 20 minutes, sufficient nucleation and capacitive charging had occurred to bring the necessary voltage below 20.20 V, at which it consistently drove the desired current.

The concentration change over time, both measured by ISE and estimated by change in pH, are presented in Fig. 5.2.21. Both indicate that the concentration should effectively be zero after 120 minutes, with the only difference between them being the relative magnitude change. Measurements with the ISE suggest that the concentration starts only at 22.9 $\pm$ 6.3 ppm, even though it was prepared as a 40 $\pm$ 2 ppm solution. The pH change, in contrast, agrees with the expectation, showing that the total change in concentration after 120 minutes is approximately

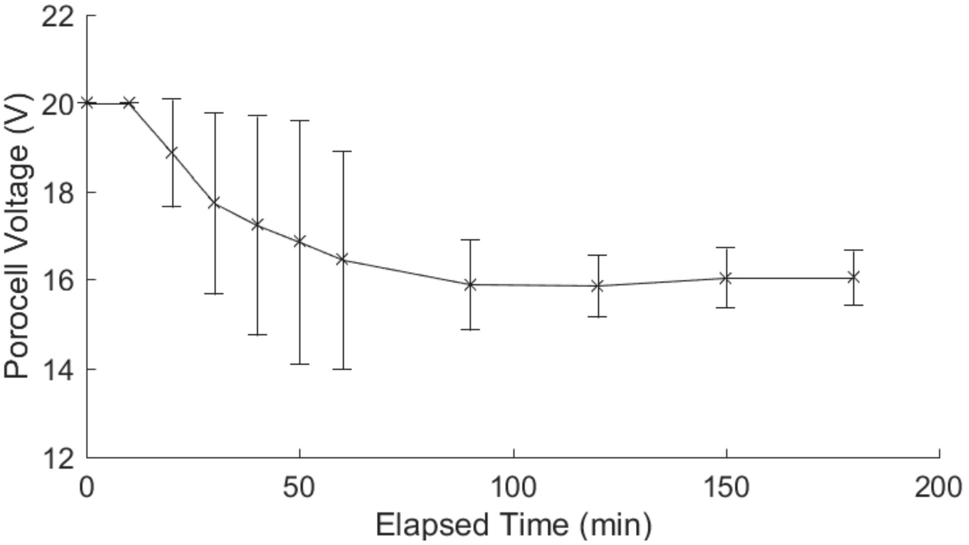

Figure 5.2.20: Porocell voltage change when operating galvanostatically at 1.05 A with a 40 ppm Cu^{2+} (pH = 4) solution. Potentials of 20 V indicate potentiostatic operation where greater than 20 V were needed to drive 1.05 A current. Error bars are the standard deviation (n = 3).

40 ppm. ISE measurements still show a concentration of 0.57 ± 0.65 ppm after 3 hours, agreeing that negligible amounts of copper remain.

The same set of calculations on the energy consumption, kinetics, and efficiency were performed, using either the measured difference in concentration or assuming the starting concentration of 40 ± 2 ppm. Based on the expectation from the change in pH, the assumed calculation is more likely to be accurate (Table 5.2.4).

It is clear that the total and mass-normalized energy consumption are much higher than previous tests to the extent that it is not industrially feasible to apply such high current. However, based on the concentration changes with time, the operation time should not be the full 3 hours, instead taking less than 120 minutes for full copper recovery. Even disregarding the final hour, which amounts to 60.4 kJ of electrical energy, the mass-normalized energy cost is still 483 GJ/tonne, which is nearly 50 times higher than the cost of primary mining.

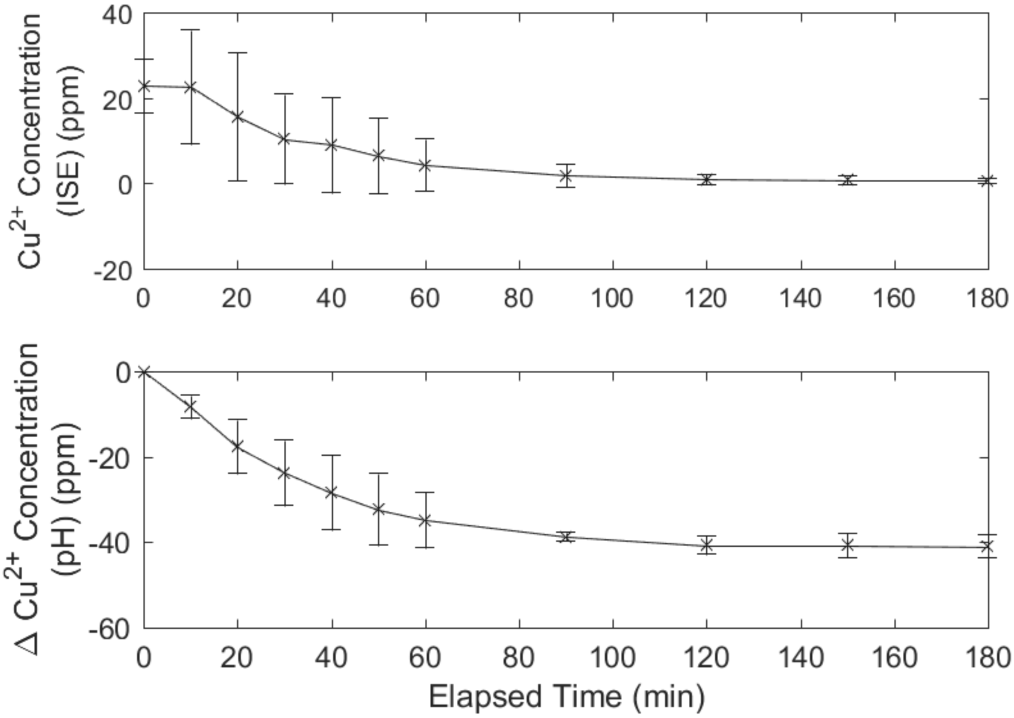

Figure 5.2.21: Measured copper concentration (top) and the change predicted by the change in pH and Eq. 5.3 (bottom) when recovering using 1.05 A in the Porocell. Error bars are the standard deviation (n = 4).

Table 5.2.4: Key values from galvanostatic Porocell operation at 1.05 A from a feed solution of 40 ppm Cu^{2+} (pH = 4).
*Using the measured starting concentration
**Using the assumed starting concentration of 40 $\pm$ 2 ppm as prepared

		Mean	SD (n = 3)	R^2
Energy consumption	Total (kJ)	177.1	4.2	
	Normalized* (kJ/g)	1770	500	
	Normalized** (kJ/g)	998	29	
Kinetics	Zeroth order (ppm/min)	0.119	0.025	0.713
	First order (min^{-1})	0.0228	0.0015	0.963
Net Coulombic efficiency (%)	Relative to measured concentration*	48.7	13.9	
	Relative to known concentration**	86.1	1.4	

From the kinetic fits, the concentration decrease strongly follows first order kinetics, indicating that the current quickly becomes higher than the transport limited current. Despite this, the net Coulombic efficiency is still high at 86.1 %, supporting the hypothesis that the primary driver for low efficiencies at low current is the relative contribution of the corrosion reaction. It is likely that a maximum current efficiency exists somewhere between 105 mA and 1.05 A, at which point the current is low enough that the limiting current is not a factor, but high enough that corrosion is negligible.

However, this maximum in efficiency is not necessarily the optimal current for operation, as it is apparent that the energy cost also increases between 105 mA and 1.05 A. Instead, further tests should combine the studies from Section 5.3.4 and 5.3.5 to identify the current which leads to the minimum energy cost to reduce the concentration to 2 ppm. For instance, a calculation for the energy cost of 70 and 105 mA when operated until steady state, rounded up to the nearest hour, shows that operating 105 mA requires 10.1 kJ, whereas operating at 70 mA requires 12.9 kJ due to its longer operation time. Based on that calculation and the estimate for 1.05 A, it is believed that a minimum will lie between 70 mA and 1.05 A, likely between 105 mA and 1.05 A.

5.2.6 Discussion

Complete optimization of the Porocell was not achieved with these tests as originally intended, predominantly due to the limitations of the instrumentation. The optimal operating current lies outside of the 10 V limit of the potentiostat that was used, although additional tests with a power supply bound the optimum current between 105 mA and 1.05 A (steady-state voltages between 10 and 20 V).

Instead, these tests establish two things: (1) copper can be recovered despite limitations posed by the solution composition and measurement methods, and

(2) the primary variable of concern for optimal Porocell operation is the current density, not the flow rate.

Based on the known compounds in distillery spent lees, they can be approximated as copper sulphate solution at 40 ppm Cu and a pH of 4. This solution is highly resistive, to the point that greater than 10 V must be applied to reach the mass transport limiting current for copper reduction. Despite this, the copper concentration has been reduced to as low as 10 ppm after 3 hours of applying 105 mA.

The exact concentration is a point of uncertainty, however, as the measurements with the ISE are highly variable across replicate tests. An alternative method based on the by-product production of protons suggests that the final concentration of the aforementioned condition is roughly 20 ppm. Despite slight differences in the exact values for the copper concentration change, the results with this alternative calculation agree with many of the conclusions made, notably related to flow rate.

Statistical tests across all variables except net Coulombic efficiency show insignificant effects of flow rate ($p > 0.05$), and even effects that are observed seem to diminish as current increases. Flow rate does not appear to influence copper plating as much as the corrosion rate, with faster transport affording faster corrosion. The effect of corrosion, which is likely at a relatively constant background rate, diminishes as the current, and thus the rate of copper plating, increases. This is believed to be the primary cause for the increase in net Coulombic efficiency with current.

Due to the uncertainties of these results, two more tests were conducted to investigate the process further. While kinetic analyses of the concentration change over time were used to predict the minimum process duration required to treat the copper concentration sufficiently, the duration exceeded the 3 hour tests and could be much longer than predicted. Extending the tests to 26 hours confirmed that after a day of operation, applying greater than 70 mA led to > 95 % of the copper being recovered, based on both the ISE measurements and the pH change. This test also confirms the validity of the pH change as a proxy for copper concentration change, as the pH change predicts a copper concentration change of 40 ppm exactly, which is the known concentration of the starting solution.

Due to physical limitations, samples could not be collected for the time in which the concentration reached the desired target. Instead, the voltage, which reflects the increase in conductivity associated with the production of protons, was used as an analogue. When the system is no longer plating copper due to the sufficiently low concentration, no net change should occur to the solution composition, specifically its conductivity, leading to a constant voltage.

The estimate of 5.6 hours for the 105 mA condition is slightly shorter than the 6.37 ± 0.17 hours predicted by the kinetics, whereas the estimate of 13.3 hours for the 70 mA condition is slightly longer than the 10.28 ± 0.40 hours predicted. They are, however, within a reasonable margin of error given that only a single 26 hour test was conducted.

Higher current tests provided additional information related to the impact of corrosion. By applying an order of magnitude greater current, the current efficiency increased from 22.4 ± 1.3 % to 86.1 ± 1.4 %, supporting the hypothesis that the low Coulombic efficiency at low current is related to a background reversal of the plating reaction via corrosion. The higher efficiency at 1.05 A is not necessarily better, though, as the energy cost is much higher.

In fact, all of the tests, both at low and high current, consume more than 40 GJ/tonne, with many test conditions and calculation assumptions estimating upwards of 100 GJ/tonne. This is at least four times higher than the energy cost of current pyrometallurgical metal production [20] and at least forty times higher than a published copper recovery tests with the Porocell [24]. Given that the previous test with the Porocell recovered copper from similar concentration wastes at lower Coulombic efficiency, the difference in energy cost is likely entirely related to the solution resistance.

One could feasibly reduce the Ohmic drop by adding significant amounts of a salt known not to interfere with copper electroplating, such as sodium sulphate. However, doing so requires an additional input, which is inconsistent with the principles of green chemistry [26]. With that said, inert salts such as sodium sulphate often cause small environmental effects if at all - to the extent that EQS do not exist for sodium or sulphate ions [11] - so it may be both cost effective and environmentally sound to reduce the amount of electrical energy through this method.

One should, however, consider possible engineering changes, such as modifying the geometry of the reactor so the anode and cathode are closer together, before adding more to the waste. In addition to being more environmentally sustainable, engineering changes would be a single cost rather than a recurring cost of additional salt, potentially making it cheaper in the long term.

One possible simple approach would be to take advantage of the heat used in distillation. Spent lees would initially be heated from the distillation process, and they have been reported to be used as a heat exchange fluid to reduce water use [13]; if the process were conducted with higher temperature solution, the conductivity would increase due to the increase in the mobility of the ions. This may, however, accelerate the corrosion reaction, so further testing is required to determine the optimal combination of process temperature and current.

Ultimately, these results suggest that copper recovery is possible from spent lees, although without changing the system or process, it would require significant amounts of electrical energy to do. This result is unoptimized, though, and there may be a current density between 105 mA and 1.05 A where the energy cost reaches a minimum, but rigorous testing within that range is not feasible with the potentiostat used in these experiments.

5.3 Validation against Spent Lees

The results just presented should take into context that they rely on the assumption made in Section 5.1 where spent lees can be approximated as weakly acidified copper sulphate solution. Validation with spent lees should be performed to confirm this assumption. Real spent lees were provided by the Glengoyne Distillery for testing, allowing for confirmation of both this initial assumption and the validity of the simulated spent lees as a proxy for real spent lees. For these tests, unless otherwise stated, the errors indicate one standard deviation, $n = 4$ for tests with pure copper solution and Glengoyne spent lees, $n = 3$ for simulated spent lees.

5.3.1 Results

Qualitatively, the three solutions are nearly identical. All three had similar viscosities indiscernible from water and a slight blue color associated with cupric hydrates. The primary distinguishing feature between them is their odour: while pure copper sulphate is odourless, simulated spent lees smell strongly of their butyric acid. Spent lees, in contrast, have a similar odour profile to the whiskey of which they are a by-product, suggesting that the simulated lees are missing many volatile organic compounds present in spent lees.

The concentration change over the course of Porocell operation at 105 mA shows little difference between the solutions (Fig. 5.3.1). Simulated spent lees appear to start at a lower concentration than the other solutions, but this is likely associated with the errors related to the ISE previously mentioned in Section 5.3.1, as this solution was prepared at 40 ± 2 ppm like the pure copper solution. The real spent lees also seem to have a starting concentration at 39.4 ± 24.6 ppm, which is unexpectedly high given that the average solution reported is at 20 ppm, with only the most concentrated lees containing 40 ppm [6].

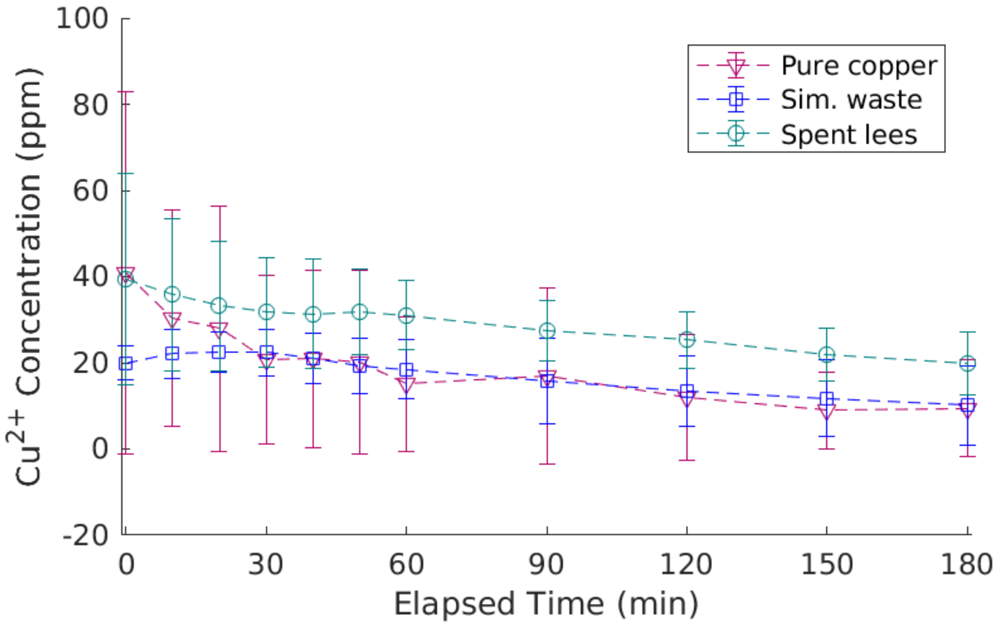

Figure 5.3.1: Copper concentration over the course of Porocell operation at 105 mA. Pure copper = 40 ppm Cu^{2+}, pH = 4, Sim. waste = see Table 1.2; Spent lees = waste provided by Glengoyne Distillery.

Throughout the recovery process, the spent lees appear to have a consistently high concentration relative to the other two solutions. While pure copper and simulated waste converge in their concentration measurements after 30 minutes, the Glengoyne spent lees are consistently 10 ppm higher after about 50 minutes. This continues until the end of the test (Table 5.3.1).

Table 5.3.1: Measurements and calculations for comparison of pure copper sulphate (40 ppm Cu^{2+}, pH = 4) (n = 4) to simulated spent lees per Table 1.2 (n = 3) and Glengoyne spent lees (n = 4). Uncertainties represent one standard deviation.

	Pure copper	Simulate waste	Spent lees
Concentration (ppm)			
t = 0	40.9 ± 42.1	19.9 ± 3.9	39.4 ± 24.6
t = 3 hours	9.5 ± 11.3	10.1 ± 9.2	19.8 ± 7.3
0th order kinetic fit			
R^2	0.750	0.927	0.953
k_0 (ppm/min)	0.14 ± 0.03	0.072 ± 0.007	0.096 ± 0.007
1st order kinetic fit			
R^2	0.894	0.942	0.973
k_1 (min^{-1})	0.0076 ± 0.0009	0.0046 ± 0.0004	0.0035 ± 0.0002
Net Coulombic efficiency (%)			
vs $[Cu^{2+}]_{t\,=\,0,\ measured}$	37.9 ± 43.6	11.8 ± 12.1	23.7 ± 30.9
vs $[Cu^{2+}]_{t\,=\,0}$ = 40 ppm	36.8 ± 11.3	36.0 ± 11.1	NA
Energy consumption			
Total over 3 hours (kJ)	6.22 ± 0.29	5.40 ± 0.63	9.87 ± 0.31
Normalized (GJ/tonne)	45.3 ± 16.3	40.2 ± 13.3	111.8 ± 164.1

Performing the same analysis as before, the kinetics of simulated waste and real spent lees are not clearly zeroth or first order, with all coefficients of determination greater than 0.92 (Table 5.3.1). There is a slight preference for first order kinetics, but as shown in the table, the first order rate constants are so low that on this time scale, it is effectively a linear equation. In fact, for both simulated waste and real spent lees, the time constant ($1/k_1$) is longer than 3 hours, so approximating the system as zeroth order is simpler without significantly sacrificing accuracy.

The Coulombic efficiencies calculated from the ISE measurements are also reported in Table 5.3.1. While pure copper seems to be the most efficient when calculating the concentration difference as measured, it is known that the first measurement of simulated spent lees is unusually low at 19.9 ± 3.9 ppm compared to the known 40 ± 2 ppm. As a result, the measured change in copper ion concentration is low, resulting in a lower calculated Coulombic efficiency than what should be expected. When performing the calculation with the known starting concentration, pure copper and simulated waste are similar ($p = 0.93$). This assumption cannot be extended to real spent lees, though, as the exact starting concentration is unknown, leading to a best estimate of 23.7 ± 30.9 % Coulombic efficiency. Due to the large standard deviation, this value is insignificantly different than either other condition ($p = 0.61$).

While Coulombic efficiency may be roughly similar, the total energy cost is not (Table 5.3.1). As expected from previous tests, simulated waste is indistinguishable from pure copper, with a total electrical energy cost of 5.40 ± 0.63 kJ for the 3 hour duration. However, real spent lees require nearly double that amount at 9.87 ± 0.31 kJ, associated with the higher potential needed to drive 105 mA current (Fig. 5.3.2). This results in an energy cost per gram of copper nearly 3 times higher, although the uncertainty associated with the ISE measurement leaves these values statistically similar ($p = 0.49$).

Based on previous results, pH would provide a more reliable method for estimating the change in copper concentration. However, looking at the change in pH with time, the difference is much smaller when using real spent lees (Fig. 5.3.3). While all solutions start at roughly similar pH values, pure copper and simulated waste both decay rapidly to around 3.3, whereas spent lees remain above 4. This estimates a decrease of only 2.04 ppm over the course of 3 hours, equating to a Coulombic efficiency of 2 % (Fig. 5.3.4). It is possible interferents in the spent lees are causing low Coulombic efficiency, but they may also be invalidating the core assumption behind relating pH and copper concentration change.

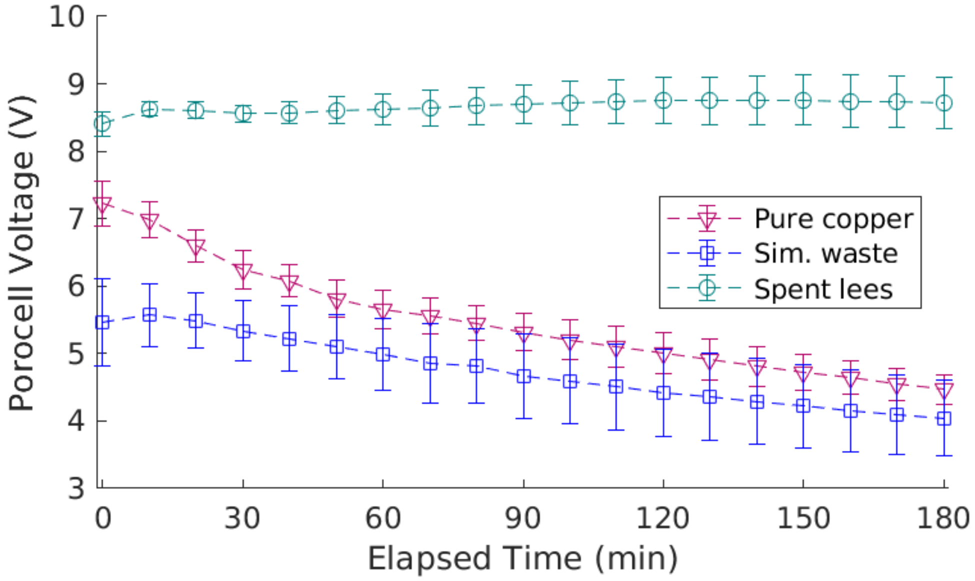

Figure 5.3.2: Porocell voltage profile over the course of operation at 105 mA. Error bars for all groups represent one standard deviation (n = 4).

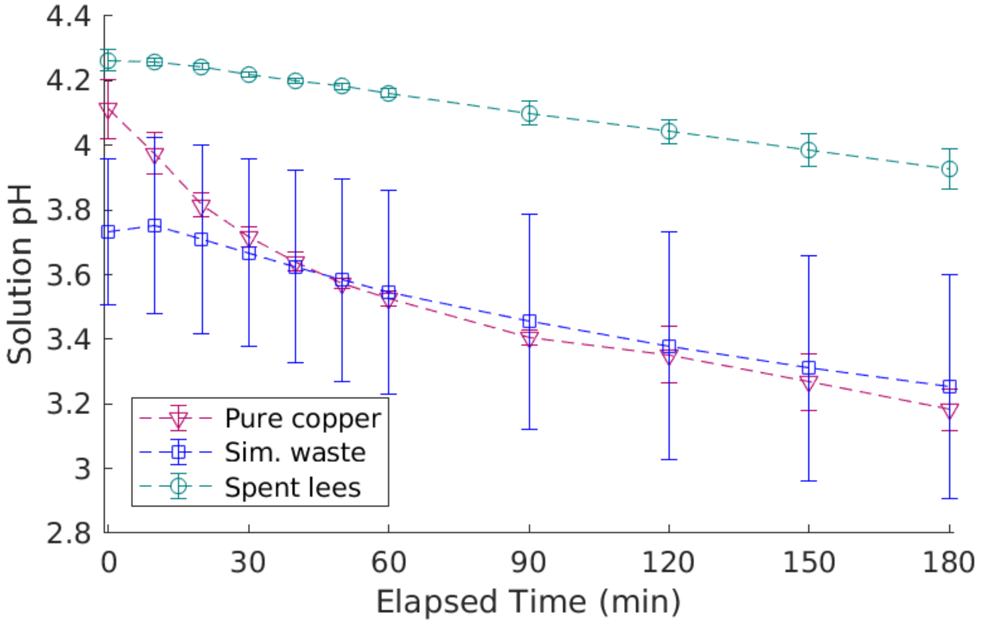

Figure 5.3.3: Change in solution pH over the course of galvanostatic Porocell operation at 105 mA. Error bars for all groups represent one standard deviation (n = 4).

Given the knowledge that the scent of spent lees is different and the exact composition differences between spent lees and simulated waste is unknown, it is

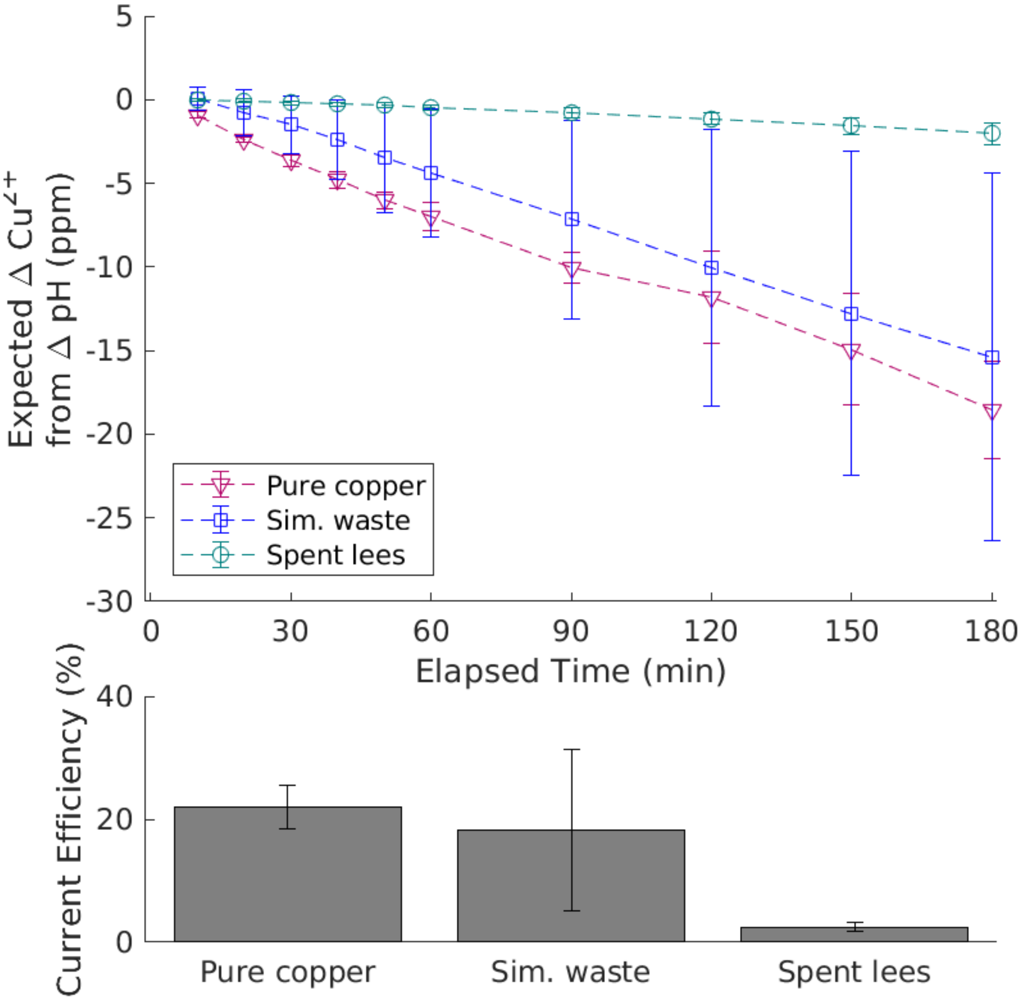

Figure 5.3.4: (top) Anticipated change in copper concentration during galvanostatic Porocell operation at 105 mA based on the change in pH. Error bars for all groups represent one standard deviation (n = 4). (bottom) Net current efficiency after 3 hours using the change in pH to estimate the change in copper concentration.

possible that there are a number of other organic acids present in spent lees that were not previously measured. These acids may act as pH buffers, limiting the pH change by taking up protons generated by the anodic half-reaction, particularly if their pK_a is close to 4, of which there are many.

The high organic content also explains the high voltage observed in Fig. 5.3.2. While one could predict that the organic compounds would complex to copper ions, stabilizing both the Cu^{2+} and Cu^{+} species and decreasing their redox potentials [82]. As a result, one might expect that the cell voltage would increase; however, this decrease in redox potential is often on the order of hundreds of millivolts, and thus cannot explain the full observed difference. Even accounting for the complexes being larger, and thus having lower diffusion coefficients and higher charge transfer kinetics [44], the observed difference of multiple volts is too large to be solely the result of the copper speciation.

Instead, a holistic consideration to the solution chemistry must be taken. Many organic molecules are large, and many lack functional groups with ionic charges, making them poor charge carriers. As a result, they are generally more resistive than even the aqueous solvent. Measurements of the solution conductivities were taken before and after 3 hours of operation, showing that while all solutions are incredibly resistive relative to a typical electrolyte for an electrochemical process, spent lees are 30 to 50 % less conductive than the pure copper solution (Table 5.3.2).

Table 5.3.2: Conductivities of pure copper, simulated waste, and Glengoyne spent lees before and after testing in the Porocell (105 mA for 3 hours).

	Starting conductivity (μS/cm)	n	Conductivity (t = 3 hr) (μS/cm)	n
Pure copper solution	135.4 ± 14.1	3	195	1
Simulated waste	177.2 ± 1.8	2		
Spent lees	97.2 ± 2.5	3	87.1 ± 4.4	3

The measured conductivity change with pure copper solution corroborates the decrease in voltage over time observed in Fig. 5.2.12, as the net reaction ($Cu^{2+} + H_2O \rightarrow Cu + 2H^+ + \frac{1}{2}O_2$) exchanges cupric ions with protons, which will lead to a more conductive solution. Compared to simulated waste, pure copper solution is slightly more resistive despite being at roughly the same pH. This is consistent with the lower observed voltage (Fig. 5.3.2). The difference is likely the result of the trace metals that were added. While one might expect the organic compounds in spent lees to counteract this effect, all of the organic compounds added to make the simulated solution contained carboxylic acid functional groups which deprotonate at or near this pH, and thus the added resistivity may not be as substantial as the influence of the additional metal ions.

Conversely, real spent lees are more resistive than pure copper solution, and become more resistive over the course of the process. The increased resistivity is consistent with the small change in pH (Fig. 5.3.3) and subsequently higher and stable voltage (Fig. 5.2.12). It is likely that some of the unidentified organic compounds in real spent lees are negatively charged proton acceptors. As a result, the protons generated by the above reaction would be lost, as would the anionic charge of these organic molecules, leading to consumption of the charge carriers in solution and a subsequent increase in solution resistance.

These differences in conductivity account for most of the deviation from pure copper solution. The starting conductivity of simulated waste is 31 % greater than that of pure copper solution, equivalent to 76 % of the solution resistance, and the starting voltage changes from 7.2 V with pure copper solution to 5.5 V after trace metals and organics are added, equivalent to 77 % of the voltage. The consistency between the percent change in solution resistance and percent change in voltage suggests that this difference can be attributed predominantly to the Ohmic drop.

With regard to real spent lees, the starting resistance is 39.3 % higher and the final resistance is 124 % higher than that of pure copper solution at those times. Similarly, the voltage for spent lees is 16 % higher to start and 95 % higher at 3 hours. While these values are not nearly identical as was the case with simulated waste, the lower than expected voltage change is likely a result of the assumption that the Ohmic resistance is so large that the other voltage drops could be ignored.

Accounting for the other voltage drops would result in more similar percent differences. For example, a cursory approximation of these overpotentials of 1.5 V for all solution compositions and time points leads to Ohmic drop differences of 21 % to start and 143 % at the end between real waste and copper alone. As evident, accounting for these other overpotentials results in a larger percent change in Ohmic drop as a result of the additional components in spent lees, and increasing the contribution of these overpotentials results in a larger difference in the Ohmic drop between pure copper and spent lees. With this rough estimate of 1.5 V, it is believed that Ohmic drop accounts for a smaller fraction of the overall cell voltage at the start than it does at the end. Based on the increased difficulty of nucleation compared to grain growth in electroplating [50], it makes sense that the activation overpotential at the start of the test would be larger than it would be at the end, providing a basis for the difference between the percent change in resistivity compared to the percent change in voltage.

5.3.2 Discussion

The results indicate that while the belief that simulated spent lees are effectively similar to pure copper is true, simulated lees are not an accurate representation of real lees. Unidentified organic compounds present in real lees are likely the cause of the differences observed, and these differences make copper recovery more difficult to perform and quantify.

The effect of the high organic content is most obvious in the voltage profiles, where driving 105 mA requires a consistent 8.5 to 8.7 V with spent lees, compared to pure copper requiring 7.5 V to start and less than 5 V after 3 hours. While the net reaction with pure copper solution led to a decrease in pH and subsequent increase in conductivity, the unknown organic molecules may be buffering the pH, resulting smaller changes to the conductivity, keeping the voltage high.

This buffer capacity means the results of the ISE cannot be checked against the expected copper concentration changes based on pH, as the pH change is not reflective of all of the protons generated by the anodic reaction. The prediction of a 2.04 ± 0.64 ppm Cu^{2+} decrease from the pH change is nearly one order of magnitude different than the 19.6 ± 25.6 ppm Cu^{2+} decrease measured by ISE.

One could possibly use the pH as a proxy for copper concentration if a titration curve for spent lees were performed. Doing so would relate the amount of acid added to the observed pH change, thereby developing a relationship back to amount of copper plated. Due to the small expected pH changes, though, a more precise pH probe would likely be necessary.

The large uncertainty associated with the ISE means that another method should be used in the future. This is particularly true because while calibrations with the ISE with simulated spent lees were consistent with those of pure copper solution, it is not known how the unidentified compounds in spent lees could be interfering with the ISE measurement. Methods such as ICP should be used instead to obtain a more reliable measurement.

This would in turn give greater confidence to the differences in energy cost and efficiency observed, for while the absolute differences are large (Table 5.3.1), they are not statistically significant ($p > 0.45$). The only confident conclusion that can be made with this data is simply that spent lees are more resistive, leading to a higher required voltage for the same current, and solutions to this problem have been previously discussed in Section 5.3.6.

5.4 Copper Plating Distribution

One of the initial intents with this set of experiments was to determine if the sources of Coulombic inefficiencies could be related to the distribution of copper plating on the electrode, as highly localized plating suggests higher than expected current densities. These could potentially be related to current and flow rate [28, 29], and having a detailed study could make optimization easier.

However, the scope of the project did not allow for full optimization of these parameters, as the range of currents and flow rates possible was too narrow. As a result, each electrode sample reflects all test conditions in aggregate, in part to provide sufficient copper for image analysis and in part due to the small differences observed between these conditions that can be attributed to causes other than plating localization. Consequently, these results instead allow for an understanding of how the cathode could be modified to reduce operation costs.

5.4.1 Physical appearance

Representative photographs of the outside face of the cathode are presented in Fig. 5.4.1. When assembled, this outside face is the side closest to the anode, and thus the side where the electric field is strongest. The reverse side of the electrode shows no copper plating and resembles base carbon felt.

This side of the electrode shows the distinct grid pattern of the plastic mesh used to hold the electrode in place, only showing the reddish color of copper

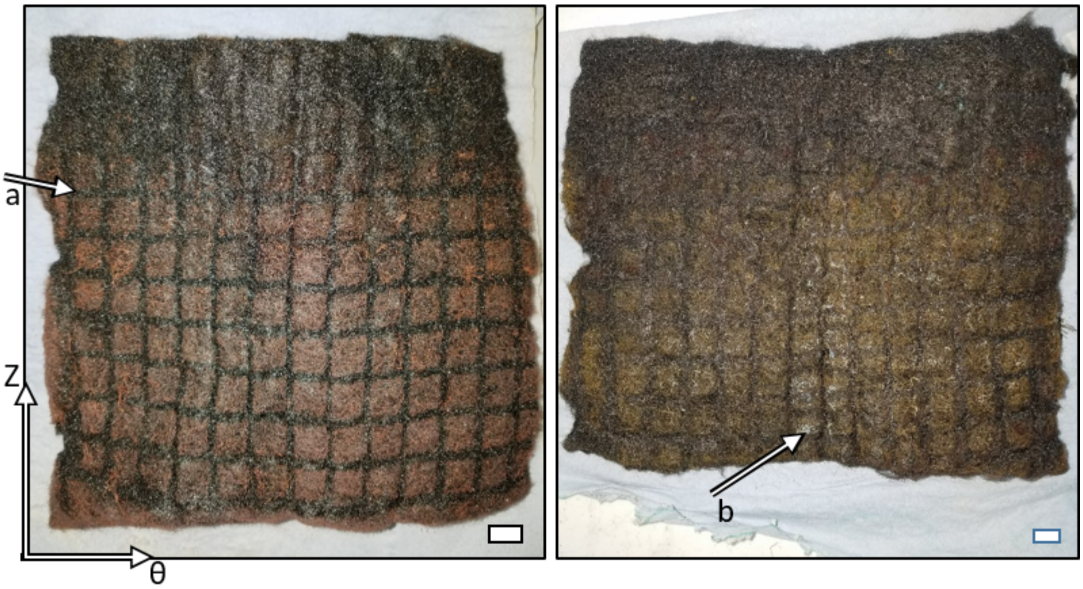

Figure 5.4.1: Photographs of the outside face of the carbon felt. Axes denote the direction of flow (Z) and the direction of radial symmetry (Θ). Scale bars in the bottom right of each image measure 1 cm across. (left) Representative electrode after 10 tests with the Porocell using copper only solution. (right) The electrode used only for tests involving simulated spent lees or Glengoyne spent lees.
Arrow (a) designates the height at which copper stops being plated.
Arrow (b) indicates a region where the copper appears blue instead of red, suggesting a hydrated form of copper (II) ions.

where the gaps in the mesh are. This is due to the plastic blocking the electric field, limiting the ability of copper ions to plate there.

Regardless, the copper is clearly visible starting from the edge nearest the inlet, and continues until approximately two-thirds of the height, noted by arrow (a) in the figure. As expected, there is no easily identifiable pattern in the radially symmetric direction.

While this red grid pattern is present with the electrode used for recovery from simulated and Glengoyne spent lees, the color is slightly different, showing slightly more yellow than red. This may be due to performing fewer tests, where the color is simply less saturated and appears lighter due to less copper having been plated. Additionally, there are locations in the electrode used with spent lees that are slightly blue, noted with arrow (b) in the figure.

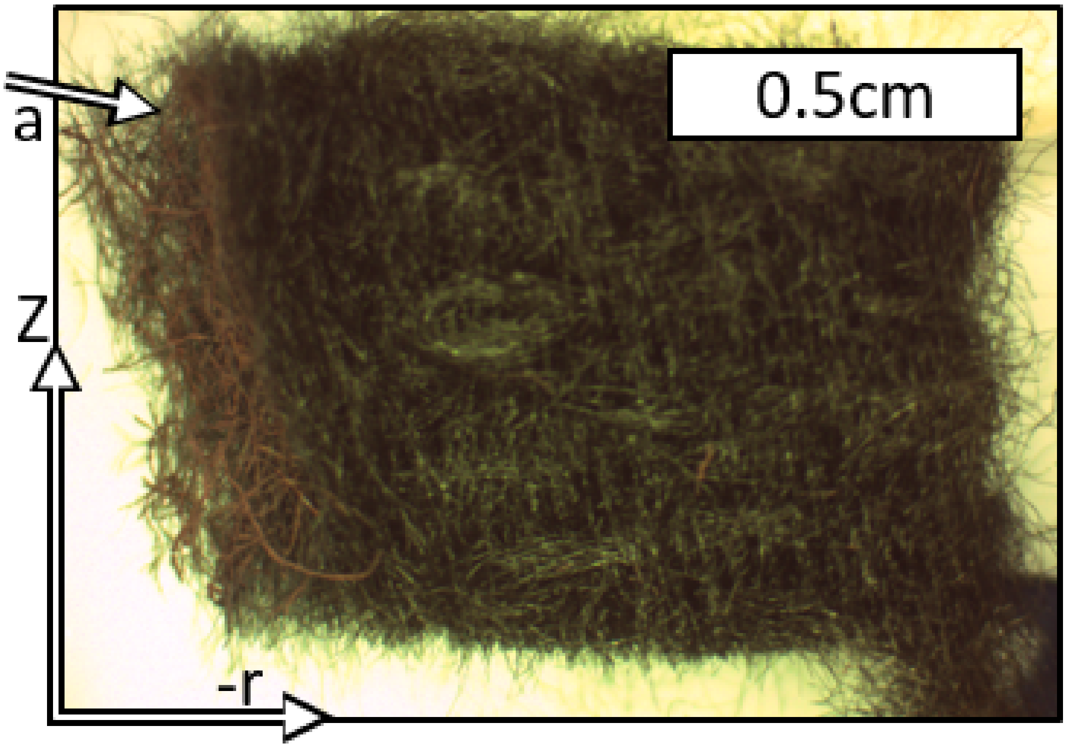

Figure 5.4.2: Sample photograph of an electrode cross section. Axes denote the direction of flow (Z) and the depth (r); the outside edge nearest the anode when assembled is to the left of the image. Scale bar measures 0.5 cm horizontally. Arrow (a) points out a slight amount of copper on the face of the electrode, indicated by the reddish tint of the fibers.

This pale blue color is associated with hydrated copper (II) species. While it may be due to insufficient rinsing of the electrode after removal, where copper (II) ions adsorbed to the surface formed hydroxides as it dried, it could be due to a corrosion reaction oxidizing plated copper back to the 2+ state. The fact that this feature is present only in the electrode used for treating spent lees suggests it may be related to the chemistry, not the rinsing, but with only one electrode sample used with spent lees compared to the three identical electrodes used with pure copper sulphate, it is difficult to make conclusions.

A sample microscopy image of the cross section is presented in Fig. 5.4.2. The photo shows the outside face on the left of the image has a layer of copper on it (arrow (a)), which quickly is lost among the black of the bare carbon felt. Bright spots in the bulk of the electrode are simply reflected light. The background is tinted slightly yellow due to differences in the microscope lighting compared to the ambient light, as well as the different color sensitivities of the two cameras.

5.4.2 Image processing algorithm proof of concept

To analyze these photographs, the images were separated into their red, green, and blue color channels. The primary distinction between copper, carbon felt, and the background of the image is the color, where copper is more red, carbon felt has lower but relatively even intensity values, and the background is pale blue for the front-facing images or yellow for the cross sections.

To determine how best to isolate the copper from the front-facing photographs, images were made using the difference between the red and green channels ($R-G$) and the difference between the red and blue channels ($R-B$) (Fig. 5.4.3). From those two images, it appears that the $R-G$ is a better representation of the copper, as the reddish copper region is clearly and selectively lighter than the rest of the image, whereas the light parts of $R-B$ show the entire cathode, independent of material.

The best image for isolating the cathode from the background, though, was seen to be the red channel. The histogram for this image is distinctly bimodal (Fig. 5.4.4), allowing Otsu's method to be used to find the threshold. Applying this threshold isolates the regions of background from the rest of the image, only incorrectly designating some of the electrode as background near the center of the image.

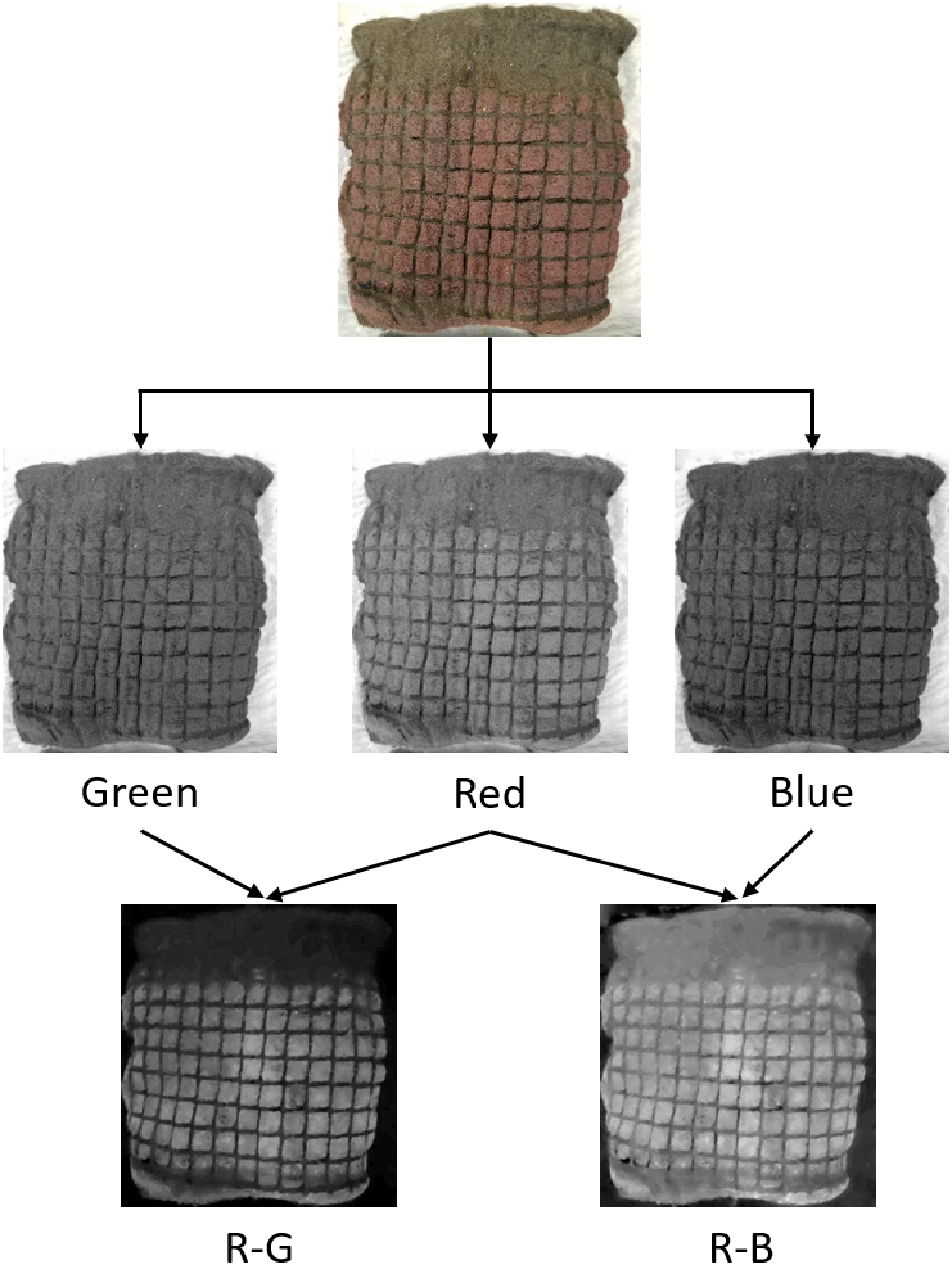

Figure 5.4.3: Example of the basic breakdown of the front-facing image. (Top) The full color image, which is stored as (middle) relative contributions of green, red, and blue channels. (Bottom) The difference between the red channel and the other two channels gives a slightly clearer image of the copper. The images for the difference have had their intensities rescaled for ease of visualization.

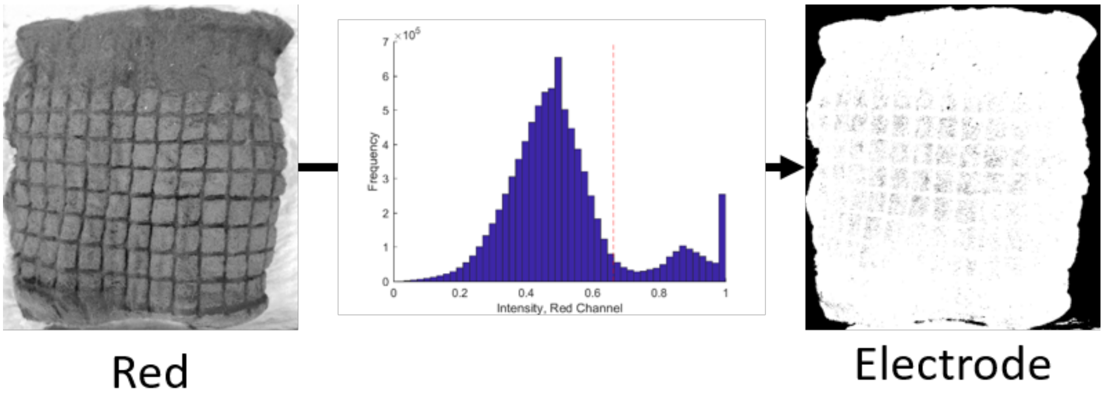

Figure 5.4.4: Demonstration of the processing used to isolate the electrode from the background. A threshold value for the red channel was determined using Otsu's method to obtain a binary filter.

For $R - G$, the histogram is not as smooth, but it still appears to have a bimodal character, and the peaks are separated by the threshold from Otsu's method (Fig. 5.4.5). Applying the threshold to the image shows the copper-containing regions clearly. Combining the two filters together creates the final image (Fig. 5.4.6), where the white and black represent the copper and carbon parts of the cathode, respectively, with the mid-tone used to represent the background.

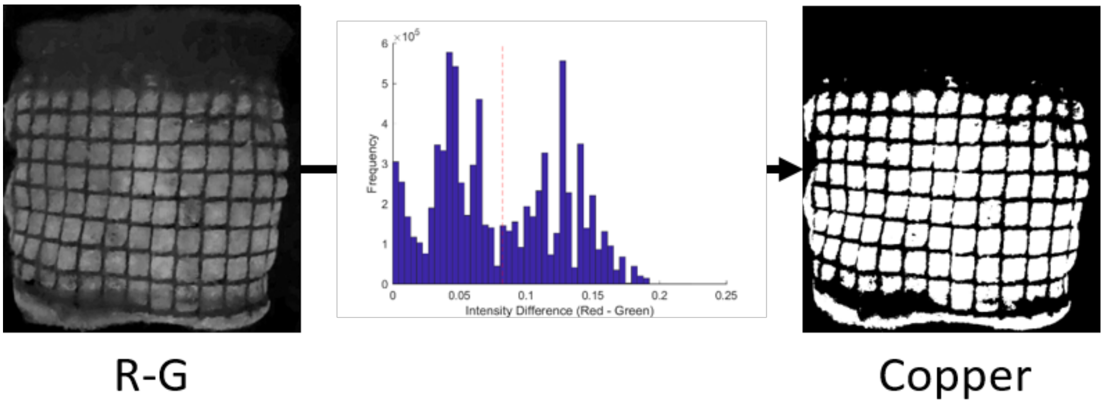

Figure 5.4.5: Demonstration of the processing used to isolate the copper from the rest of the image. A threshold value for the difference between the red and green channels was determined using Otsu's method to obtain a binary filter.

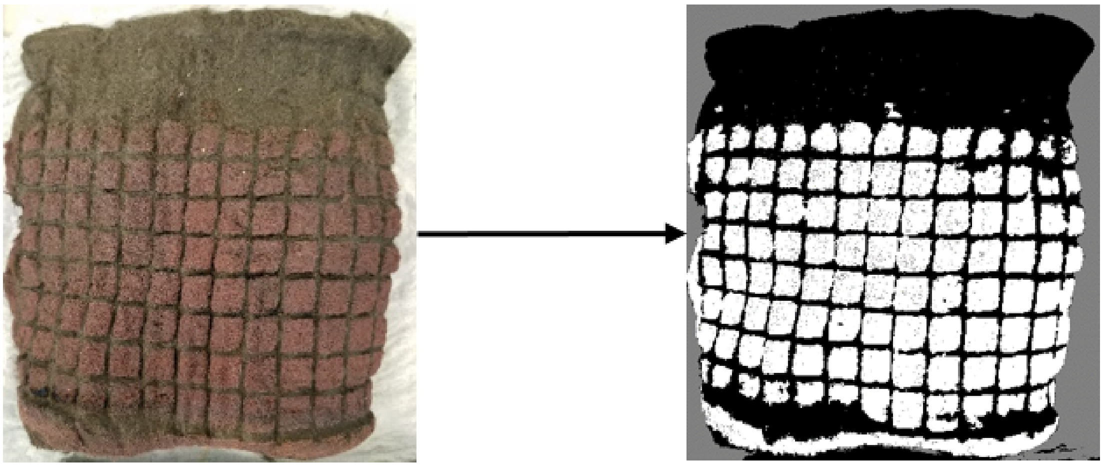

Figure 5.4.6: Visual comparison of the original front-facing photograph and the processed image. White designates copper, black indicates carbon felt, and gray indicates the background.

Images from the microscope required a slightly different algorithm, as there is less copper present, making it more difficult to isolate. As the region of interest is smaller, the brightness values of copper-containing and non-copper regions need to have a larger difference for Otsu's method to be viable. Therefore, these values, which ranged from 0 (black) to 1 (full brightness) for each color, were squared, for while all values would decrease, the darkest parts would decrease more, causing a larger difference between the brightest and darkest regions. This results in greater contrast in the image, as seen in Fig. 5.4.7.

While $R^2 - G^2$ seems to show a larger contrast, it also seems to highlight some of the reflected light elsewhere in the image. Therefore, $R^2 - B^2$ was used to establish the threshold. The histogram only appears to contain a single peak (Fig. 5.4.8), but this may be attributed to the fact that there are significantly fewer bright pixels associated with copper in the image, such that the peak would be too small to see in the histogram. This does put some degree of uncertainty in the conclusions made from these images, but using this threshold is the most unbiased and systematic method for analyzing the images as they are.

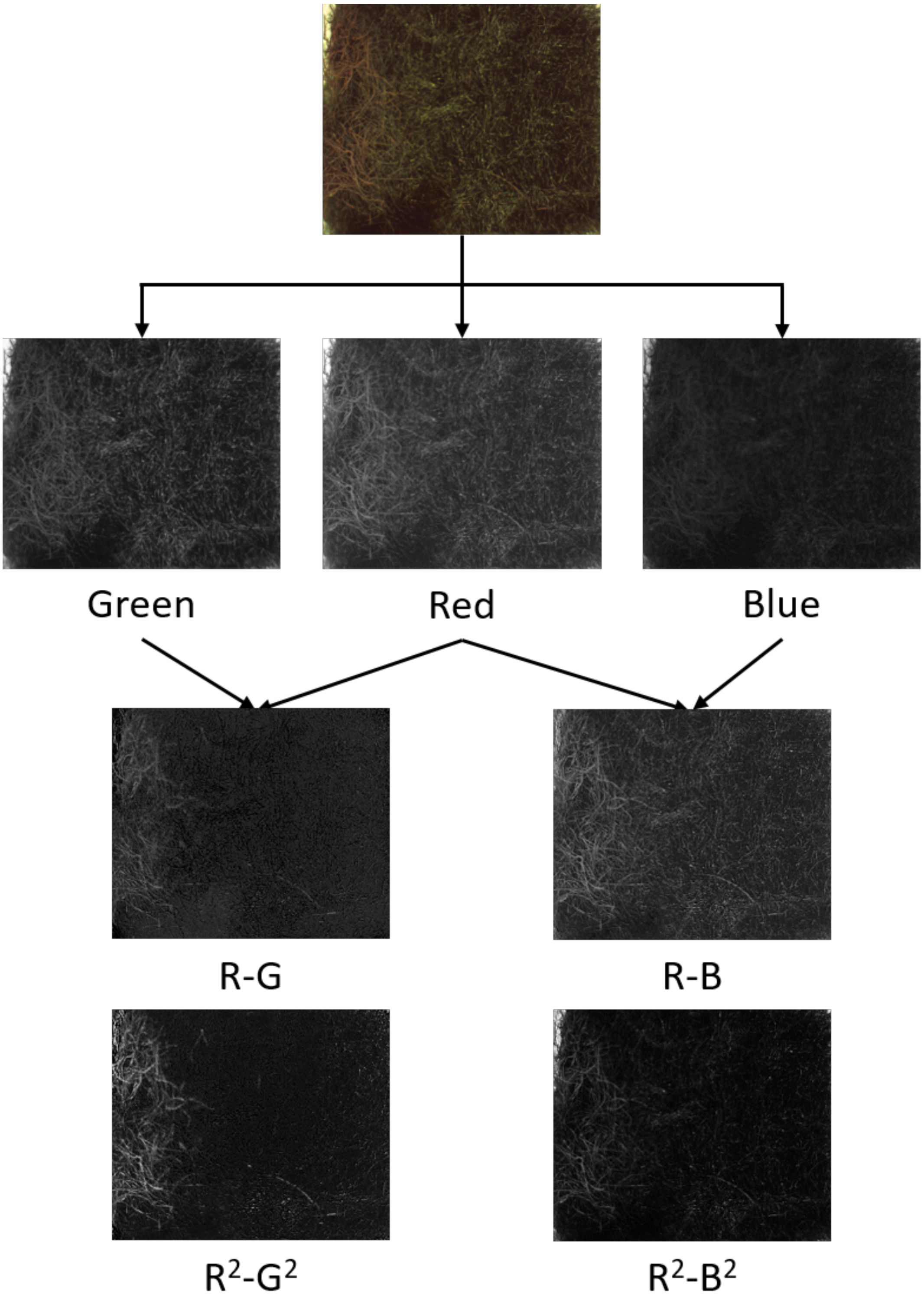

Figure 5.4.7: Example of the basic breakdown and calculation for the cross section image. (Top) The full color image, which is stored as (row 2) relative contributions of green, red, and blue channels. (Row 3) The difference between the red channel and the other two channels gives a slightly clearer image of the copper. (Bottom) Squaring the original color channels, which have intensities from 0 to 1, causes greater separation between the lightest and darkest regions, allowing for sharper distinction when calculating the difference between red and the other channels.

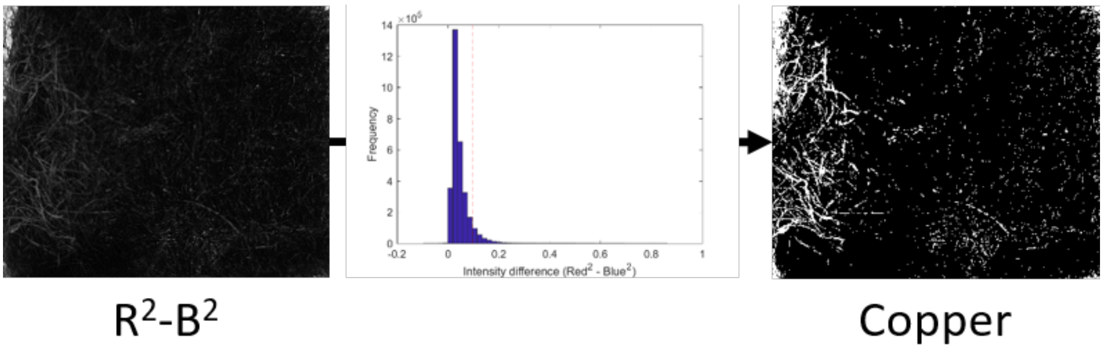

Figure 5.4.8: Demonstration of Otsu's method to isolate the regions likely to be copper.

The threshold still picks up some of the reflected light, but much of that light also meets the criteria for the background color (Fig. 5.4.9). Due to the image cropping, much of the yellow of the background was removed, but some remained due to slight warping of the sample during handling.

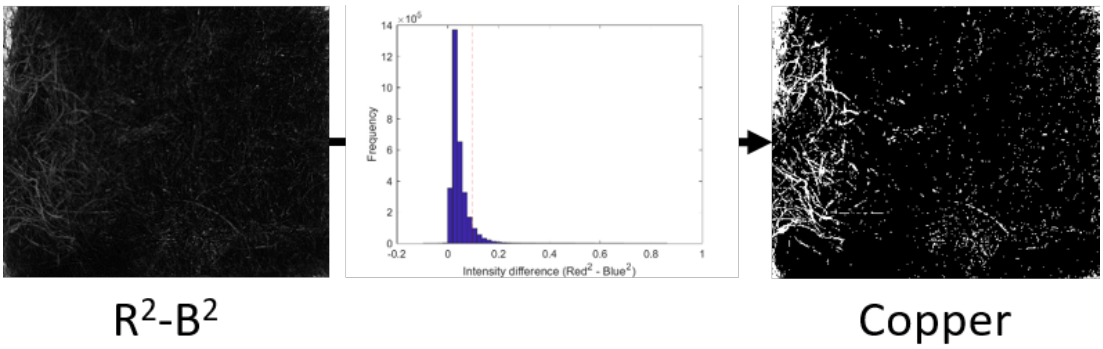

Figure 5.4.9: Demonstration of the processing used to isolate an electrode cross section from the background. The yellow hue was isolated based on its expected relative intensities of red, green, and blue.

Combining the two masks produces the image in Fig. 5.4.10, which is able to strongly define the red copper-containing region, though it does also misrepresent some of the deeper parts of the electrode as copper instead of reflected light. Therefore, the data is analyzed assuming that there is a background level of perceived copper that is actually reflected light and looks for deviations from the

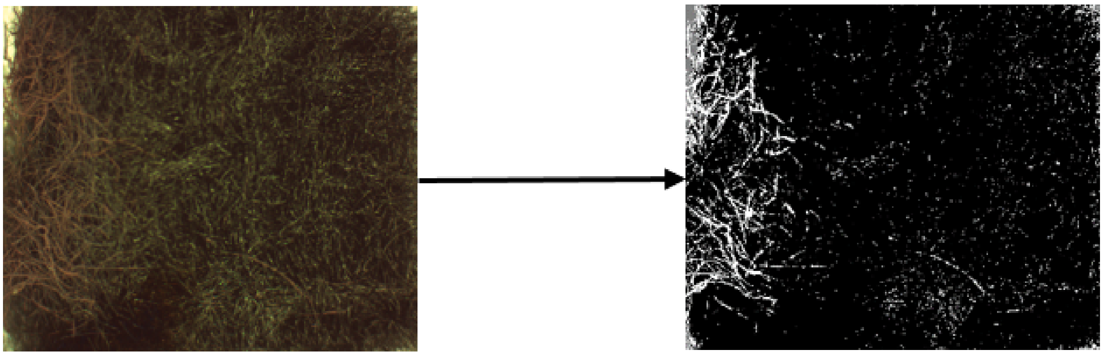

Figure 5.4.10: Visual comparison of the original cross section and the processed image. White designates copper, black indicates carbon felt, and gray indicates the background.

middlemost region of the image.

5.4.3 Quantification of plating

Three separate electrodes were imaged from both the front and for all cross sections. The copper distribution with height can be seen in Fig. 5.4.11. It is evident that in all three replicates, the grid pattern of the plastic mesh causes distinct dips in the fraction of the electrode surface believed to be copper. For the first two electrodes, there is also a clear delineation between where there is copper plating and the region at which there is no longer any copper. For the third electrode, peaks in the mesh are still visible beyond about 11 cm in height, suggesting there is some copper in that region, albeit less than the amount observed at heights below 10 cm.

For all three electrodes, it is clear that copper begins to stop being plated as frequently at about 10 cm from the base. Using the derivative of copper fraction with respect to distance (Fig. 5.4.12), one can isolate the inflection points associated with the decline, as well as the final inflection point associated with the mesh pattern that designates the highest point at which copper has been plated. Between these two distances, copper may be present, but at lower frequency than

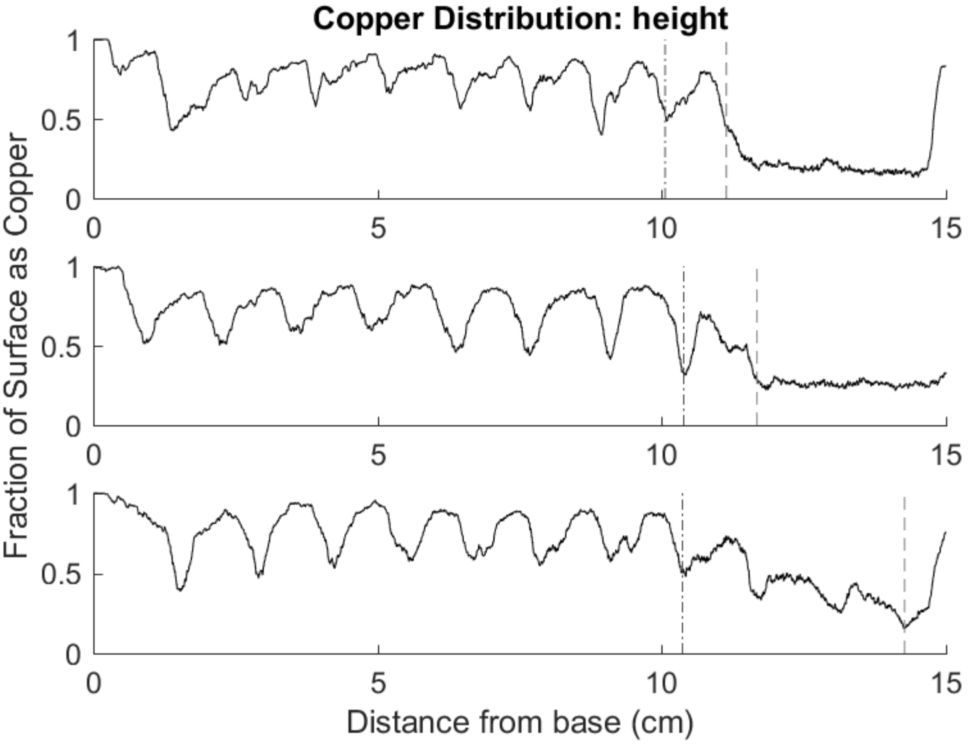

Figure 5.4.11: Relative fraction of copper at each height increment for 3 independent electrodes. Vertical dashed and dotted (—.—) lines represent the height at which copper begins to disappear, and vertical dashed lines (——) represent the point highest point at which copper is present.

closer to the base of the cathode.

These values for all three electrodes, designated E3, E4, and E5, are presented in Table 5.4.1. Generally, the height at which copper starts to disappear is 10 cm, with a margin of error associated with the precise location of the mesh. It may begin to decrease at roughly the same height, but the pattern of the mesh dominates over any natural decrease that may be occurring.

On the other hand, the point at which copper stops being plated is usually within the next 1 cm grid block of the mesh, but E5 shows copper plating for another 4 centimeters. While all electrodes underwent the roughly the same number of experiments, plating near the top may be related to the order in which those tests were performed, as the order was changed for each electrode to avoid

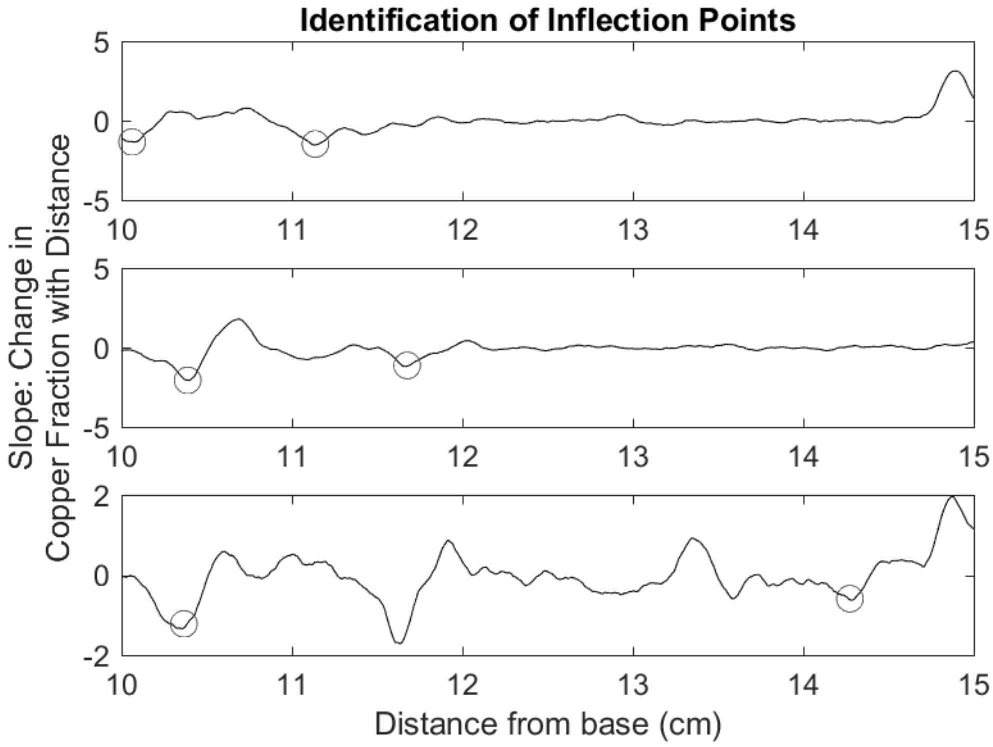

Figure 5.4.12: Change in copper fraction with change in distance. The circled minima are capable of noting when copper begins to disappear and when it ceases to appear.

any unexpected order effects. E5 was also used in troubleshooting high power tests, which may explain additional plating at this height due additional tests with a stronger electric field.

With regards to depth, the data is much less clear. Sample profiles of the cross sections at the base, middle, and top of the electrode are presented in Fig. 5.4.13. All samples show both the outside (depth = 0 cm) and inside (depth = 1 cm) have high estimated fractions of copper.

However, by visual inspection, there is no copper on the inside of the electrode, so this is likely related to the edge effects. This is particularly true for the sample at a height of 13 cm, as it is known that next to no plating occurs at this height (Fig. 5.4.11). These high fractions are likely related to the sparseness of the

Table 5.4.1: Calculated values for the point at which copper starts to disappear and the point at which it ceases to appear. E3, E4, and E5 represent electrodes used in 8 tests of copper recovery each, all from solutions of pure copper.

	Start (cm)	End (cm)
E3	10.06	11.14
E4	10.39	11.68
E5	10.37	14.27
Mean	10.27 ± 0.15	12.36 ± 1.37

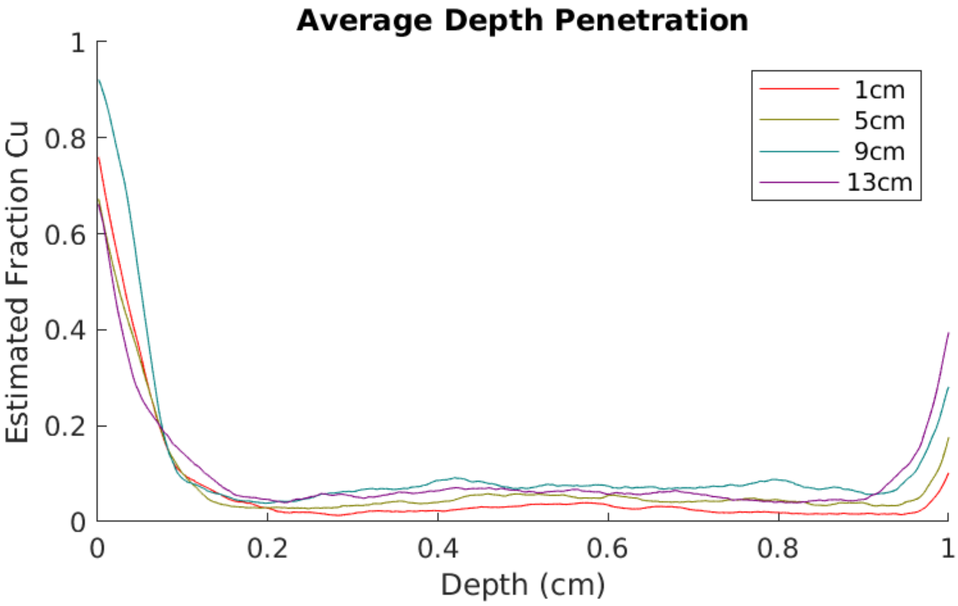

Figure 5.4.13: Average profile for copper fraction with depth (n = 3) at sections close to the inlet (1 cm) and outlet (13 cm). Profiles have been smoothed using a 41 point linear interpolation window.

carbon felt fibres near the edges, which allow for some amount of background to be interpreted as copper instead.

Looking at depths of 0.2 to 0.8 cm, it is clear that while the lower heights show low baseline fractions, the image processing algorithm is less selective for copper, likely because there is little visible copper. As a result, Otsu's method is placing the threshold lower, causing more of the reflected light to be interpreted as copper.

This causes the baseline fraction of copper to appear to increase with height (Fig. 5.4.14) despite no visual indication of this trend in the images themselves (Appendix C). In fact, there is a generally increasing trend from 1 cm to 7 cm, after which the analysis suggests approximately 7 % of the surface is copper in the middle of the electrode.

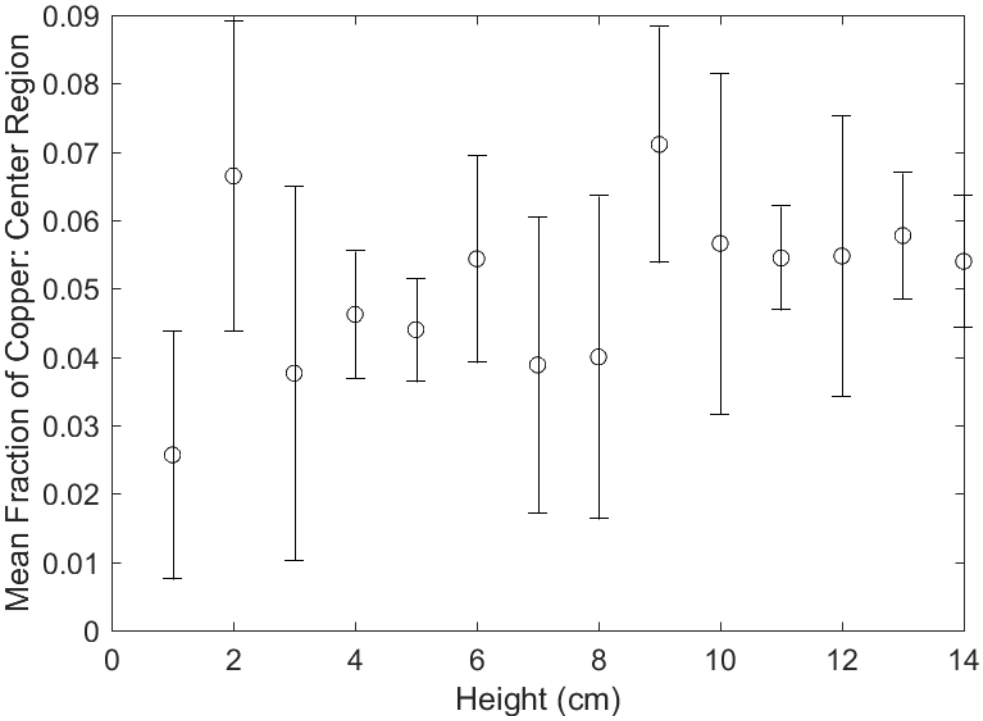

Figure 5.4.14: Perceived copper fraction of the centermost depths, 0.2 cm in from each edge. Error bars are one standard deviation (n = 3).

Since it is expected that most of the copper plating will occur on the outside edge nearest the anode, additional attention was paid to the first 0.2 cm. In this region, it may be possible to discern copper from carbon due to the higher copper fraction, allowing for quantification of how deep into the electrode copper could be plated. Attempts to quantify the depth that copper can penetrate based on deviation from the baseline fraction, however, show no difference between sections nearest the inlet and sections nearest the outlet (Fig. 5.4.15), despite Fig. 5.4.11

showing that negligible amounts of copper are plated on the outside surface above heights of about 12 cm.

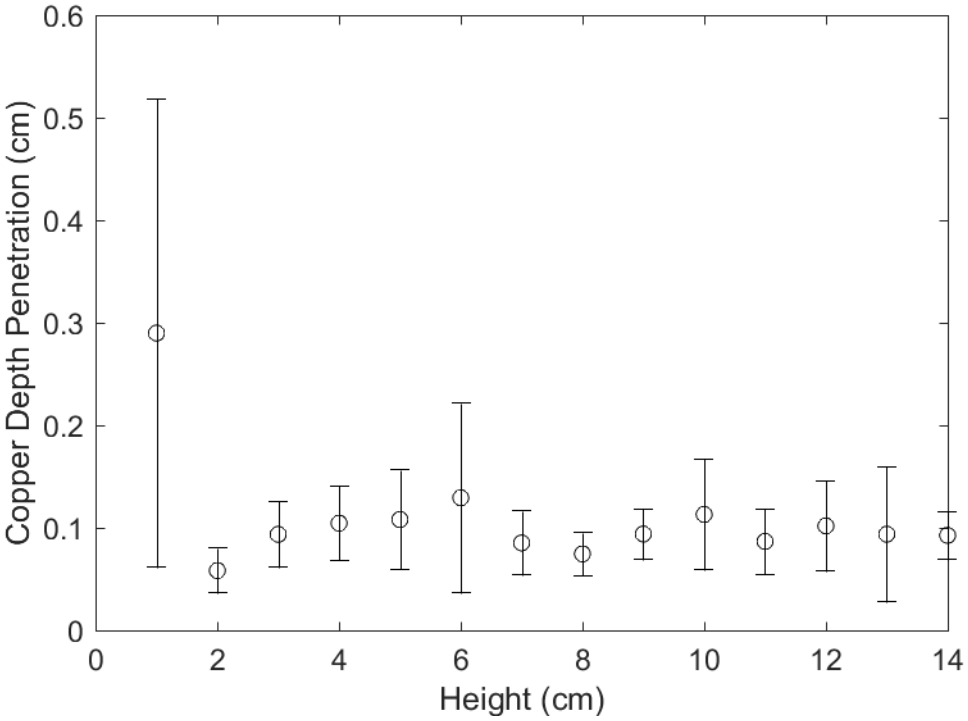

Figure 5.4.15: Estimated copper deposition depth penetration at each height increment. This depth represents the point at which the copper fraction is first becomes equal to the mean plus one standard deviation of the centermost region. Error bars are one standard deviation (n = 3).

At best, this data is purely a result of the edge effects, which are large enough to mask the distribution profile for copper plating. As a result, these values can be used as a coarse overestimate, indicating that copper plating only occurs at most in the outermost 0.1 cm, with a shallower region being more likely.

5.4.4 Discussion

Images of the electrode from the front are able to discern what fraction of the electrode surface is covered by copper at each height increment. Across three independent electrodes, copper begins to stop being plated at a height of 10.27

± 0.15 cm, after which the fraction of copper decays for another 1 to 4 cm. On average, no copper is observed above the height of 12.36 ± 1.37 cm.

The 10 cm estimate of initial decline in copper plating aligns with two features on the Porocell. First, this is the height at which the blockage in the pipe is located, forcing flow through the cathode. Below this height, flow is forced radially outward, supplying solution to the reactor chamber, and above this height, flow is forced radially inward to exit the reactor chamber. Second, this is also the highest point at which the current collector makes contact with the cathode; above this height, the current collector is insulated, and thus does not charge the cathode directly.

Both of these features are independently capable of causing the decline in copper plating at this height. The switch from solution flowing into the chamber to solution flowing out means that the copper concentration should be lower as it exits the chamber, as it would have reacted with the outer surface of the cathode when it first passed through it. This lower concentration means that there is less copper to plate, causing the observation.

Alternatively, the insulation of the current collector above this point means that the electric field is weaker, thereby reducing the driving force for copper reduction. This would then reduce the reaction rate, causing less to plate at those heights.

In order to test which of these two hypotheses dominates the observation, modifications would need to be made to the design. This can be done simply by adding more conductive leads or covering up the existing material of the current collector so direct contact with the carbon felt stops above or below the blockage. Decoupling these factors could inform better design decisions, adjusting the reactor design to have a largest possible active surface area for the fastest possible recovery.

Even in the absence of this information, at present, the fact that copper plating is limited above a height just greater than 10 cm suggests that the carbon felt need only be 10 to 11 cm in that dimension. Using 10 cm instead of 15 cm would reduce the cost of the electrode by 33 %, which, while not a particularly expensive material, could reduce operation costs in the long term.

On the other hand, cross section images of the electrode were not able to yield useful information. While images from the front contained large areas of easy-to-detect copper, cross sections only appeared to have copper on the outermost edge, making up less than 1 % of the image. As a result, the histogram was not distinctly bimodal as it was with the images of the electrode front, meaning the thresholds selected with Otsu's method are not accurate.

This proved to be the case, as a baseline quantity of copper appeared to exist in the middle of the electrode despite visual inspection by eye only seeing reflected light, not the red hue of copper, in that region. Edge effects on both sides were also prominent, to the extent that one could not quantify the deepest part of the electrode where copper was plated. This does place an upper bound on the depth penetration of copper plating, as it must stop being plated at depths shallower than the maximal depth where the edge effect of the image is observed.

In order to quantify the depth profile of copper plating, one would need to perform a more precise method, such as EDX, to more clearly identify where copper is and is not. It would also be useful to plate more copper, as while each electrode was used in 10 tests, using the estimates from Fig. 5.2.16, that still amounts to less than 1 g that could potentially be distributed across the entire

210 cm^3 volume.

Like with the height distribution, this does still provide some insight on a method to reduce cost, as an upper bound for the depth penetration was established. Since no plating is likely to have occurred more than 0.1 cm from the surface, the 1 cm thick electrode could be reduced by an order of magnitude. While the thickness should not be made too thin in order to prevent flow channelling or cause problems with the electric field, if suitable thinner electrodes can be found, it may reduce the material costs of operation.

These two reductions to the electrode size are incredibly long-term cost-savings, though, as the electrode can be reused for multiple batches until the copper plating is sufficient to prevent flow, and no significant changes to the flow rate due to pore clogging were observed after at least 10 recovery trials. Therefore, performing the suggested tests with additional plated copper to make it easier to identify would provide more useful information with regard to optimization of the reactor design as a whole.

Chapter 6

Conclusion

6.1 Summary

The scotch whiskey industry is a major economic force in Scotland, and as a result, it is also one of the largest producers of waste [1]. For instance, for every liter of whiskey, about 10 liters of spent lees, the by-product of the second distillation, are produced [8, 9].

Spent lees are a relatively dilute solution, composed primarily of a variety of organic acids and metal ions. The most prevalent component in spent lees is copper (II) ions, which are the result of low levels of corrosion from the copper stills used in whiskey distillation. Despite being extremely dilute at an average of 21.4 ppm and highest reported measurements of 41.3 ppm [6], the copper content may need to be reduced further prior to discharge in order to comply with environmental protections [11].

Additionally, copper is a resource of concern, as some projections of copper mining predict that reserves will be depleted or nearly depleted by the end of the century [19, 23]. New methods and systems need to be developed for recycling and recovering copper from waste in order for current technological growth and development to persist. These recycling and recovery processes have the added environmentally sustainable benefit of typically requiring about an order of magnitude less energy than mining and purifying primary ores [22].

Electrochemical copper recovery is promising as it can be used as an alternative to treating copper from aqueous waste prior to discharge. This process adheres to many of the green chemistry principles [26], particularly since it only requires the input of electrical energy. As a result, no secondary by-product is produced, for the only input of electrons are consumed when converting cupric ions to usable metallic copper.

This work uses electrochemical copper recovery as a means of treating scotch whiskey distillery spent lees. Tests were performed using the Porocell, a commercial 4.5 L electrochemical reactor. The reactor is designed to use a porous carbon felt cathode, allowing reasonably high currents despite low metal ion concentrations by forcing flow through small tortuous pores to enhance mass transport.

Bench scale tests compared pure copper sulphate solution to simulated spent lees, made according to the reported composition [6], in order to attempt to simplify the test conditions. This simplification was believed to be possible because copper is at molar concentrations at least one order of magnitude higher than most other waste constituents. These tests indicate that the other compounds in spent lees only cause small changes if they are at all statistically significant, and many of the differences can be ignored when considering the demands at the 4.5 L scale.

Many of the insignificant effects are partly due to the low concentration of copper, which reduced the clarity with which copper reduction-related features could be discerned. However, since these features were near or below the limit of detection, their changes are likely to be small as well, allowing those effects to be ignored. The only notable electrochemically relevant difference between electrolytes containing only copper sulphate and simulated spent lees was a decrease in the reduction potential from 271 ± 38 mV to 245 ± 46 mV (vs Ag/AgCl, 3M NaCl). This suggests the organic acids may act to chelate copper, making reduction slightly less favorable, but this difference is small relative to the voltages required in the Porocell.

Tests with the Porocell showed that copper could be recovered from spent lees, albeit with a large energy cost. The copper corrosion reaction proved to be the primary source of inefficiency at the low current densities tested. As a result, increasing the flow rate caused the efficiency to decrease by accelerating corrosion, but increasing the current from 35 mA to 105 mA increases the net Coulombic efficiency of 3 hours of operation from 13.5 ± 4.5 % to 25.2 ± 2.5 %. This increases further to 86.1 ± 1.4 % when applying 1.05 A current.

These values are slightly uncertain due to the imprecision of the ion selective electrode (ISE) used to detect changes in copper concentration, particularly at the higher concentrations tested. Results could be confirmed against the changes in pH based on the reaction stoichiometry, allowing for some confidence in the relative differences between conditions, although not necessarily with the exact values.

Despite the high efficiencies compared to other tests with copper recovery from similar concentration solutions [24], the smallest amount of energy required to reduce a 40 ppm copper solution to the drinking water standard of 2 ppm was approximately 10.1 kJ, equating to 59 GJ/tonne. This can be attributed to the high resistivity of the solution. However, the trends suggest that a minimum energy cost may exist between 105 mA and 1.05 A, as this range of currents could not be tested intensively due to instrument limits.

Results were validated against both simulated spent lees and real spent lees provided by the Glengoyne Distillery. While pure copper sulphate solution was not significantly different than simulated spent lees, real spent lees were significantly more resistive. This is likely related to the high organic content, as the literature reports of the composition only identified 12 % of the total organic content. Many of these organic compounds likely have pK_a values near 4 as the pH of this solution appeared buffered. As a result, the aforementioned measurement method of using the reaction stoichiometry and change in pH to infer cupric ion concentration changes yielded vastly different results compared to the ISE measurements.

Photographs of the electrodes after copper plating allowed for analysis of the distribution of copper throughout the electrode surface. As expected based on the electric field, copper only appeared to plate on the outside face nearest the anode. With respect to height, plating only occurred only on the lower 10 cm of the electrode, potentially a result of the hydrodynamics or the electric field. With respect to depth, plating could only be observed on the surface. Although the exact thickness of the layer in which copper plated could not be determined from the images, it is known to be smaller than the edge effects of the analysis, which were observed up to depths of 0.1 cm. While these profiles cannot be related to current density or flow rate, the small region in which plating occurs indicates that the electrode can be made smaller without affecting the process.

Overall, these results indicate that copper recovery from extremely dilute waste, such as distillery spent lees, is possible using a flow-through electrode setup like the Porocell. However, the high resistivity caused by the low salinity results in high energy costs that likely make it too expensive to be industrially viable without significant modification to the process.

6.2 Future Work

A number of experiments should be conducted to validate the presented data or to test hypotheses further. Due to the uncertainties associated with copper concentration measurements, many of the tests with the Porocell should be repeated with an analytical method more accurate at this concentration such as ICP. This would clarify some of the uncertainties in the results due to the large measurement errors, and grant tighter confidence intervals for comparison with future changes.

Due to the difference between real spent lees provided by the Glengoyne Distillery and the simulated lees, a full chemical analysis by GC-MS should be done to identify other major organic compounds besides the organic acids. One could also perform a titration with the spent lees, creating a relationship between the amount of additional acid and the pH, allowing pH to be used as an indirect means of measuring changes to copper concentration.

Tests should be conducted between currents of 105 mA and 1.05 A, as it is possible that a maximum in current efficiency and a minimum in total process energy exists in this region. This would require an instrument capable of applying greater than 10 V, but based on the data from 1.05 A, would not require excess of 20 V.

Design changes to the Porocell could be tested to attempt to reduce the influence of the solution resistance. For instance, one could simply move the anode and cathode closer together to reduce Ohmic loss. These design changes should be wary of how changing the location of the anode and cathode would influence the hydrodynamics in order to minimize stagnant areas within the reaction chamber. Alternatively, one could add sodium sulphate, an environmentally benign salt known to be inert to the copper reduction reaction, to improve the conductivity. Tests should be conducted to determine the minimum amount of sodium sulphate required to achieve the maximum reduction in energy cost.

One could also test the hypotheses related to copper plating distribution by adding or covering conductive material between the current collector and the cathode. Doing so would decouple the hydrodynamic and electric field effects by moving the topmost connection point between the electrode and current collector to other heights, allowing for one to discern which parameter to adjust to maximize the active electrode surface area.

Finally, one can then attempt to enhance the process using alternative anode materials such as boron doped diamond. These materials poison the oxygen evolution reaction sufficiently to allow for the oxidation of some organic compounds, allowing simultaneous treatment of copper and organics. This may also have the added benefit of increasing the solution conductivity over time, as the organic compounds typically will decompose into carbon dioxide, which then forms carbonic acid. This possibility is of lowest importance, though, as anodes such as boron doped diamond are expensive and still being developed and optimized for this function.

Bibliography

[1] J. Graham, B. Peter, G. M. Walker, A. Wardlaw, and E. Campbell, "Chapter 43: Characterisation of the pot ale profile from a malt whisky distillery," in *Worldwide Distilled Spirits Conference* (G. M. Walker, I. Goodall, R. Fotheringham, and D. Murray, eds.), Nottingham University Press/The Institute of Brewing and Distilling, 2012.

[2] R. Smithers, "Scotch whisky industry bigger than uk iron and steel or computers," 2015 Jan 27.

[3] M. Tokuda, N. Ohta, S. Morimura, and K. Kidaz, "Methane fermentation of pot ale from a whisky distillery after enzymatic or microbial treatment," *Journal of Fermentation and Bioengineering*, vol. 85, no. 5, pp. 495–501, 1998.

[4] B. Harrison, O. Fagnen, F. Jack, and J. Brosnan, "The impact of copper in different parts of malt whisky pot stills on new make spirit composition and aroma," *Journal of the Institute of Brewing*, vol. 117, no. 1, pp. 106–112, 2011.

[5] Y. Kharayat, "Distillery wastewater: bioremediation approaches," *Journal of Integrative Environmental Sciences*, vol. 9, no. 2, pp. 69–91, 2012.

[6] E. H. Yu, "Copper revmoal and recovery from whisky distillery wastewater," 27 Jun 2017.

[7] T. K. Grose, "Whisky a go go: Can Scotlands distillery waste boost biofuels?," *National Geographic*, 15 June 2013.

[8] J. R. Piggott, R. Sharp, R. Erskine, and B. Duncan, *The Science and Technology of Whiskies.* Longman Scientific and Technical, 1989.

[9] I. Russell, *Whisky: Technology, Production, and Marketing.* Academic Press, 2003.

[10] K. Kida, S. Morimura, Y. Mochinaga, and M. Tokuda, "Efficient removal of organic matter and NH_4^+ from pot ale by a combination of methane fermentation and biological denitrification and nitrification processes," *Process Biochemistry*, vol. 34, no. 6-7, pp. 567–575, 1999.

[11] SEPA, "Environmental quality standards and standards for discharges to surface waters: WAT-SG-53," Dec 2015.

[12] S. France and T. Zabel, "Assessment of programmes under Article 7 of council Directive 76/464/EEC," 2001.

[13] R. Hughes, "Personal communication," 2018 Aug 15.

[14] W. Environmental, "Wastewater treatment case study: Glenallachie Distillery, Scotland," report, 2008.

[15] T. A. Bringhurst and J. Brosnan, *Whisky: Technology, Production and Marketing.* Elsevier, 2015.

[16] K. Rajeshwar, J. Ibanez, and G. M. Swain, "Electrochemistry and the environment," *Journal of Applied Electrochemistry*, vol. 24, pp. 1077–1091, 1994.

[17] J. Bell, C. Morgan, G. Dick, and G. Reid, "Distillery feed by-products briefing: An AA211 special economic study for the Scottish government," 2012.

[18] S. Parliament, “The water supply (water quality) (Scotland) regulations 2001,” 2001.

[19] A. Elshkaki, T. E. Graedel, L. Ciacci, and B. K. Reck, “Copper demand, supply, and associated energy use to 2050,” *Global Environmental Change*, vol. 39, pp. 305–315, 2016.

[20] T. Norgate and S. Jahanshahi, “Low grade ores - smelt, leach, or concentrate?,” *Minerals Engineering*, vol. 23, pp. 65–73, 2010.

[21] I. Gaballah and N. Kanari, “Recycling policy in the European Union,” *Journal of Metals*, vol. 53, no. 11, pp. 24–27, 2001.

[22] T. Norgate and W. J. Rankin, “The role of metals in sustainable development,” 29-31 May 2002 2002.

[23] P. Crowson, “Some observations on copper yields and ore grades,” *Resources Policy*, vol. 37, no. 1, pp. 59–72, 2012.

[24] S. A. Northcote and A. Aldridge, “The recovery of copper from hydrochloric acid process liquors,” report, EA Technology Ltd, 1995.

[25] A. E. Marteel, J. A. Davies, W. W. Olson, and M. A. Abraham, “Green chemistry and engineering: Drivers, metrics, and reduction to practice,” *Annual Review of Environment and Resources*, vol. 28, pp. 401–428, 2003.

[26] P. Anastas and J. C. Warner, *Green Chemistry: Theory and Practice.* Oxyford Univresity Press, 2000.

[27] R. Buckle and S. Roy, “The recovery of copper and tin from waste tin stripping solution,” *Separation and Purification Technology*, vol. 62, no. 1, pp. 86–96, 2008.

[28] A. Z. Medvedev, A. F. Zherebilov, A. I. Masliiy, and N. P. Poddubnyi, “Effect of solution flow rate and direction on copper electrodeposition process from

sulfuric acid electrolyte on porous electrode with high electric conductivity," *Russian Journal of Electrochemistry*, vol. 44, no. 6, pp. 761–766, 2008.

[29] N. C. Hoyt, K. L. Hawthorne, R. F. Savinell, and J. S. Wainright, "Plating utilization of carbon felt in a hybrid flow battery," *Journal of the Electrochemical Society*, vol. 163, no. 1, pp. A5041–A5048, 2016.

[30] K. Rajeshwar and J. Ibanez, *Environmental Electrochemistry.* Elsevier, 1997.

[31] D. Pletcher and F. Walsh, *Industrial Electrochemistry.* Netherlands: Springer, 1993.

[32] C. Comninellis and G. H. Chen, *Electrochemistry for the Environment.* New York: Springer, 2010.

[33] D. A. Campbell, I. M. Dalrymple, J. G. Sunderland, and D. Tilston, "The electrochemical recovery of metals from effluent and process streams," *Resources Conservation and Recycling*, vol. 10, no. 1-2, pp. 25–33, 1994.

[34] S. S. A. El Rehim, S. M. Sayyah, and M. M. El Deeb, "Electroplating of copper films on steel substrates from acidic gluconate baths," *Applied Surface Science*, vol. 165, no. 4, pp. 249–254, 2000.

[35] B. J. Sabacky and J. W. Evans, "Electrodeposition of metals in fluidized-bed electrodes: 2. Experimental investigation of copper electrodeposition at high current density," *Journal of the Electrochemical Society*, vol. 126, no. 7, pp. 1180–1187, 1979.

[36] S. Silva-Martnez and S. Roy, "Copper recovery from tin stripping solution: Galvanostatic deposition in a batch-recycle system," *Separation and Purification Technology*, vol. 118, pp. 6–12, 2013.

[37] F. C. Walsh, N. A. Gardner, and D. R. Gabe, "Development of the eco-cascade cell reactor," *Journal of Applied Electrochemistry*, vol. 12, no. 3, pp. 299–309, 1982.

[38] B. Beverskog and I. Puigdomenech, "Revised Pourbaix diagrams for copper at 5-150^{o}C," report, Swedish Nuclear Power Inspectorate, 1995.

[39] A. C. T. Inc, "Cyanide and heavy metal removal."

[40] B. Volesky, *Biosorption of Heavy Metals*. Boca Raton: CRC Press, 1990.

[41] S. G. Lu and S. W. Gibb, "Copper removal from wastewater using spent-grain as biosorbent," *Bioresource Technology*, vol. 99, no. 6, pp. 1509–1517, 2008.

[42] J. Varia, A. Zegeye, S. Roy, S. Yahaya, and S. Bull, "*Shewanella putrefaciens* for the remediation of Au^{3+}, Co^{2+} and Fe^{3+} metal ions from aqueous systems," *Biochemical Engineering Journal*, vol. 85, pp. 101–109, 2014.

[43] S. P. Cheng, W. Grosse, F. Karrenbrock, and M. Thoennessen, "Efficiency of constructed wetlands in decontamination of water polluted by heavy metals," *Ecological Engineering*, vol. 18, no. 3, pp. 317–325, 2002.

[44] R. S. Yeh, Y. Y. Wang, and C. C. Wan, "Removal of Cu-EDTA compounds via electrochemical process with coagulation," *Water Research*, vol. 29, no. 2, pp. 597–599, 1995.

[45] F. Jack, J. Bostock, D. Tito, B. Harrison, and J. Brosnan, "Electrocoagulation for the removal of copper from distillery waste streams," *Journal of the Institute of Brewing*, vol. 120, no. 1, pp. 60–64, 2014.

[46] S. Miura and H. Honma, "Advanced copper electroplating for application of electronics," *Surface and Coatings Technology*, vol. 169, pp. 91–95, 2003.

[47] M. Lefebvre, G. Allardyce, M. Seita, H. Tsuchida, M. Kusaka, and S. Hayashi, "Copper electroplating technology for microvia filling," *Circuit World*, vol. 29, no. 2, pp. 9–14, 2003.

[48] J. T. Hinatsu and F. R. Foulkes, "Diffusion coefficients for copper (II) in aqueous cupric sulfate-sulfuric acid solutions," *Journal of The Electrochemical Society*, vol. 136, no. 1, pp. 125–132, 1989.

[49] J. T. Hinatsu and F. R. Foulkes, "Electrochemical kinetic parameters for the cathodic deposition of copper from dilute aqueous acid sulfate solutions," *Canadian Journal of Chemical Engineering*, vol. 69, no. 2, pp. 571–577, 1991.

[50] C. N. Liao, C. Y. Lin, C. L. Huang, and Y. S. Lu, "Morphology, texture and twinning structure of cu films prepared by low-temperature electroplating," *Journal of the Electrochemical Society*, vol. 160, no. 12, pp. D3070–D3074, 2013.

[51] P. H. Britto-Costa, E. R. Pereira-Filho, and L. A. M. Ruotolo, "Copper electrowinning using a pulsed bed three-dimensional electrode," *Hydrometallurgy*, vol. 144, pp. 15–22, 2014.

[52] F. Coeuret, "The fluidized-bed electrode for the continuous recovery of metals," *Journal of Applied Electrochemistry*, vol. 10, no. 6, pp. 687–696, 1980.

[53] D. Hutin and F. Coeuret, "Experimental study of copper deposition in a fluidized bed electrode," *Journal of Applied Electrochemistry*, vol. 7, no. 6, pp. 463–471, 1977.

[54] P. A. Shirvanian and J. M. Calo, "Copper recovery in a spouted vessel electrolytic reactor (sber)," *Journal of Applied Electrochemistry*, vol. 35, no. 1, pp. 101–111, 2005.

[55] K. L. Hawthorne, J. S. Wainright, and R. F. Savinell, "Maximizing plating density and efficiency for a negative deposition reaction in a flow battery," *Journal of Power Sources*, vol. 269, pp. 216–224, 2014.

[56] J. Gonzalez-Garcia, V. Montiel, A. Aldaz, J. A. Conesa, J. R. Perez, and G. Codina, "Hydrodynamic behavior of a filter-press electrochemical reactor with carbon felt as a three-dimensional electrode," *Industrial and Engineering Chemistry Research*, vol. 37, no. 11, pp. 4501–4511, 1998.

[57] M. Kyuzou, W. Mori, and J. Tanaka, "Electronic structure and spectra of cupric acetate mono-hydrate revisited," *Inorganica Chimica Acta*, vol. 363, no. 5, pp. 930–934, 2010.

[58] G. H. Chen, "Electrochemical technologies in wastewater treatment," *Separation and Purification Technology*, vol. 38, no. 1, pp. 11–41, 2004.

[59] P. Grimshaw, J. M. Calo, P. A. Shirvanian, and G. Hradil, "II. electrodeposition/removal of nickel in a spouted electrochemical reactor," *Industrial and Engineering Chemistry Research*, vol. 50, no. 16, pp. 9525–9531, 2011.

[60] A. I. Maslii, N. P. Poddubnyi, A. Z. Medvedev, and O. V. Karunina, "The effect of the solution flow rate on the final mass of metals deposited into a porous electrode at individual and joint deposition. frontal delivery of solution," *Russian Journal of Electrochemistry*, vol. 50, no. 10, pp. 909–917, 2014.

[61] A. I. Maslii, N. P. Poddubnyi, A. Z. Medvedev, and O. V. Karunina, "The effect of the solution flow rate on the final mass of metals deposited into a porous electrode at individual and joint deposition. rear delivery of solution," *Russian Journal of Electrochemistry*, vol. 50, no. 10, pp. 918–925, 2014.

[62] J. Trainham and J. Newman, “A flow through porous electrode model: Application to metal-ion removal from dilute streams,” *Journal of The Electrochemical Society*, vol. 124, no. 10, pp. 1528–1540, 1977.

[63] R. Alkire and P. Ng, “Studies on flow-by porous electrodes having perpendicular directions of current and electrolye flow,” *Journal of The Electrochemical Society*, vol. 124, no. 8, pp. 1220–1227, 1977.

[64] A. Wragg, “Effect of flow rate and constant operating current on the behaviour of a recirculating electrochemical reactor system,” *Journal of Applied Electrochemistry*, vol. 13, pp. 507–517, 1982.

[65] Y. Wang and Y. Hasebe, “Carbon felt-based bioelectrocatalytic flow-through detectors: 2,6-dichlorophenol indophenol and peroxidase coadsorbed carbon-felt for flow-amperometric determination of hydrogen peroxide,” *Materials*, vol. 7, pp. 1142–1154, 2014.

[66] N. S. Lawrence, J. Davis, F. Marken, L. Jiang, T. G. J. Jones, S. N. Davies, and R. G. Compton, “Electrochemical detection of sulphide: a novel dual flow cell,” *Sensors and Actuators B: Chemical*, vol. 69, pp. 189–192, 2000.

[67] F. C. Walsh, L. F. Arenas, C. Ponce de Leon, G. W. Reade, I. Whyte, and B. G. Mellor, “The continued development of reticulated vitreous carbon as a versatile electrode material: Structure, properties and applications,” *Electrochimica Acta*, vol. 215, pp. 566–591, 2016.

[68] G. Mohanakrishna, S. V. Mohan, and P. N. Sarma, “Bio-electrochemical treatment of distillery wastewater in microbial fuel cell facilitating decolorization and desalination along with power generation,” *Journal of Hazardous Materials*, vol. 177, no. 1-3, pp. 487–494, 2010.

[69] X. M. Chen, G. H. Chen, and P. L. Yue, "Anodic oxidation of dyes at novel Ti/B-diamond electrodes," *Chemical Engineering Science*, vol. 58, no. 3-6, pp. 995–1001, 2003.

[70] C. Terashima, R. Hishinuma, N. Roy, Y. Sugiyama, S. S. Latthe, K. Nakata, T. Kondo, M. Yuasa, and A. Fujishima, "Charge separation in TiO_2/BDD heterojunction thin film for enhanced photoelectrochemical performance," *ACS Applied Materials and Interfaces*, vol. 8, pp. 1583–1588, 2016.

[71] J. G. Sunderland and I. M. Dalrymple, "Cell and method for the recovery of metals from dilute solutions," 1997.

[72] J. Bancroft and I. M. Dalrymple, "Porocell: A dramatic improvement in the extraction of metals from waste solutions," report, EA Technology Ltd, 1996.

[73] T. Group, "Porocell operational procedures," report, EA Technology Ltd, 1996.

[74] S. A. Northcote, "Laboratory scale feasibility study into the removal of cadmium from aqueous streams in the porocell," report, EA Technology Ltd, 1994.

[75] P. G. Griffiths, C. P. Jones, and A. R. Junkison, "The removal of technetium from EARP waste streams, Phase III," Report RandD Technical Report P55, AEA Technology, 1996.

[76] P. T. Huyen, T. D. Dang, M. T. Tung, N. T. T. Huyen, T. A. Green, and S. Roy, "Electrochemical copper recovery from galvanic sludge," *Hydrometallurgy*, vol. 164, pp. 295–303, 2016.

[77] A. G. Tyson and T. D. Tilston, "Copper recovery from a nitrate stream," report, EA Technology Ltd, 1998.

[78] M. F. N. Noh and I. E. Tothill, "Development and characterisation of disposable gold electrodes, and their use for lead (II) analysis," *Analytical and Bioanalytical Chemistry*, vol. 386, no. 7-8, pp. 2095–2106, 2008.

[79] C. Spegel, A. Heiskanen, J. Acklid, A. Wolff, R. Taboryski, J. Emneus, and T. Ruzgasd, "On-chip determination of dopamine exocytosis using mercaptopropionic acid modified microelectrodes," *Electroanalysis*, vol. 19, no. 2-3, pp. 263–271, 2006.

[80] N. Otsu, "A threshold selection method from gray-level histograms," *IEEE Transactions of Systems, Man, and Cybernetics*, vol. SMC-9, no. 1, pp. 62–66, 1979.

[81] N. F. I. I. Nestle and R. Kimmich, "Concentration-dependent diffusion coefficients and sorption isotherms. application to ion exchange processes as an example," *Journal of Physical Chemistry*, vol. 100, pp. 12569–12573, 1996.

[82] K. Scott, X. Chen, J. Atkinson, M. Todd, and R. Armstrong, "Electrochemical recycling of tin, lead, and copper from stripping solution in the manufacture of circuit boards," *Resources Conservation and Recycling*, vol. 20, pp. 43–55, 1997.

[83] M. R. King and N. A. Mody, *Numerical and Statistical Methods for Bioengineering.* Cambridge: Cambridge University Press, 2010.

[84] H. Scheffe, "A method for judging all contrasts in the analysis of variance," *Biometrika*, vol. 40, no. 1-2, pp. 87–104, 1953.

Appendix A

Statistical and Computational Methods

A.0.1 Power consumption

Electrical power is defined as the product of voltage and current. While in these experiments, the current is set to be constant, variations may occur due to noise or instrument problems. As a result, both voltage and current can potentially change with time. To obtain the complete electrical power consumption, numerical integration of the instantaneous current-voltage product across the test duration was performed using the trapezoidal Riemann sum.

A.1 Linear regression analyses

In many calculations, the desired value for comparison is not the output value measured, but the relationship between the output value (y) and the input value (x). For all calculations in this report, all relationships were either linear or could be linearized by performing a simple calculation on the measured or input values. Fits to linear equations, generic form of power N shown in Eq. A.1, were calculated in accordance with the linear least squares method [83].

$$\hat{y} = \sum_{n=0}^{N} a_n x^n \tag{A.1}$$

Briefly, the values of constants a_n are selected to minimize the sum of squared of errors (SSE), defined by Eq. A.2, where $\hat{y}$ is the predicted value using the fit and m is the number of data points used in the fit. This minimization process is expressed by the solution to the matrix equation Eq. A.3.

$$SSE = \sum_{i=1}^{m} (\hat{y} - y_i)^2 \tag{A.2}$$

$$\begin{bmatrix} m & \dots & \sum_{i=1}^{m} z_i^N \\ \vdots & \ddots & \vdots \\ \sum_{i=1}^{m} x_i^N & \dots & \sum_{i=1}^{m} x_i^{2N} \end{bmatrix} \begin{bmatrix} a_0 \\ \vdots \\ a_N \end{bmatrix} = \begin{bmatrix} \sum_{i=1}^{m} y_i \\ \vdots \\ \sum_{i=1}^{m} x_i^N y_i \end{bmatrix} \tag{A.3}$$

Doing so allows for the calculation of values such as the coefficient of determination (R^2) and the variance of the fit line (s_y^2), defined by Eq. A.4-A.5. The coefficient of determination was used as a general measure for the quality of fit lines, as it describes the percentage of variability observed in the output value that can be explained by the fit line. The variance of the fit line can then be used to calculate the variance of the coefficients a_n. The equations used for calculation of $s_{a_0}^2$ and $s_{a_1}^2$ for a linear equation of power $N = 1$ are provided in Eq. A.6-A.7.

$$R^2 = 1 - \frac{SSE}{\sum_{i=1}^{m} \left(y - \frac{\sum y}{m} \right)^2} \tag{A.4}$$

$$s_y^2 = \frac{SSE}{m - 2} \tag{A.5}$$

$$s_{a_0}^2 = s_y^2 \frac{m \sum x_i^2}{\left(m \sum z_i^2 - (\sum x_i)^2 \right)^2} \left(\left(\sum x_i \right)^2 - 4 \sum x_i + m \right) \tag{A.6}$$

$$s_{a_1}^2 = s_y^2 \frac{m}{\left(m \sum z_i^2 - \left(\sum x_i\right)^2\right)^2} \left(m \sum x_i^2 - \left(\sum x_i\right)^2\right) \tag{A.7}$$

A.2 Statistical testing: ANOVA and Scheffe comparison

All data was analyzed for statistical significance, taking the values of independent replicates and making comparisons for statistical significance. In cases where a calculated value (f) used multiple uncertain values in its determination (x_n), the variance of the calculated value (s_f^2) was determined by the commonly accepted method for propagation of error using the input values and their variances ($s_{x_n}^2$) (Eq. A.8) [83].

$$s_f^2 = \sum s_{x_n}^2 \left(\frac{df}{dx_n}\right)^2 \tag{A.8}$$

All comparisons made were calculated via ANOVA ($\alpha = 0.05$). For cases where the comparison is among calculated values with propagated errors, particularly those from regressions such as the diffusion coefficient, a modified algorithm was developed in MatLab to calculate ANOVA table values from the means, standard deviation, and degrees of freedom.

While most built-in algorithms for the analysis of variance (ANOVA) rely on input of the individual trials, this process does not account for propagated uncertainties associated with calculated values. As a result, the standard equations based on individual tests were modified to be related to the means and standard deviations. The modified version for a 2-way ANOVA, which tests for effects of 2 independent variables, also called factors, are presented.

$$SS_{row} = \sum n_{row,i} \left(x_{row,i} - x_{grand}\right)^2 \tag{A.9}$$

Table A.1: List of variables used in 2-way ANOVA

$x_{i,j}$, $s_{i,j}$, $n_{i,j}$	Mean, standard deviation, and number of replicates of each individual experimental condition, combining condition i of variable 1 and j of variable 2
$\bar{x}_{row,i}$, $n_{row,i}$, $s_{row,i}$	Mean, standard deviation, and number of replicates of all tests for which condition i of variable 1 (row) was used, independent of the condition for the second variable
$\bar{x}_{col,i}$, $n_{col,i}$	Mean and total number of replicates for condition j of variable 2 (col), independent of condition for the first variable
$\bar{x}_{grand}$	Mean across all conditions
m_{row}, m_{col}	Number of conditions tested for variable 1 and 2, respectively
SS_{var}	Sum of squares of error due to var
MS_{var}	Degrees of freedom of var
ν_{var}	Mean across all conditions
F_{var}	F-statistic of var

$$SS_{column} = \sum n_{col,j} \left(x_{col,ji} - x_{grand}\right)^2 \tag{A.10}$$

$$SS_{error} = \sum \sum \left(n_{i,j} - 1\right) * s_{i,j}^2 \tag{A.11}$$

$$SS_{interference} = \sum \sum \left(x_{i,j} - x_{row,i} - x_{col,j} + x_{grand}\right)^2 \tag{A.12}$$

$$MS_{var} = \frac{SS_{var}}{\nu_{var}} \tag{A.13}$$

$$F_{var} = \frac{MS_{var}}{MS_{error}} \tag{A.14}$$

In cases where calculated values used means composed of different numbers of degrees of freedom (e.g. f is a function of x_1 and x_2; x_1 is composed of 3 replicates to give 2 degrees of freedom and x_2 is from a linear regression with 5 data points and 2 variables, giving 3 degrees of freedom), the smaller number was used in the statistical test for maximum confidence.

Significance of differences between groups was determined using Scheffe's method (Eq. A.15) [84].

$$\Delta_{crit}^2 = \nu_{gr} F(\alpha, \nu_{gr}, \nu_{err}) MSE \left(\frac{1}{n_1} + \frac{1}{n_2} \right) \tag{A.15}$$

In this equation, Δ_{crit} is the minimum difference among group means (μ_1 and μ_2) necessary for significance level α, ν_{gr} is the degrees of freedom among the groups, ν_{err} is the degrees of freedom from error, F is the f-statistic function, MSE is the mean sum of squares of error defined by the ANOVA calculation, and n_1 and n_2 are the degrees of freedom of the two groups being compared plus 1, equivalent to number of replicates in a simple comparison. This method was selected over the more often used Tukey-Kramer method due to the narrower confidence intervals, the ability to compare groups with different numbers of replicates, and the ability to obtain the p-value of each individual comparison (Eq. A.16) using the inverse F-statistic.

$$F(p, \nu_{gr}, \nu_{err}) = \frac{(\mu_1 - \mu_2)^2}{(\nu_{gr} MSE) \left(\frac{1}{n_1} + \frac{1}{n_2} \right)} \tag{A.16}$$

Appendix B

Development of Procedures

In order to test the Porocell, an initial characterization of its limitations is necessary in order to establish the test parameters. Additionally, the Porocell is capable of plating copper, but not quantifying how much has been plated, so an analytical technique that is reliable in the relevant concentration range is needed to be able to analyze its effectiveness. This is particularly important given the results at the bench scale, which showed that gravimetric methods have notable uncertainty if insufficient amounts of copper are plated. Given that the current efficiencies of previous Porocell tests at this dilute concentration are low and variable [24, 77], a gravimetric method should be avoided even if the batch volume and electrode size are significantly larger, as it is uncertain how much copper must be deposited to obtain a reliable measurement. This also alleviates any handling issues that may arise, as the carbon felt often loses loose fibres with handling, leading to underestimates in the measurements.

B.1 Copper measurement method

Two methods for measuring copper concentrations were tested: UV-vis spectroscopy and use of an ion selective electrode. Calibration curves for the two methods are presented in Fig. B.2 and B.3, respectively.

The absorption spectra of weakly acidic 40 ppm Cu^{2+} and that of the solvent without any copper sulphate are included in the Fig. B.1. It is apparent that at this concentration, the difference between the solvent alone and with copper sulphate is small as a result of the extremely dilute concentration. While the instrument was able to discern the largest difference with wavelenths of 760 nm, prior work with spectrophotometric copper detection used 805 nm [36]. Due to the small difference between 0 and 40 ppm copper, it is likely that the disagreement is due to inherent inaccuracies when comparing these spectra. An initial test with both wavelengths (Table B.1) shows that while both wavelengths have strong linear relationships with concentration ($R^2 > 0.95$), 805 nm is more sensitive to concentration changes with a slightly higher slope compared to the measurement error.

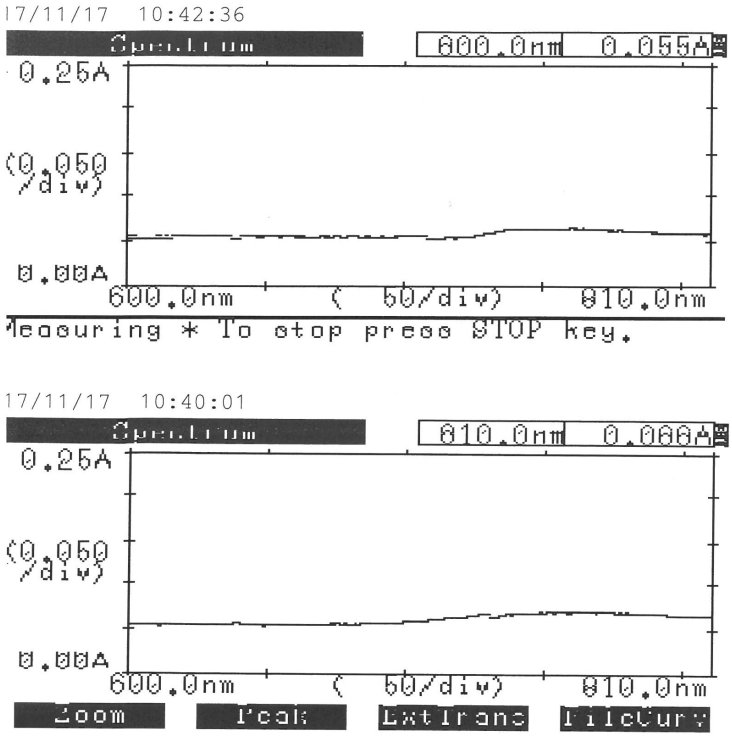

Measuring * To stop press STOP key.

Figure B.1: Absorption spectra of dilute sulphuric acid, pH = 4 (approximately 65 μM) (top) and 40 ppm copper in dilute sulphuric acid, pH = 4 (bottom).

Table B.1: Comparison between absorbance wavelengths of 760 nm and 805 nm for detection of copper at concentrations below 40 ppm. Values are mean ± measurement error (1 standard deviation of absorbance for the same solution, n = 3).

Concentration (ppm)	Absorbance 760 nm	Absorbance 805 nm
40	0.071 ± 0.003	0.069 ± 0.004
25	0.068 ± 0.006	0.066 ± 0.007
10	0.064 ± 0.004	0.062 ± 0.006
4	0.064 ± 0.005	0.061 ± 0.007
2.5	0.064 ± 0.006	0.061 ± 0.008
1	0.064 ± 0.005	0.061 ± 0.007
0.4	0.064 ± 0.006	0.061 ± 0.008

	Absorbance 760 nm	Absorbance 805 nm
Coefficient of determination	0.987	0.986
Slope (abs/ppm)	$2.03*10^{-4}$	$2.15*10^{-4}$

As a result, absorption with 805 nm was repeated to obtain a reliable relationship between absorbance and concentration. Absorption at 805 nm shows a relatively linear trend with concentration, agreeing with the prediction by Beer-Lambert Law. However, while the mean absorbance was initially strongly linearly related to concentration, adding in additional replicates uncovered day-to-day variability that weakened the fit quality ($R^2 = 0.843$), with the majority of the deviation at the lowest concentrations. Additionally, it is apparent that the standard deviations are quite large, particularly relative to the slope of the line. Thus, when using this fit line to determine the concentration from the absorbance, there will be notable error associated with the method.

In contrast, using the cupric ion selective electrode led to a very strong correlation ($R^2 = 0.995$) between the log_{10} of the concentration and the measured potential for concentrations from 2 to 100 ppm. Other fits were performed with larger or narrower ranges to determine the apparent concentration range for which

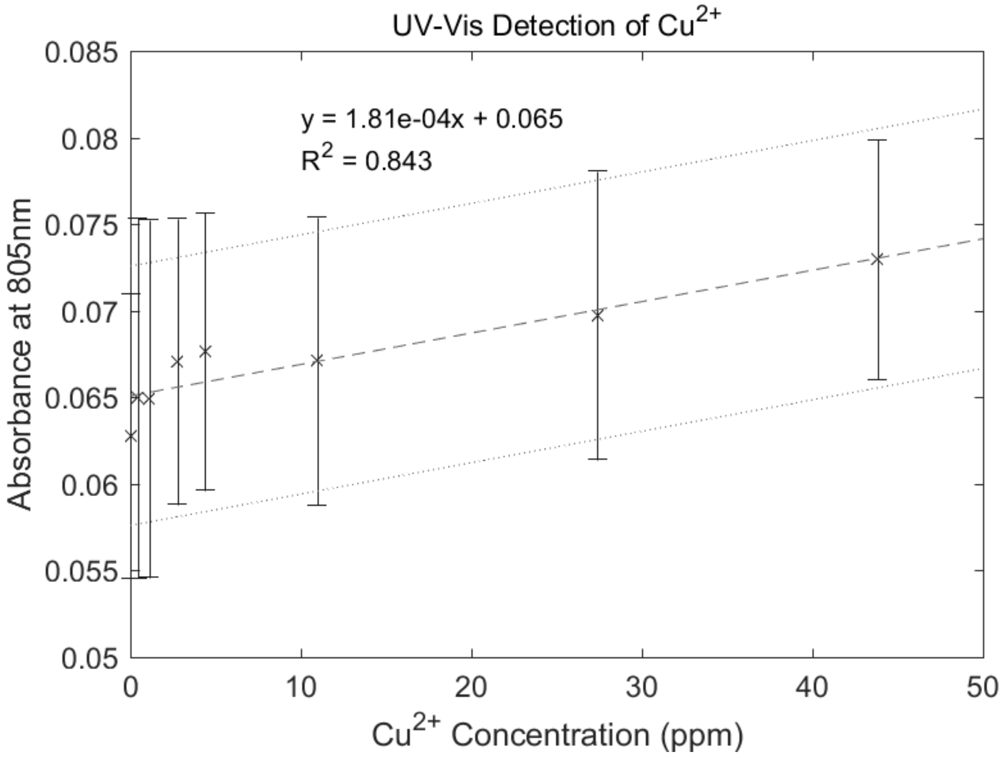

Figure B.2: Calibration of UV-vis measurements for cupric ion detection. Error bars indicate the standard deviation (n = 3); the dotted line indicates the standard deviation of the fit line.

it is accurate (Table B.2). Importantly, the slope of this fit line is much larger than the standard deviation, particularly compared to that of the UV-vis calibration. This allows for more reliable measurements which can discern high and low concentrations from one another.

Measurements do deviate from the fit line below 2 ppm, but the deviation is mostly apparent in two of the three replicates, and could simply be the result of an experimental error on those days. It is possible that it is simply an artefact where the ISE was not fully equilibrated, as the ISE is stored in 100 ppm Cu^{2+} (pH = 4 ± 0.1) when in daily use, and measurements were typically taken from low to high concentration. Even if this is not the case, the target final concentration for recovery is 2 ppm, so the deviation is not relevant to the experiments as designed.

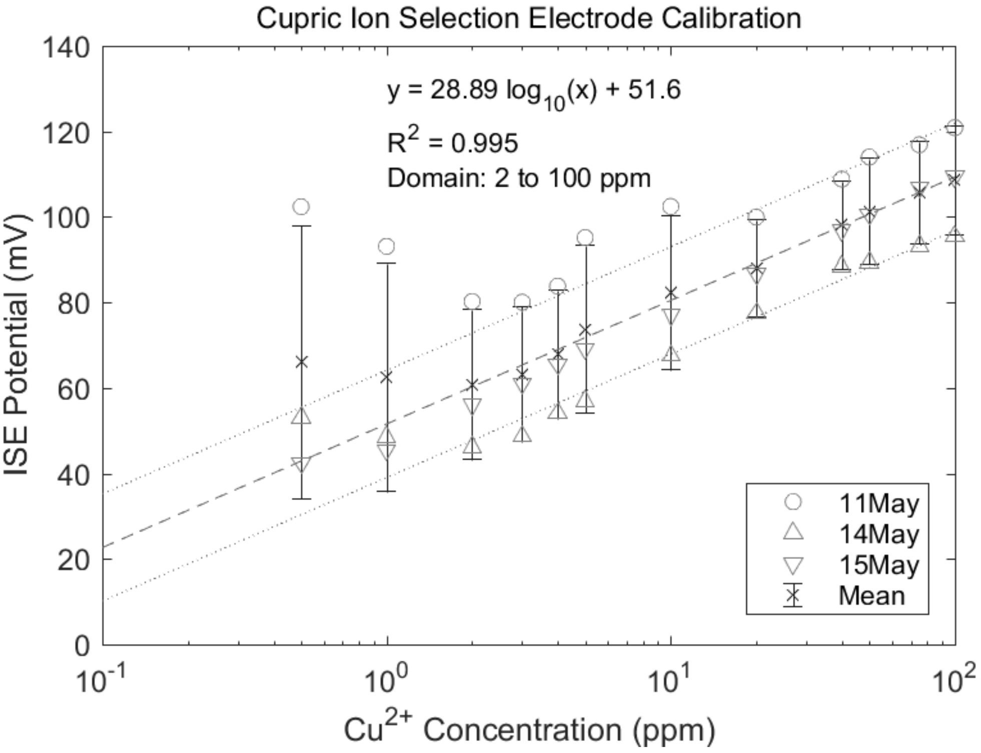

Figure B.3: Calibration of the ion selective electrode for cupric ion detection. Error bars indicate the standard deviation (n = 3); individual replicates are also presented. The dotted line indicates the standard deviation of the fit line from 2 to 100 ppm.

Table B.2: Quality of the fit line to the ISE calibration for different regions of interest. Data was fit to the following equation:
$V_{ISE} = slope * \log_{10}[Cu^{2+}] + intercept$

Lower bound (ppm)	Upper bound (ppm)	Slope	Intercept	R^2
0.5	100	22.8	60.1	0.908
1	100	26.5	55.1	0.972
2	100	28.9	51.6	0.995
3	100	29.1	51.3	0.993

Based on these two results, the ISE is the more appropriate method for measuring copper concentrations throughout recovery experiments. Not only is it more sensitive with a larger change due to change in concentration, but also is more reproducible with each measurement.

B.2 Calibration of the cupric ion selective electrode

Notably, there is a difference in the dates of each replicate used in the initial ISE calibration (Fig. B.3), and they follow a trend where the later the date of the calibration, the lower the measured potential. Across the span of those four days, the potential decreased by slightly more than 10 mV across all concentrations measured. As a result, it is necessary to fully characterize the ISE's behaviour over time to assess whether this trend is consistent and needs to be accounted for in copper measurements, or if this pattern was from random chance.

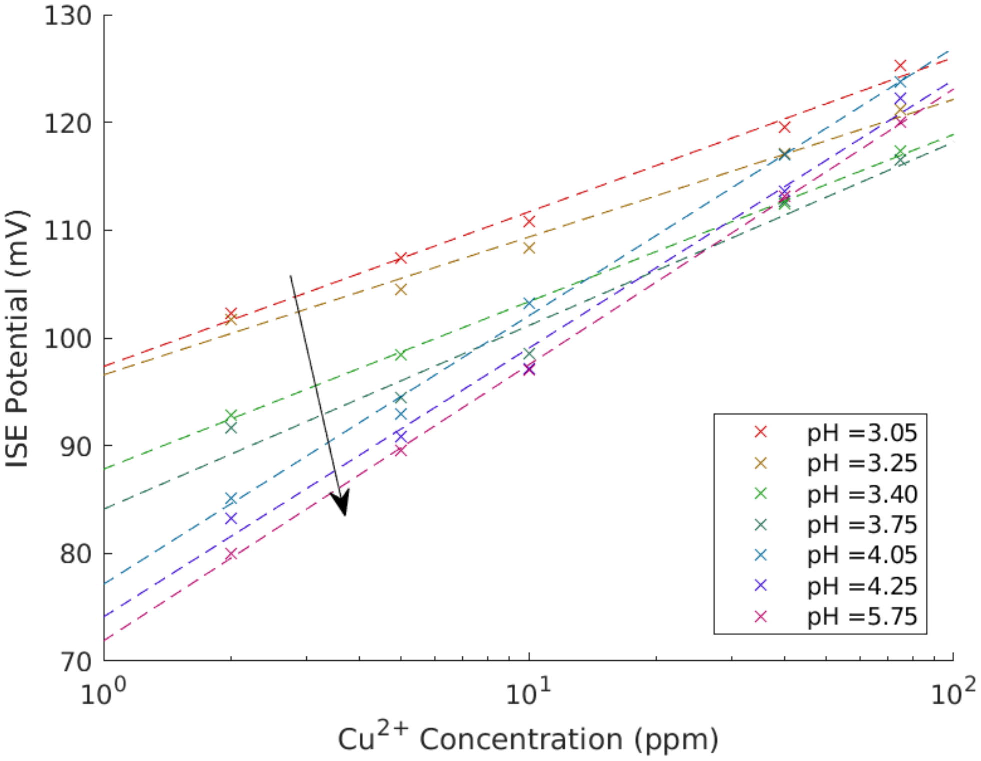

Figure B.4: Calibrations of the ion selective electrode at different pH values. The arrow shows the direction of increasing pH.

In addition to time, one other possible variable affecting ISE results is the pH. While the ISE used in the experiments is designed to be operational in the pH range of 2 to 7, the concentration of protons are likely to affect the potential reading if the membrane is not completely selective for cupric ions. The solution acidity should also become stronger over the course of the process, as the anodic counter reaction to copper plating is the oxygen evolution reaction ($H_2O \rightarrow 2H^+ + \frac{1}{2}O_2 + 2e^-$), which generates protons. A series of calibrations were then performed across a range of expected pH values from 4.25 to 3.05, including an additional higher pH test of 5.75 as a near-neutral reference (Fig. B.4). A qualitative assessment of the figure shows that at low concentrations, the measured potential drops as pH increases, decreasing from 102 mV at pH 3.05 to 83 mV at pH 4.25. At high concentrations, there is less of a trend, as the slope of the potential-concentration relationship becomes steeper at high pH values.

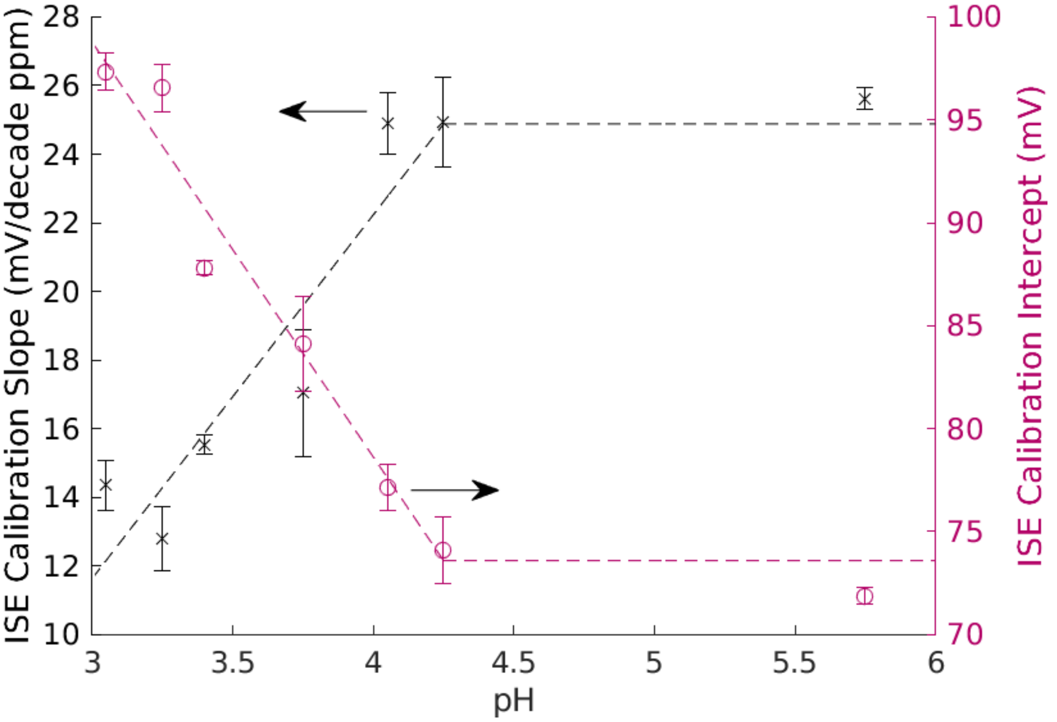

Figure B.5: Quantification of the pH effect on the ISE calibration's slope (-x-, left axis) and intercept (-o-, right axis). Error bars indicate the uncertainty in the calibration fit line.

A more quantitative assessment of this relationship is presented in Fig. B.5. Here, it is apparent that the slope generally increases with pH while the intercept decreases, but only until about a pH of 4.25. After this point, the pH dependence is much weaker. This dependence is roughly linear ($R^2 = 0.873$ for slope, $R^2 = 0.963$ for intercept), so a correction to the calibration curve and its associated error using the pH can be done.

Based on the Pourbaix diagram (Fig. 3.4), pH 4.25 is roughly a transition between the $Cu^{2+} \rightarrow Cu^0$ reaction in more acidic pH to the $Cu^{2+} \rightarrow Cu_2O$ reaction in more alkaline pH. This means that at neutral pH values, there is only one electron transfer, but in more acidic solutions, a greater fraction of those Cu^{2+} ions would undergo two electron transfers instead due to preference for the Cu (s) state over the Cu_2O state. Based on the Nernst equation (Eq. 2.2), the slope of the ISE should be inversely related to number of electron transfers, z, explaining why the slope would be lower in acidic solution, as a greater number of those reactions at the electrode would transfer two electrons instead of just one. Likewise, if the apparent E^0 is related to the relative fraction of one and two electron transfers, it should also be related to pH. Since $Cu^{2+} \rightarrow Cu$ has a standard potential of 0.34 V vs SHE and $Cu^{2+} \rightarrow Cu^+$ has a standard potential of 0.16 V vs SHE, it makes sense that the intercept would increase at more acidic pH.

Looking at these relationships over a series of days (Fig. B.6), it is seen that while the intercept seems to decrease over time, the slope increases slightly. The trends with pH are generally quite strong (Table B.3), indicating that this relationship is ongoing and not the result of a limited reaction with protons. The manufacturer does note in its documentation that the ISE may experience slight decreases in potential over time, so the decrease in intercept is expected. This trend is roughly -0.562 mV/day (Fig. B.7), which is lower than the expected 2

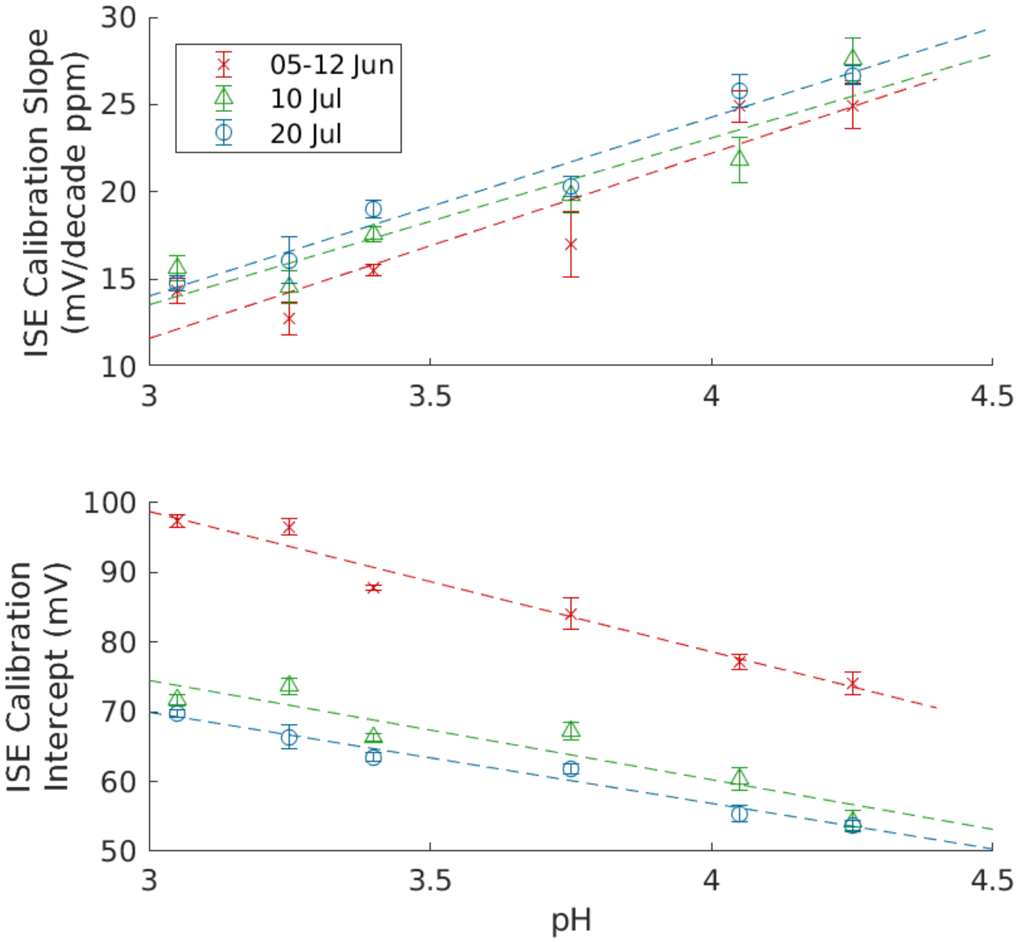

Figure B.6: Change in the ISE calibration's slope (top) and intercept (bottom) with respect to pH and time. Error bars indicate the uncertainty in the calibration fit line.

mV/day drift reported by the manufacturer's operation manual.

Table B.3: Coefficients of determination of the ISE calibration variables with respect to pH for each test date in July.

	Slope vs pH	Intercept vs pH
05-12 June	0.873	0.963
10 July	0.887	0.860
20 July	0.967	0.973

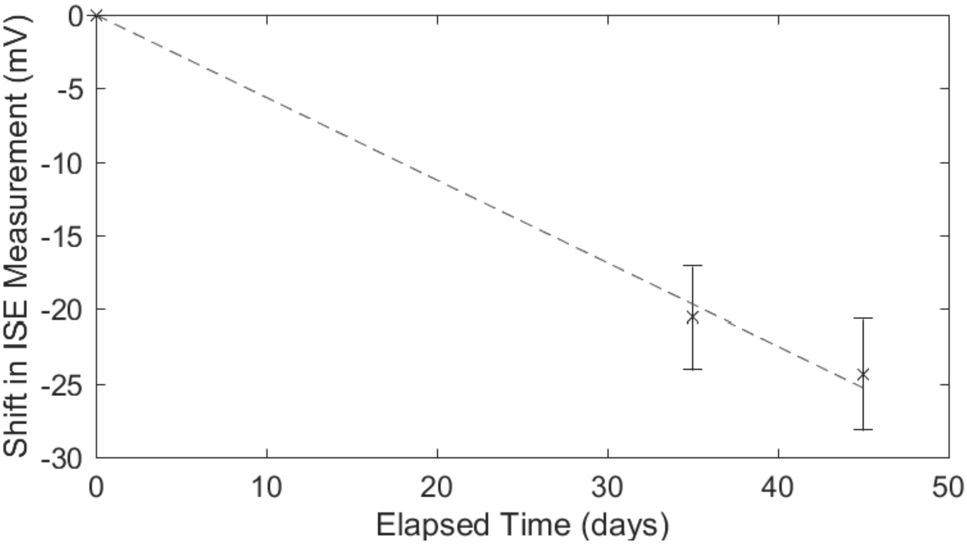

Figure B.7: Shift in the ISE measurement over time. Error bars indicate the standard deviation across all tested concentrations (n = 5).

With regard to the increase in slope over time, it is possible that the membrane used to make the ISE selective to cupric ions is acid or water sensitive, and prolonged storage in weakly acidic solutions may slightly widen those pores to allow greater access to the electrode surface. Alternatively, consistent use may release air bubbles trapped in the membrane over time by agitation in solution when moving it between samples, so this change could stabilize over enough use. Regardless, the shift between days is small, amounting to an increase of less than 3 mV/decade ppm over the course of a month, and thus was not corrected in the calibration.

While these trends initially seemed consistent, there was a period of time from 21 July to 6 August where the ISE was stored dry, as no tests were being performed during this timeframe and dry storage is best for long-term ISE maintenance. After allowing the ISE to soak in 100 ppm copper solution to rewet the membrane, subsequent tests did not clearly show such pH and time trends (Fig. B.8). In fact, the intercept no longer shows a reliable pH trend, while the slope did not initially show a trend (Table B.4).

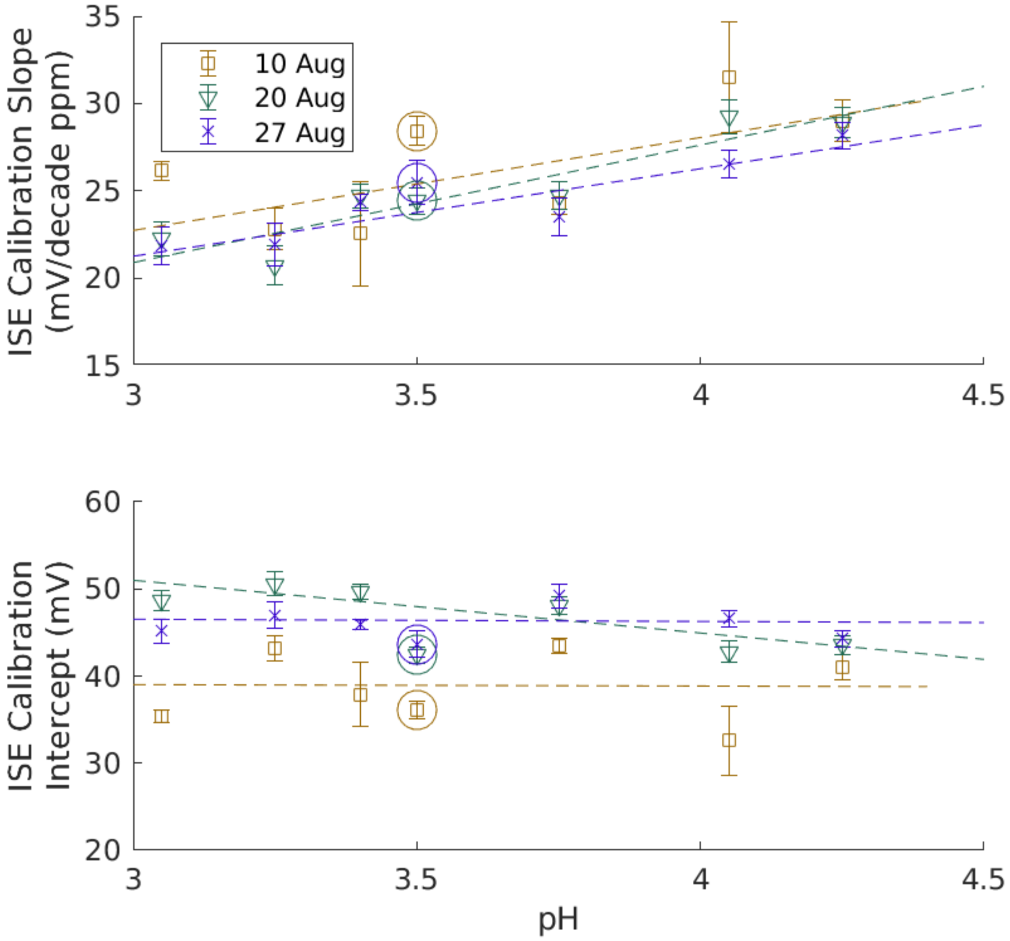

Figure B.8: Change in the ISE calibration's slope (top) and intercept (bottom) with respect to pH during the month of August. Error bars indicate the uncertainty in the calibration fit line. Circled data points indicate tests with simulated spent lees.

Table B.4: Coefficients of determination of the ISE calibration variables with respect to pH for each test date in August.

	Slope vs pH	Intercept vs pH
10 Aug	0.488	0.000
21 Aug	0.849	0.759
27 Aug	0.866	0.005

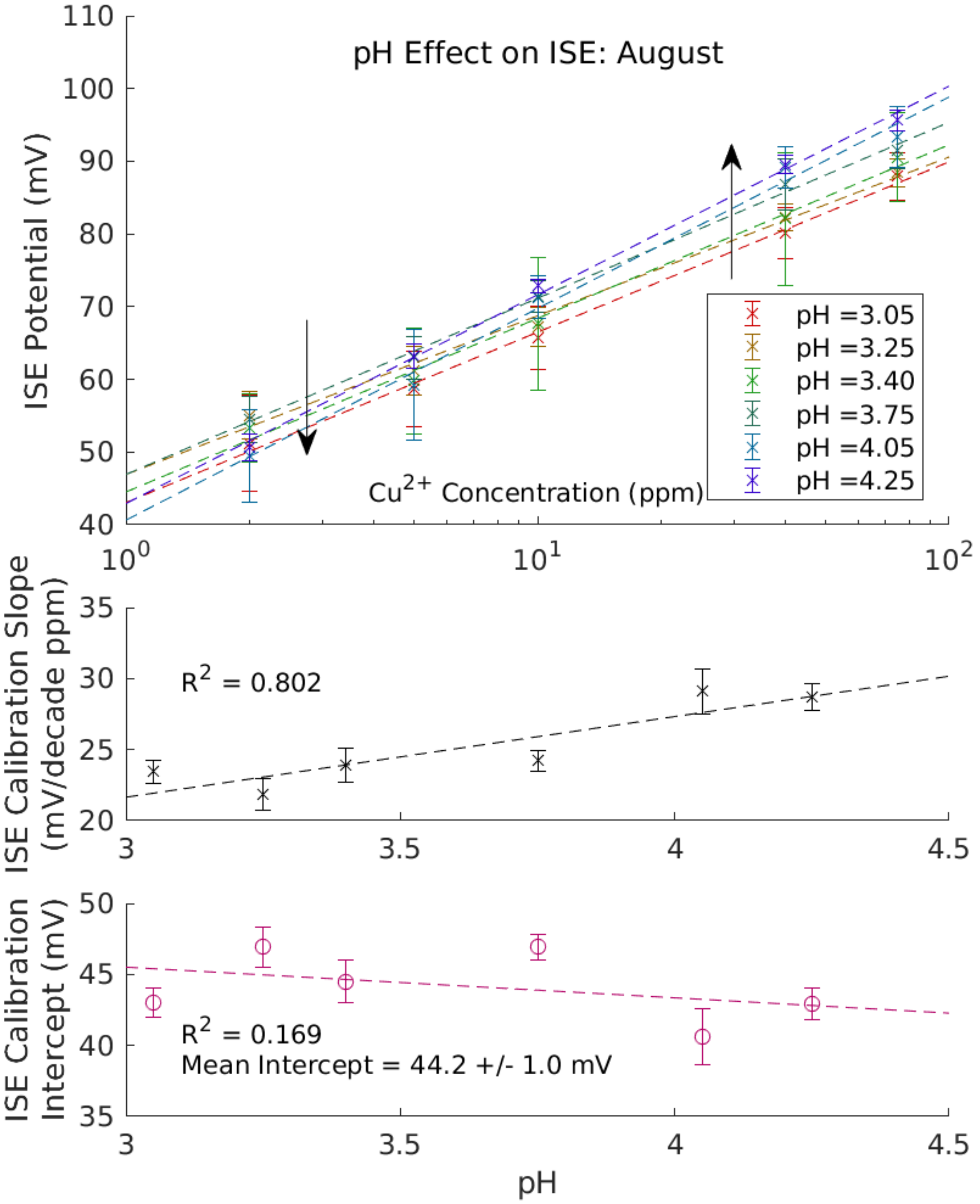

Figure B.9: Calibrations of the ion selective electrode at different pH values, aggregating tests performed in August together. (top) Error bars indicate the standard deviation. The arrows show the direction of increasing pH. (middle and bottom) pH dependence on the calibration slope and intercept. Error bars show the uncertainty in the fit line.

As a result, tests after 6 August could not rely on the same pH and time corrections. Instead, these three calibration curves were aggregated together, which did seem to show a relatively strong pH dependence with slope while taking into account the variability among the days (Fig. B.9). The weak relationship between pH and intercept led to using the intercept and error of the fit line should all pH values be aggregated together, resulting in a single intercept with a large error instead of a function between intercept and pH.

More specifically, the calibrations and errors in both July and August relied on the Nernstian relationship between equilibrium potential and copper ion concentration. Simplification of the Nernst equation allows one to use a generic slope (slp) and voltage offset (int).

$$V_{ISE} = slp * \log_{10}[Cu^{2+}] + int \tag{B.1}$$

$$[Cu^{2+}] = 10^{\frac{V_{ISE} - int}{slp}} \tag{B.2}$$

As previously mentioned, the equation for the change in copper concentration is then:

$$d\left[Cu^{2+}\right] = \left[Cu^{2+}\right]\left(dV_{ISE} - d(int) + \frac{int - V_{ISE}}{slp^2} d(slp)\right) \tag{B.3}$$

Combining this with the general form for propagation of error (Eq. A.8):

$$s_{[Cu^{2+}]} = \left[Cu^{2+}\right]\sqrt{s_{V_{ISE}}^2 + s_{int}^2 + \left(\frac{int - V_{ISE}}{slp^2}\right)^2 s_{slp}^2} \tag{B.4}$$

However, it has been established that both int and slp are functions of pH in conditions more acidic than pH 4.25, and V_{ISE} requires a correction for time. Additionally, these variables differ whether the test was performed in July or August due to changes in the storage condition of the electrode.

For July, the values were based on the original calibration from 5-12 June, which all future calibrations were similar to after performing the correction for the date to V_{ISE} (-0.5622 mV/day). Afterwards, the values of *int* and *slp* could be determined based on the pH according to the following relationships:

$$int = -20.14 * pH + 159.2 \tag{B.5}$$

$$slp = 10.60 * pH - 20.18 \tag{B.6}$$

The equation for *int* fits the data with a coefficient of determination of 0.963, allowing for relatively small error of approximately 2.08. The equation for *slp* fits with a coefficient of determination of 0.873, so despite *slp* generally being significantly smaller than *int* (in the relevant range of pH values, *slp* varies ranges from 10.5 to 24.9; *int* ranges from 73.6 to 101), its error is also approximately 2.13.

In August, the dependence was weakened, requiring aggregation of the data to find a fair quality ($R^2 > 0.8$) fit for slope. The error, s_{slp}, is 1.49.

$$slp = 5.680 * pH + 4.507 \tag{B.7}$$

The intercept, on the other hand, was determined by finding the intercept of all pH solutions aggregated together, giving a single intercept ($int = 44.16$) and corresponding standard deviation ($s_{int} = 1.047$). As a result, the date correction was not application for August tests, as this s_int value is a result of the data across a the wide range of calibration dates, and accounts for drift in its uncertainty.

In addition to performing calibrations with only copper, an additional set of standards were made with all of the other waste constituents known to be present in spent lees at a pH of 3.5. These calibration can be seen circled in Fig. B.8.

While this calibration's intercept and slope do not fall directly on the trend lines with respect to pH for copper only solutions, the deviation is not significant compared to the deviations of pure copper solution. All of the values are generally consistent with each other, meaning the additional components in the solution do not impact ISE measurements in an appreciable manner. As a result, tests with simulated spent lees can be analyzed using the same method without need for a separate set of calibration curves, and it is possible that the same can be said when performing tests with real spent lees.

B.3 Flow rate validation

The initial desire with the Porocell was to test how the flow rate and current density would affect the current efficiency and energy cost of copper recovery, and as a result, a characterization of the Porocell's flow rate and current limits with these solutions is needed. Specifically, a confirmation of the flow rates achievable by the Porocell must be conducted in order to be confident that the readings given by instrument are the actual flow rates.

A test was performed where fluid was pumped at a set flow rate, comparing the Porocell's nominal reading to the actual volume passed (Fig. B.10). This data shows that the flow meter actually underestimates the flow rate. The flow rate does follow a linear trend ($R^2 = 0.992$, $\dot{V}_{real} = 0.899\dot{V}_{nominal} + 0.572$).

Additionally, the nominal flow rate can only reach upper limits of approximately 3.5 L/min, and can only reliably generate flow above 0.5 L/min. This corresponds to a real flow rate of about 1.0 L/min to 3.7 L/min, so the lowest and highest flow rates differ by less than a factor of 4. As a result, tests were only performed at the upper and lower limits, as differences in efficiency and energy are only expected by order of magnitude differences [28].

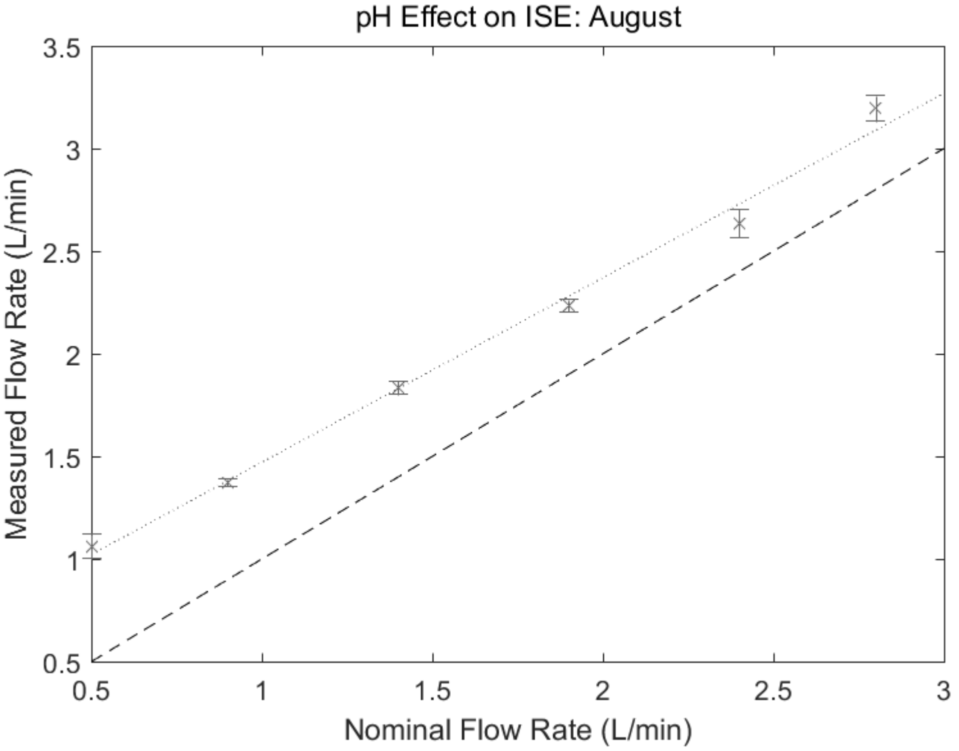

Figure B.10: Comparison between the nominal flow rate displayed on the Porocell (abscissa) and the experimentally measured flow rate (ordinate). Error bars indicate the standard deviation (n = 3). The dashed line shows the expected values should the nominal and measured flow rates be equivalent.

B.4 Comparison of carbon felt pre-treatments

One concern when operating the Porocell is that the carbon felt electrode tends to have poor wettability, thereby reducing the effective electrode area. Attempts were made to improve the surface hydrophilicity, specifically attempting to improve copper access by using methods that are reported to make the surface negatively charged [58].

Tests were performed in the Porocell using the steel anode as the working electrode such that positive current led to copper plating on the carbon felt (Fig. B.11). While there does not appear to be a large difference between untreated and treated carbon felts when polarizing with 65 μM sulfuric acid, a large difference is seen when copper is added. Interestingly, simply submerging the electrode in deionized water for at least 1 hour resulted in a 10-fold increase to current magnitude that was specific to the presence of copper. While one would expect the submersion to forcibly degas the carbon felt to allow better solution access, that difference should also be observed when polarizing dilute acid, as increased electrode surface area should also affect the ionic current, not just Faradaic current.

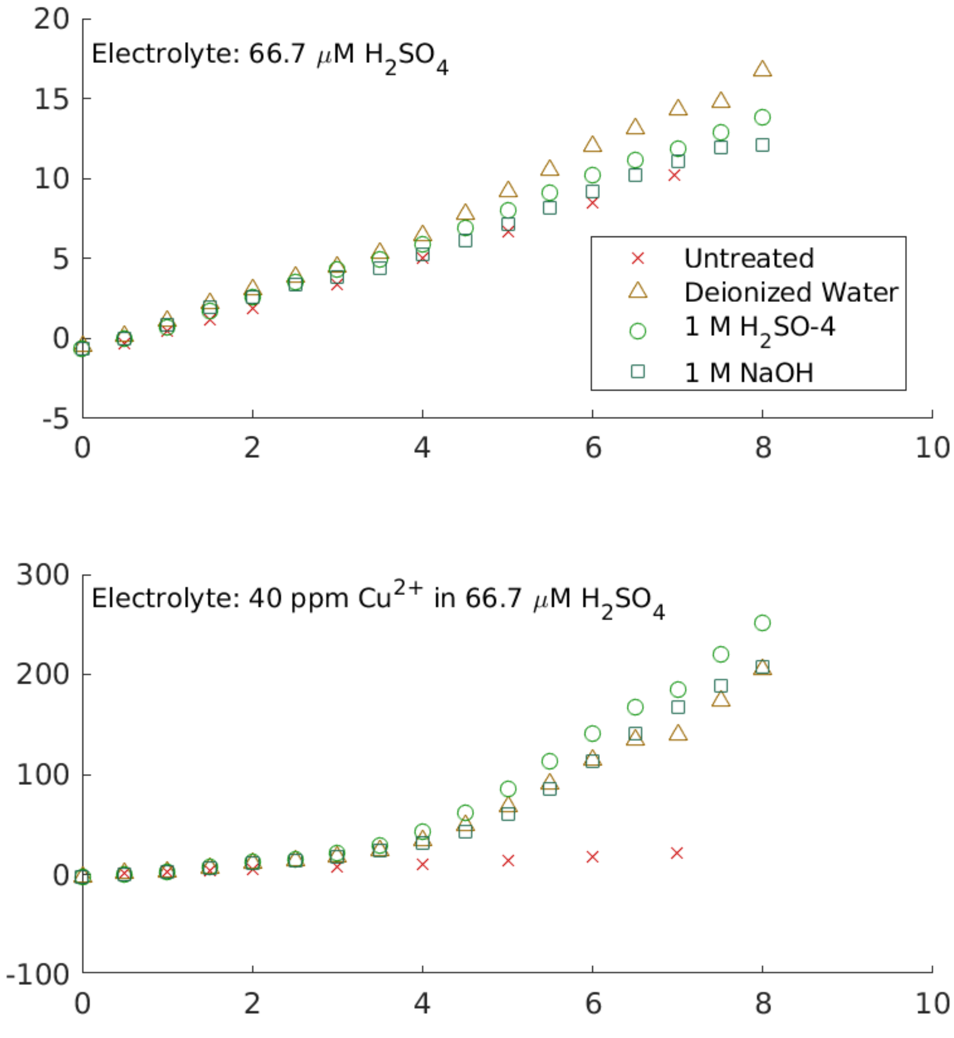

Figure B.11: Comparison of the steady state current when using carbon felt pre-treated under various conditions, using dilute sulphuric acid (top) or 40 ppm Cu^{2+} in dilute sulphuric acid. Untreated tests were performed with the Porocell circulating at 3.5 L/min; all other tests were performed with a static solution.

It is possible that the lack of difference with only acid electrolyte is because the untreated felt was tested at a high flow rate, whereas the treated felts were tested in stagnant solution. Alternatively, it is possible that the carbon felt has some hydrolyzable groups on its surface that produced negatively charged surfaces, increasing copper adsorption when using only deionized water. Regardless, surface changes are more obvious when treating with strong base or acid due to the acids and bases reacting at the surface to produce carbonyl or sulphide groups, which adsorb copper ions for faster reduction [58]. Given that the acidic treatment led to the highest currents, all tests with the Porocell utilized acid-treated carbon felt.

B.5 Determination of current limits

It is apparent from Fig. B.11 that the current passed is more than 1 order of magnitude lower than the 4 A passed with previous Porocell tests, likely due to the highly resistive solution. Therefore, to determine the range of currents for copper recovery, the current was measured at potentials up to 9 V due to the ±10 V limit of the potentiostat. These tests could also confirm the earlier prediction that only the highest and lowest flow rates would show any difference, if any difference existed.

An initial voltage sweep was performed at four flow rates to check this prediction (Fig. B.12). While these plots appear to be voltammograms, they are instead current-voltage plots, for the Porocell only allows for a 2-electrode setup, causing the voltages to be relative to a floating counter electrode potential. In each of the flow rates, a clear shoulder is visible around -0.7 to -1.0 V in the cathodic scan, likely associated with copper reduction, and has a magnitude independent of flow rate.

The only flow rate effect observed is that the slowest flow rate shows the feature most obviously, where the current is stable for a wider range of voltages. Higher flow rates instead proceed to the natural increase in current with voltage more quickly. This may be due to the faster flow rates making a subsequent reaction, such as hydrogen evolution or sulphate reduction at such negative potentials, more favorable due to better transport to the electrode.

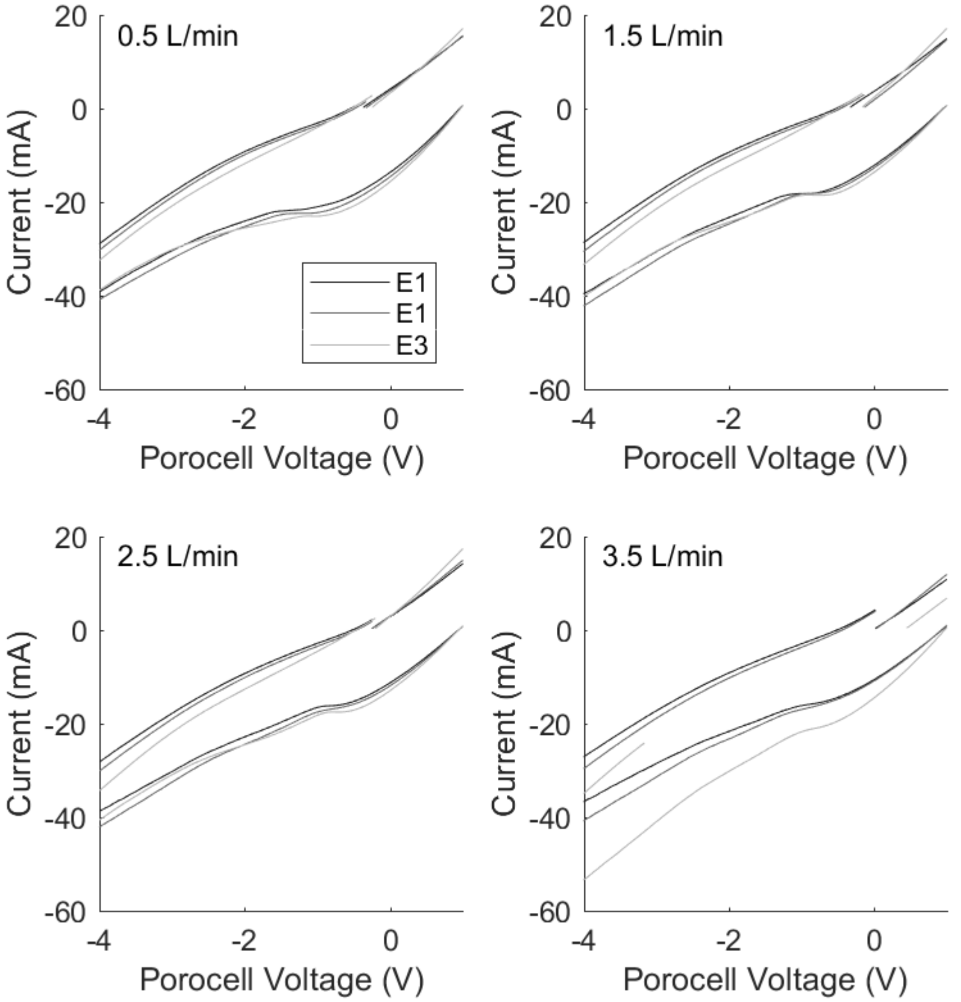

Figure B.12: Current-voltage plot of 40 ppm Cu^{2+} in dilute sulphuric acid under each flow rate tested. Each trace indicates an independent replicate. Titles refer to the uncorrected nominal flow rate.

Since the shoulder itself does not appear to change in magnitude with flow rate, it does not appear that there is a large effect of flow rate on the current associated with copper reduction. While one would expect copper reduction to show some flow rate dependence given that it tends to operate under mass transport control (Fig. 5.1.12), the less than 4-fold difference in flow rate from the slowest to the fastest and the high solution resistivity may mitigate this effect. It is not likely that the observation is due to chance, as results are highly reproducible, where most independent scans lie on top of each other, despite using different carbon felt electrodes.

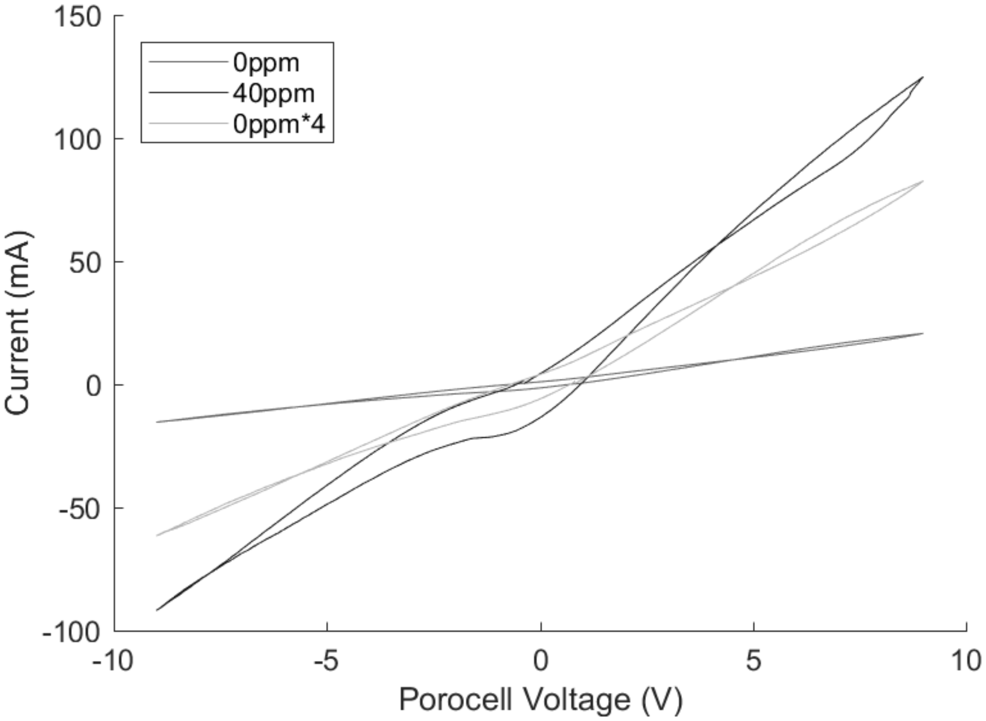

Figure B.13: Current-voltage plot comparing 65 μM sulphuric acid to 65 μM sulphuric acid with 40 ppm Cu^{2+}. An additional curve of 65 μM sulphuric acid scaled by a factor of 4 is included due to a factor of 4 increase in conductivity for more direct comparison.

Tests performed with no copper indicate that this shoulder is, in fact, attributable to copper (Fig. B.13), as without copper is cannot be seen. Addition-

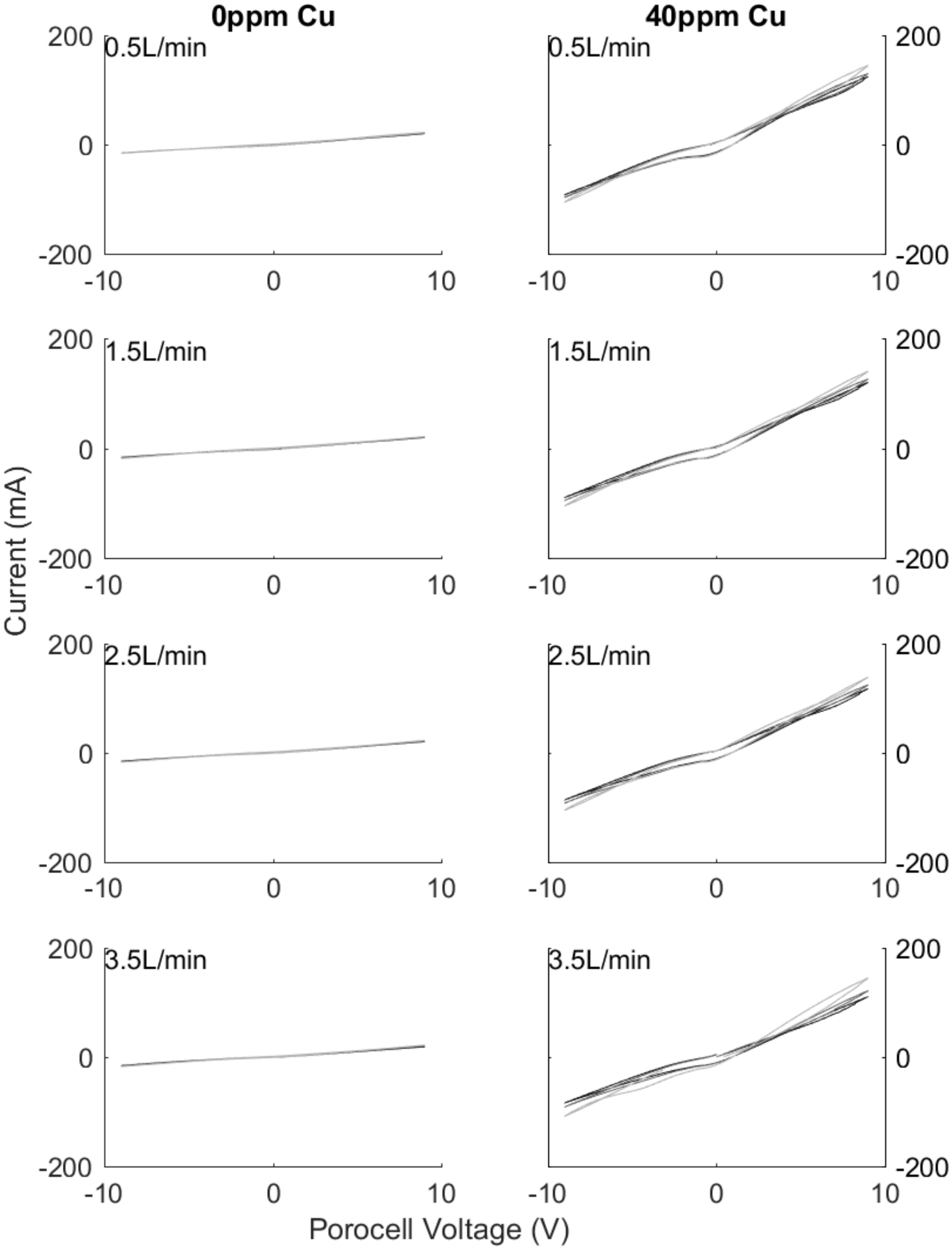

Figure B.14: Current-voltage plot for each flow rate (rows) and concentration (columns) tested. Titles refer to the uncorrected nominal flow rate.

ally, the majority of the current appears to be related to copper even at higher voltages. While the current is partially due to the higher conductivity when Cu^{2+} and SO_4^{2-} are added, multiplying the current of the scan without copper by the difference in their conductivities (a factor of 4) shows that about half of the difference cannot simply be explained with conductivity alone. Instead, the difference is likely the Faradaic copper reduction and oxidation reactions. As with the shoulder believed to be associated with copper reduction, these findings are consistent with individual replicates and flow rate (Fig. B.14).

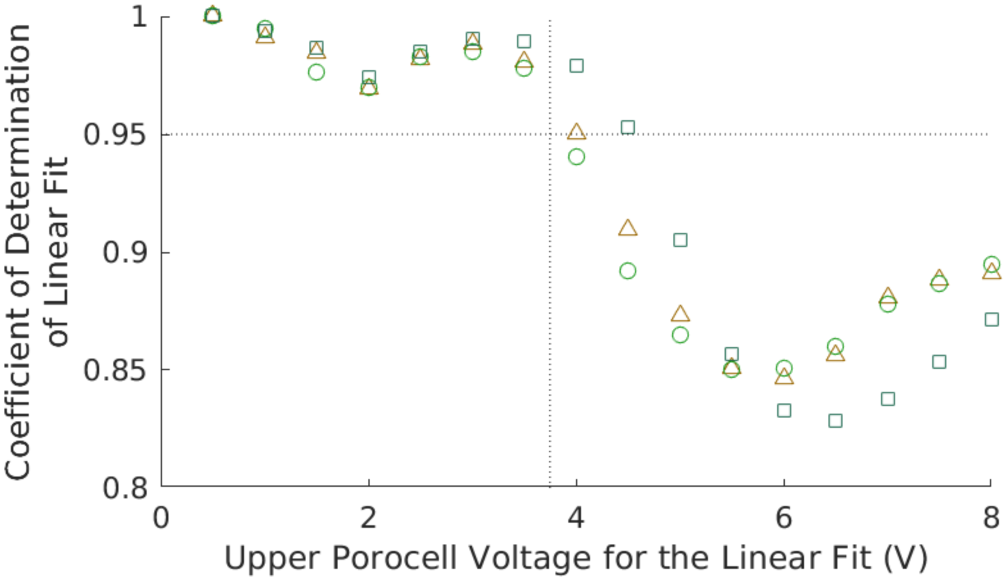

Figure B.15: Coefficient of determination of the linear fit of the steady state current (Fig. B.11) from 0 V to the specified upper voltage. The horizontal dotted line indicates the 0.95 cut-off point for a strong linear fit. The vertical dotted line is the estimated potential where the linear fit is no longer applicable.

With these results in mind, the determination of the lower limit of current is important. The solution is highly resistive, so a sufficiently high voltage is needed to accommodate the high Ohmic overpotential. Using the steady-state current when initially testing the electrode treatment (Fig. B.11), linear fits were performed from 0 V up to each higher voltage to obtain the coefficient of determination (Fig. B.15). The region in which the Ohmic overpotential dominates would strongly fit Ohm's law, and thus a linear relationship, but at sufficiently large voltages, the Faradaic current, modeled by the Butler-Volmer equation, would deviate from a simple line fit. Based on this assessment, it appears that the current deviates from a simple resistor at voltages above 3.5 V, which equates roughly to a current of 35 mA. On the other hand, the current at 8 V, chosen as the upper bound to allow for some tolerance with the 10 V potentiostat limit, resulted in a steady state current of about 105 mA.

Appendix C

Additional Data and Statistical Tables

For ease of discussion, representative figures were presented in Chapter 5. This was done to remove excess clutter from the figures so they could be more easily understood. Additionally, not all statistical tests that were performed were reported in the main chapter, as many were not directly relevant to the arguments made. For tests that were reported, many of the insignificant differences were only reported as being greater than a lower threshold to give an estimate of the significance, rather than give the exact value. This data is presented here.

C.1 Bench scale tests

The cyclic voltammorgrams are presented, with the current and voltage circled. Note that the peak may be slightly off of what is expected from visual inspection in part due to the removal of the background current when determining the peak. There are also some tests which have been expanded or narrowed their potential windows compared to the intended 0.1 to 0.6 V. A wider window is desired, but the background behaviour, potentially due to parasitic oxygen evolution, would often mask the copper behaviour.

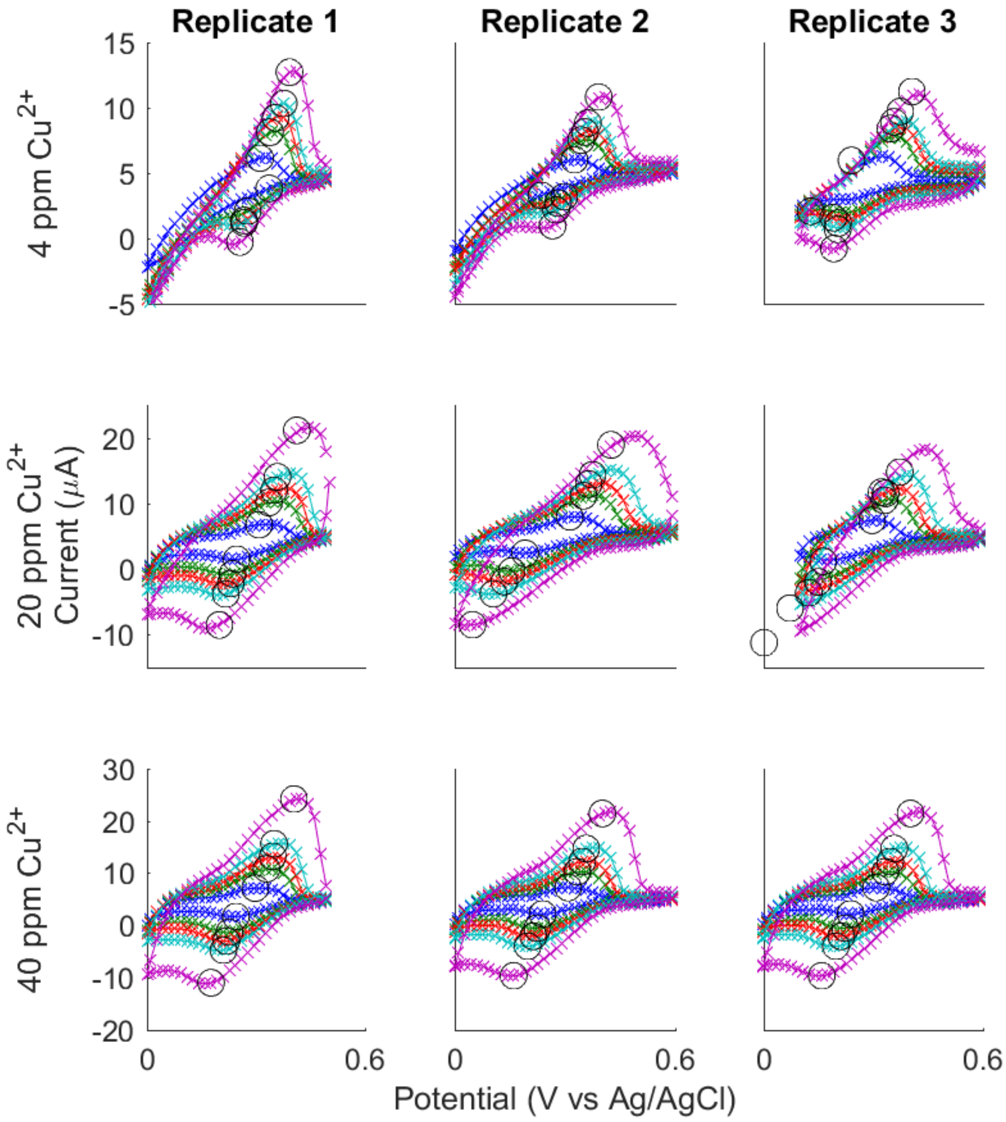

Figure C.1: Cyclic voltammetry with weakly acidified copper solution. Each row uses the same scale for the y-axis; each column uses the same scale for the x-axis. The estimated peak is circled.

Table C.1: Current for each voltammogram peak: copper only. Current in μA. Uncertainty is one standard deviation.

	4 ppm				20 ppm				40 ppm			
Scan rate (mV/s)	Individual trials			Mean + SD	Individual trials			Mean + SD	Individual trials			Mean + SD
Oxidation peak												
10	5.99	6.04	6.16	6.16 ± 0.12	7.44	7.97	6.76	7.36 ± 0.61	7.81	7.22	7.09	7.35 ± 0.35
25	8.43	7.54	8.14	7.83 ± 0.30	10.5	11.2	10.2	10.5 ± 0.6	11.8	10.2	10.8	11.0 ± 0.8
35	8.93	8.16	9.25	8.61 ± 0.57	11.6	13.0	12.0	12.1 ± 0.8	13.9	12.2	13.2	13.1 ± 0.9
50	9.72	8.84	10.34	9.36 ± 0.85	11.7	14.4	14.1	13.5 ± 1.3	15.1	14.7	15.6	15.1 ± 0.46
100	11.3	10.8	12.7	11.5 ± 1.1	14.8	19.0	21.2	18.4 ± 3.19	17.9	21.4	24.1	21.4 ± 2.7
Reduction peak												
10	2.10	3.31	3.85	3.38 ± 0.43	1.14	2.39	1.49	1.66 ± 0.66	0.90	2.17	1.67	1.61 ± 0.60
25	1.61	3.21	2.11	2.44 ± 0.67	-1.99	-0.32	-0.76	-0.91 ± 0.68	-2.90	-0.56	-1.33	-1.58 ± 1.17
35	1.20	2.72	1.40	1.85 ± 0.76	-3.66	-1.93	-2.24	-2.49 ± 0.72	-4.98	-2.11	-3.01	-3.40 ± 1.53
50	0.72	2.22	1.22	1.43 ± 0.71	-6.00	-3.80	-3.83	-4.34 ± 0.91	-8.19	-4.00	-4.75	-5.58 ± 2.12
100	-0.75	1.00	-0.24	0.00 ± 0.90	-11.3	-8.54	-8.56	-9.48 ± 1.61	-18.0	-9.65	-11.0	-12.8 ± 4.3

Table C.2: Potential for each voltammogram peak, and the estimated reduction potential: copper only. Potential in mV vs Ag/AgCl.

	4 ppm			20 ppm			40 ppm		
Scan rate (mV/s)	Individual trials			Individual trials			Individual trials		
Oxidation peak									
10	241	326	310	297	313	308	296	308	297
25	348	344	338	331	351	335	328	334	328
35	357	355	353	334	365	349	341	347	345
50	374	363	376	323	375	358	331	358	349
100	406	392	391	373	426	411	354	402	403
Reduction peak									
10	129	236	336	164	191	246	217	239	244
25	191	298	276	150	155	235	201	224	226
35	204	281	267	124	134	229	164	213	218
50	203	276	266	73	104	216	131	198	210
100	193	266	255	1.87	47.2	198	0.479	160	176
Reduction potential $E = (E_{ox} + E_{re})/2$									
10	185	281	323	230	252	277	256	274	271
25	269	321	307	240	253	285	265	279	277
35	281	318	310	229	249	289	252	280	281
50	289	319	321	198	240	287	231	278	279
100	300	329	323	187	237	305	177	281	290

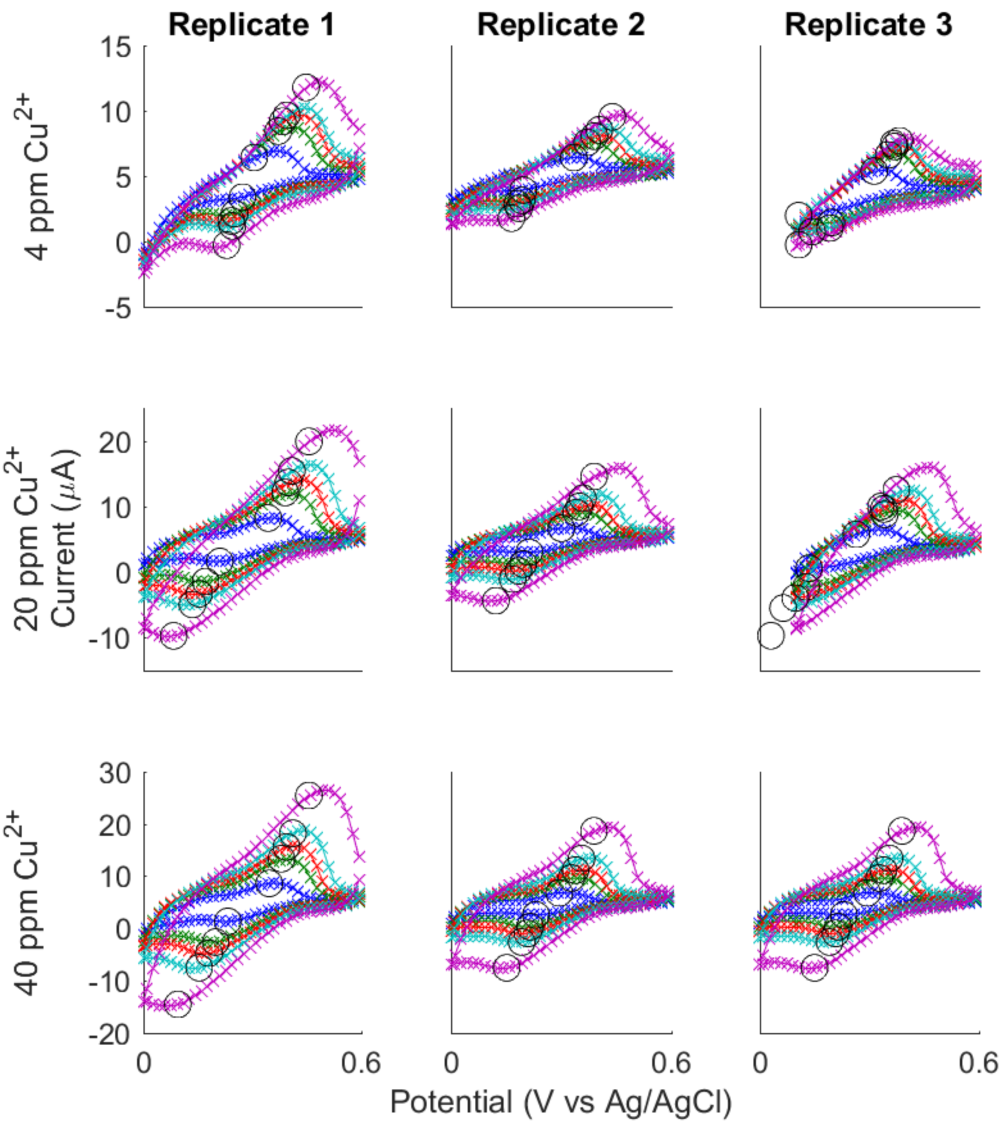

Figure C.2: Cyclic voltammetry with weakly acidified copper solution with trace metals found in spent lees. Each row uses the same scale for the y-axis; each column uses the same scale for the x-axis. The estimated peak is circled.

Table C.3: Current for each voltammogram peak: copper and trace metals. Current in μA. Uncertainty is one standard deviation.

	4 ppm				20 ppm				40 ppm			
Scan rate (mV/s)	Individual trials			Mean + SD	Individual trials			Mean + SD	Individual trials			Mean + SD
Oxidation peak												
10	6.44	6.43	5.41	6.09 ± 0.59	8.24	6.67	5.74	6.88 ± 1.26	8.58	6.76	6.34	7.23 ± 1.19
25	8.46	7.60	6.64	7.57 ± 0.91	12.1	9.07	8.79	10.0 ± 1.86	13.3	9.60	10.3	11.1 ± 1.97
35	9.20	8.07	7.29	8.19 ± 0.96	13.7	10.0	9.63	11.1 ± 2.23	15.6	11.1	12.0	12.9 ± 2.34
50	9.66	8.56	7.49	8.57 ± 1.08	15.4	11.3	10.0	12.2 ± 2.84	18.2	13.3	13.5	15.0 ± 2.73
100	11.8	9.55	7.73	9.69 ± 2.04	20.0	14.6	12.5	15.7 ± 3.83	25.4	18.6	17.0	20.3 ± 4.45
Reduction peak												
10	3.41	3.94	2.00	3.12 ± 1.01	1.60	3.03	0.56	1.73 ± 1.24	1.31	2.57	0.28	1.39 ± 1.15
25	2.15	3.17	1.47	2.26 ± 0.85	-1.46	1.21	-2.28	-0.84 ± 1.82	-2.62	0.30	-3.32	-1.88 ± 1.92
35	1.59	2.91	1.04	1.85 ± 0.96	-3.35	0.17	-3.98	-2.39 ± 2.23	-4.76	-0.99	-5.26	-3.67 ± 2.33
50	1.22	2.56	0.77	1.52 ± 0.93	-4.98	-1.10	-5.53	-3.87 ± 2.41	-7.54	-2.63	-7.72	-5.96 ± 2.89
100	-0.26	1.81	-0.23	0.44 ± 1.18	-9.77	-4.41	-9.74 ± -7.97	3.09	-14.5	-7.56	-14.9	-12.3 ± 4.14

Table C.4: Potential for each voltammogram peak, and the estimated reduction potential: copper and trace metals. Potential in mV vs Ag/AgCl.

	4 ppm			20 ppm			40 ppm		
Scan rate (mV/s)	Individual trials			Individual trials			Individual trials		
Oxidation peak									
10	304	335	314	342	300	265	346	295	294
25	370	371	353	390	341	342	379	328	349
35	383	391	370	398	350	341	393	339	352
50	394	405	367	408	359	332	411	356	354
100	447	440	383	455	390	374	454	389	384
Reduction peak									
10	272	196	107	210	212	135	232	231	211
25	250	192	197	171	196	128	198	215	181
35	241	180	192	153	183	98	180	208	164
50	244	185	144	134	167	64.6	153	192	127
100	228	163	108	82.7	121	31.3	94.3	151	49.0
Reduction potential $E = (E_{ox} + E_{re})/2$									
10	288	265	210	276	256	200	289	263	253
25	310	282	275	280	269	235	289	271	265
35	312	285	281	276	266	219	286	274	258
50	319	295	255	271	263	198	282	274	241
100	338	302	245	269	256	203	274	270	217

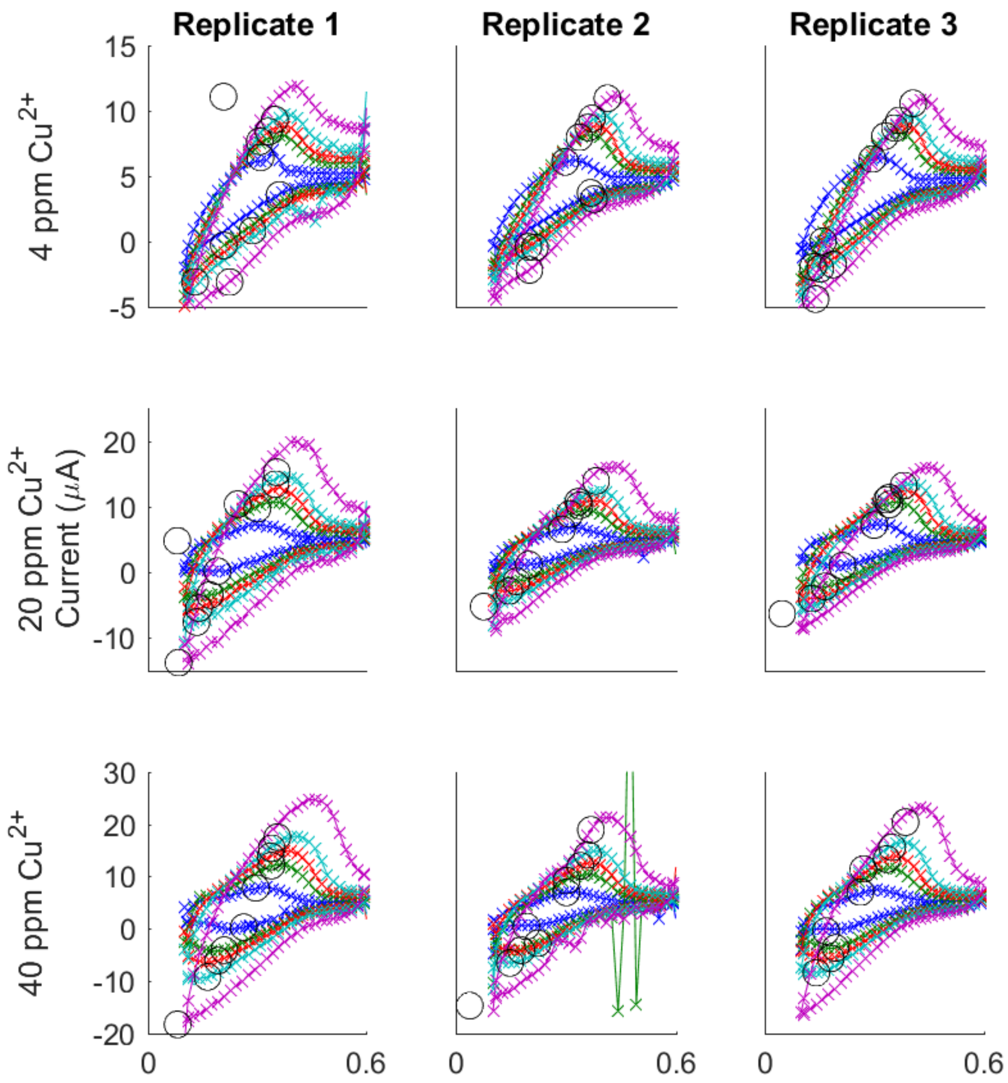

Figure C.3: Cyclic voltammetry with simulated spent lees. Each row uses the same scale for the y-axis; each column uses the same scale for the x-axis. The estimated peak is circled.

Table C.5: Current for each voltammogram peak: simulated waste. Current in μA. Uncertainty is one standard deviation.

	4 ppm				20 ppm				40 ppm			
Scan rate (mV/s)	Individual trials			Mean + SD	Individual trials			Mean + SD	Individual trials			Mean + SD
Oxidation peak												
10	6.44	6.12	6.33	6.30 ± 0.17	4.80	6.55	7.20	6.19 ± 1.25	7.79	6.94	6.99	7.24 ± 0.48
25	7.68	7.99	8.08	7.92 ± 0.21	9.72	8.91	10.3	9.65 ± 0.71	12.1	9.19	11.4	10.9 ± 1.51
35	8.43	8.74	8.70	8.62 ± 0.17	10.4	10.2	11.4	10.7 ± 0.62	13.8	12.0	13.3	13.0 ± 0.95
50	9.34	9.44	9.28	9.35 ± 0.08	13.4	10.8	11.1	11.8 ± 1.47	15.4	14.1	15.6	15.0 ± 0.78
100	11.1	11.0	10.6	10.9 ± 0.27	15.3	13.9	13.2	14.2 ± 1.04	17.5	18.9	20.4	18.9 ± 1.44
Reduction peak												
10	3.59	3.74	0.04	2.46 ± 2.09	0.14	1.16	0.99	0.76 ± 0.55	0.27	0.44	-0.47	0.08 ± 0.49
25	-0.28	3.26	-1.93	0.35 ± 2.65	-3.49	-1.40	-2.20	-2.36 ± 1.05	-4.10	-2.77	-3.68	-3.52 ± 0.68
35	0.86	-0.38	-2.06	-0.53 ± 1.46	-5.48	-2.87	-4.03	-4.13 ± 1.31	-6.09	-4.13	-5.67	-5.30 ± 1.03
50	-3.06	-0.43	-1.73	-1.74 ± 1.31	-7.62	-5.24	-6.36	-6.41 ± 1.19	-9.20	-6.53	-8.41	-8.04 ± 1.37
100	-3.07	-2.15	-4.37	-3.20 ± 1.12	-13.8	-11.5	-13.7	-13.0 ± 1.35	-18.3	-14.7	-19.9	-17.6 ± 2.65

Table C.6: Potential for each voltammogram peak, and the estimated reduction potential: simulated waste. Potential in mV vs Ag/AgCl.

	4 ppm			20 ppm			40 ppm		
Scan rate (mV/s)	Individual trials			Individual trials			Individual trials		
Oxidation peak									
10	309	298	295	80.0	289	300	296	301	263
25	307	337	330	300	310	342	339	301	271
35	331	361	357	246	337	341	337	339	334
50	348	371	369	350	333	334	340	359	349
100	207	413	407	354	382	381	355	368	386
Reduction peak									
10	361	367	160	191	198	213	263	191	169
25	208	376	133	169	165	165	209	223	195
35	287	197	153	140	145	130	192	178	182
50	129	215	188	133	75.3	48.4	163	147	142
100	224	200	140	83.7	-47.3	-138	80.8	37.0	-12.8
Reduction potential $E = (E_{ox} + E_{re})/2$									
10	335	333	228	135	244	257	279	246	216
25	257	356	232	235	237	254	274	262	233
35	309	279	255	193	241	236	265	259	258
50	239	293	278	242	204	191	252	253	246
100	215	306	273	219	167	121	218	202	187

Table C.7: Slope and subsequent diffusion coefficient when fitting the mean oxidation peak current and scan rate to the Randles-Sevcik equation. Uncertainty is one standard deviation.

	Slope ($*10^5$)	Coefficient of determination	Diffusion coefficient ($*10^5$ cm^2/s)
Oxidation peak			
Copper only			
4 ppm Cu^{2+}	2.43 ± 0.10	1.64 ± 0.00	0.995
20 ppm Cu^{2+}	5.02 ± 0.13	0.28 ± 0.01	0.998
40 ppm Cu^{2+}	6.49 ± 0.10	0.12 ± 0.00	0.999
Copper and trace metals			
4 ppm Cu^{2+}	1.61 ± 0.21	0.72 ± 0.01	0.951
20 ppm Cu^{2+}	3.97 ± 0.25	0.17 ± 0.01	0.988
40 ppm Cu^{2+}	6.03 ± 0.13	0.10 ± 0.00	0.999
Simulated waste			
4 ppm Cu^{2+}	2.09 ± 0.17	0.54 ± 0.01	0.980
20 ppm Cu^{2+}	3.54 ± 0.47	0.14 ± 0.02	0.950
40 ppm Cu^{2+}	5.39 ± 0.40	0.08 ± 0.01	0.984
Reduction peak			
Copper only			
4 ppm Cu^{2+}	-1.55 ± 0.05	0.67 ± 0.00	0.997
20 ppm Cu^{2+}	-5.19 ± 0.15	0.30 ± -0.01	0.998
40 ppm Cu^{2+}	-6.68 ± 0.34	0.12 ± -0.01	0.992
Copper and trace metals			
4 ppm Cu^{2+}	-1.22 ± 0.06	0.41 ± 0.00	0.993
20 ppm Cu^{2+}	-4.49 ± 0.07	0.22 ± 0.00	0.999
40 ppm Cu^{2+}	-6.38 ± 0.18	0.11 ± -0.01	0.998
Simulated waste			
4 ppm Cu^{2+}	-2.60 ± 0.31	0.83 ± -0.02	0.959
20 ppm Cu^{2+}	-6.41 ± 0.25	0.46 ± -0.01	0.995
40 ppm Cu^{2+}	-8.22 ± 0.68	0.19 ± -0.04	0.980

Table C.8: p-values for the comparison of each pair of solution compositions for results from bench scale studies.

Condition 1	Copper only	Copper only	Copper + trace metals
Condition 2	Copper + trace metals	Simulated spent lees	Simulated spent lees
Diffusion coefficient	0.650	0.832	0.946
Reduction potential	0.862	0.007	0.030
Tafel slope	0.992	0.302	0.261
Exchange current	0.995	0.922	0.955
Total energy consumption	0.023	0.006	0.474
Anode potential	0.025	0.007	0.490
Cathode potential	$1*10^{-6}$	$3*10^{-7}$	0.002

Condition 1	12.5 μA	12.5 μA	25 μA
Condition 2	25 μA	50 μA	50 μA
Total energy consumption	0.061	0.005	0.128
Anode potential	0.007	$1*10^{-4}$	0.003
Cathode potential	0.982	0.563	0.664

Condition 1	Copper only	Copper and trace metals	Simulated waste
Condition 2	Literature value		
Diffusion coefficient	0.988	0.418	0.679

C.2 Porocell Copper Recovery Under Ideal Conditions

Included here are the results from each individual trial with respect to pH and ISE measured concentration. The tables also note which electrode was used in each test, as well as the date it was performed.

Table C.9: Solution pH of each individual sample from the Porocell when comparing different flow rate and current conditions.

Current	0 mA							
Flow rate	Low				High			
Date	11-Jun	22-Jun	5-Jul	12-Jul	13-Jun	26-Jun	3-Jul	18-Jul
Electrode	E3	E2	E4	E5	E3	E2	E4	E5
Time (min)	pH							
0	3.97	4.18	4.00	4.05	3.99	4.20	4.05	4.12
10	4.05	4.39	4.09	4.15	4.75	4.74	4.36	4.26
20	4.14	4.46	4.14	4.22	4.67	5.04	4.58	4.57
30	4.22	4.66	4.18	4.29	4.65	5.12	4.69	4.74
40	4.32	4.72	4.22	4.36	4.66	5.29	4.87	4.90
50	4.40	4.82	4.25	4.42	4.66	5.35	5.00	5.03
60	4.47	4.97	4.29	4.47	4.67	5.28	5.09	5.10
90	4.70	4.97	4.36	4.64	4.71	5.46	5.26	5.29
120	4.92	5.09	4.41	4.80	4.73	5.56	5.34	5.36
150	5.11	5.13	4.45	4.95	4.76	5.58	5.46	5.46
180	5.25	5.21	4.49	5.06	4.80	5.59	5.49	5.52

Current	35 mA							
Flow rate	Low				High			
Date	14-Jun	18-Jun	6-Jul	11-Jul	15-Jun	19-Jun	4-Jul	17-Jul
Electrode	E3	E2	E4	E5	E3	E2	E4	E5
Time (min)	pH							
0	4.57	4.37	4.22	4.06	4.13	4.23	4.20	4.22
10	4.38	4.38	4.21	4.14	4.30	4.19	4.27	4.32
20	4.30	4.20	4.11	4.10	4.26	4.13	4.24	4.11
30	4.20	4.08	4.02	4.04	4.24	4.09	4.21	4.26
40	4.15	4.01	3.99	3.99	4.23	4.06	4.18	4.24
50	4.12	3.97	3.91	3.95	4.22	4.02	4.16	4.21
60	4.10	3.91	3.87	3.92	4.22	4.00	4.13	4.17
90	4.06	3.84	3.79	3.84	4.21	3.94	4.09	4.10
120	4.03	3.80	3.73	3.80	4.22	3.91	4.05	4.03
150	4.02	3.76	3.69	3.75	4.22	3.89	4.01	3.98
180	4.01	3.73	3.68	3.71	3.94	3.88	4.00	3.93

Current	70 mA							
Flow rate	Low				High			
Date	8-Jun	20-Jun	28-Jun	10-Jul	11-Jun	20-Jun	27-Jun	12-Jul
Electrode	E3	E2	E4	E5	E3	E2	E4	E5
Time (min)	pH							
0	4.07	4.09	4.05	4.19	4.26	4.00	4.02	4.06
10	4.25	4.01	4.04	4.06	4.33	3.85	3.95	3.95
20	4.11	3.86	3.84	3.97	4.21	3.76	3.86	3.85
30	3.97	3.73	3.78	3.86	4.12	3.68	3.77	3.78
40	3.87	3.68	3.70	3.77	4.05	3.64	3.71	3.70
50	3.79	3.61	3.68	3.70	4.00	3.57	3.65	3.66
60	3.75	3.57	3.63	3.65		3.54	3.59	3.64
90	3.65	3.48	3.52	3.53	3.87	3.44	3.48	3.56
120	3.58	3.41	3.46	3.45	3.81	3.36	3.41	3.50
150	3.55	3.34	3.40	3.38	3.75	3.29	3.32	3.43
180	3.53	3.33	3.34	3.29	3.76	3.23	3.26	3.36

Current	105 mA							
Flow rate	Low				High			
Date	5-Jun	21-Jun	4-Jul	9-Jul	6-Jun	22-Jun	2-Jul	17-Jul
Electrode	E3	E2	E4	E5	E3	E2	E4	E5
Time (min)	pH							
0	4.24	4.19	4.00	3.99	4.24	4.09	4.10	4.02
10	4.10	3.94	3.88	3.92	4.05	3.95	4.00	3.90
20	3.89	3.73	3.72	3.76	3.86	3.82	3.81	3.77
30	3.76	3.61	3.61	3.65	3.73	3.72	3.74	3.67
40	3.67	3.53	3.54	3.56	3.64	3.66	3.66	3.60
50	3.60	3.47	3.49	3.53	3.57	3.58	3.59	3.55
60	3.54	3.42	3.44	3.43	3.50	3.55	3.54	3.51
90	3.39	3.32	3.36	3.30	3.39	3.39	3.44	3.40
120	3.31	3.25	3.29	3.21	3.29	3.48	3.34	3.30
150	3.23	3.18	3.23	3.15	3.22	3.39	3.27	3.19
180	3.17	3.12	3.16	3.08	3.16	3.27	3.18	3.12

Table C.10: Solution cupric ion concentration of each individual sample from the Porocell when comparing different flow rate and current conditions. Concentration determined from the ISE measurements.

Current	0 mA							
Flow rate	Low				High			
Date	11-Jun	22-Jun	5-Jul	12-Jul	13-Jun	26-Jun	3-Jul	18-Jul
Electrode	E3	E2	E4	E5	E3	E2	E4	E5
Time (min)	Cu^{2+} Concentration (ppm)							
0	31.8	59.6	43.2	75.1	65.3	19.8	56.4	73.3
10	44.4	56.7	51.4	81.9	53.7	28.9	70.2	91.5
20	39.8	56.6	54.9	83.0	70.2	23.2	69.6	89.9
30	58.1	57.4	57.0	78.8	73.5	22.0	71.7	94.7
40	38.2	55.6	62.8	96.6	69.1	26.0	74.3	88.1
50	45.9	54.7	64.8	93.3	77.5	27.2	72.9	101.8
60	51.0	78.0	63.6	79.9	75.1	23.6	80.5	99.6
90	52.3	61.5	74.8	83.9	78.8	29.4	81.1	101.7
120	69.1	65.1	77.2	94.8	95.6	28.7	83.6	113.5
150	52.2	79.2	78.8	93.1	89.2	29.6	93.7	105.6
180	60.3	83.8	81.7	107.7	72.0	29.6	91.0	106.8

Current	35 mA							
Flow rate	Low				High			
Date	14-Jun	18-Jun	6-Jul	11-Jul	15-Jun	19-Jun	4-Jul	17-Jul
Electrode	E3	E2	E4	E5	E3	E2	E4	E5
Time (min)	Cu^{2+} Concentration (ppm)							
0	46.7	36.5	76.5	80.0	92.0	66.3	16.0	98.7
10	47.4	38.6	86.7	81.1	56.1	67.0	17.2	74.4
20	48.8	29.0	84.6	72.4	64.6	83.8	15.3	60.9
30	49.8	26.2	82.7	71.7	60.9	54.4	14.5	86.2
40	42.0	27.8	85.3	63.3	57.6	63.8	15.2	107.2
50	47.5	33.8	74.2	64.1	58.6	54.5	15.1	91.7
60	36.3	23.7	80.2	66.3	56.2	55.4	15.4	86.3
90	42.7	24.0	82.0	66.3	40.0	62.5	13.8	93.7
120	41.5	22.6	78.9	58.0	64.2	53.3	18.0	81.4
150	32.2	19.1	65.7	55.9	57.9	57.8	13.6	118.9
180	40.8	22.8	78.4	65.2	48.1	53.0	14.3	78.9

Current	70 mA							
Flow rate	Low				High			
Date	8-Jun	20-Jun	28-Jun	10-Jul	11-Jun	20-Jun	27-Jun	12-Jul
Electrode	E3	E2	E4	E5	E3	E2	E4	E5
Time (min)	Cu^{2+} Concentration (ppm)							
0	37.5	39.9	82.9	73.5	72.2	62.9	23.9	9.8
10	34.3	41.5	79.0	73.1	36.0	41.7	20.2	8.6
20	45.4	31.6	70.8	79.3	44.6	58.1	18.5	7.1
30	36.5	24.4	74.4	64.2	35.2	47.3	16.0	5.3
40	36.2	31.8	69.4	63.9	32.3	46.0	18.7	4.0
50	30.5	29.1	56.4	48.7	31.8	33.4	13.0	5.0
60	31.1	18.9	62.6	48.8		40.0	12.8	4.3
90	28.8	18.5	50.2	41.3	35.8	28.8	11.6	3.8
120	23.8	10.9	66.3	39.1	31.2	44.0	9.0	2.9
150	42.6	13.6	60.0	28.6	32.9	46.6	7.8	2.2
180	34.1	9.8	47.8	19.8	34.5	66.3	6.6	1.8

Current (mA)	105 mA							
Flow rate	Low				High			
Date	5-Jun	21-Jun	4-Jul	9-Jul	6-Jun	22-Jun	2-Jul	17-Jul
Electrode	E3	E2	E4	E5	E3	E2	E4	E5
Time (min)	Cu^{2+} Concentration (ppm)							
0	23.5	22.4	63.6	68.2	102.0	34.0	88.9	88.3
10	27.1	14.1	57.0	69.8	65.0	30.3	93.9	86.6
20	24.5	12.1	53.2	59.0	68.6	26.0	71.3	73.1
30	27.5	7.1	37.0	50.3	48.5	19.7	65.0	72.5
40	27.5	7.1	44.1	39.0	50.2	19.8	65.7	70.4
50	24.9	6.7	39.6	37.3	50.9	17.1	64.4	74.1
60	21.1	6.2	33.2	37.6	37.5	13.8	49.9	64.7
90	39.1	5.1	29.5	27.4	46.6	13.5	47.4	58.1
120	23.7	4.6	29.6	20.0	33.4	7.5	52.5	57.5
150	11.3	2.7	26.6	18.6	20.3	11.8	33.0	42.2
180	17.9	3.9	18.7	9.6	25.9	7.0	58.2	42.2

Table C.11: Tabular version of Figure 5.2.8: Coefficient of determination (R^2) when fitting the mean measured concentration profile to the zeroth and first order kinetics.

Current (mA)	0	35	70	105	0	35	70	105
Flow rate	Low				High			
Zeroth order	0.919	0.782	0.683	0.163	0.843	0.151	0.828	0.750
First order	0.906	0.756	0.665	0.170	0.876	0.122	0.893	0.894

Table C.12: p-values from the 2-way ANOVA of the concentration at three hours, as measured by ISE.

Condition 1	Condition 2	p-value
Low flow rate	High flow rate	0.200
0 mA	35 mA	0.137
0 mA	70 mA	0.007
0 mA	105 mA	0.0002
35 mA	70 mA	0.567
35 mA	105 mA	0.048
70 mA	105 mA	0.485

While a qualitative assessment was made showing that one could calculate efficiency and total recovery from (a) the ISE measurements alone, (b) the final ISE measurement and the known starting concentration, or (c) the change in pH, a statistical test was also performed to show that equivalence. This was done by comparing the total quantity of copper recovered based on the change in concentration and the known batch volume. Performing this as a 2-way ANOVA, where both the calculation method and the applied current magnitude are compared, allows for discernment of how much error can be attributed to each, allowing for higher confidence conclusions when comparing the amount of copper recovered at each current (Table C.13).

Table C.13: p-values from the 2-way ANOVA of the mass of copper recovered after three hours. Comparison factors are the calculation method (top) and the current (bottom). The flow rate is known to have an insignificant effect compared to the effects of these factors and was ignored. Calculation method definition:
Measured = uses the measured concentrations from ISE for both t = 0 and t = 3 hours
Assumed = uses the measured concentrations from ISE for t = 3 hours and the known starting concentration of 40 ± 2 ppm
pH = uses the change in copper ion concentration based on the change in [H^+] and the stoichiometric relation

Condition 1	Condition 2	p-value
Measured	Assumed	0.113
Measured	pH	0.791
Assumed	pH	0.351
0 mA	35 mA	0.045
0 mA	70 mA	0.005
0 mA	105 mA	$7*10^{-5}$
35 mA	70 mA	0.830
35 mA	105 mA	0.134
70 mA	105 mA	0.529

C.3 Validation Against spent lees

Included here are the results from each individual trial with respect to pH and ISE measured concentration. The table also notes which electrode was used in each test, as well as the date it was performed (Table C.14).

C.4 Electrode image analysis

For ease of visualization of the data, not all of the images of the electrodes were provided, nor were all height segments presented. These photographs are presented below.

Table C.14: Solution pH (top) and cupric ion concentration (bottom) of individual samples when validating Porocell behaviour with spent lees.

	Simulated spent lees			Glengoyne spent lees			
Date	10-Aug	16-Aug	20-Aug	22-Aug	23-Aug	24-Aug	27-Aug
Electrode	E4	E3	E6	E6	E6	E6	E6
Time (min)	pH						
0	3.82	3.51	3.59	4.30	4.26	4.27	4.22
10	3.90	3.50	3.55	4.27	4.26	4.26	4.24
20	3.88	3.42	3.51	4.25	4.25	4.24	4.23
30	3.83	3.39	3.46	4.22	4.22	4.23	4.21
40	3.79	3.34	3.41	4.20	4.21	4.20	4.19
50	3.76	3.28	3.36	4.17	4.19	4.19	4.18
60	3.72	3.25	3.31	4.15	4.18	4.17	4.15
90	3.64	3.15	3.20	4.05	4.12	4.13	4.10
120	3.57	3.06	3.11	3.99	4.05	4.08	4.05
150	3.46	3.00	3.05	3.92	3.97	4.04	4.01
180	3.37	2.95	3.00	3.85	3.91	3.99	3.96

Time (min)	Cu^{2+} Concentration (ppm)						
0	22.8	21.5	15.5	33.1	48.5	8.9	67.0
10	26.1	24.5	15.7	26.9	51.0	15.1	50.1
20	26.5	23.4	17.5	25.0	44.9	16.2	46.7
30	28.2	21.6	17.3	20.2	42.3	21.2	43.2
40	27.5	19.9	15.7	19.5	42.1	21.1	42.6
50	26.4	17.6	13.8	21.8	39.1	25.0	41.6
60	26.1	16.5	12.8	21.8	36.5	26.9	39.2
90	27.4	10.6	9.7	17.4	30.9	29.0	32.7
120	22.8	10.6	7.2	16.4	27.6	25.4	31.7
150	22.0	6.9	6.3	13.4	21.6	25.1	27.2
180	20.8	4.5	5.1	10.5	17.3	25.7	25.5

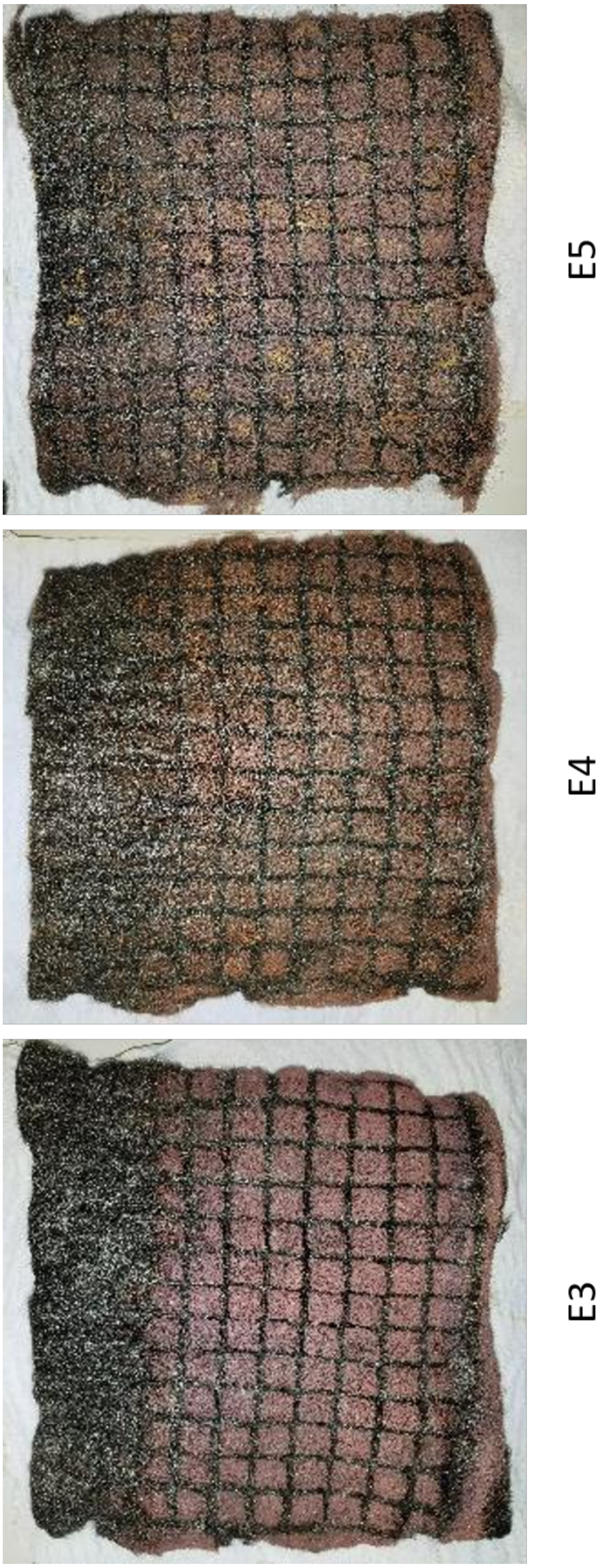

Figure C.4: Photographs of the electrodes' outer face.

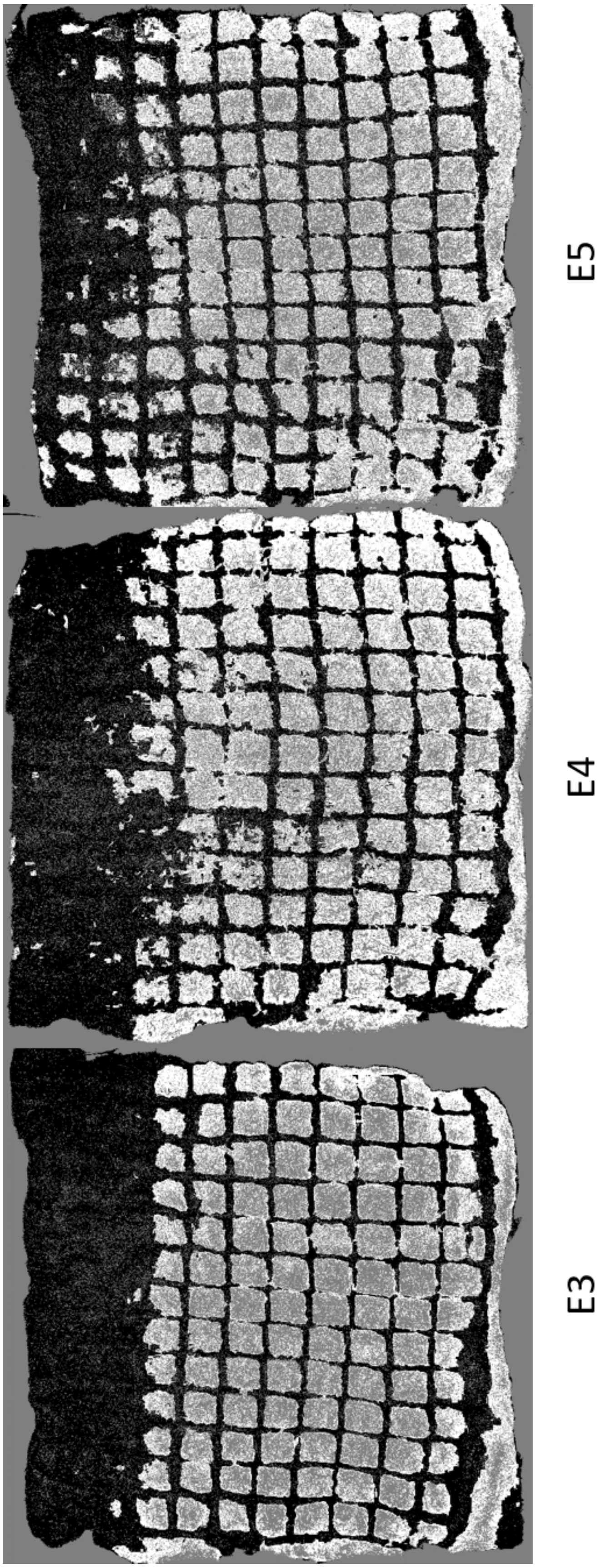

Figure C.5: Processed photographs of the electrodes' outer face. White regions are copper; black regions are the rest of the electrode surface.

E3	Raw Image	Binary Image
Depth = 1 cm	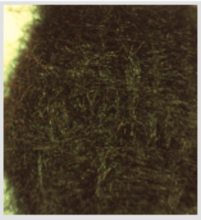	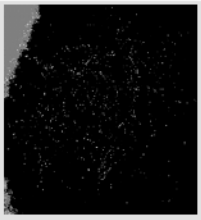
Depth = 2 cm	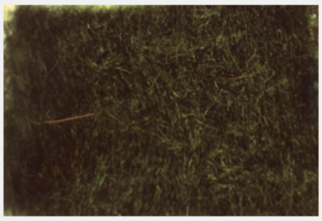	
Depth = 3 cm	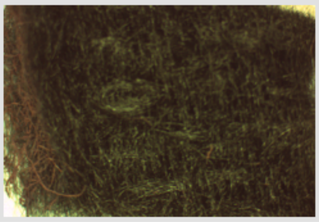	
Depth = 4 cm	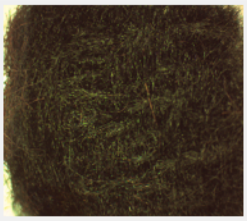	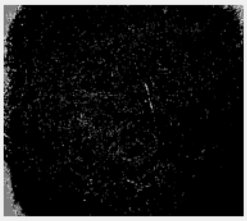
Depth = 5 cm	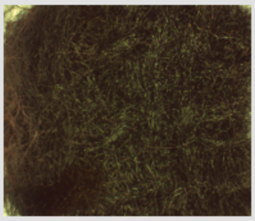	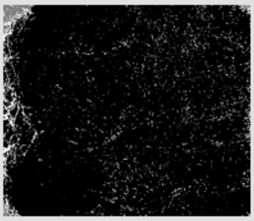
Depth = 6 cm	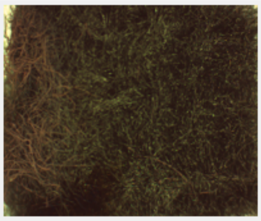	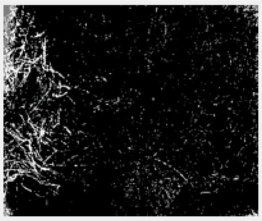
Depth = 7 cm	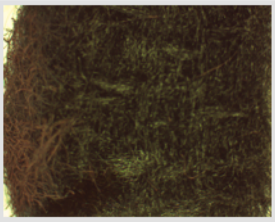	

Table C.15: Photographs and processed images of electrode E3 cross sections.

E3	Raw Image	Binary Image
Depth = 8 cm		
Depth = 9 cm	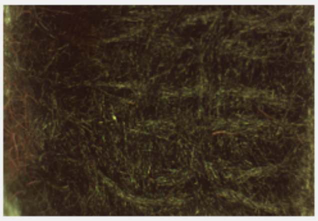	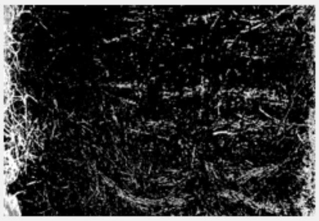
Depth = 10 cm		
Depth = 11 cm	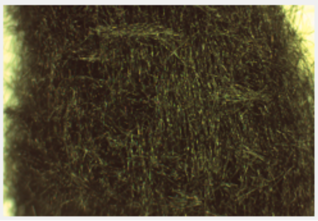	
Depth = 12 cm		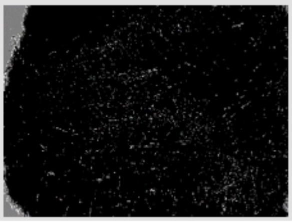
Depth = 13 cm	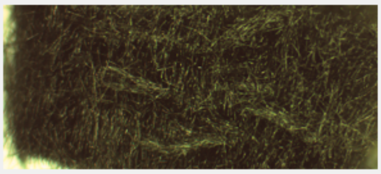	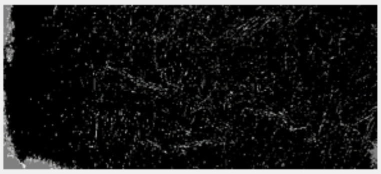
Depth = 14 cm	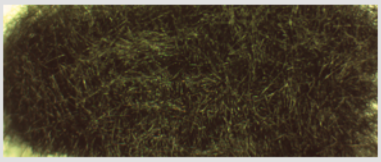	

Figure C.6: Photographs and processed images of electrode E3 cross sections.

E4	Raw Image	Binary Image
Depth = 1 cm	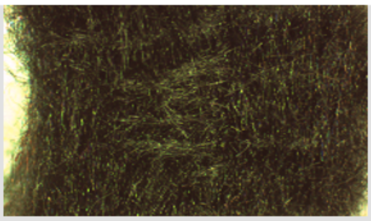	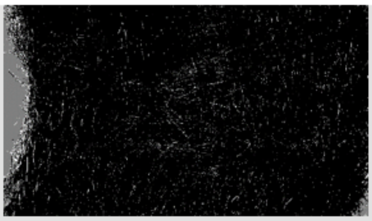
Depth = 2 cm	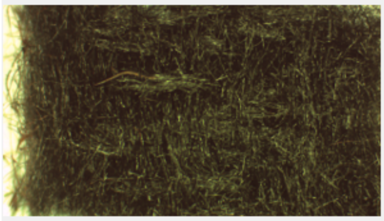	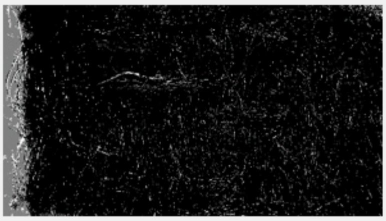
Depth = 3 cm	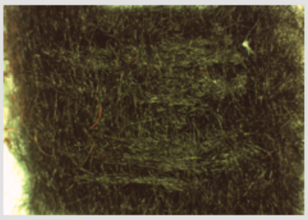	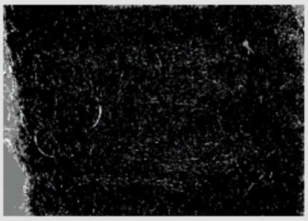
Depth = 4 cm	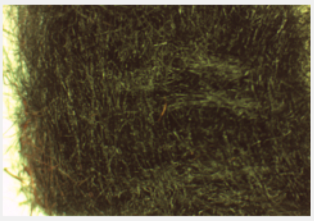	
Depth = 5 cm	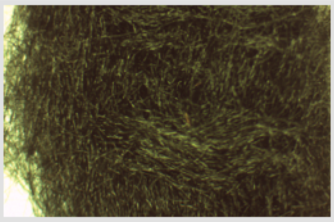	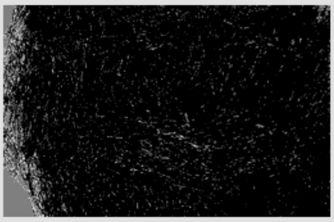
Depth = 6 cm	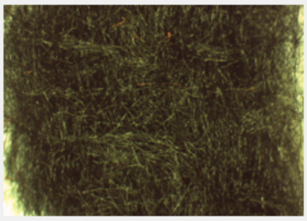	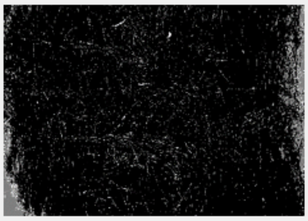
Depth = 7 cm	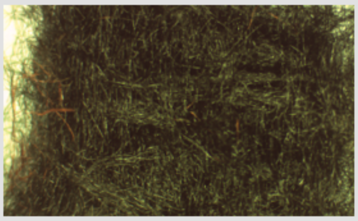	

Table C.16: Photographs and processed images of electrode E4 cross sections.

E4	Raw Image	Binary Image
Depth = 8 cm	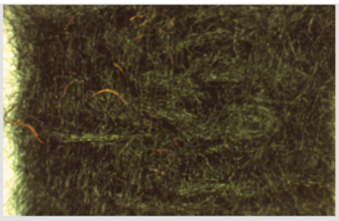	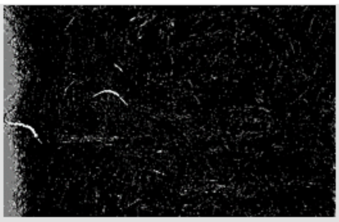
Depth = 9 cm	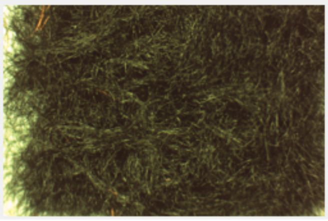	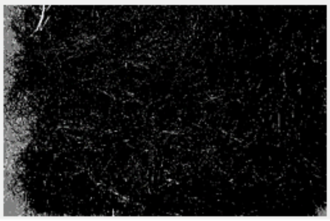
Depth = 10 cm		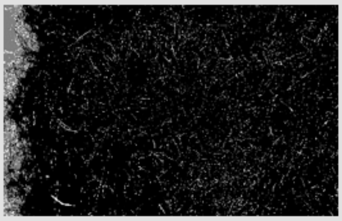
Depth = 11 cm	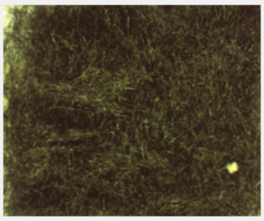	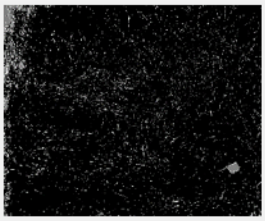
Depth = 12 cm		
Depth = 13 cm	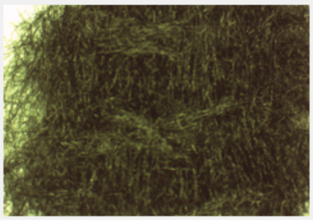	
Depth = 14 cm	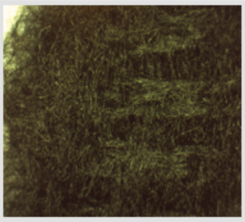	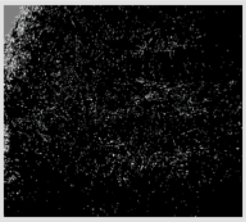

Figure C.7: Photographs and processed images of electrode E4 cross sections.

E5	Raw Image	Binary Image
Depth = 1 cm	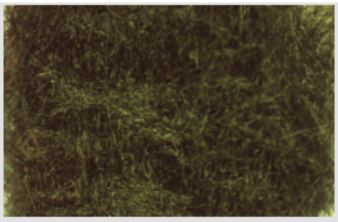	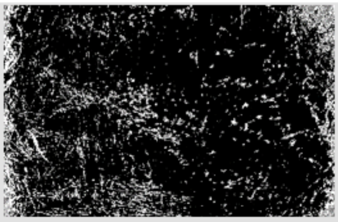
Depth = 2 cm	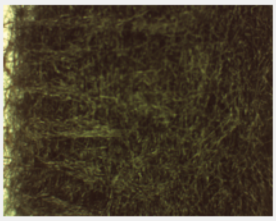	
Depth = 3 cm	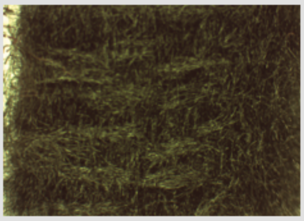	
Depth = 4 cm	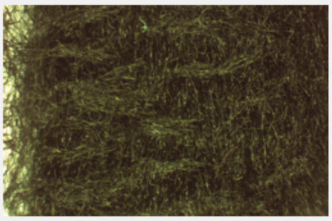	
Depth = 5 cm	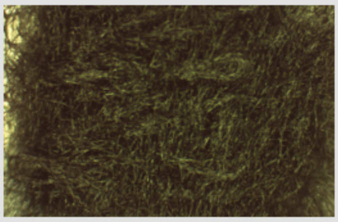	
Depth = 6 cm	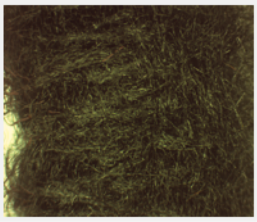	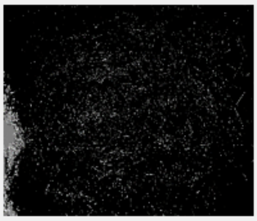
Depth = 7 cm	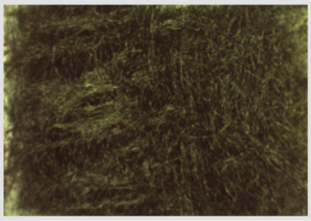	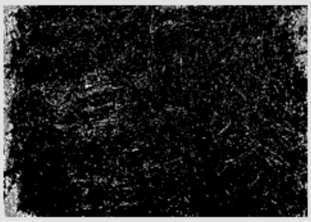

Table C.17: Photographs and processed images of electrode E5 cross sections.

E5	Raw Image	Binary Image
Depth = 8 cm	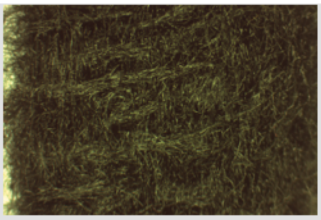	
Depth = 9 cm		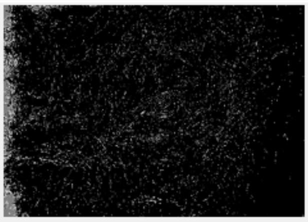
Depth = 10 cm	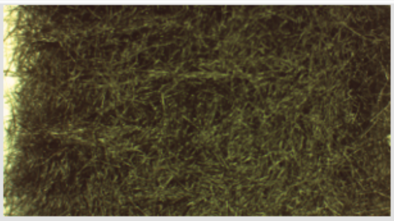	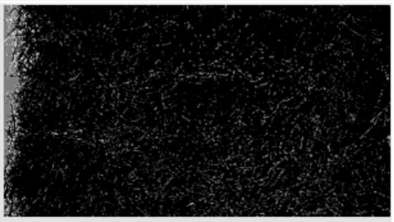
Depth = 11 cm	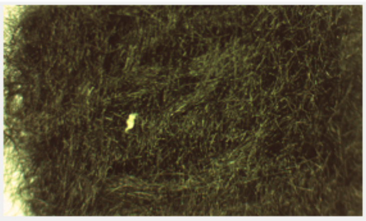	
Depth = 12 cm		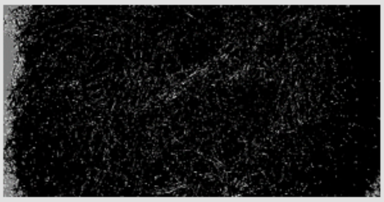
Depth = 13 cm	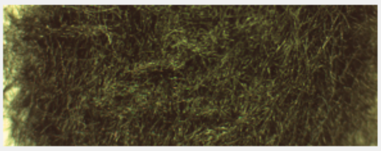	
Depth = 14 cm	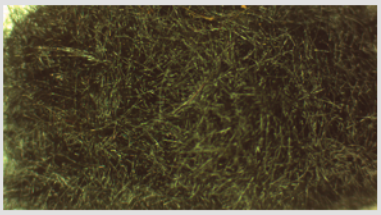	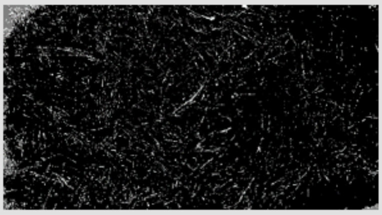

Figure C.8: Photographs and processed images of electrode E5 cross sections.

For simplicity of the discussion, only 4 of the 14 height segments were presented in the main document, as there was little difference or pattern that could be determined when seeing all 14 at the same time. These figures show all 14 for each electrode (E3 - E5), as well as the mean value, smoothed by a 41-point linear approximation.

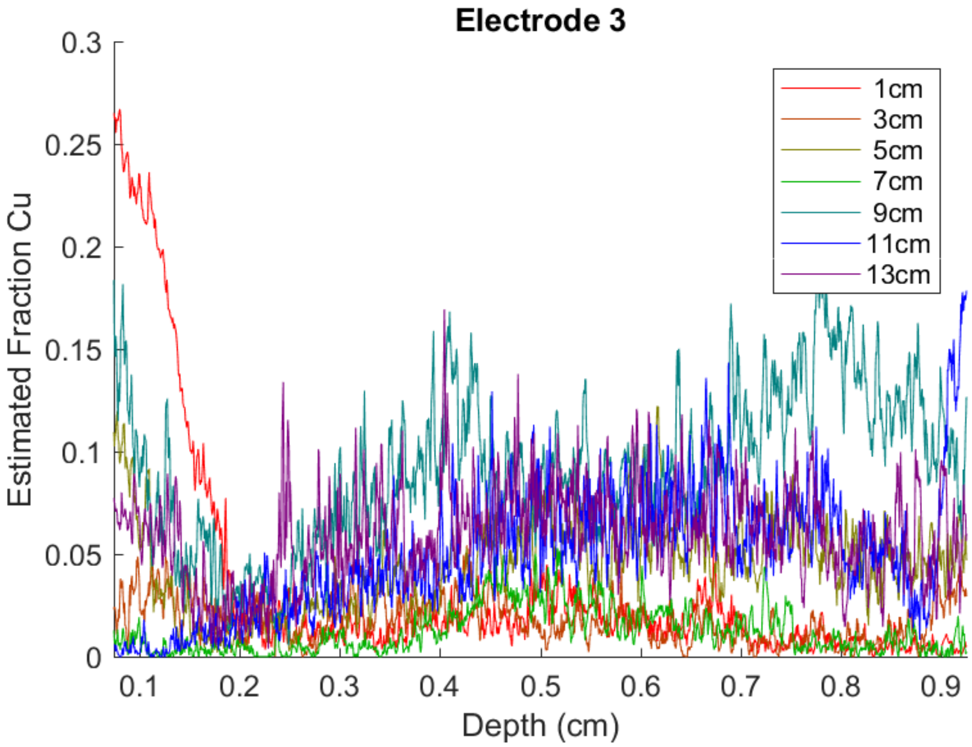

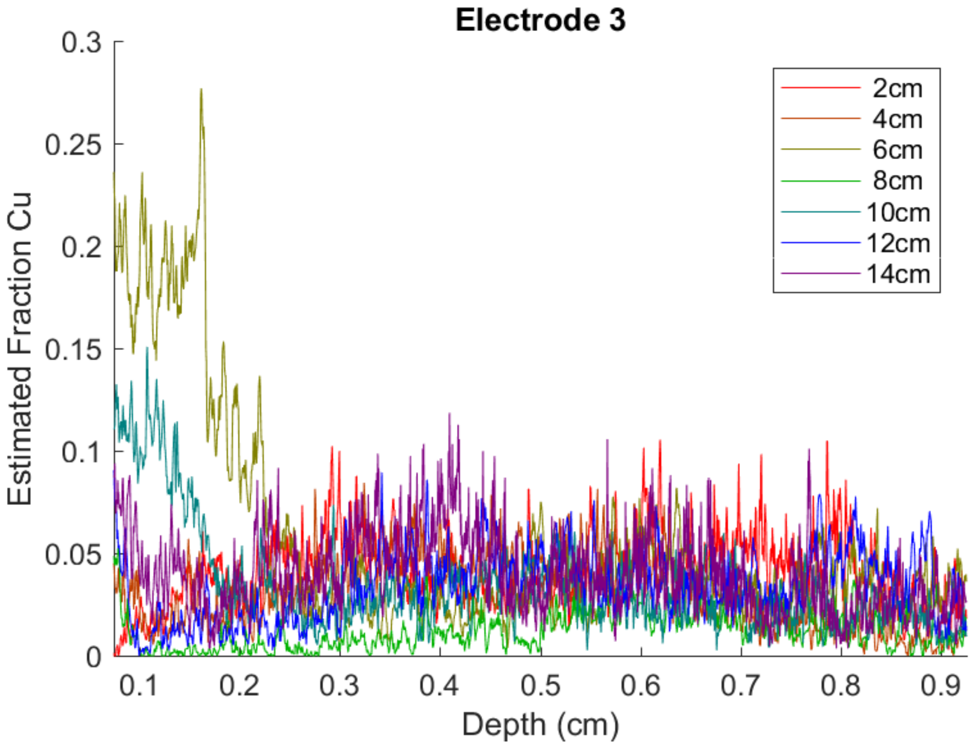

Figure C.9: E3 cross sections: profile of copper with depth.

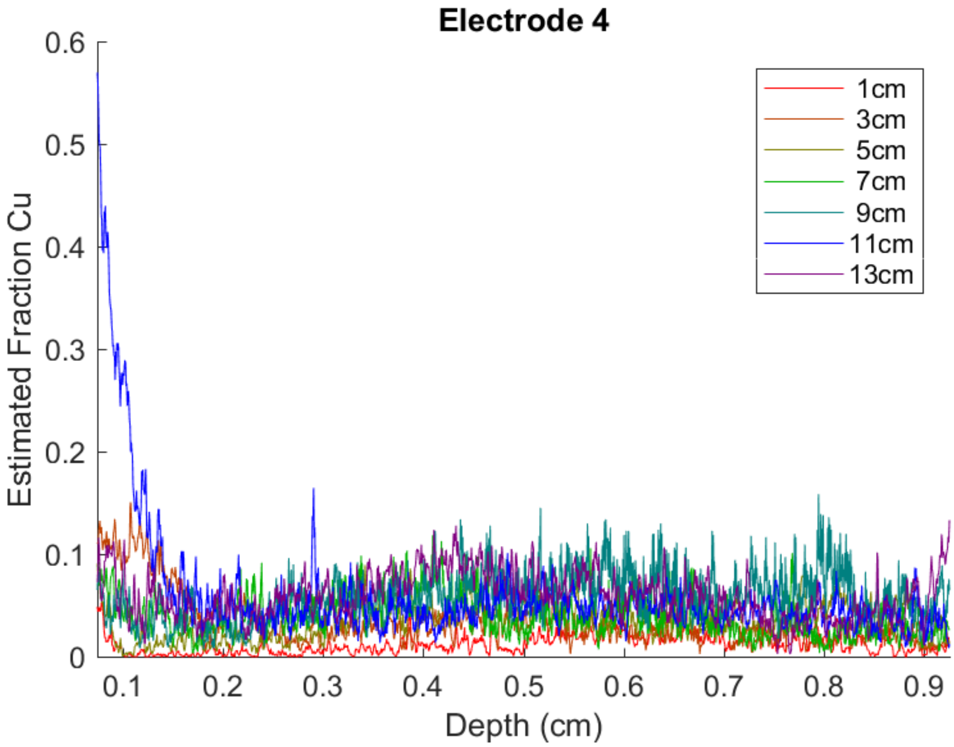

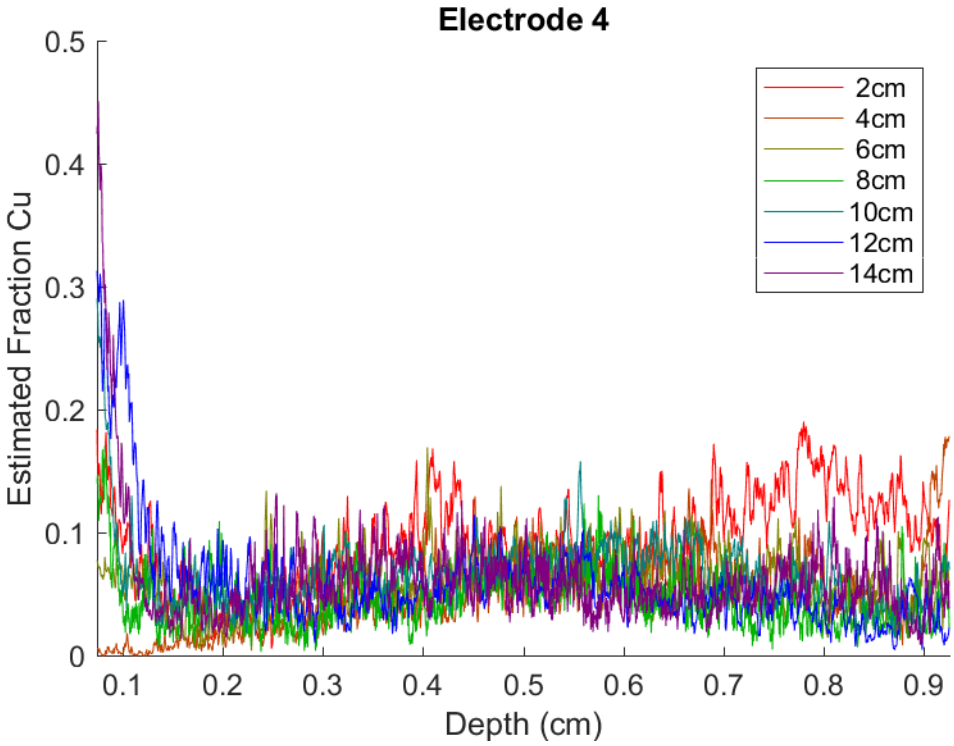

Figure C.10: E4 cross sections: profile of copper with depth.

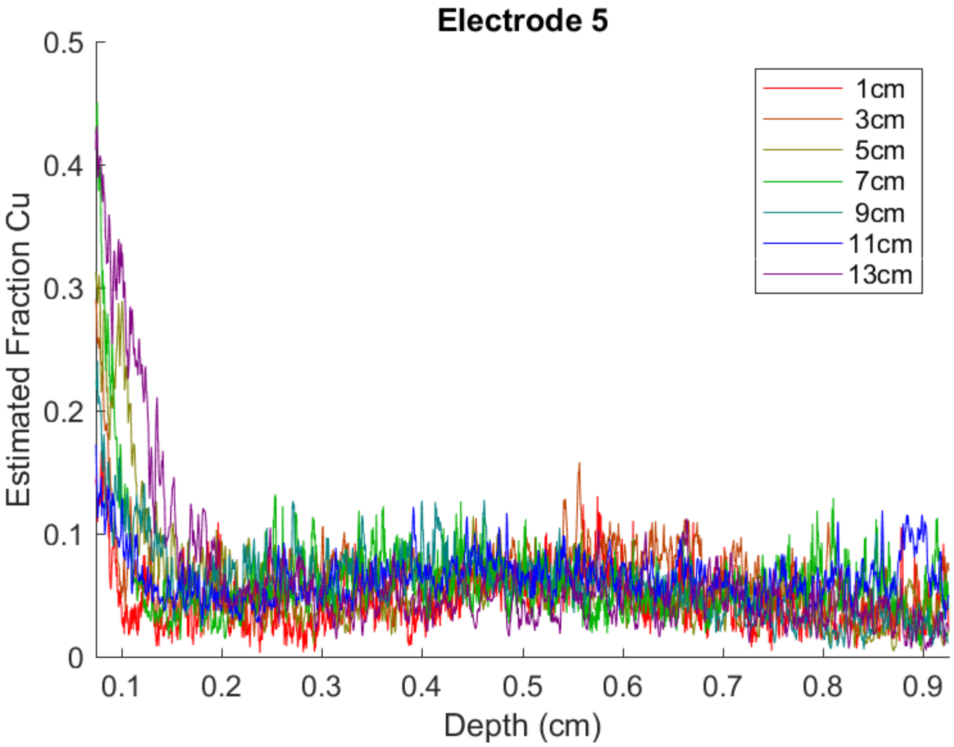

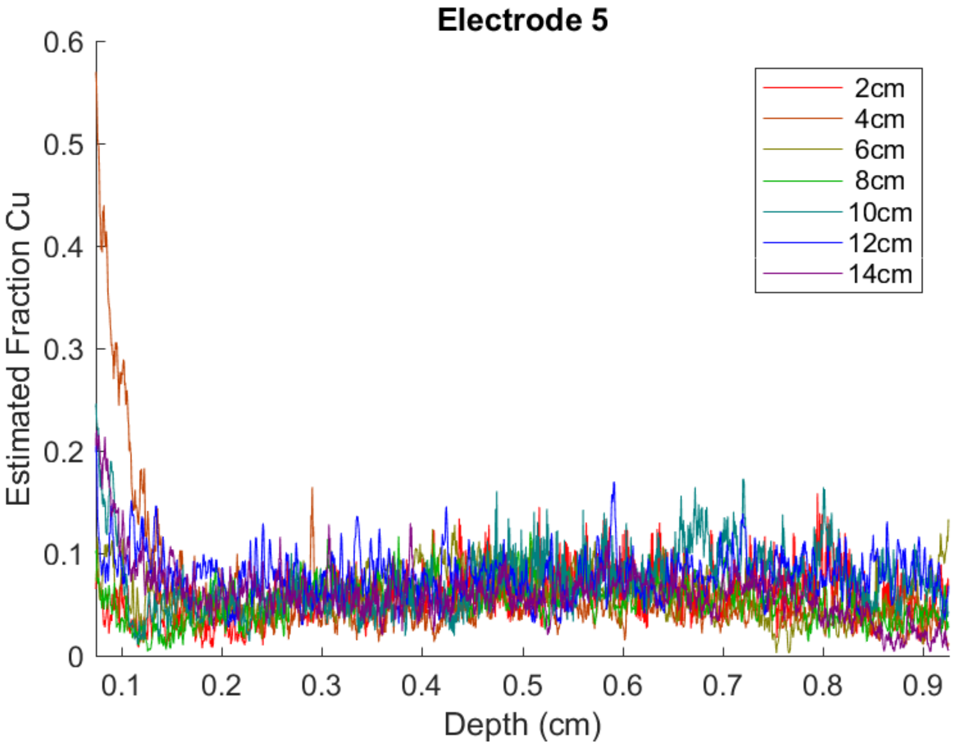

Figure C.11: E5 cross sections: profile of copper with depth.

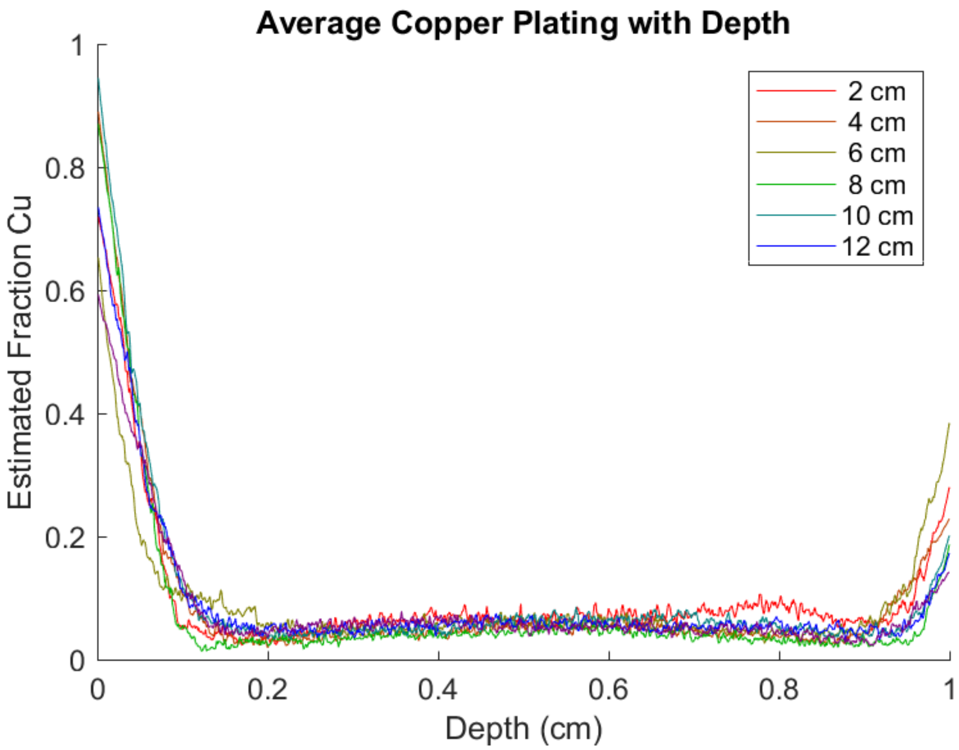

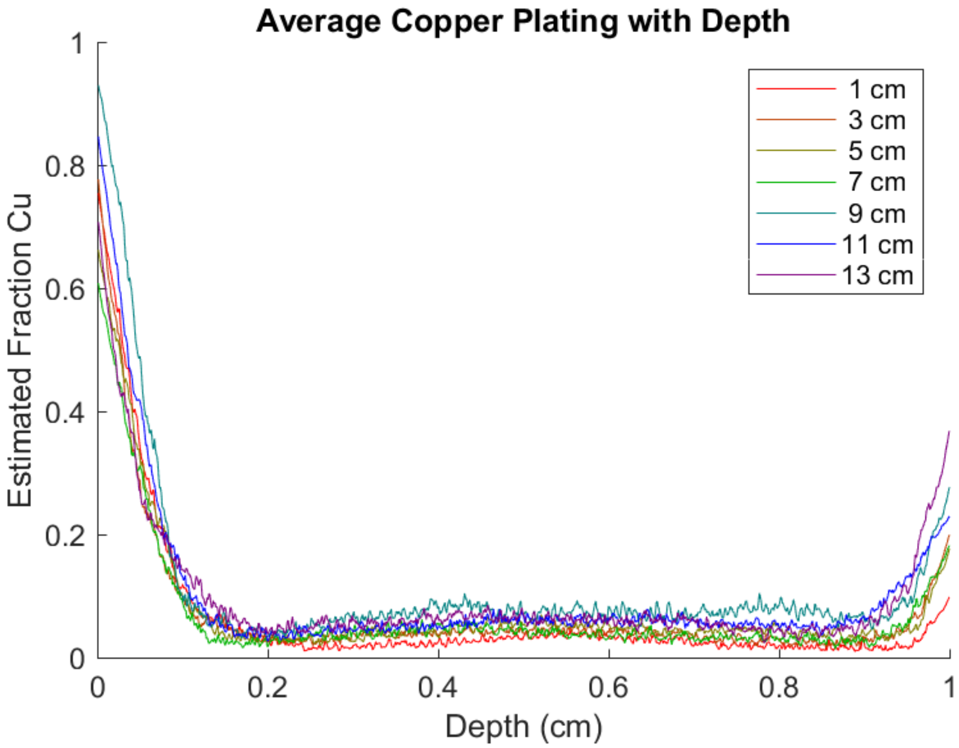

Figure C.12: Electrode cross sections: mean profile of copper with depth, smoothed by a 41 point slope (40 mm window).